UNIVERSITY OF CALIFORNIA
RIVERSIDE

Pulmonary Inflammation, Aerosol Exposure, and Health Impacts

A Dissertation submitted in partial satisfaction
of the requirements for the degree of

Doctor of Philosophy

in

Biomedical Sciences

by

Keziyah Yisrael-Gayle

September 2024

Dissertation Committee:
Dr. David D. Lo, Chairperson
Dr. Byron Ford
Dr. Erica Heinrich
Dr. Marcus Kaul

The Dissertation of Keziyah Yisrael-Gayle is approved:

Committee Chairperson

University of California, Riverside

ACKNOWLEDGMENTS

The text of chapters 3 and 4 of this dissertation is a reprint of the material as it appears in Science of the Total Environment (2021/10/20 and 2023/2/1 publications), experiments performed in earlier experiments of my lab led by Dr. Trevor Biddle. Experiments described in this dissertation were directed and supervised by my thesis mentor, Dr. David D. Lo. Dr. Qi Li, Dr. Mia R. Maltz, Purvi N. Tandel, and Jasmine Yu, Dr. Ryan Drover, Caroline Hung, and Edward E. Helderop assisted with figure production. Malia L. Shapiro, Diana del Castillo, Sumaya Alaama, Emily Tran, Martha Anguiano, Rishi Kongari, Abby Choy, Elyse Moy, and Amy Guillen aided in data collection. Ryan Drover, Daniel Gonzalez, and Hovanness Dingilian operated the environmental aerosol exposure chambers used in various studies described here. Trevor Biddle, Hannah L. Freund, Mark P. Swenson, Talyssa M. Topacio, and Robin Merwyn collected and processed water and dust samples used in chapters 3-5. Jon K. Botthoff designed the passive dust collectors used in chapters 3-5. Dr. Emma Aronson and Dr. David R. Cocker III helped to edit and review manuscripts described in chapters 3 and 4. The work described in this dissertation is truly a collaborative effort. I would like to thank everyone listed above for their contribution to my research, especially Dr. Trevor Biddle who led the studies described in chapters 3 and 4.

DEDICATION

I dedicate this thesis to my family, especially my amazing husband, Kevaughn, and my beautiful mother, Namiyah, whose endless support has carried me through this journey. To my sisters, Kashara, Keyislah, and Fatemah, my nephew, Kezari, and my friend, Aneesah—your love, support, and month-long visits brought me the reassurance, joy, and determination I needed to complete my Ph.D. To my husband and my mother, you are my backbone and the most incredible support system I could have ever asked for. This work is dedicated to you all, as without you, I would not have been able to persevere.

ABSTRACT OF THE DISSERTATION

Pulmonary Inflammation, Aerosol Exposure, and Health Impacts

by

Keziyah Yisrael-Gayle

Doctor of Philosophy, Graduate Program in Biomedical Sciences
University of California, Riverside, September 2024
Dr. David D. Lo, Chairperson

The work described in this dissertation delves into the intricate relationship between environmental exposures, inflammation, and pulmonary health, with a focus on the impact of chronic exposure to environmental particulate matter from the Salton Sea, TGF-β signaling in allergic asthma, and the therapeutic potential of antimicrobial peptides.

The Salton Sea is California's largest inland lake, bordering Riverside and Imperial Counties. The impoverished communities surrounding the lake have been documented to suffer from abnormally high rates of asthma. My studies investigated the effects of aerosolized particulate matter from the Salton Sea on pulmonary health. Using a novel aerosol exposure chamber system, I generated murine models to understand the health impacts of chronic particulate matter exposure. My research revealed that exposure to Salton Sea dust elicited distinct inflammatory and gene expression profiles in the lungs. Mice exposed to the dust showed elevated levels of pro-inflammatory cytokines and significant gene

expression changes. My studies identified the bacterial toxin, Lipopolysaccharide (LPS), in the dust, linking environmental degradation to public health issues. I found that endotoxins produced by bacteria entrained in the dust triggered severe neutrophilic inflammatory responses in the respiratory system.

In my research on TGF-β signaling, I demonstrated that Vactosertib, a TGF-β RI antagonist, significantly reduces eosinophil recruitment and lung tissue fibrosis. Mice treated with Vactosertib exhibited reduced airway hyperresponsiveness and inflammation compared to untreated controls. These findings underscore the potential of targeted molecular therapies in managing chronic inflammatory diseases and suggest that Vactosertib could be a promising treatment for severe allergic asthma.

Finally, my exploration of antimicrobial peptides from the HLB-resistant Australian Finger Lime revealed their potential as a sustainable alternative to traditional antibiotics. My research showed that these peptides exhibited promising bacteriostatic effects against pathogens such as *Salmonella typhimurium* and *Pseudomonas aeruginosa*. By disrupting bacterial cell membranes and affecting biofilm formation, these peptides demonstrated significant bacterial growth inhibition, offering a new avenue for combating resistant pathogens.

Table of Contents

List of Figures

Chapter 5: Evidence for Aerosolized Bacterial Endotoxin as an Environmental Health Hazard

Chapter 6: Effects of TGF-βRI Signaling Prevention on Protection From Airway Remodeling in Murine Model of Allergic Inflammation

Chapter 7: Antimicrobial Activity of Stable Antimicrobial Peptides Extracted From the Citrus-greening Huanglongbing resistant Australian Finger Lime Plant

List of Tables

Chapter 1: Introduction

Lung Anatomy and Physiology

The primary function of the lung is respiration. This process of respiration involves the inhalation of oxygen and exhalation of carbon dioxide, the byproduct of converting oxygen into energy. In humans, the lung has two main lobes, the left and the right lobes. Although the structural organization of each lobe is similar, they differ in their anatomical arrangement. The right lung is divided into 3 segments, the right upper, right middle, and right lower lobes. While the left lung is only composed of two lobes, the upper and the lower segments[1]. While the lungs serve as the centerpiece of the respiratory system, this system also includes additional organs. This complex system is divided into two tracts, with the upper respiratory tract consisting of the nose, nasal cavity, mouth, sinuses, throat, and the trachea.

The nasal cavity is typically the first to interact with inspired air[2]. As air passes through the nasal cavity, it is humidified, warmed and filtered. This filtering that takes place in the nasal cavity, is the respiratory immune systems initial clearance of debris. It is lined with ciliated pseudostratified columnar epithelium and mucosal cells responsible for mucus secretion to facilitate mucociliary clearance of microscale aerosolized particles that become trapped in the nasal passages. Mucociliary clearance is the lungs' first line of defense in the upper respiratory tract. The ciliated epithelium of the nasal cavity assists in expelling inhaled particles out of the respiratory system[3]. This mechanism also

takes place directly within the lungs as the ciliated pseudostratified epithelium and mucus producing goblet cells line the respiratory tract, trapping particulate matter and/or pathogens that have made it past the nasal passages and propelling these particles from the respiratory system by coughing to stimulate phlegm expulsion[3].

The lower respiratory system is often split into two zones, the conducting zone and the respiratory zone. The conducting zone is formed by the trachea, as well as the bronchi and bronchioles, while the respiratory zone is formed by respiratory bronchioles, alveolar ducts, and alveoli[3]. As air passes from the nose through the trachea, it travels through the two large primary right and left bronchi branching off from the trachea. These bronchi branch into smaller airways known as secondary bronchi which branch into tertiary bronchi and eventually bronchioles[3]. Bronchioles terminate in tiny air sacs known as alveoli, whose ultimate function is to facilitate gas exchange. While the structure of bronchi is supported and maintained by smooth muscle encased by thick rings of hyaline cartilage, as you progress through the respiratory tree, the amount of cartilage and smooth muscle significantly decreases[4]. In fact, as you enter the bronchioles and alveoli, structure and stability are solely reliant on elastic fibers as well as the production of surfactant. Surfactant is a compound produced by cells in the lung with the role of decreasing surface tension between the gaseous-aqueous interphase within alveoli[5].

Encasing the lungs is a serous membrane known as the pleura. The pleura is a multi-layered membranous sac, consisting of the outermost layer known as the parietal pleura which attaches to the chest wall and the inner layer called the visceral pleura which directly lines the lungs[6]. In between these two membranes is pleural fluid which lubricates the pleural surface to allow for smooth, unimpeded movement of the lungs. The pleural fluid also creates surface tension to secure 4the visceral and parietal layers together.

Respiratory Mechanics

The anatomy of the lung is carefully designed to optimize its functional properties. With extensive branching, the lung has optimal surface area to maximize oxygen transport, respiration, and gas exchange[7]. This branching structure creates distinct patterns of air flow within the lungs and its individual regions. Air flows into the lungs due to pressure differences between the atmosphere, intraalveolar, and intrapleural regions[7].

The active process of respiration begins with inhalation. During inhalation, the diaphragm contracts as the volume in the intrathoracic cavity increases[8]. This increase in volume causes a decrease in intrathoracic pressure. Expiration on the other hand is the passive process of respiration as the diaphragm relaxes and the surrounding tissue undergoes elastic recoil, decreasing the thoracic volume while increasing the intraalveolar pressure[8].

Due to the function of the lungs, its tissue must have elastic properties to allow for expansion and contraction. The deposition of elastic and collagen fibers within the connective tissue governs the mechanical ability of this organ. Although widely distributed throughout the lungs, the highest concentrations of elastin are found in the parenchyma, accounting for almost 30% of the lungs connective tissue[9]. This network of elastic fibers allows the lungs to recoil in order to expel carbon dioxide. Contrarily, collagen fibers are present in the parenchyma to maintain shape due to persistent stretching and recoiling of the tissue. Collagen is the most abundant protein in the connective tissue of the lungs. The primary role of this fiber is to provide structure and stability to the airways of the lungs. Many forms of collagen are found within the lungs, each with a specific contribution to its function. While type I collagen is the major contributor to respiratory mechanics, type II collagen makes up a major component of the hyaline cartilage surrounding the large airways. Type II collagen also facilitates the synthesis of extracellular matrix from chondrocytes within the interstitium. Elastin fibers allow the lung to recoil upon exhalation while collagen fibers are more rigid and prevent overextension during the process of inhalation[10]. In tandem, these fibers play crucial roles in the overall mechanics of the respiratory system[10]. The disruption of these fibrous networks can lead to severe pathology, a concept which we will discuss in the upcoming sections of this dissertation.

The Immune System

A proper functioning immune system is fundamental for survival. The immune system exists as a complex network of cellular and humoral interactions and processes that protects nearly all organisms. The immune system is predetermined and begins its development during early phases of embryogenesis. During initial phases of human hematopoiesis, mesenchymal cells originating from the mesoderm differentiate into hematopoietic cells with primitive macrophages, megakaryocytes, and erythroblasts being some of the first cells to be identified within the yolk sac[11,12]. As development progresses, the genesis of other vital immune cells such as dendritic cells, neutrophils, eosinophils, lymphocytes, and natural killer (NK) cells begins. Each of these hematopoietic cell types have distinct functions in the immune response as well as tissue homeostasis.

Innate and Adaptive Immunity (cell-mediated vs humoral)

The complexity of the immune system can be highlighted by the recognition of not only the many cell types involved in immune processes but also by its overarching processes. The immune system is historically recognized as having two arms: Innate and adaptive immunity. Innate immunity involves first responding cells such as granulocytes (neutrophils, eosinophils, basophils, and mast cells), NK cells, monocytes, macrophages, and dendritic cells (DCs)[13]. The initial onset of cell-mediated innate immune responses begin within minutes to

hours after detection of foreign elements. The process is initiated by detection of an invading element by antigen presenting cells (APCs). These antigen presenting cells play a vital role in innate immune responses as they are the first to recognize foreign elements due to germ-line encoded pattern recognition receptors (PRR)[14]. These receptors recognized conserved molecular patterns and consists of receptors such as the large family of Toll-like receptors (TLRs), C-type lectin receptors (CLRs), Retinoic acid-inducible gene (RIG)-I-like receptors (RLRs), and NOD-like receptors (NLRs)[14]. These receptors differ not only by their localization but also their ligands and ligand origins. For example, TLRs and CLRs are typically situated on the plasma membrane of innate immune cells while NLRs and RLRs are found in the cytoplasm. These receptors also differ greatly in their ligands as TLRs recognize components of bacterial, parasitic, and viral cell walls. RLRs are known to be activated by the detection of short dsRNA, and long dsRNA of many viruses[15]. Contrarily, NLRs detect motifs of bacterial peptidoglycan such as *γ*-D-glutamyl-*meso*-diaminopimelic acid (iE-DAP) and muramyl dipeptide (MDP)[16,17]. Lastly, CLRs detect β-Glucan, a component of the cell walls of fungi, and spliceosome-associated protein 130 (SAP130), a small endogenous nuclear ribonucleoprotein associated with fungi. Although triggered by distinct ligands, activation of any of these receptor results in proinflammatory responses characterized by the production of pleotropic proteins such as tumor necrosis factor (TNF), interleukin-1 (IL-1), and IL-6 which will be discussed more mechanistically in the coming sections[16].

For the purposes of this dissertation, I will focus on the contribution of Toll-like receptors to innate immunity. TLRs are a large class of receptors each playing crucial roles in the recognition of pathogenic bacterial components such as lipopolysaccharide (LPS), lipoteichoic acid (LTA), lipoproteins from the cell membrane, as well as flagellin, a structural component of bacterial cell walls. TLRs are able to signal through both the adaptor protein, myeloid differentiation primary response protein (My-D88), dependent pathways as well as through My-D88 independent signaling processes. TLR-mediated intracellular signaling is initiated by Toll/interleukin-1 receptor (TIR) dependent interactions with the TIR domain-containing cytosolic adapters such as My-D88, TIR domain-containing adapter protein (TIRAP), TIR domain-containing adapter inducing IFNβ (TRIF), and Trif-related adapter molecule (TRAM)[18]. While each TLR recognizes unique bacterial components, they each converge at their use of My-D88 signaling pathways. Upon activation of TLRs, cytosolic TIR domains dimerize[19]. This dimerization is detected by TRIF and TRAM which then recruit My-D88 to the cytoplasmic domain of the TLRs to initiate proinflammatory signal transduction. Upon this recruitment, My-D88 then induces downstream signaling molecules to form a Myddosome, containing interleukin-1 receptor-associated kinase 4 (IRAK4) and IRAK1/2. IRAK1 then activates the R3 ubiquitin ligase-TRAF6 to form K63-linked polyubiquitin chains, leading to recruitment and activation of the TAK1 complex. The activated TAK1 complex phosphorylates the IKK complex to

result in the activation of both NF- κB and MAPKs. Ultimately allowing for the translocation of NF- κB to the nucleus and the transcription of proinflammatory proteins such as Type I interferons (IFNs), IFN- α and -β, IL-1β, and TNF- α[20]. Additionally, TLRs can signal through non-My-D88 dependent pathways such as the TRIF-dependent pathway. Signaling through this pathway also leads to the production of Type I IFNs and other proinflammatory cytokines to drive inflammation.

Upon activation of TLRs, hematopoietic cells are recruited to initiate fighting off the invading pathogen. Neutrophils are the first to respond and traffic to the site of infection or damage. These cells are recruited due to activation of endothelial cells which release proinflammatory proteins as a result of stimulation of TLRs and other PRRs[21]. Activation of endothelial cells allows for the initiation of the leukocyte recruitment cascade, beginning with upregulation of adhesion molecules such as P- and E-selectin. P- and E-selectin bind their glycosylated ligands, such as P-selectin glycoprotein ligand 1 (PSGL1), on the surface of the endothelium to tether circulating neutrophils to the endothelium[21]. Following neutrophil tethering, these cells then roll along the vessel with the help of the adhesion molecules selectins until they find a point of extravasation in which they can then exit the vessel and enter the site of infection. During this process, other cells of the innate immune system are also activated and recruited to the tissues.

In addition to the cellular mediated component of innate immunity, there is also humoral contribution[22]. The humoral arm of innate immunity involves microbe sensing molecules such as mannose-binding protein (MBP) and other associated molecules that recognize peptidoglycan from the cell wall of microbes. In addition to MBP, the innate immune system also incorporates lipopolysaccharide binding protein (LBP), CD14, C-reactive protein, and antimicrobial peptides such as defensins and cathelicidins. The processes that these molecules follow converge at their activation of the complement cascade[23]. The complement system consists of plasma proteins that lead to a cascade of reactions on the surface of pathogens[24]. This is a complex system that ultimately leads to pathogen opsonization, engulfment, and clearance of the inflammatory trigger.

Innate immunity is ultimately characterized by nonspecific acute inflammatory processes that resolve within hours to days[13]. However, certain inflammatory conditions can lead to persistent inflammation, necessitating the activation of the adaptive immune system.

In contrast to the broad responses produced by the innate immune system, adaptive immunity produces targeted cellular and humoral responses. This process is driven by T and B lymphocytes. The responses of adaptive immunity heavily rely on innate immune processes. Innate immunity drives

adaptive responses through antigen presentation capabilities as well as the secretion of cytokines which lead to recruitment and activation of lymphocytes. Innate cells such as dendritic cells are critical in lymphocyte activation as they specialize in antigen presentation to these cells via major histocompatibility complexes class I and II (MHC class I/II)[26]. Activated dendritic cells upregulate their expression of MHC II as well as CD40 and CD86 which are co-stimulatory and lymph node-homing chemokines. These cells then migrate to the lymph nodes where they can present antigen peptides to T cells to activate effector T cell responses. This is done by DCs internalizing and breaking down peptides for presentation to T cells on MHC II molecules.

T Cells:

T cells are a crucial component of the adaptive immune system. These cells are capable of directly targeting antigens to facilitate clearance of pathogens which evaded the innate immune responses. These cells originate from a common lymphoid progenitor in the bone marrow and migrate to the thymus where they mature and differentiate[27]. The thymus is a highly specialized lymphoid organ where T cell progenitors are developed and selected[28]. The development of these cells within the thymus is a complex process that involves T cell receptor (TCR) rearrangement to generate double positive T cells which express both CD4 and CD8 co receptors. These double positive cells then undergo additional selection to give rise to CD4+ or CD8+ single positive

populations. These cells are then subjected to positive selection in which their affinity for antigen/MHC I/II interactions with self-peptides is tested. T cells which express appropriate affinity for antigen/MHC I/II complexes, survive this phase and migrate to the medulla of the thymus to undergo negative selection. During this process, these cells are presented self-antigens by APCs[29]. If the T cell interacts with a strong affinity for self-antigens, it is programmed to undergo apoptosis, while appropriately binding cells then exit the thymus and enter peripheral circulation as naïve CD4 or CD8 single positive cells[29]. In the periphery, T cells have a variety of subsets as well as functions. There are 5 main categories of T cells, Th1 cells responsible for cellular immune responses, Th2 cells for humoral responses, Th17 cells for protection against extracellular pathogens, regulatory T cells to suppress inflammatory responses, and cytotoxic T cells to target specific foreign elements[30,31]. The involvement of these cells in adaptive immunity is crucial for survival and health.

B Cells:

Also originating from a common lymphoid progenitor within the bone marrow, B cells are also crucial for adaptive inflammatory responses[32]. These cells can be activated in both a T cell dependent as well as a T cell independent manner[32]. T cell dependent B cell activation involves interaction of B cells with activated T helper cells. This interaction is initiated by B cells recognizing antigen and processing this antigen to be presented to T helper cells via MHC class II

molecules. This interaction induces expression of the B-cell stimulatory molecule CD40 ligand (CD40L) on the T helper cell, leading to production of effector molecules which then activates the B cell to proliferate and differentiate into antibody secreting plasma cells[33].

B cells can also be stimulated in a T cell independent manner in which antigens can activate these cells directly. This activation is induced by cross-linking of B cell receptors which in turn stimulates the cell to proliferate and produce antibodies. However, this method of activation is less effective and leads to the production of less diverse antibodies which have lower affinity[34].

The effectiveness of B cells is regulated by a highly orchestrated genetic process known as V(D)J recombination[35]. This process enables B cells to produce a wide array of distinct antigen receptors capable of recognizing a large variety of foreign antigens[35]. V(D)J recombination involves the rearrangement of gene segments encoding the variable (V), diversity (D), and joining (J) regions of the B cell receptor genes[35]. These gene segments are scattered throughout germline DNA and must be recombined in a particular arrangement to create functional BCR genes. Defects in this process can lead to severe immunodeficiencies, emphasizing the crucial function of these cells in adaptive immune processes.

Lung Immunology

The lung is a unique organ due to its constant direct exposure to the environment. Making it a prime place for infection/inflammation due to airborne particles. Due to these constant perturbations, it is imperative for the lung to have a host of immune responses capable of mitigating these environmental insults. Immunological responses within the lung involves a complex interplay between various cells and immune components to protect the respiratory system while maintaining tolerance to ensure homeostasis. A variety of cells participate in lung inflammatory responses, ranging from tissue-resident cells to recruited immune cells. Tissue-resident cells such as Type 1 alveolar epithelial cells aid in inflammatory responses by producing antimicrobial peptides to protect the lower airways[36]. These cells are also responsible for release of cytokines and chemokines to activate and recruit a variety of inflammatory cells[37]. Ciliated epithelial cells of the lungs also participate in inflammatory responses by secreting a broad spectrum of antimicrobial factors such as lysozymes, lactoferrin, defensins, cathelicidins, and pentraxin[38,39]. Additionally, the lung has a community of resident cells which aid in rapid detection and clearance of pathogens. Dendritic cells and macrophages are residential lung cells which function to phagocytize and eliminate inhaled allergens and airborne pathogens[40,41]. In addition to DCs and macrophages, mast cells are also a population of residential lung cells. These cells reside in the connective tissue and participate in innate and adaptive immune processes, releasing inflammatory

mediators as well as engulfing bacteria. Interstitial macrophages also reside within the lung parenchyma. At steady-state, these cells secrete Interleukin (IL)-10 to maintain homeostasis and anti-inflammatory conditions within the respiratory system[42].

In addition to these cells, lung endothelial cells also participate in its complex inflammatory responses by allowing for the recruitment and movement of inflammatory cell into the tissue. These recruited immune cells can be macrophages, neutrophils, T cells, B cells, eosinophils, and other inflammatory cells. These cells are responsible for promoting rapid and coordinated responses to invading pathogens to quickly restore balance within the airways. Together, these cells provide a complex network of sentinel cells aiding in tissue homeostasis.

Chronic Respiratory Diseases

Chronic respiratory disease is an ever-increasing health and economic burden[43]. The most prevalent chronic respiratory diseases are asthma, chronic obstructive pulmonary disorder (COPD), cystic fibrosis, and interstitial pulmonary fibrosis[44]. Among these, asthma and COPD are particularly pertinent to the research described in this thesis. According to the Institute for Health Metrics and Evaluation, chronic respiratory disease is the third leading cause of death globally, leading to death in 1.3 million people. These values stress the

importance of an in-depth understanding of disease pathologies of chronic respiratory diseases to develop better tailored therapeutic efforts and strategies. Each of the above-mentioned illnesses possess distinct pathologies and have different effects on lung physiology.

Asthma

Asthma is a chronic inflammatory disorder of the airways characterized by temporary airflow obstruction, and airway hyperresponsiveness (AHR). Clinically, asthma is diagnosed by presences of a cohort of symptoms such as cheat tightness, wheezing, coughing, and breathlessness. The disease manifestation as well as etiology of asthma is very complex and involves multiple cellular and molecular mechanisms. Asthma develops as a result of very complex interactions between a variety of inflammatory cells, cytokines, and mediators. The inflammatory profile of asthma is frequently characterized by the abundant infiltration of inflammatory cells into the airways. The hallmark cell populations commonly seen in allergic inflammation are eosinophils while nonallergic inflammation is characterized by the infiltration of neutrophils[45,46]. These cells interact with cells such as mast cells, macrophages, and epithelial cells to trigger a cascade of processes which lead to chronic inflammation and ultimately, clinical features of asthma. This cascade of events leads to the release and production of various mediators such as histamine, prostaglandins, and cysteinyl leukotrienes. These mediators lead to the attraction of additional inflammatory

cells into the airways, amplifying the host immune responses. This leads to bronchoconstriction, increased mucus secretion, as well as damage to epithelial cells due to proteins released by recruited eosinophils[47]. In asthmatics, resident cells such as macrophages are activated to produce a variety of cytokines and mediators such as tumor necrosis factor (TNF), Interleukin 1β (IL-1β), IL-2, IL-6, and granulocyte-macrophage colony-stimulating factor (GM-CSF)[48,49,50]. These proteins have effects on other resident and inflammatory cell types, leading to the continuous cascade of inflammation in asthmatics, resulting in chronic inflammation and lung damage affecting the small and the large airways.

AHR is a hallmark feature of asthma and is due to airway smooth muscle (ASM) contraction around large airways. This process also features increased intraluminal mucus production and airway wall edema, making airways more sensitive to triggers and more prone to contraction[51]. In healthy lungs, airway smooth muscle surrounds the airways in a circumferential pattern and is responsible for contracting the airway to aid in exhalation; however, in asthmatics, the ability of ASM to relax is severely impaired. This impaired airway relaxation can result in severe bronchoconstriction and airflow obstruction even to low doses of stimuli.

Asthma is a chronic disease with various etiologies ranging from allergies and obesity to occupational hazards and climate change[52]. To expound upon the

heterogeneity of asthma, in addition to the variety of triggers, there are also a multitude of distinct inflammatory profiles associated with asthma phenotypes. The most common forms of asthma are allergic and nonallergic pulmonary inflammation, as briefly mentioned above.

Allergic Asthma

Allergic inflammation is the most prevalent and well understood form of asthma. Its phenotype is characterized by allergen-induced immune responses resulting in increased recruitment of eosinophils into the airways. Common allergens include pollen, mold spores, dust mites, and even various food proteins[53]. Upon initial exposure to allergens, predisposed individuals develop inflammatory responses characterized by production of allergen-specific immunoglobulin E (IgE) antibodies. This process is driven by the presentation of the allergen to T lymphocytes by APCs such as dendritic cells. These primed T lymphocytes differentiate into Th2 T cells to produce type 2 cytokines such as IL-4, IL-13, and IL-5 to progress inflammatory responses[54]. These activated T cells then prime B lymphocytes to produce IgE antibodies to directly target the invading antigen. The produced IgE is then capable of binding to high-affinity IgE receptors on the surface of mast cells and basophils. This initial exposure leads to sensitization of inflammatory responses to the allergen, leading to rapid reaction to subsequent exposures and exacerbated inflammatory responses.

Nonallergic Asthma

Nonallergic inflammation refers to a more severe form of the disease that is less responsive to standard treatment methods. This endotype is described by neutrophilia resulting from exposure to a stimulus that is non-allergenic. Research has established connections between neutrophilic asthma and both Th1 and Th17 T cell subtypes, each possessing distinct downstream mechanisms. Th1 driven responses are initiated by detection of pathogen/danger associated molecular patterns (PAMPs/DAMPS) that activate TLRs on dendritic cells[55]. These cells then migrate to the lymph node where they illicit the differentiation of CD4+ T helper cells into Th1 cells[56]. While previously thought to be protective against allergic asthma, a pathogenic role of these cells has been elucidated. Th1s produce IFN-γ, TNF- α, and IL-2 to drive inflammatory responses distinct from allergic asthma, differentiated by the recruitment of neutrophils[57]. The prevalence of Th1 cells in disease manifestation is linked to increased severity of disease and decreased sensitivity to common therapeutic approaches such as corticosteroids. Conversely, Th17 driven asthma is initiated by exposure to non-allergenic stimuli which leads to the production of proinflammatory cytokines such as IL-1β, IL-6, IL-21, and IL-23, each linked to Th17 differentiation[58]. Th17 cells secrete IL-17A, IL-17F, and IL-22, with increasing data highlighting the proinflammatory potential of these cytokines[59]. Both Th1 and Th17 high asthma are defined by severe neutrophilia with distinct biological mechanisms inducing refractory asthma phenotypes.

Paucigranulocytic Asthma

Paucigranulocytic asthma (PGA) has recently been recognized as a distinct clinical entity within the spectrum of asthma. PGA is a subtype of asthma characterized by persistent symptoms despite low sputum eosinophil and neutrophil counts. This endotype typically presents with severe symptoms of asthma even in the absence of inflammation[60]. Although the underlying mechanisms are poorly understood, PGA is believed to be a subtype of eosinophilic asthma. Current findings indicate that this phenotype may be driven by macrophages or mast cells while other studies hint to the involvement on neuronal control of ASM contractility as a possible mechanism for promoting AHR in this disease phenotype. However, the mechanism is very poorly understood and little supporting data exists to help elucidate this endotype of asthma.

As highlighted here, asthma is a complex heterogenous disease with pathogenesis that warrants additional studies. Although allergic asthma is comparably well understood, disease pathology and mechanisms of nonallergic and paucigranulocytic asthma remain insufficiently comprehended. For this reason, it is imperative that additional studies be done to elucidate molecular mechanisms of asthma pathogenesis in order to better understand therapeutic strategies for better management, especially in cases of severe asthma.

COPD

Chronic Obstructive Pulmonary Disease (COPD) has a complex pathology which includes both chronic bronchitis and emphysema[61]. Its disease manifestation is variable with some patients presenting with only symptoms of one form of the disease while others present with dual disease phenotypes. The etiology of COPD is due to the repeated exposure to environmental pollutants and persistent smoking[62]. These respiratory stressors induce a heterogenous, progressive respiratory condition defined by persistent airflow limitation and chronic airway inflammation. Central to COPD pathology are multiple cellular and molecular processes involving various immune and structural cells as well as their inflammatory mediators. In fact, macrophages have been documented to play a major role in disease pathogenesis[63]. In COPD, these cells are induced to release various inflammatory chemokines and mediators which directly contribute to initiation and perpetuation of airway inflammation, impaired phagocytosis, and promote tissue remodeling. Cells such as macrophages and neutrophils are commonly attributed with the role of producing key cytokines observed in COPD, including TNF-α, IL-1, IL-6, and IL-8[63]. These cells and their mediators play critical roles in perpetuating the inflammatory phenotype of COPD. Due to persistent inflammation, this disease typically leads to structural changes of the airway epithelium, mucus hypersecretion, and airway remodeling, one link between COPD and asthma. Understanding the mechanisms underlying COPD pathogenesis is essential for

understanding its relation to other chronic respiratory diseases as well as for development of effective therapeutic interventions. Emphysema and Chronic Bronchitis are two manifestations of COPD and frequently coexist.

Emphysema

Emphysema is a chronic lung disease which is attributed to damaged alveolar sacs, causing for air to be trapped within the lungs[61]. This disease pathology leads to decreased lung function and severely impaired gas exchange. This condition is commonly imputable to long-term exposure to irritants such as cigarette smoke, the principle causative factor of emphysema[64]. This frequent subjection to harmful chemicals leads to the disruption of the fragile connections between alveoli, causing the inner walls of the air sacs to weaken and eventually rupture. This causes enlargement of the airways, preventing the lungs from properly recoiling in order to expel air; hence why this condition is frequently characterized by the key feature of air trapping[64]. This trademark of emphysema relates closely to asthma as it is also commonly observed in asthmatics due to the overproduction of mucus and tightening of airways, limiting airflow[64]. Furthermore, the two conditions also share similarities in their manifestation of symptoms. For instance, both can result wheezing, shortness of breath, as well as excessive mucus production.

Other significant parallels between asthma and emphysema include documented airway remodeling, suspected genetic involvement, as well as

absence of a cure [65]. Even with such commonality, there remains profound differences between emphysema and asthma. These differences are mainly documented as the variance of immune modulation between the two diseases. Asthma can be distinguished into a few different categories, with the principal classifications being either allergic or nonallergic. The characteristics of these two differ upon common cell types seen during surveys of the immune system. In nonallergic asthma, literature documents a high presence of neutrophils, whereas, in allergic asthma, eosinophils are the most abundant cell type. Emphysema more closely resembles the immune profile of nonallergic asthma, with a high prevalence of neutrophils within the airways. An important distinction between emphysema and asthma lies in the source of the symptomology. Emphysema is caused by constant cellular damage and loss of connection between alveoli, whereas symptoms of asthma are typically caused by bronchoconstriction due to the upregulation of smooth muscle mass and collagen deposition.

Chronic Bronchitis

Chronic bronchitis (CB) is defined by irreversible airway obstruction due to the persistent inflammation of the bronchial tubes[66]. Common symptoms of this illness include severe coughing, increased mucus production, as well as shortness of breath. The main process which attributes to the pathophysiology of chronic bronchitis is the mucous metaplasia, leading to the overproduction of

mucus in response to inflammatory prompting. Similar to emphysema, there are many similarities between CB and asthma. These commonalities include the process of mucus overproduction as recently mentioned, a narrowing of the airways, gene-environment interaction contribution, as well as airway remodeling[67]. Another intriguing commonality between these two diseases is the documentation of an upregulation of matrix metalloproteinases[68]. These proteinases are tasked with degrading extracellular matrix proteins as well as activating several cytokines and chemokines which help to regulate tissue remodeling[69]. In comparison with asthma, CB differs in the population of cells recruited as well as the region of the airway affected by these infiltrates. In CB, it is frequently noted that there is destruction and fibrosis of the alveolar walls; a feature that is not commonly associated with asthma[70]. The most crucial cellular contribution in CB comes from CD8 T cells and neutrophils as opposed to the upregulation of eosinophils noted in allergic asthma. These differences raise critical questions regarding the variation of inflammatory response and the role this may play in connection with the molecular mechanisms of airway remodeling and lung physiology.

Airway Remodeling

Airway remodeling (AWR) is a complex process characterized by structural changes to the airways and parenchyma of the lungs[71]. This pathology can occur in various respiratory diseases, including asthma and COPD[72].

Remodeling involves alterations in the airway epithelium, subepithelial fibrosis, increased smooth muscle mass, and mucus gland hyperplasia, leading to irreversible changes in lung function and airflow limitation[71]. Various cell subsets and cytokines participate in the dynamic process of AWR. Epithelial cells, in particular, are known to play a pivotal role in initiating and orchestrating remodeling processes. These cells secrete cytokines and growth factors that stimulate fibroblasts, smooth muscle cells, and inflammatory cells[73]. Fibroblasts, in turn, produce extracellular matrix proteins such as collagen and elastin, which directly induce airway fibrosis[74]. Smooth muscle cells undergo hypertrophy and hyperplasia, leading to increased airway smooth muscle mass and ultimately, airway narrowing. Additionally, inflammatory cells including eosinophils, neutrophils, and T lymphocytes release proinflammatory cytokines and chemokines that further promote tissue remodeling and inflammation[71]. Cytokines such as transforming growth factor-beta (TGF-β), IL-4, -13, and tumor necrosis factor-alpha (TNF-α) are key mediators involved in mechanisms of airway remodeling[75]. Understanding the cellular and molecular mechanisms underlying airway remodeling is essential for developing targeted therapeutics to prevent or mitigate these structural changes within the airways.

AWR in chronic respiratory inflammatory diseases directly corresponds to increased severity of clinical presentation. Firstly, due to structural changes in the airways such as thickening of the basement membrane, increased smooth muscle mass, and goblet cell hyperplasia, directly causing airflow obstruction[76].

These structural alterations lead to reduced lung function and exacerbation of respiratory symptoms such as wheezing, shortness of breath, and coughing. AWR also contributes to persistent inflammation and exacerbation of inflammatory responses within the airways[77]. Altered epithelial barrier function and increased deposition of extracellular matrix proteins provide a favorable environment for recruitment and activation of inflammatory cells such as eosinophils, neutrophils, and T lymphocytes, perpetuating a cycle of chronic inflammation and tissue damage.

Remodeling is also known to occur in COPD patients and tends to affect peripheral airways causing a thickening of the lung walls as well as narrowing of the bronchial lumen[78]. It has been broadly accepted that COPD is a small airway disease; however, in more recent research, it has been highlighted that this process may also occur in both larger and central airways of COPD patients[79]. These pathophysiological changes are thought to occur due to the increased deposition of extracellular matrix as well as hypertrophy of smooth muscles in the walls of the airway.

AWR is a multifaceted process characterized by structural alterations in the airways and lung parenchyma. This phenomenon is observed in various respiratory diseases and leads to irreversible changes in lung function and airflow. This process of lung damage could have significant implications for

individuals with asthma, especially in areas with significant factors contributing to persistent pulmonary inflammation such as air pollution, dust storms, and agricultural activities.

The Salton Sea

Situated at the Riverside-Imperial county border is California's largest inland lake, The Salton Sea. The modern-day Salton Sea was preceded by the ancient freshwater lake, lake Cahuilla. Natural flooding of the Colorado River has cyclically formed bodies of water within the Salton Sea basin for decades[80]. This water body has experienced fluctuations between fresh water, highly saline conditions, and periodic desiccation. A breach in a levee of the Colorado River filled the Salton Sea basin and created the modern-day Salton Sea, a vast, shallow lake. In the early 20th century, the land surrounding the Salton Sea was recognized for its agricultural potential, leading to the construction of irrigation canals and one of the world's largest agricultural regions[81]. In the mid 20th century, the sea had become a critical habitat for various species of fish as well as migratory birds flying the Pacific flyway path[82]. However, in modern times, the Salton Sea has been designated as an agricultural sump, serving as wastewater for agricultural run-off from the surrounding fields[83]. Additionally, due to water diversion and processes of climate change, the Salton Sea is rapidly desiccating, leading to increased salinity and exposure of playa (lakebed). This has led to the rapid deterioration of this once thriving ecosystem, resulting in immense fish die-

offs, declining bird populations, and puzzling health effects in the surrounding community.

The declining ecosystem of the Salton Sea has been linked to detrimental health effects within the region, plaguing the community with severe symptoms of asthma. The community living near the Salton Sea is a particularly vulnerable population as most are impoverished, immigrant families. These communities lack proper access to healthcare both due to physical and financial limitations[84]. Studies have shown that on average, Salton Sea residents have to travel nearly 50-60 minutes to access Imperial County emergency healthcare facilities, highlighting the severe lack of accessible healthcare in this community[84,85]. Additionally, the residents of the Salton Sea region are significantly impoverished with the median income being around $35,000, almost two times below that of the rest of California, which is estimated to be about $61,400[86]. The vulnerability of this community directly translates into poor health outcomes within the region.

The Imperial Valley is heavily plagued with a high respiratory disease prevalence. This is made evident by the two-fold increase in pediatric asthma-related emergency room visits and hospitalizations in this region when compared to the state average[84]. A study done in 2019 reported an asthma prevalence of 22.4% in the northern Imperial Valley region, compared to the national average of 7.7%, documented in 2021[87]. These statistics demonstrate the overwhelming

prevalence of respiratory disease affecting this underrepresented community group. The elevated incidence of respiratory ailments in the region is hypothesized to be correlated with the heightened dust emissions in the Salton Sea region[85].

Due to the rapid desiccation of the Salton Sea, there is progressive exposure of the lakebed, generating increased particulate matter via dust emissions. Due to the arid conditions of the Salton Sea as well as the frequent high winds, this area experiences frequent dust storms, many times requiring residents to remain inside. As mentioned above, increased dust generation has been linked to increasing pulmonary health issues affecting residents. The Salton Sea as it stands is heavily polluted, containing numerous potentially harmful chemicals and high nutrient loads from fertilizer runoff. This is believed to contribute to the transportation of these toxic substances through transmission via dust particles, allowing these particles to become airborne and inhaled, leading to respiratory complications[88].

The modern-day Salton Sea serves as a reminder of the dynamic nature of environmental challenges associated with human intervention and health issues. However, these issues are not isolated to just this region. The presence of anthropogenic alterations to the environment in other areas of the world also show significant ramifications on human health. For example, the desiccation and

drought-related health impacts of the Aral Sea Basin in central Asia has been well documented and offer opportunities for comparison to the health issues around the Salton Sea[81]. In the mid-1900s, the Aral Sea underwent rapid desiccation, leading to increased respiratory disease in countries surrounding the sea. These residents also experienced higher rates of cancer, hepatic and renal diseases, as well as pregnancy complications as a result of toxic chemicals present in drinking water from agricultural runoff in the region. This warns of further consequences to areas like the Salton Sea that are facing similar issues. In addition to the Aral Sea, the consequences of anthropogenic intervention and climate change has also been demonstrated in other areas such as Mono Lake, The Great Salt Lake, The Red Sea, and Owens Lake. Increased evaporation and decreased water input has negatively impacted each of these bodies of waters, leading not only to decreased water volume but also increases in salinity[89]. These changes are detrimental to the ecosystems of these water bodies, impacting their biodiversity and overall health[89]. Additionally, these environmental alterations pose significant risks to the well-being of communities residing in proximity to these areas. Our lab explores this connection between lake desiccation, dust exposure, and the associated health outcomes with a focus on the Salton Sea, serving as a model for global lake desiccation and its potential impacts.

To advert global crisis, it is crucial to recognize the link between particulate matter (PM), aerosol exposure, and health impacts. Particulate matter is typically categorized based on diameter with PM10 referring to particles with a diameter of 10 microns or less, and PM2.5 indicating particles with a diameter of 2.5 microns or less[90]. These size particles are of particular concern due to their ability to penetrate deep into the respiratory system. While PM10 is generally trapped in the nose and throat, PM2.5 can penetrate the deepest regions of the lungs[91]. Exposure to PM, especially PM2.5, has been linked to a wide range of health complications including respiratory infections, exacerbation of pre-existing conditions like asthma and COPD, and even cardiovascular diseases. These finer particles can directly cause inflammation and tissue damage.

Particular Matter Exposure and Health Consequences

PM and dust are commonly emitted from a range of sources, including vehicle exhaust, industrial activities, agricultural operations[92,93]. In regions like the Salton Sea area, natural phenomena such as increased lakebed exposure and dust storms also contribute to the release of PM and dust into the atmosphere. These particles are able to penetrate the lungs and lead to various respiratory health issues. Vulnerable populations such as children and individuals with pre-existing respiratory conditions are especially susceptible to the adverse effects of PM and dust emissions.

Dust particles are often composed of a mixture of material as dust can frequently act as a vehicle to allow aerosolization of materials such as soil, pollen, allergens, organic matter, various pollutants, and even biological material[94]. Although exposure to dust is known to be linked to irritation within the airways and upper respiratory tract, the disease phenomenon noted within the Salton Sea region cannot be summarized simply by exposure to dust and irritation of the respiratory system[95],[96]. In fact, our studies focus on the ability of dust to act as a method of transport for other organic material and toxins which may lead to the health issues observed within the region.

The potential for negative health impacts due to PM and aerosol exposure highlights the need for additional air quality regulations as well as technological advancements to reduce emissions. For a decade, atmospheric particulate matter in the Salton Sea region has exceeded California and National Ambient air quality standards[97]. This is attributed not only to the Salton Sea itself but also to factors including industrial farming, factory emissions from Mexicali, as well as heavy commercial traffic along the Mexico-California border[98]. While the connection between water and air quality and their impact on health is well-established, there has been limited research specifically exploring direct links, particularly in the Salton Sea region.

Environmental Aerosol Exposure Chambers

To investigate aerosol exposure and linked pathology, our lab developed environmental aerosol exposure chambers (EAEC) as described in Peng et al[99]. Our lab utilizes these chambers to facilitate translational research on health effects of PM exposure. Their design enables natural inhalation of aerosolized PM, allowing us to simulate real-world conditions and better understand the health impacts of PM exposure. During exposure, the EAEC controls particle size distribution as well as PM mass concentration to allow for tightly regulated aerosol exposures[99]. In our laboratory, we have developed two whole-body chambers for animal studies. One chamber functions as a clean air/control system, receiving laboratory compressed air that undergoes filtration using a Speedaire Compress Air Filter prior to being dispensed into the chamber through an atomizer dispenser. The exposure chamber is equipped with an atomizer that generates aerosol sprays from an ultrapure water solution of the desired material.

Throughout the exposure, aerosol size distribution and concentration are recorded using the Scanning Mobility Particle Sizer and Condensation Particle Counter systems. The chambers are also equipped with a DustTrak aerosol monitor which utilizes a light-scattering laser photometer to generate real-time aerosol mass readings. Utilizing this system, our lab is able to address aerosol exposure and related health impacts in a clinically translatable manner.

Conclusion

The anatomy and physiology of the lung are foundational to its critical role in the respiratory system. The lung's intricate structure, characterized by extensive branching from the trachea to the alveoli, maximizes surface area and airflow efficiency, facilitating optimal gas exchange. Each alveolus, surrounded by a network of capillaries, serves as the site for oxygen and carbon dioxide exchange, vital for maintaining homeostasis. The mechanisms of mucociliary clearance and surfactant production are essential in protecting the respiratory system from pathogens and preventing alveolar collapse, highlighting the lung's multifaceted protective functions.

Understanding lung mechanics is crucial in appreciating respiratory health. The roles of elastin and collagen fibers in the lung's extracellular matrix are paramount in maintaining lung elasticity and structural integrity. Elastin allows the lungs to expand and recoil during breathing, while collagen provides tensile strength, preventing over-distension. Disruptions in these fibrous networks, such as those seen in diseases like pulmonary fibrosis and emphysema, lead to significant respiratory dysfunction. Airway remodeling, characterized by changes in the structural components of the airway wall, is a critical aspect of chronic respiratory diseases. It includes goblet cell proliferation, increased smooth muscle mass, and extracellular matrix deposition, contributing to airflow limitation and persistent symptoms. This emphasizes the importance of ongoing research

to elucidate the molecular pathways involved in maintaining and repairing lung tissue.

The immune system within the lungs, comprising both innate and adaptive responses, is vital for defending against environmental insults and maintaining respiratory health. Alveolar macrophages, dendritic cells, and lymphocytes play key roles in recognizing and responding to pathogens, allergens, and pollutants. Chronic inflammation and immune dysregulation are central to the pathophysiology of respiratory diseases such as asthma and chronic obstructive pulmonary disease (COPD). Understanding the interactions between immune cells and the lung microenvironment can inform the development of targeted therapies to modulate immune responses and improve disease management. Chronic respiratory diseases like asthma have a significant global health impact, contributing to substantial morbidity and mortality. Asthma, characterized by reversible airway obstruction and hyperresponsiveness, involves complex interactions between genetic and environmental factors. Advances in understanding the molecular and cellular mechanisms underlying this disease is crucial for developing novel therapeutic strategies. The detriment of fibrosis, characterized by excessive deposition of fibrous connective tissue, cannot be overstated, as it leads to irreversible scarring and loss of lung function. Detailed studies on airway remodeling and fibrosis are imperative to uncover potential therapeutic targets, prevent disease progression, and improve patient outcomes.

Overall, this thesis provides a comprehensive foundation for further exploration into the intricate interplay between lung anatomy, physiology, and immunology. By advancing our knowledge of these fundamental aspects, we can better understand and treat respiratory diseases, ultimately improving respiratory health and patient care.

References

1. Chaudhry, Raheel, and Bruno Bordoni. “Anatomy, Thorax, Lungs.” *National Library of Medicine*, StatPearls Publishing, 13 Jan. 2019, www.ncbi.nlm.nih.gov/books/NBK470197/

2. Sobiesk, John L., and Sunil Munakomi. “Anatomy, Head and Neck, Nasal Cavity.” *PubMed*, StatPearls Publishing, 2023, www.ncbi.nlm.nih.gov/books/NBK544232/

3. Bustamante-Marin, Ximena M., and Lawrence E. Ostrowski. “Cilia and Mucociliary Clearance.” *Cold Spring Harbor Perspectives in Biology*, vol. 9, no. 4, 18 Nov. 2017, www.ncbi.nlm.nih.gov/pmc/articles/PMC5378048/

4. Ball, Matthew, et al. “Anatomy, Airway.” *PubMed*, StatPearls Publishing, 2023, www.pubmed.ncbi.nlm.nih.gov/29083624/#:~:text=The%20bronchi%2C%20the%20main%20bifurcation.

5. Seadler, Benjamin D, and Sandeep Sharma. “Physiology, Alveolar Tension.” *Nih.gov*, StatPearls Publishing, 20 Sept. 2019, www.ncbi.nlm.nih.gov/books/NBK539825/.

6. Mahabadi, Navid, et al. “Anatomy, Thorax, Lung Pleura and Mediastinum.” *PubMed*, StatPearls Publishing, 17 Oct. 2022, www.ncbi.nlm.nih.gov/books/NBK519048/

7. National Cancer Institute. “Mechanics of Ventilation | SEER Training.” *Cancer.gov*, 2019, www.training.seer.cancer.gov/anatomy/respiratory/mechanics.html

8. Shahid, Zainab, and Bracken Burns. “Anatomy, Abdomen and Pelvis: Diaphragm.” *PubMed*, StatPearls Publishing, 2023, www.ncbi.nlm.nih.gov/books/NBK470191

9. Mecham, Robert P. “Elastin in Lung Development and Disease Pathogenesis.” *Matrix Biology*, vol. 73, Nov. 2018, pp. 6–20, www.ncbi.nlm.nih.gov/pmc/articles/PMC6041195/

10. Liu, Lumei, et al. “Role of Collagen in Airway Mechanics.” *Bioengineering*, vol. 8, no. 1, 16 Jan. 2021, p. 13, https://doi.org/10.3390/bioengineering8010013

11. Canu, Giovanni, and Christiana Ruhrberg. “First Blood: The Endothelial Origins of Hematopoietic Progenitors.” *Angiogenesis*, vol. 24, no. 2, 30 Mar. 2021, pp. 199–211, https://doi.org/10.1007/s10456-021-09783-9

12. Sreejit, Gopalkrishna, et al. “Origins and Diversity of Macrophages in Health and Disease.” *Clinical & Translational Immunology*, vol. 9, no. 12, Jan. 2020, https://doi.org/10.1002/cti2.1222

13. Aristizábal, Beatriz, and Ángel González. *Innate Immune System*. *Www.ncbi.nlm.nih.gov*, El Rosario University Press, 18 July 2013,

www.ncbi.nlm.nih.gov/books/NBK459455/#:~:text=Effector%20cells%20of%20innate%20immunity&text=Phagocytic%20cells%20consist%20of%20granulocytes

14. Mogensen, T. H. “Pathogen Recognition and Inflammatory Signaling in Innate Immune Defenses.” *Clinical Microbiology Reviews*, vol. 22, no. 2, 2009, pp. 240–273, https://doi.org/10.1128/cmr.00046-08

15. Takeuchi, Osamu, and Shizuo Akira. “Pattern Recognition Receptors and Inflammation.” *Cell*, vol. 140, no. 6, Mar. 2010, pp. 805–820, www.sciencedirect.com/science/article/pii/S0092867410000231

16. Wang, Yan, et al. “IE-DAP Induced Inflammatory Response and Tight Junction Disruption in Bovine Mammary Epithelial Cells via NOD1-Dependent NF-KB and MLCK Signaling Pathway.” *International Journal of Molecular Sciences*, vol. 24, no. 7, 27 Mar. 2023, p. 6263, www.ncbi.nlm.nih.gov/pmc/articles/PMC10094069/

17. Ogawa, Chikako, et al. “Muramyl Dipeptide and Its Derivatives: Peptide Adjuvant in Immunological Disorders and Cancer Therapy.” *Current Bioactive Compounds*, vol. 7, no. 3, 1 Sept. 2011, pp. 180–197, www.ncbi.nlm.nih.gov/pmc/articles/PMC3241611/

18. Kawai, T, and S Akira. “TLR Signaling.” *Cell Death and Differentiation*, vol. 13, no. 5, 20 Jan. 2006, pp. 816–825, https://doi.org/10.1038/sj.cdd.4401850

19. Duan, Tianhao, et al. “Toll-like Receptor Signaling and Its Role in Cell-Mediated Immunity.” *Frontiers in Immunology*, vol. 13, 3 Mar. 2022, https://doi.org/10.3389/fimmu.2022.812774

20. Swiecki, Melissa, and Marco Colonna. “Type I Interferons: Diversity of Sources, Production Pathways and Effects on Immune Responses.” *Current Opinion in Virology*, vol. 1, no. 6, Dec. 2011, pp. 463–475, https://doi.org/10.1016/j.coviro.2011.10.026

21. Kolaczkowska, Elzbieta, and Paul Kubes. “Neutrophil Recruitment and Function in Health and Inflammation.” *Nature Reviews. Immunology*, vol. 13, no. 3, 2013, pp. 159–75, https://doi.org/10.1038/nri3399

22. Beutler, B. “Innate Immunity: An Overview.” *Molecular Immunology*, vol. 40, no. 12, Feb. 2004, pp. 845–859, https://doi.org/10.1016/j.molimm.2003.10.005

23. Bjerre, Anna, et al. “Complement Activation Induced by Purified*Neisseria Meningitidis*Lipopolysaccharide (LPS), Outer Membrane Vesicles, Whole Bacteria, and an LPS-Free Mutant.” *˜ the œJournal of Infectious Diseases (Online. University of Chicago Press)/˜ the œJournal of Infectious*

Diseases, vol. 185, no. 2, 15 Jan. 2002, pp. 220–228, www.academic.oup.com/jid/article/185/2/220/2191299

24. Charles A Janeway, Jr, et al. “The Complement System and Innate Immunity.” *Immunobiology: The Immune System in Health and Disease. 5th Edition*, vol. 5, 2001, www.ncbi.nlm.nih.gov/books/NBK27100/#:~:text=Complement%20is%20a%20system%20of%20plasma%20proteins%20that%20can%20be

25. Ness, Sara, et al. “Regulatory Dendritic Cells, T Cell Tolerance, and Dendritic Cell Therapy for Immunologic Disease.” *Frontiers in Immunology*, vol. 12, 10 Mar. 2021, https://doi.org/10.3389/fimmu.2021.633436

26. Charles A Janeway, Jr, et al. “Generation of Lymphocytes in Bone Marrow and Thymus.” *Immunobiology: The Immune System in Health and Disease. 5th Edition*, 2001.

27. Gameiro, Jacy, et al. “The Thymus Microenvironment in Regulating Thymocyte Differentiation.” *Cell Adhesion & Migration*, vol. 4, no. 3, July 2010, pp. 382–390, https://doi.org/10.4161/cam.4.3.11789

28. Shah, Divya K. “T-Cell Development in Thymus | British Society for Immunology.” *Www.immunology.org*, www.immunology.org/public-

information/bitesized-immunology/immune-development/t-cell-development-thymus

29. Tesmer, Laura A., et al. “Th17 Cells in Human Disease.” *Immunological Reviews*, vol. 223, no. 1, June 2008, pp. 87–113, https://doi.org/10.1111/j.1600-065x.2008.00628.x

30. Krammer, Peter H., et al. “Life and Death in Peripheral T Cells.” *Nature Reviews Immunology*, vol. 7, no. 7, July 2007, pp. 532–542, https://doi.org/10.1038/nri2115

31. LeBien, T. W., and T. F. Tedder. “B Lymphocytes: How They Develop and Function.” *Blood*, vol. 112, no. 5, 25 Aug. 2008, pp. 1570–1580, www.ncbi.nlm.nih.gov/pmc/articles/PMC2518873/, https://doi.org/10.1182/blood-2008-02-078071

32. Charles A Janeway, Jr, et al. “B-Cell Activation by Armed Helper T Cells.” *Immunobiology: The Immune System in Health and Disease. 5th Edition*, 2001, www.ncbi.nlm.nih.gov/books/NBK27142/#:~:text=Helper%20T%20cells%20stimulate%20the

33. Yin, Zhaojun, and Xuefei Huang. “Recent Development in Carbohydrate Based Anticancer Vaccines.” *Journal of Carbohydrate Chemistry*, vol. 31,

no. 3, Mar. 2012, pp. 143–186, https://doi.org/10.1080/07328303.2012.659364

34. Roth, David B. “V(D)J Recombination: Mechanism, Errors, and Fidelity.” *Microbiology Spectrum*, vol. 2, no. 6, 1 Dec. 2014, www.ncbi.nlm.nih.gov/pmc/articles/PMC5089068/

35. Chuquimia, Olga D., et al. “Alveolar Epithelial Cells Are Critical in Protection of the Respiratory Tract by Secretion of Factors Able to Modulate the Activity of Pulmonary Macrophages and Directly Control Bacterial Growth.” *Infection and Immunity*, vol. 81, no. 1, 12 Nov. 2012, pp. 381–389, https://doi.org/10.1128/iai.00950-12

36. Standiford, Theodore J, et al. “Alveolar Macrophage-Derived Cytokines Induce Monocyte Chemoattractant Protein-1 Expression from Human Pulmonary Type II-like Epithelial Cells.” *Journal of Biological Chemistry*, vol. 266, no. 15, 25 May 1991, pp. 9912–9918, https://doi.org/10.1016/s0021-9258(18)92905-4

37. Grubor, B., et al. “Collectins and Cationic Antimicrobial Peptides of the Respiratory Epithelia.” *Veterinary Pathology*, vol. 43, no. 5, 1 Sept. 2006, pp. 595–612, www.ncbi.nlm.nih.gov/pmc/articles/PMC2786072/, https://doi.org/10.1354/vp.43-5-595

38. Rogan, Mark P, et al. “Antimicrobial Proteins and Polypeptides in Pulmonary Innate Defence.” *Respiratory Research*, vol. 7, no. 1, 17 Feb. 2006, https://doi.org/10.1186/1465-9921-7-29

39. Savina, Ariel, and Sebastian Amigorena. “Phagocytosis and Antigen Presentation in Dendritic Cells.” *Immunological Reviews*, vol. 219, no. 1, 1 Oct. 2007, pp. 143–156, www.ncbi.nlm.nih.gov/pubmed/17850487

40. Kopf, Manfred, et al. “The Development and Function of Lung-Resident Macrophages and Dendritic Cells.” *Nature Immunology*, vol. 16, no. 1, 1 Jan. 2015, pp. 36–44, www.nature.com/articles/ni.3052, https://doi.org/10.1038/ni.3052

41. Liegeois, Maude, et al. “The Interstitial Macrophage: A Long-Neglected Piece in the Puzzle of Lung Immunity.” *Cellular Immunology*, vol. 330, Aug. 2018, pp. 91–96, https://doi.org/10.1016/j.cellimm.2018.02.001

42. Naghavi, Mohsen, et al. “Global Burden of Chronic Respiratory Diseases and Risk Factors, 1990–2019: An Update from the Global Burden of Disease Study 2019 | the Institute for Health Metrics and Evaluation.” *Www.healthdata.org*, 25 Apr. 2023, www.healthdata.org/research-analysis/library/global-burden-chronic-respiratory-diseases-and-risk-factors-1990-2019#:~:text=Findings

43. Shukla, Shakti D., et al. “Chronic Respiratory Diseases: An Introduction and Need for Novel Drug Delivery Approaches.” *Targeting Chronic Inflammatory Lung Diseases Using Advanced Drug Delivery Systems*, 2020, pp. 1–31, https://doi.org/10.1016/b978-0-12-820658-4.00001-7

44. Bakakos, Agamemnon, et al. “Severe Eosinophilic Asthma.” *Journal of Clinical Medicine*, vol. 8, no. 9, 2 Sept. 2019, p. 1375, https://doi.org/10.3390/jcm8091375

45. Esteban-Gorgojo, Ignacio, et al. “Non-Eosinophilic Asthma: Current Perspectives.” *Journal of Asthma and Allergy*, vol. Volume 11, Oct. 2018, pp. 267–281, www.ncbi.nlm.nih.gov/pmc/articles/PMC6211579/, https://doi.org/10.2147/jaa.s153097

46. Oddera, S., et al. “Airway Eosinophilic Inflammation, Epithelial Damage, and Bronchial Hyperresponsiveness in Patients with Mild-Moderate, Stable Asthma.” *Allergy*, vol. 51, no. 2, 1 Feb. 1996, pp. 100–107, pubmed.ncbi.nlm.nih.gov/8738515/, https://doi.org/10.1111/j.1398-9995.1996.tb04565.x

47. Lechner, Antonie, et al. “Macrophages Acquire a TNF-Dependent Inflammatory Memory in Allergic Asthma.” *The Journal of Allergy and Clinical Immunology*, vol. 149, no. 6, 1 June 2022, pp. 2078–2090, pubmed.ncbi.nlm.nih.gov/34974067/, https://doi.org/10.1016/j.jaci.2021.11.026

48. van der Veen, T. Anienke, et al. “The Different Faces of the Macrophage in Asthma.” *Current Opinion in Pulmonary Medicine*, vol. 26, no. 1, Jan. 2020, pp. 62–68, http://dx.doi.org/10.1097%2FMCP.0000000000000647

49. Saha, S, et al. “Granulocyte–Macrophage Colony-Stimulating Factor Expression in Induced Sputum and Bronchial Mucosa in Asthma and COPD.” *Thorax*, vol. 64, no. 8, 1 Aug. 2009, pp. 671–676, www.ncbi.nlm.nih.gov/pmc/articles/PMC2712140/

50. Doeing, Diana C., and Julian Solway. “Airway Smooth Muscle in the Pathophysiology and Treatment of Asthma.” *Journal of Applied Physiology*, vol. 114, no. 7, 1 Apr. 2013, pp. 834–843, www.ncbi.nlm.nih.gov/pmc/articles/PMC3633438/

51. National Heart, Lung, and Blood Institute. “Asthma - Causes and Triggers | NHLBI, NIH.” *Www.nhlbi.nih.gov*, 24 Mar. 2022, www.nhlbi.nih.gov/health/asthma/causes

52. National Institute of Environmental Health Sciences. “Allergens.” *National Institute of Environmental Health Sciences*, www.niehs.nih.gov/health/topics/agents/allergens

53. Baos, Selene, et al. “Nonallergic Asthma and Its Severity: Biomarkers for Its Discrimination in Peripheral Samples.” *Frontiers in Immunology*, vol. 9, 21 June 2018, www.ncbi.nlm.nih.gov/pmc/articles/PMC6021512/

54. Luo, Weihang, et al. “Distinct Spatial and Temporal Roles for Th1, Th2, and Th17 Cells in Asthma.” *Frontiers in Immunology*, vol. 13, 12 Aug. 2022, https://doi.org/10.3389/fimmu.2022.974066

55. Terhune, Julia, et al. “Dendritic Cell-Induced Th1 and Th17 Cell Differentiation for Cancer Therapy.” *Vaccines*, vol. 1, no. 4, 21 Nov. 2013, pp. 527–549, https://doi.org/10.3390/vaccines1040527

56. Trentini, Monalisa M., et al. “The Role of Neutrophils in the Induction of Specific Th1 and Th17 during Vaccination against Tuberculosis.” *Frontiers in Microbiology*, vol. 7, 10 June 2016, https://doi.org/10.3389/fmicb.2016.00898

57. Tsai, Hsing-Chuan, et al. “IL-17A and Th17 Cells in Lung Inflammation: An Update on the Role of Th17 Cell Differentiation and IL-17R Signaling in Host Defense against Infection.” *Clinical and Developmental Immunology*, vol. 2013, 2013, pp. 1–12, https://doi.org/10.1155/2013/267971

58. Fouser, Lynette A., et al. “Th17 Cytokines and Their Emerging Roles in Inflammation and Autoimmunity.” *Immunological Reviews*, vol. 226, no. 1, Dec. 2008, pp. 87–102, https://doi.org/10.1111/j.1600-065x.2008.00712.x

59. Papaioannou, Andriana I., et al. “Paucigranulocytic Asthma: Potential Pathogenetic Mechanisms, Clinical Features and Therapeutic

Management." *Journal of Personalized Medicine*, vol. 12, no. 5, 23 May 2022, p. 850, https://doi.org/10.3390/jpm12050850

60. ---. "COPD - What Is COPD?" *Www.nhlbi.nih.gov*, 25 Oct. 2023, www.nhlbi.nih.gov/health/copd

61. Association, American Lung. "COPD and Particulate Matter." *Www.lung.org*, 3 Nov. 2023, www.lung.org/blog/copd-particulate-matter#:~:text=Specifically%2C%20air%20pollution%20in%20the

62. King, Paul T. "Inflammation in Chronic Obstructive Pulmonary Disease and Its Role in Cardiovascular Disease and Lung Cancer." *Clinical and Translational Medicine*, vol. 4, no. 1, 29 July 2015, www.ncbi.nlm.nih.gov/pmc/articles/PMC4518022/

63. Sharafkhaneh, A., et al. "Pathogenesis of Emphysema: From the Bench to the Bedside." *Proceedings of the American Thoracic Society*, vol. 5, no. 4, 1 May 2008, pp. 475–477, www.ncbi.nlm.nih.gov/pmc/articles/PMC2645322/

64. Kim, Victor, and Gerard J. Criner. "Chronic Bronchitis and Chronic Obstructive Pulmonary Disease." *American Journal of Respiratory and Critical Care Medicine*, vol. 187, no. 3, Feb. 2013, pp. 228–237, www.ncbi.nlm.nih.gov/pmc/articles/PMC4951627/

65. de Oliveira, Júlio César Mendes, et al. “Clinical Significance in COPD Patients Followed in a Real Practice.” *Multidisciplinary Respiratory Medicine*, vol. 8, no. 1, 28 June 2013, https://doi.org/10.1186/2049-6958-8-43

66. Buist, A.S. “Similarities and Differences between Asthma and Chronic Obstructive Pulmonary Disease: Treatment and Early Outcomes.” *European Respiratory Journal*, vol. 21, no. Supplement 39, 1 Jan. 2003, pp. 30S35S, https://doi.org/10.1183/09031936.03.00404903

67. Wang, Yujie, et al. “Role of Inflammatory Cells in Airway Remodeling in COPD.” *International Journal of Chronic Obstructive Pulmonary Disease*, vol. 13, Oct. 2018, pp. 3341–3348, www.ncbi.nlm.nih.gov/pmc/articles/PMC6190811/

68. Yabluchanskiy, Andriy, et al. “Matrix Metalloproteinase-9: Many Shades of Function in Cardiovascular Disease.” *Physiology*, vol. 28, no. 6, Nov. 2013, pp. 391–403, www.ncbi.nlm.nih.gov/pmc/articles/PMC3858212/

69. Saetta, M., and G. Turato. “Airway Pathology in Asthma.” *European Respiratory Journal*, vol. 18, no. 1, 2 July 2001, pp. 18–23, https://doi.org/10.1183/09031936.01.00229501

70. Busse, William, et al. “Airway Remodeling and Repair.” *American Journal of Respiratory and Critical Care Medicine*, vol. 160, no. 3, Sept. 1999, pp. 1035–1042, https://doi.org/10.1164/ajrccm.160.3.9902064

71. Kistemaker, Loes E.M., et al. “Regulation of Airway Inflammation and Remodeling by Muscarinic Receptors: Perspectives on Anticholinergic Therapy in Asthma and COPD.” *Life Sciences*, vol. 91, no. 21-22, Nov. 2012, pp. 1126–1133, https://doi.org/10.1016/j.lfs.2012.02.021

72. Davies, D. E. “The Role of the Epithelium in Airway Remodeling in Asthma.” *Proceedings of the American Thoracic Society*, vol. 6, no. 8, 15 Dec. 2009, pp. 678–682, https://doi.org/10.1513/pats.200907-067dp

73. Ball, Stephen L., et al. “The Role of the Fibroblast in Inflammatory Upper Airway Conditions.” *The American Journal of Pathology*, vol. 186, no. 2, 1 Feb. 2016, pp. 225–233, www.ncbi.nlm.nih.gov/pmc/articles/PMC4729240/

74. Ji, Tong, and Hequan Li. “T-Helper Cells and Their Cytokines in Pathogenesis and Treatment of Asthma.” *Frontiers in Immunology*, vol. 14, 12 June 2023, https://doi.org/10.3389/fimmu.2023.1149203

75. James, A. L., and S. Wenzel. “Clinical Relevance of Airway Remodelling in Airway Diseases.” *European Respiratory Journal*, vol. 30, no. 1, 1 July 2007, pp. 134–155, https://doi.org/10.1183/09031936.00146905

76. TIDDENS, HARM, et al. “The Role of Inflammation in Airway Disease.” *American Journal of Respiratory and Critical Care Medicine*, vol. 162, no. supplement_1, Aug. 2000, pp. S7–S10, https://doi.org/10.1164/ajrccm.162.supplement_1.maic-2

77. Hogg, James C, et al. “The Nature of Small-Airway Obstruction in Chronic Obstructive Pulmonary Disease.” *The New England Journal of Medicine*, vol. 350, no. 26, 2004, pp. 2645–53, www.ncbi.nlm.nih.gov/pubmed/15215480

78. Pini, Laura, et al. “Central Airways Remodeling in COPD Patients.” *International Journal of Chronic Obstructive Pulmonary Disease*, Sept. 2014, p. 927, https://doi.org/10.2147/copd.s52478

79. Edge Institute UC Riverside. “Lake Cahuilla Research Coalition | the EDGE Institute.” *Edge.ucr.edu*, www.edge.ucr.edu/research/lake-cahuilla-research-coalition

80. Doede, Aubrey L., and Pamela B. DeGuzman. “The Disappearing Lake: A Historical Analysis of Drought and the Salton Sea in the Context of the GeoHealth Framework.” *GeoHealth*, vol. 4, no. 9, Sept. 2020, https://doi.org/10.1029/2020gh000271

81. California Department of Fish and Wildlife. “Background Information on the Salton Sea.” *Wildlife.ca.gov*, www.wildlife.ca.gov/Regions/6/Salton-Sea-Program/Background

82. “What’s Wrong with the Salton Sea?” *Audubon California*, 28 Apr. 2020, www.ca.audubon.org/news/whats-wrong-salton-sea

83. Juturu, Preeti. “Assessing Emergency Healthcare Accessibility in the Salton Sea Region of Imperial County, California.” *PLOS ONE*, vol. 16, no. 6, 30 June 2021, p. e0253301, https://doi.org/10.1371/journal.pone.0253301

84. Marshall, John. “Why Emergency Physicians Should Care about the Salton Sea.” *Western Journal of Emergency Medicine*, vol. 18, no. 6, 18 Oct. 2017, pp. 1008–1009, https://doi.org/10.5811/westjem.2017.8.36034

85. United States Census Bureau. “U.S. Census Bureau QuickFacts: Imperial County, California.” *Www.census.gov*, www.census.gov/quickfacts/imperialcountycalifornia

86. Farzan, Shohreh F., et al. “Assessment of Respiratory Health Symptoms and Asthma in Children near a Drying Saline Lake.” *International Journal of Environmental Research and Public Health*, vol. 16, no. 20, 11 Oct. 2019, p. 3828, www.ncbi.nlm.nih.gov/pmc/articles/PMC6843482/

87. Ather, Binish, et al. “Airborne Precautions.” *PubMed*, StatPearls Publishing, 2023, www.pubmed.ncbi.nlm.nih.gov/30285363/#:~:text=The%20microorganisms%20transmitted%20by%20an

88. Oren, Aharon, et al. “The Aral Sea and the Dead Sea: Disparate Lakes with Similar Histories.” *Lakes & Reservoirs: Research & Management*, vol. 15, no. 3, 16 Sept. 2010, pp. 223–236, https://doi.org/10.1111/j.1440-1770.2010.00436.x

89. California Air Resources Board. “Inhalable Particulate Matter and Health (PM2.5 and PM10) | California Air Resources Board.” *Ca.gov*, 2015, ww2.arb.ca.gov/resources/inhalable-particulate-matter-and-health

90. Xing, Yu-Fei, et al. “The Impact of PM2.5 on the Human Respiratory System.” *Journal of Thoracic Disease*, vol. 8, no. 1, Jan. 2016, pp. E69-74, https://doi.org/10.3978/j.issn.2072-1439.2016.01.19

91. Dheeraj Alshetty, V., and S.M. Shiva Nagendra. “Impact of Vehicular Movement on Road Dust Resuspension and Spatiotemporal Distribution of Particulate Matter during Construction Activities.” *Atmospheric Pollution Research*, Nov. 2021, p. 101256, https://doi.org/10.1016/j.apr.2021.101256

92. Farhang Akbar-Khanzadeh, et al. “Particulate Matter (PM) Exposure Assessment—Horizontal and Vertical PM Profiles in Relation to Agricultural Activities and Environmental Factors in Farm Fields.” *Journal of Occupational and Environmental Hygiene*, vol. 9, no. 8, 1 Aug. 2012, pp. 502–516, https://doi.org/10.1080/15459624.2012.695216

93. None Ormstad, et al. “Airborne House Dust Particles and Diesel Exhaust Particles as Allergen Carriers.” *Clinical & Experimental Allergy/Clinical and Experimental Allergy*, vol. 28, no. 6, 1 June 1998, pp. 702–708, https://doi.org/10.1046/j.1365-2222.1998.00302.x

94. Rylander, Ragnar. “Organic Dusts and Lung Reactions — Exposure Characteristics and Mechanisms for Disease.” *Scandinavian Journal of Work, Environment & Health*, vol. 11, no. 3, 1985, pp. 199–206, www.jstor.org/stable/40965212?seq=2

95. Biddle, Trevor A., et al. “Salton Sea Aerosol Exposure in Mice Induces a Pulmonary Response Distinct from Allergic Inflammation.” *Science of the Total Environment*, vol. 792, Oct. 2021, p. 148450, https://doi.org/10.1016/j.scitotenv.2021.148450

96. Zaremba, Melissa. “SPECIAL REPORT: Imperial Valley Gets a Failing Grade for Unhealthy Air Quality.” *KYMA*, 22 Mar. 2023, www.kyma.com/news/special-reports/2023/03/22/special-report-imperial-valley-gets-a-failing-grade-for-unhealthy-air-quality/

97. Gewin, Virginia. “As the Salton Sea Shrinks, Agriculture’s Legacy Turns to Dust.” *Civil Eats*, 17 July 2023, www.civileats.com/2023/07/17/as-the-salton-sea-shrinks-agricultures-legacy-turns-to-dust/

98. Peng, Xinze, et al. “Establishment and Characterization of a Multi-Purpose Large Animal Exposure Chamber for Investigating Health Effects.” *Review of Scientific Instruments*, vol. 90, no. 3, 1 Mar. 2019, https://doi.org/10.1063/1.5042097

Glossary of Terms:

Asthma: A chronic respiratory disease characterized by reversible airway obstruction, airway inflammation, and increased airway hyperresponsiveness to various stimuli.

Immunology: The branch of biomedical science that studies the immune system, its functions, disorders, and the body's defense mechanisms against pathogens.

Innate Immunity: The body's first line of defense against pathogens, consisting of physical barriers, immune cells, and various molecules that provide immediate but non-specific responses.

Adaptive Immunity: The immune system's ability to recognize and remember specific pathogens, leading to a stronger and more targeted response upon subsequent exposures.

Particulate Matter: Tiny particles or droplets suspended in the air, including dust, dirt, soot, and smoke, which can be inhaled and cause health problems.

Aerosol: A suspension of fine solid particles or liquid droplets in the air, which can be natural or anthropogenic, and can impact air quality and health.

COPD (Chronic Obstructive Pulmonary Disease): A group of progressive lung diseases, including chronic bronchitis and emphysema, characterized by airflow limitation and chronic respiratory symptoms.

Chronic Bronchitis: A form of COPD marked by chronic inflammation of the bronchi, leading to persistent cough and mucus production.

Emphysema: A type of COPD characterized by damage to the alveoli, resulting in reduced surface area for gas exchange and difficulty breathing.

Airway Remodeling: Structural changes in the airway walls, including epithelial cell proliferation, increased smooth muscle mass, and extracellular matrix deposition, commonly seen in chronic respiratory diseases.

Fibrosis: The formation of excess fibrous connective tissue in an organ or tissue, often resulting in scarring and impaired function.

Antigen Presenting Cells (APCs): Immune cells, such as dendritic cells and macrophages, that process and present antigens to T cells, initiating an adaptive immune response.

Pattern Recognition Receptors (PRR): Receptors on immune cells that recognize pathogen-associated molecular patterns (PAMPs) and initiate innate immune responses.

Toll-like Receptors (TLRs): A type of PRR that recognizes distinct PAMPs and activates immune responses, playing a key role in the innate immune system.

C-type Lectin Receptors (CLRs): A family of PRRs that recognize carbohydrate structures on pathogens, leading to immune cell activation and pathogen clearance.

Retinoic Acid-Inducible Gene (RIG)-I-like Receptors (RLRs): Cytoplasmic PRRs that detect viral RNA and initiate antiviral immune responses.

NOD-like Receptors (NLRs): A family of intracellular PRRs that detect microbial components and stress signals, contributing to the regulation of inflammation and immune responses.

Airway Hyperreactivity: Increased sensitivity of the airways to various stimuli, leading to exaggerated bronchoconstriction and airflow obstruction, commonly seen in asthma.

Antigen: A molecule or molecular structure, often a protein, recognized by the immune system as foreign, triggering an immune response.

Antibody: A protein produced by B cells in response to an antigen, specifically binding to that antigen to neutralize or mark it for destruction by other immune cells.

Cytokines: Small proteins released by immune cells that act as signaling molecules, regulating immune responses, inflammation, and cell communication.

Chemokine: A subset of cytokines that specifically induce chemotaxis, guiding the migration of immune cells to sites of infection, inflammation, or injury.

Chapter 2: Route of Administration Significantly Affects Particle Deposition and Cellular Recruitment

Abstract

Lung exposures to dusts, pollutants, and other aerosol particulates are known to be associated with pulmonary diseases such as asthma and Chronic Obstructive Pulmonary Disease. These health impacts are attributed to the ability of aerosol components to induce pulmonary inflammation, which promotes tissue remodeling, including fibrosis, tissue degradation, and smooth muscle proliferation. Consequently, the distribution of these effects can have a significant impact on the physiologic function of the lung. In order to study the impact of distribution of inhaled particulates on lung pathogenesis, we compared the effect of different methods of particle delivery. By comparing intranasal versus aerosol delivery of fluorescent microspheres, we observed strikingly distinct patterns of particle deposition; intranasal delivery provided focused deposition concentrated on larger airways, while aerosol delivery showed uniform deposition throughout the lung parenchyma. Recognizing that the impacts of inflammatory cells are contingent upon their recruitment and behavior, we postulate that these variations in distribution patterns can result in significant alterations in biological responses. To elucidate the relevance of these findings in terms of biological representation, we subsequently conducted an investigation into the responses elicited by the administration of endotoxin (bacterial Lipopolysaccharide, or LPS) in a transgenic neutrophil reporter mouse model. As with the microsphere results,

patterns of recruited neutrophil inflammatory responses matched the delivery method; that is, despite the active migratory behavior of neutrophils, inflammatory histopathology patterns were either focused on large airways (intranasal administration) or diffusely throughout the parenchyma (aerosol). These results demonstrate the importance of modes of aerosol delivery as different patterns of inflammation and tissue remodeling will have distinct impacts on lung physiology.

Introduction

Despite its position as an internal organ, the lung provides a major interface with the environment, with a high volume of airflow across its large surface area. While it provides the critical surface for gas exchange, it also comprises a major mucosal barrier against aerosol particulates, toxins, and infectious organisms. The anatomy of the lung must provide an efficient path for airflow during respiration; yet also enable immune system mechanisms for maintaining clear airways and alveoli. Innate immune cells such as resident alveolar macrophages provide an important scavenging function, but the warm moist environment can promote invasion or colonization by infectious microbes that are not as easily eliminated[1]. Thus, lung tissue must enable the efficient recruitment of blood-borne inflammatory cells including neutrophils, monocytes, and lymphocytes, as well as mechanisms to ensure effective clearance of the products of inflammation [2,3]. Pulmonary diseases demonstrate the limits of these

mechanisms, and studies on the pathogenesis of various pulmonary inflammatory diseases are dependent on disease models that replicate the physiological mechanisms protecting the lung.

In addition to lung resident immune cells, this organ also provides a partial physical barrier via the branched structure of the airways[4,5,6]. These bifurcations represent a partial anatomical obstruction impeding the flow of particles and microbes from making it into the distal airways. Although the threat of adverse reactions to inhaled particulate matter varies depending on their size and content, airborne particles can elicit some degree of an inflammatory response. Airborne particulate matter (PM) refers to a complex mixture of aerosols, which are present in the ambient air. PM is characterized by particle diameter with particles with a diameter of 10 microns or larger categorized as “coarse”, particles $\leq$ 10 microns are referred to as PM_{10}, and those which are $\leq$ 2.5 microns are referred to as $PM_{2.5}$. Particles which fall into the $PM_{2.5}$ category are of most concern as these particles are able to reach deep into the distal lung parenchymal tissue and airways and induce adverse health effects[7]. Many studies have shown links to health effects in as little as 24 hours with exposure to $PM_{2.5}$ particulates[8]. A study done by Wang et. al revealed that exposure to $PM_{2.5}$ was associated with risks of cardiovascular disease, respiratory illness, as well as some forms of cancer[9]. These particles can be directly emitted from a source such as motor vehicle exhaust or from chemical reactions of gases within the

atmosphere. Frequent particulate matter exposure has also been linked to various health conditions such as asthma exacerbations, decreasing lung function, increased irritation of airways, coughing, and difficulty breathing. Due to the frequency of exposure to particulate matter, many studies have investigated these exposures and the related health impacts.

Most in vivo studies regarding PM and aerosol exposures have been done through the traditional intranasal administration method. However, this episodic method of exposure is not representative of chronic human exposure to particulates. In addition, it is difficult to ensure that all liquid is inhaled through the nasal passages and deposited directly into the lung; this may not only lead to inaccurate estimates of delivered dose but may also have off target effects as much of the solution may be swallowed and deposited in the digestive tract. Moreover, intranasally administered particle suspensions are likely to get fixed in the upper respiratory tract and may not penetrate the airways, leading to inaccurately skewed results. To address these limitations, we developed an environmental exposure chamber to study health impacts of suspended PM exposure[10]. To verify the efficacy of our chamber, we studied the impacts of differences in particle deposition in response to the method of administration. The results of this study elucidate the significance of method of administration on the pattern of particle deposition and cellular recruitment.

Materials and methods

Microspheres

Ready-made 1-micron FluoSpheres Carboxylate-Modified microspheres (FluoSpheres, Molecular Probes) were used to assess particle deposition as a result of exposure method. These polystyrene microspheres are loaded with red fluorescent dye, detectable with fluorescence microscopy at a wavelength of 580-605nm. As these microspheres are biologically inert, we used these to characterize the simple distribution of particle deposition in the lung of mice without any superimposed biological effects.

Aerosol Exposure Chamber

Aerosol exposures were conducted using dual animal chambers as developed and characterized in Peng et al. (2019) and used in Biddle et al. (2021, 2023) [10,11]. The conditions in the chambers were monitored for the duration of the exposures, including relative humidity, temperature, and atmospheric pressure. Aerosol-exposed mice were administered aerosols generated from an aqueous solution (of the chosen aerosol, microspheres or LPS, at a concentration determined to achieve the target aerosol concentration within the chamber), dried by two in-line silica gel columns (3.5-4.5 LPM) mixed with dry filtered air (0.5-1.0 LPM) to balance chamber volume exchange rates, as previously applied in Peng et al. Particulate matter in the chamber was monitored using a scanning mobility particle sizer (SMPS, including Series 3080

Electrostatic Classifier and Ultrafine Condensation Particle Counter 3776, TSI) and a laser aerosol spectrometer (LAP 323, Topas GmbH) to assist in maintaining stable and repeatable environmental PM exposure conditions.

As discussed in Peng et al. (2019), the animal exposure chambers provide the ability to expose mice to a targeted aerosol for a determined duration of time, while they can move and live unimpeded by the experimental procedures. The chambers are characterized to ensure a well-dispersed distribution of aerosol throughout the chamber so that a given volume of air inhaled by a mouse is equivalent in aerosol concentration to any other pocket of air inhaled by other mice, throughout the duration of an exposure period and across multiple exposure tests. Beyond controlling the aerosol concentration, deposition in the lungs of the mice is subject to additional factors including obstruction by whiskers, nasal passages, bronchial passage bifurcation, and airway anatomy, but are consistent across exposure methods. In this study 1-micron microspheres were used in order to minimize the variance of these effects for evaluating deposition, as physical properties including the size, shape, hygroscopicity, volatility, and the electrostatic charge of the particle are maintained, while particle coagulation can be measured by the PM instruments to confirm that particulate size does not significantly vary during the exposure. The size of the 1- μm particles also is in the size range to remain suspended in the air column, minimally affected by the anatomy of the airways and able to reach the alveoli largely unimpeded. This provides for consistency in the repeated exposures in

this study; although the exposure (environmental aerosol presence through the exposure duration) is held constant, accumulated deposition in the lungs of the mice (delivered dose) cannot be directly measurable in real-time.

Mouse Models and Exposure Conditions

All animal procedures were performed according to protocol AUP #20210011 approved by the UCR IACUC and consistent with institutional and NIH guidelines. 8-week-old C57BL/6J (B6) mice were obtained from The Jackson Laboratory. Mice were exposed to the microspheres by either method of administration at a concentration of 1.71E+09/mL for the duration of 1-hour. For environmental chamber aerosol exposures, a suspension of microspheres was continuously injected through an atomizer nozzle, and then passed through two drying columns on their way into the environmental chamber. Continuous monitoring of the aerosol suspension in the chamber (Fig 2.1A) confirmed that the microspheres were in a single-particle suspension with a measured monodisperse particle size distribution of 1-micron (Fig 2.1B).

Figure 2.1: Quantification of fluorescent microsphere aerosols.
(A) Total number concentration of particles within 0.5–1.3μm. **(B)** Average size distribution of particles injected into chamber.

Mice exposed via the aerosol chamber were continuously exposed for 1-hour and permitted to rest for 1-hour before processing. Intranasally exposed mice were given one dose of 40 μl of the solution containing the microspheres

and were allowed to rest for 1-hour prior to processing. To alleviate suffering, animals were placed in an isoflurane chamber before cervical dislocation and processing. Mice were also intranasally exposed to one dose of 20 µl, alternating nostrils and administering 5 µl at a time. Another group of intranasally exposed mice were given one large dose of 20 µl at a single time. All mice were permitted to rest for 1-hour before sacrifice. Upon sacrifice, left lobes were collected and analyzed via fluorescence microscopy.

PGRP-S-dsRed transgenic reporter mice rely on the peptidoglycan recognition protein-S (PGRP-S) promoter sequences driving expression of the dsRed express2 coding sequence[12]. In this mouse model, cells such as neutrophils, eosinophils, and epithelial M cells will fluoresce red upon detection due to their regulated expression of PGRP-S. These mice were exposed to LPS via either exposure method and differences in distribution of dsRed expressing cellular recruits were assessed via Python software. Mice exposed to LPS intranasally were administered a concentration of 75 µg/mL. Mice were administered 40 µl doses at two time points 6 hours apart and were allowed to rest for 24 hours before sacrifice. This method was established through optimization of both the time and concentration for intranasal administration. Mice exposed via the aerosol chamber were exposed to a concentration of 15 $\mu g/m^3$ for the duration of 24 hours and sacrificed after 1-hour of rest. Mice were sacrificed in the same manner as described for the microsphere exposures.

Mice utilized for all aerosol exposures, were housed two per cage in a home cage lined with a thin layer of bedding. Mice were supplied ample food and water and were allowed to freely drink and eat in their home cages. The mice were housed within their home cages inside of the larger exposure chamber used for aerosol delivery, equipped with an automatic day/night light cycle. Intranasally exposed mice were housed identical to the chamber cohort.

Histology

For hematoxylin and eosin staining (H&E), mice were exposed to lipopolysaccharide under the aforementioned conditions; however, for this processing, these mice were sacrificed before performing intratracheal instillation to inflate lungs with 0.3mL of a 1:1 mixture of optimal cutting temperature compound (OCT) and phosphate-buffered saline (PBS). These lungs were then dissected and flash frozen. Cryostat sectioning was performed on the fresh frozen tissue followed by H&E staining to assess cellular infiltrations.

Neutrophil recruitment was confirmed through the utilization of spinning disc confocal microscopy in conjunction with the Keyence system, as described below. The procedures employed for this approach were identical to those described previously for the microsphere exposure cohort. However, the specimens under examination only received DAPI nuclear staining to visualize the multilobed nuclei of the recruited neutrophils. As previously mentioned, based

on the transgenic reporter in these mice, dsRed+ cells were detected and recorded within the Texas Red channel.

Microscopy

A Keyence BZX800 and a custom Yokogawa/Zeiss spinning disc confocal microscope setup were used to image both microsphere deposition as well as dsRed positive cells in either study. All images were taken using either 10x or 20x objectives and tiled together to generate the whole lobe images; scale bars are included in the images. The larger stitched images were then used for analysis using a custom Python script.

Analysis

Automated image analysis was used to quantify fluorescent microsphere and cell distribution throughout the tissue analysis. A stand-alone script was built using the IPython kernel (Python (3.9.7)) in JupyterLab (3.2.1, Jupyter) through Anaconda Navigator (2.1.4, Anaconda Inc.), with the libraries Matplotlib (3.6.0), NumPy (1.11.3), pandas (1.5.1), Python Imaging Library (Pillow/PIL, 9.3.0), and OpenCV (4.6.0.66) used to support functionality without modification to the image files from the Keyence microscope (.TIFF file formatting)[13]. This script was paired with the open-source image processing platform ImageJ (NIH) in order to preliminarily identify neutrophils during the PGRP experimental portion of the

study[14]. Images were minimally processed at all stages of analysis to minimize manipulation biasing the analysis.

Preliminary analysis performed on fluorescent microsphere images centered on color analysis, identifying, and quantifying characteristic colors present to differentiate non-fluorescent tissue, auto-fluorescent tissue (as commonly present near airways), and fluorescent microspheres. These separations provided exclusionary criteria for identifying microspheres in the final analysis of measuring localized deposition to evaluate the dispersion of deposition within the lung tissue. The whole-lung analysis was performed by 1) creating a *mask* image to filter the characteristic color of fluorescent microspheres, 2) overlaying a grid of square cells a given size (100, 200, or 500 μm), which was used 3) to subdivide the image into a numerical output based on the measured intensity of the fluorescent microspheres (as filtered for in (1)). 4) Following this, the tissue was re-analyzed with the *mask* image in (1) modified to include all color characteristic of tissue coverage. 5) These numerical outputs were aligned, and the output values from (4) were used to determine the proportion of tissue coverage within given grid cells. 6) Finally, the tissue coverage of a grid cell from (4) and (5) was used to include or exclude a given grid cell from analysis to ensure that tissue being analyzed was sufficiently representative of lung tissue, rather than biasing the analysis due to the inclusion

of non-tissue space (such as airways or external non-lung space) that would not contain fluorescent microspheres.

Grid cell sizing and use for analysis was evaluated using combinations of three grid sizes (100 μm, 200 μm, 500 μm square grids) and four tissue-coverage (50%, 75%, 90%, 98% tissue coverage within a given grid cell) criteria for the inclusion in the analysis of each lung image. The grid sizing of 200 μm with the tissue coverage criteria of 90% was used in the final image analysis as these criteria worked best to avoid biasing measurement through the inclusion of airway and non-tissue image areas. Although all size ranges tested yielded similar results, this selection criteria provided the most robust and repeatable analysis across the dataset.

Additionally, to identify distribution of particles and cells proximal to large and medium airways, deposition of microspheres and neutrophils within 200 μm of the airways was evaluated as a fraction of the total deposition/presence in the lung.

Interpretation of Data

The index of dispersion (D, the ratio of the variance to the mean $D=\sigma^2/\mu$) was used as the primary statistic for comparison of the deposition throughout the lung tissue in this dataset[15]. The index of dispersion is a useful measure of

comparison between two datasets with large differences in means to account for the larger variance due to larger means. In interpreting the index of dispersion, the threshold of D=1 is commonly used, as Poissonian distribution has an equal variance and mean, resulting in an index of dispersion of D=1. In the case of the random distribution of particles (or diffusion; Brownian motion; deposition in this study) the distribution of particles in a given volume is Poissonian. The index of dispersion can be used to assess a given pattern of distribution by dividing the space into equally sized segments, within each of which particles are counted, and the index of dispersion across the total space is calculated. An index of dispersion D>>1 commonly denote a clustered distribution, while an index of dispersion D<1 indicates low variance (particularly with regard to outliers/extremes that notably impact the measured variance) throughout the space.

The coefficient of variation (c_v, the ratio of the standard deviation to the mean $c_v=\sigma/\mu$, or in a sample, the ratio of the sample standard deviation to the sample mean $c_v=s/x$) was used as an initial statistic for corroborating the measure of dispersion alongside the index of dispersion. While the standard deviation is commonly reported in evaluating the dispersion of numerical data, the variance (as used in the index of dispersion) weights outliers more heavily than data very near to the mean (as in the standard deviation). Due to the need for measuring extreme areas of deposition in the dataset, the standard deviation

(and so c_v) obscured the extremes of the deposition in comparison to the index of dispersion enabling the emphasis in identification and measurement of this pattern of deposition.

Results

To model typical aerosol particulate exposures, we exposed B6 mice to 1μm fluorescent microspheres via either intranasal administration or using the aerosol exposure chamber. This chamber is unique as it allows for continuous exposure to a given concentration of aerosols for any desired length of time. The chamber allows for uninterrupted aerosol exposure in the form of natural, unassisted ventilation. The chamber also allows for continuous monitoring of particle size distribution and PM mass concentration. With this chamber system, we mimic natural inhalation of particles as a physiologically natural system to study aerosol exposure. We hypothesized that exposure via the chamber will generate uniform distribution of particles throughout the lung while intranasally exposed mice will demonstrate nonuniform microsphere deposition. Results shown in Table 2.1 as well as Figure 2.2 illustrate the differences in the overall pattern of particle distribution between exposure methods.

Figure 2.2: Tile stitched full lung lobes, chamber vs intranasal microsphere administration. (**A)** 10x tile stitched fluorescence image of WT mouse exposed to 1μm fluorescent microspheres via exposure chamber. **(B)** 10x tile stitched fluorescence image of WT mouse exposed to 1μm fluorescent microspheres via intranasal administration.

Table 2.1: Summary of results.

Method of administration alters microsphere deposition

Mice exposed to microspheres via the exposure chamber (Fig 2.3A) revealed an average index of dispersion of 0.627 as compared to animals subjected to exposure via intranasal instillation (Fig 2.3B), which had an average index of dispersion of 41.90 (Fig 2.3D). There is a significant increase in index of dispersion in mice administered the microspheres via intranasal administration when compared to the chamber group. The index of dispersion illustrated in Fig 2.3D indicates that the dispersion of particles due to administration via exposure chamber follows a uniform distribution pattern. When compared to the index of dispersion for mice exposed via the I.N. method, intranasally exposed mice showed a distinct, nonuniform, clustered phenotype. In addition to significant differences in the index of dispersion, overall variance between exposure groups also varied significantly (Fig 2.3E). Analysis revealed that chamber exposed mice demonstrated an average variance of 0.266 while I.N. exposed mice exhibited an average variance of 2043.0.

Figure 2.3: Microsphere deposition due to chamber exposure vs intranasal exposure. (A) Fluorescence images of microsphere deposition of WT mouse exposed to 1μm fluorescent microspheres via exposure chamber. Arrows highlight microspheres. **(B)** Fluorescence images of microsphere deposition of WT mouse exposed to 1μm fluorescent microspheres intranasally. Arrows highlight preferential clustering of microspheres around medium sized airways. **(C)** Fluorescence images of control WT mouse lung. **(D)** Index of Dispersion of chamber and intranasally exposed WT mice. **p-value = 0.036581 I** Raw variance of chamber and intranasally exposed WT mice. **p-value = 0.01363**.

The calculated index of dispersion values revealed that mice exposed to the 1μm fluorescent spheres in the exposure chamber showed uniform distribution with particle deposition occurring in an even pattern throughout lung parenchyma. By contrast, animals exposed via intranasal instillation, demonstrated a pattern of sporadic, nonuniform deposition (Figs 2.3 and 2.4). Not surprisingly, it was also noted that specific patterns of particle distribution varied greatly from subject to subject in intranasally exposed animals.

Figure 2.4: Microsphere deposition in intranasally exposed mouse. (A) Tile stitched fluorescence image of intranasally exposed WT mouse lung illustrating nonuniform microsphere distribution throughout entire left lung lobe. **(B)** Enlarged image of Figure **(A)** to highlight nonuniform deposition at apex of lung. **(C)** Enlarged image of Figure **(A)** to illustrate nonuniform deposition in middle area of lung. **(D)** Enlarged image of Figure **(A)** to demonstrate nonuniform deposition in distal portion of lung. Arrows highlight microsphere clustering surrounding airways.

Histologically, we noted significant differences in the general pattern of deposition of the microspheres between exposure groups. In mice exposed to the microspheres via intranasal administration, we noted significant microsphere deposition concentrated around medium and large airways; a feature exclusive to this administration method (Figs 2.2B, 2.3B, and 2.4). I.N. exposed mice also frequently demonstrated deposition of microsphere mini-aggregates at terminal portions of the airways where they empty into the smaller alveolar spaces of the lung. In these mice, the microspheres distribution was patchy, and particles were inconsistently distributed throughout the lung when compared to chamber

exposed animals (Fig 2.3). Chamber exposed mice demonstrated uniform deposition in which no clumping was observed neither around airways nor throughout the parenchyma itself (Fig 2.5). These animals demonstrated uniform delivery of the particles with broader coverage throughout the parenchyma, where nearly every region of the lung tissue contained deposited microspheres. In contrast, I.N. exposed animals showed significant gaps in deposition where large portions of the lungs had very minimal to no microsphere deposition. Another distinction in intranasally exposed mice is that there was frequent deposition within the lumen of airways; this feature was not observed in chamber exposed animals. This may be due to the preferential clustering of microspheres in and near the airway in liquid drops with aggregated microspheres, or simply due to the concentrated delivery of the particles, forcing some microspheres to be trapped within the airways.

Figure 2.5: Microsphere deposition in chamber exposed mouse. (A) Tile stitched fluorescence image of chamber exposed WT mouse lung illustrating uniform microsphere distribution throughout entire left lung lobe. **(B)** Enlarged image of Figure **(A)** to highlight uniform deposition at apex of lung. **(C)** Enlarged image of Figure **(A)** to illustrate uniform deposition in middle area of lung. **(D)** Enlarged image of Figure **(A)** to demonstrate uniform deposition in distal portion of lung. Arrows highlight microspheres.

The results of this study illustrate the need for clinically representative models to study the health effects associated with aerosol exposure. As illustrated in Fig 2.3D, particle deposition due to administration via the exposure chamber demonstrated even distribution with microspheres being uniformly

deposited throughout the parenchyma of the lungs. In contrast, mice which were exposed by using the traditional intranasal methodology, demonstrated nonuniform, sporadic deposition. This pattern of distribution is critical to consider when assessing experimental designs attempting to study exposure to aerosols and the possible associated health effects. As previously mentioned, our data revealed significant variation in intranasal administration. In preliminary preparation for this study, we used a method of one dose of 20 µl total, administering 5 µl per nostril at a time. In these mice, we noted varying results as some mice illustrated robust, nonuniform deposition with clustering around larger airways while others showed little to no microsphere deposition throughout the lung. Using this administration method, another cohort of mice showed very few microspheres making it through the respiratory tract and depositing in only the apex of the lungs, incapable of penetrating past the larger airways (Fig 2.6A and 2.6B). The clustering of microspheres around airways following intranasal administration suggests that this method of exposure could produce a response, which is not fully representative of the immune response in humans. This could ultimately mean that cellular responses will subsequently target the parenchyma and conducting airways of the lung differently leading to different areas of the lung itself being affected unevenly. The pattern of cellular recruitment is critical to understanding the behavior of the immune response. If cells are preferentially recruited to specific areas due to administration method, this may lead to varying immune responses when compared to an exposure done utilizing a method more

similar to the natural route of inhalation such as those done utilizing an exposure chamber.

Figure 2.6: Inconsistent deposition and cellular recruitment in intranasally exposed mice. (A) Tile stitched fluorescence image of full left lobe of intranasally exposed WT mouse illustrating microsphere deposition at apex of the lung only. **(B)** Enlarged image of Figure **(A)** to highlight deposition in apex of lung. Arrows highlight clustering of microspheres around airways. **(C)** Representative tile stitched fluorescence image of full left lobe of control WT mouse exposed to PBS intranasally **(D)** Enlarged image of Figure **(C). (E)** Fluorescence image of PGRP+ mouse intranasally exposed to LPS illustrating preferential clustering around airways. White square highlights neutrophil clustering surrounding airways. White circle highlights minimal neutrophil deposition in parenchyma of lung. Arrows highlight PGRP+ cells recruited into the lung.

Method of administration influences cellular recruitment pattern and behavior

To assess clinical implications of particle deposition, we exposed PGRP-S mice to 75 μg/mL of Lipopolysaccharide either intranasally or via the exposure chamber. During initial studies, it was difficult to estimate comparable concentrations for intranasal versus chamber aerosol delivery due to the differences in how solutions entered the lungs; for example, while the input solution of 15 μg/mL of LPS was able to induce a response as an aerosol, when delivered intranasally this concentration was insufficient to induce cellular recruitment. Through optimization, we found that 75 μg/mL was a concentration able to reliably induce significant cellular recruitment. We also found that administration must be done in one single bolus of 40 μl rather than delivering 5

μl/nostril at a single time; we previously found in the microsphere administration that small volumes often led to microspheres being embedded in the nasal passages and not entering the lungs. Upon administering LPS, we noted significant airway infiltration in lungs of mice both chamber exposed (Fig 2.7A) and intranasally exposed (Fig 2.7B). Quantitative analysis of dsRed fluorescence in the lungs of PGRP-S animals revealed results similar to those generated by microsphere administration (Figs 2.7D-F). Analysis of neutrophil distribution throughout lung parenchyma of both exposure groups revealed that mice exposed to LPS intranasally demonstrated nonuniform distribution while chamber exposed mice exhibited uniform deposition. H&E histological staining and confocal imaging was done to verify establishment of inflammation and the cellular recruitment of neutrophils (Figs 2.8 and 2.9). Fig 2.8 illustrates a representative image of immune cell recruitment in intranasally exposed PGRP+ mice. To verify neutrophil recruitment, we conducted higher magnification confocal imaging on samples stained with a DAPI nuclear stain (Fig 2.9) to visualize multilobular nuclei of the recruited neutrophils. Mice exposed to LPS intranasally showed an average index of dispersion of 0.981 while comparatively, chamber exposed mice illustrated an index of dispersion of 0.509. Along with a higher index of dispersion, intranasally exposed mice also demonstrated an increased variance when compared to those exposed via the chamber. Thus, our data suggest that the delivery of material into the lung influences the pattern of cellular recruitment.

Figure 2.7: Cellular recruitment in PGRP+ mice. (A) Fluorescence images of cellular recruitment in PGRP+ mouse exposed to LPS via exposure chamber. **(B)** Fluorescence images of cellular recruitment in PGRP+ mouse exposed to LPS intranasally. Arrows highlight PGRP+ cells recruited into the lungs. **(C)** Fluorescence images of control lung. **(D)** Index of Dispersion of chamber and intranasally exposed PGRP+ mice. **p-value = 0.009467 (E)** Raw variance of chamber and intranasally exposed PGRP+ mice. **p-value = 0.042693 (F)** Average neutrophil density comparison of chamber and intranasally exposed mice. **p-value = 0.251384**.

Figure 2.8: Histological characterization of infiltrating cells. (A) 60X hematoxylin and eosin stain of PGRP-S-dsRed model exposed to LPS intranasally. Arrows highlight infiltrating neutrophils. **(B)** 60X hematoxylin and eosin stain of WT control mice exposed to PBS intranasally.

Figure 2.9: Fluorescence Images of I.N. LPS exposed mice (Red = PGRP signal, Blue = DAPI). (A) a.60X PGRP **b**. 60X DAPI, yellow arrows signify epithelial cell nuclei; white arrows signify neutrophil nuclei **c**. 60X Merge of PGRP and DAPI. **B)** 63X magnified DAPI stain to show multilobular neutrophil nuclei.

In histological sections, intranasally exposed PGRP mice demonstrated dsRed+ neutrophil distribution similar to that of the corresponding microsphere animals. In these mice, we noticed sporadic recruitment of these cells, which showed clustering throughout the parenchyma often leaving much of the tissue devoid of cellular recruitment. In contrast, chamber exposed mice demonstrated a distinct pattern in which cellular recruitment was uniform throughout the tissue, with no clustering and wide coverage throughout the parenchyma. This suggests that chamber exposed mice may have a broad inflammatory response due to the

dispersed recruitment of neutrophils throughout the tissue while mice exposed intranasally elicit a varied immune response due to significant differences in tissue recruitment patterns between exposure routes.

The use of the PGRP-S-dsRed transgenic mouse model allowed for an in vivo analysis of our hypothesis demonstrating that the route of administration may affect biological responses to inhaled pathogens as well as other environmental toxins[12]. As highlighted in Figures 2.7D and 2.7E, this data provides clear support of the hypothesis and shows significant effects on cellular recruitment patterns. These results strongly suggest that the distribution of particles due to administration method significantly influences the behavior and recruitment pattern of immune cells. Interestingly, although the number of neutrophils recruited into the lungs was not significantly different between exposure groups (Fig 2.7F), as highlighted in Figs 2.6E and 2.7B, we noted clustering of cells around airways in intranasally exposed mice while the recruitment pattern of neutrophils in chamber exposed animals was uniform throughout the parenchyma. The clustering of neutrophils around medium and large airways was particularly striking; despite the fact that recruited neutrophils are intrinsically migratory within tissues, the intranasal administration still directed a clear pattern of preferential clustering. This data closely mimicked the pattern of particle deposition noted in the microsphere portion of this study and illustrates the overall inconsistency of intranasal administration (Fig 2.6). The consequences of inflammatory neutrophil recruitment also will include distinct

patterns of tissue damage and fibrosis induced by cellular inflammation. Accordingly, inconsistencies among methodologies should be considered before designing studies aimed to address immunological responses to inhaled materials, whether inert, immunostimulatory, or even infectious, to ensure that studies can provide clinically relevant physiological data.

Clustering Phenotype of I.N. Exposed Animals

We observed a distinct clustering pattern of beads and recruited neutrophils around the airways following intranasal instillation. In contrast, animals exposed to microspheres or LPS in the controlled chamber exhibited an even dispersion of cells and beads throughout the lung parenchyma. As highlighted in Fig 2.10, in the microsphere experimental group, 26.48% of particles deposited near an airway in the chamber-exposed animals whereas, 52.68% of the beads exhibited a clustering phenotype within a 200 μm radius of a medium or large airway in the intranasally exposed animals. These values underscore the unique pattern of peri-airway clustering observed in the intranasally exposed animals. Similarly, PGRP-ds-Red transgenic mice exposed to LPS, 65.68% of cells clustered near the airways in the chamber-exposed animals, while 75.60% of cells demonstrated peri-airway deposition in the intranasal exposure group. Ultimately, this analysis revealed significant differences in distribution patterns between the two exposure methodologies,

highlighting the remarkable clustering phenotype observed in the intranasally exposed animals.

Figure 2.10: Percent of near-airway deposition. (A) Percent of near-airway deposition of microspheres in intranasal and chamber exposed animals. p-value = 0.004496 **(B)** Percent of near-airway deposition of recruited neutrophils in intranasal and chamber exposed animals. p-value = 0.011466.

Discussion

This study provides evidence that the method of administering materials into the lung can significantly influence immunological responses, primarily due to variations in patterns of cellular recruitment. The lung is a complex organ that comprises two main distinct tissue compartments: the conducting airways and the respiratory airways or parenchyma, each characterized by unique cellular subsets. Consequently, disease processes involving inflammatory cell recruitment and associated cytokines are expected to have disparate effects within these compartments. As demonstrated in the current study, even in cases where inflammation triggers the recruitment of highly mobile cells like neutrophils, there are discernible variations in their recruitment patterns between these tissue compartments due to the administration method utilized. Therefore, it is imperative to carefully consider the divergent impacts of such recruitment on these distinct tissue compartments given the chosen method of delivery. This becomes particularly relevant in models investigating the effects of inhaled aerosols as well as disease model development, where models utilizing

intranasal administration are prone to misrepresentation of the physiologically responses, especially those which depend on relevant impacts on the lung parenchyma.

In relation to the data presented here, other studies have aimed to highlight differences in immune response based on varying methods of administration. A recent clinical trial assessed the differences in immune response to cat allergen delivered via chamber exposure or nasal allergen challenge[16]. This study ultimately showed significant differences in overall magnitude of response with an increase in severity noted in the chamber exposed mice. In this study, they did not note significant differences in cytokine production; however, this measurement alone is not a true representation of overall immune response. A study by Hasegawa-Baba et al. sought to investigate the distribution of a test substance in rats utilizing variations of intratracheal administration[17]. This group found significant differences in distribution in regard to the technique used. In this study, they compared distribution of the substance under various conditions, altering the angle of the mouse, instillation speeds, as well as utilizing various devices. Intratracheal delivery techniques vary widely, so it may be difficult to compare results between studies utilizing this technique. The results of this study demonstrated that variation within technique of intratracheal administration alone produced significant differences in distributions of particles, highlighting the inconsistency of this method[16]. These results also raise the

question of the reproducibility of models utilizing this method of administration. As in the present study, these inconsistencies are crucial as they suggest that techniques may introduce broad variation within cohorts of animals intended to address the same question. This is important to consider as it may affect reproducibility not only between exposures but also within a single exposure group. Although intratracheal administration bypasses the limitation of intranasal administration in which solution can get trapped in the nasal passages, there are also limitations to this method as it also administers a bolus of solution as opposed to aerosolization solution. Because of this, it does not simulate natural inhalation. In addition to this, the delivery of a bolus of solution intratracheally may still result in nonuniform distribution and ultimately changes in cellular response patterns. To address this limitation for this method, further studies must be done to investigation distribution patterns and immune response.

Conclusion

Current techniques such as I.N. administration, nose-only exposure chambers, and intratracheal administration have various limitations. In addition to lack of clinical relevance of these techniques, they also pose various technical limitations as some of these methods limit animal activity during time of exposure, making chronic exposures studies difficult to perform. This is a severe limitation as human response to aerosol exposure more often occurs by chronic rather than sporadic exposure to particulate matter. Our chamber design allows

our laboratory to bypass previously mentioned limitations, allowing for generation of clinically relevant exposure models in which we can investigate the health effects of various substances. This study not only highlights the inconsistencies of intranasal administration but more specifically provides compelling information about cellular behavior. The results of this study illustrate that intranasal administration of LPS, a robust immune stimulus, leads to localized cellular recruitment with characteristic peri-airway clustering. In contrast, exposure via aerosol chamber demonstrated uniform cellular recruitment throughout the lung tissue. These findings are important as they indicate biological consequences due to method of exposure, namely variations in cellular behavior such as more dispersed cell trafficking throughout the tissues to provide broad protection, pathogen sensing, and defensive responses, as well as consequent tissue damage and fibrosis.

The data produced by this study suggests that the use of intranasal administration methods in current aerosol studies which aim to investigate the relationship between aerosol exposure and associated health effects, may not accurately represent real-world human exposure. However, these results additionally indicate that intranasal delivery may serve as a suitable administration technique for studies focused on investigating models of airway toxicity or mucosal drug delivery. Ultimately, the findings of this study provide compelling evidence for the need for further studies to be done to ensure

relevancy and accuracy of data attempting to address aerosol exposure and health implications employing the available methods of administration.

References

1. Stannard, W., & O'Callaghan, C. (2006). Ciliary function and the role of cilia in clearance. *Journal of aerosol medicine: the official journal of the International Society for Aerosols in Medicine*, *19*(1), 110–115. https://doi.org/10.1089/jam.2006.19.110
2. Ardain, A., Marakalala, M. J., & Leslie, A. (2020). Tissue-resident innate immunity in the lung. *Immunology*, *159*(3), 245–256. https://doi.org/10.1111/imm.13143
3. Naeem, A., Rai, S. N., & Pierre, L. (2022). Histology, Alveolar Macrophages. In *StatPearls*. StatPearls Publishing. https://www.ncbi.nlm.nih.gov/books/NBK513313/
4. Condon, T. V., Sawyer, R. T., Fenton, M. J., & Riches, D. W. (2011). Lung dendritic cells at the innate-adaptive immune interface. *Journal of leukocyte biology*, *90*(5), 883–895. https://doi.org/10.1189/jlb.0311134
5. L. P. Nicod. Lung defences: an overview. *European Respiratory Review* Dec 2005, 14 (95) 45-50. https://err.ersjournals.com/content/14/95/45
6. Canto, R.G., Robinson, G.R., Reynolds, H.Y. (1994). Defense Mechanisms of the Respiratory Tract. In: Chmel, H., Bendinelli, M., Friedman, H. (eds) Pulmonary Infections and Immunity. Infectious Agents

and Pathogenesis. Springer, Boston, MA. https://doi.org/10.1007/978-1-4899-1063-9_1

7. California Air Resources Board. (n.d.). Inhalable Particulate Matter and Health (PM2.5 and PM10). Inhalable Particulate Matter and Health (PM2.5 and PM10) | California Air Resources Board. Retrieved December 15, 2022, from https://ww2.arb.ca.gov/resources/inhalable-particulate-matter-and-health#:~:text=Those%20with%20a%20diameter%20of,5
8. World Health Organization. Regional Office for Europe. (2006). Air quality guidelines: global update 2005: particulate matter, ozone, nitrogen dioxide and sulfur dioxide. World Health Organization. Regional Office for Europe. https://apps.who.int/iris/handle/10665/107823
9. Wang, B., Eum, KD., Kazemiparkouhi, F. *et al.* The impact of long-term $PM_{2.5}$ exposure on specific causes of death: exposure-response curves and effect modification among 53 million U.S. Medicare beneficiaries. *Environ Health* 19, 20 (2020). https://doi.org/10.1186/s12940-020-00575-0
10. Peng, X., Maltz, M. R., Botthoff, J. K., Aronson, E. L., Nordgren, T. M., Lo, D. D., & Cocker, D. R. (2019). Establishment and characterization of a multi-purpose large animal exposure chamber for investigating health effects. *The Review of scientific instruments*, *90*(3), 035115. https://doi.org/10.1063/1.5042097

11. Biddle, T. A., Yisrael, K., Drover, R., Li, Q., Maltz, M., Topacio, T., et al. Aerosolized aqueous dust extracts collected near a drying lake trigger acute neutrophilic pulmonary inflammation reminiscent of microbial innate immune ligands. Science of The Total Environment. https://www.sciencedirect.com/science/article/pii/S0048969722069820
12. Wang, J., Gusti, V., Saraswati, A., & Lo, D. D. (2011, November 15). *Convergent and divergent development among M cell lineages in mouse mucosal epithelium*. Journal of immunology (Baltimore, Md.: 1950). Retrieved December 19, 2022, from https://www.ncbi.nlm.nih.gov/pmc/articles/PMC3208058/
13. Kluyver, T., Ragan-Kelley, B., Pérez F., Granger, B., Bussonnier, M., Fredric, J., Kelley, K., Hamrick, J., Grout, J., Corlay, S., Ivanov, P., Avila, D., Abdalla, S., Willing, C., Jupyter Development Team. (***). Jupyter Notebooks – A publishing format for reproducible computational workflows. *Positioning and Power in Academic Publishing: Players, Agents and Agendas*, 87-90., https://jupyter.org/about
14. Abramoff, M.D.; Magalhães, Paulo J.; Ram, Sunanda J. (2004)., Image processing with ImageJ. *Biophotonics international*, 11(7), 36 – 42. https://dspace.library.uu.nl/handle/1874/204900
15. National Institute of Standards and Technology. (2017, January 24). *Index of dispersion*. Index of Dispersion. Retrieved December 15, 2022, from

https://www.itl.nist.gov/div898/software/dataplot/refman2/auxillar/ind_disp.htm

16. Larson, D., Patel, P., Salapatek, A. M., Couroux, P., Whitehouse, D., Pina, A., Johnson, J. L., Sever, M. L., Sanda, S., Poyser, J., Allio, T., Scadding, G. W., Qin, T., Shamji, M. H., Kwok, W. W., James, E. A., French, D., Lelic, A., Larché, M., Altman, M. C., … Durham, S. R. (2020). Nasal allergen challenge and environmental exposure chamber challenge: A randomized trial comparing clinical and biological responses to cat allergen. *The Journal of allergy and clinical immunology*, *145*(6), 1585–1597. https://doi.org/10.1016/j.jaci.2020.02.024
17. Hasegawa-Baba, Y., Kubota, H., Takata, A., & Miyagawa, M. (2014). Intratracheal instillation methods and the distribution of administered material in the lung of the rat. *Journal of toxicologic pathology*, *27*(3-4), 197–204. https://doi.org/10.1293/tox.2014-0022

Acknowledgments

The authors would like to acknowledge staff at UCR vivarium for their assistance with maintenance and care of mouse colonies.

Figures

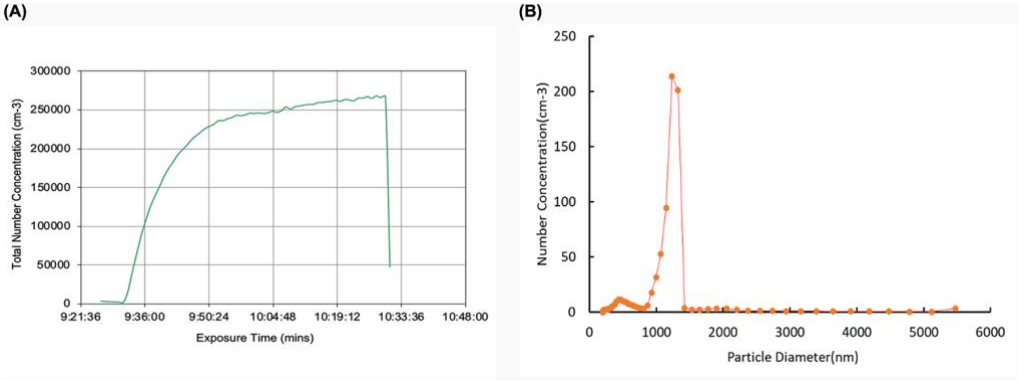

Figure 2.1 – Quantification of fluorescent microsphere aerosols. (A) Total number concentration of particles within 0.5-1.3μm. **(B)** Average size distribution of particles injected into chamber.

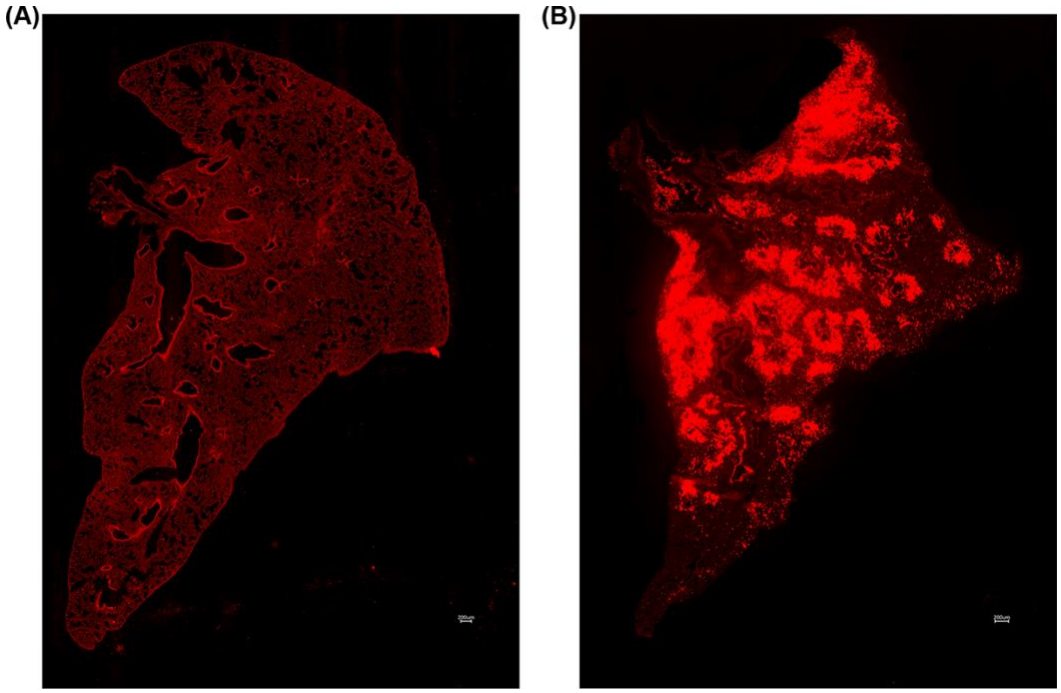

Figure 2.2 - **Tile stitched full lung lobes, chamber vs intranasal microsphere administration.** (**A)** 10x tile stitched fluorescence image of WT mouse exposed to 1µm fluorescent microspheres via exposure chamber. **(B)** 10x tile stitched fluorescence image of WT mouse exposed to 1µm fluorescent microspheres via intranasal administration.

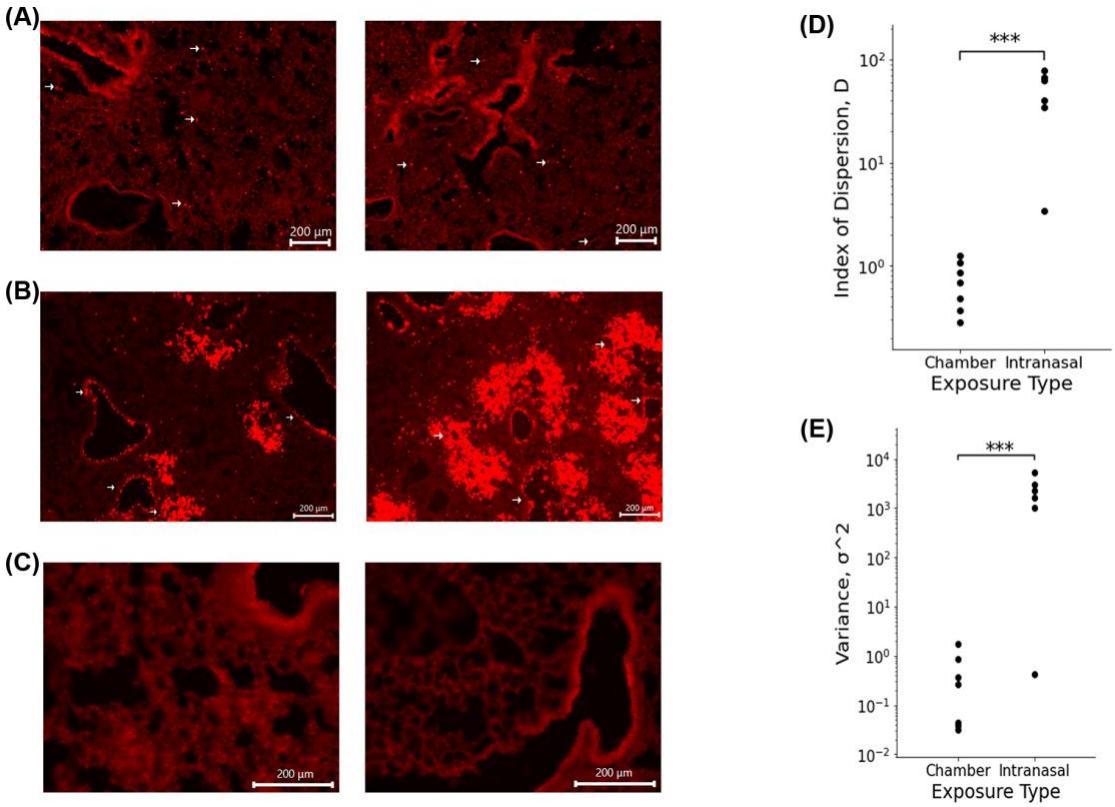

Figure 2.3 - Microsphere deposition due to chamber exposure vs intranasal exposure. (A) Fluorescence images of microsphere deposition of WT mouse exposed to 1µm fluorescent microspheres via exposure chamber. Arrows highlight microspheres. **(B)** Fluorescence images of microsphere deposition of WT mouse exposed to 1µm fluorescent microspheres intranasally. Arrows highlight preferential clustering of microspheres around medium sized airways. **(C)** Fluorescence images of control WT mouse lung. **(D)** Index of Dispersion of chamber and intranasally exposed WT mice. **p-value= 0.036581** Raw variance of chamber and intranasally exposed WT mice. **p-value= 0.01363**

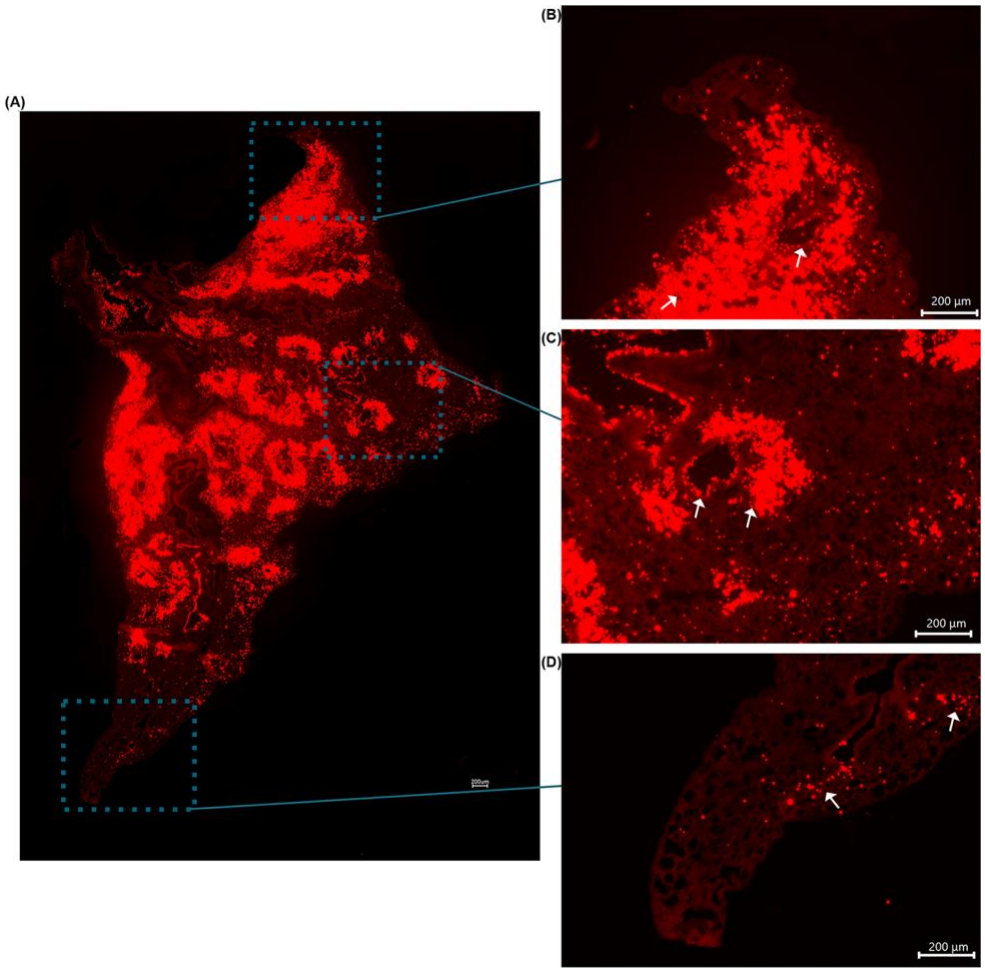

Figure 2.4 – Microsphere deposition in intranasally exposed mouse. (A) Tile stitched fluorescence image of intranasally exposed WT mouse lung illustrating nonuniform microsphere distribution throughout entire left lung lobe. **(B)** Enlarged image of Figure **(A)** to highlight nonuniform deposition at apex of lung. **(C)** Enlarged image of Figure **(A)** to illustrate nonuniform deposition in middle area of lung. **(D)** Enlarged image of Figure **(A)** to demonstrate nonuniform deposition in distal portion of lung. Arrows highlight microsphere clustering surrounding airways.

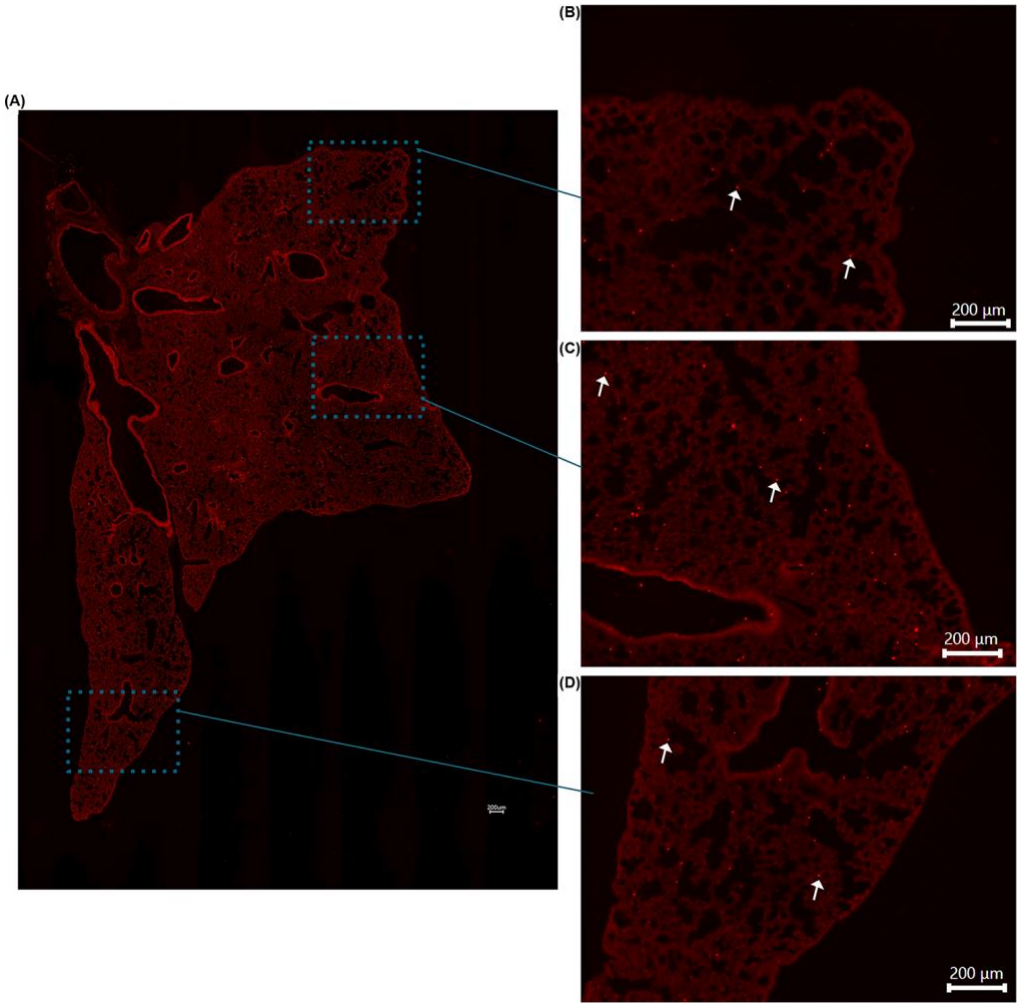

Figure 2.5 - Microsphere deposition in chamber exposed mouse. (A) Tile stitched fluorescence image of chamber exposed WT mouse lung illustrating uniform microsphere distribution throughout entire left lung lobe. **(B)** Enlarged image of Figure **(A)** to highlight uniform deposition at apex of lung. **(C)** Enlarged image of Figure **(A)** to illustrate uniform deposition in middle area of lung. **(D)** Enlarged image of Figure **(A)** to demonstrate uniform deposition in distal portion of lung. Arrows highlight microspheres.

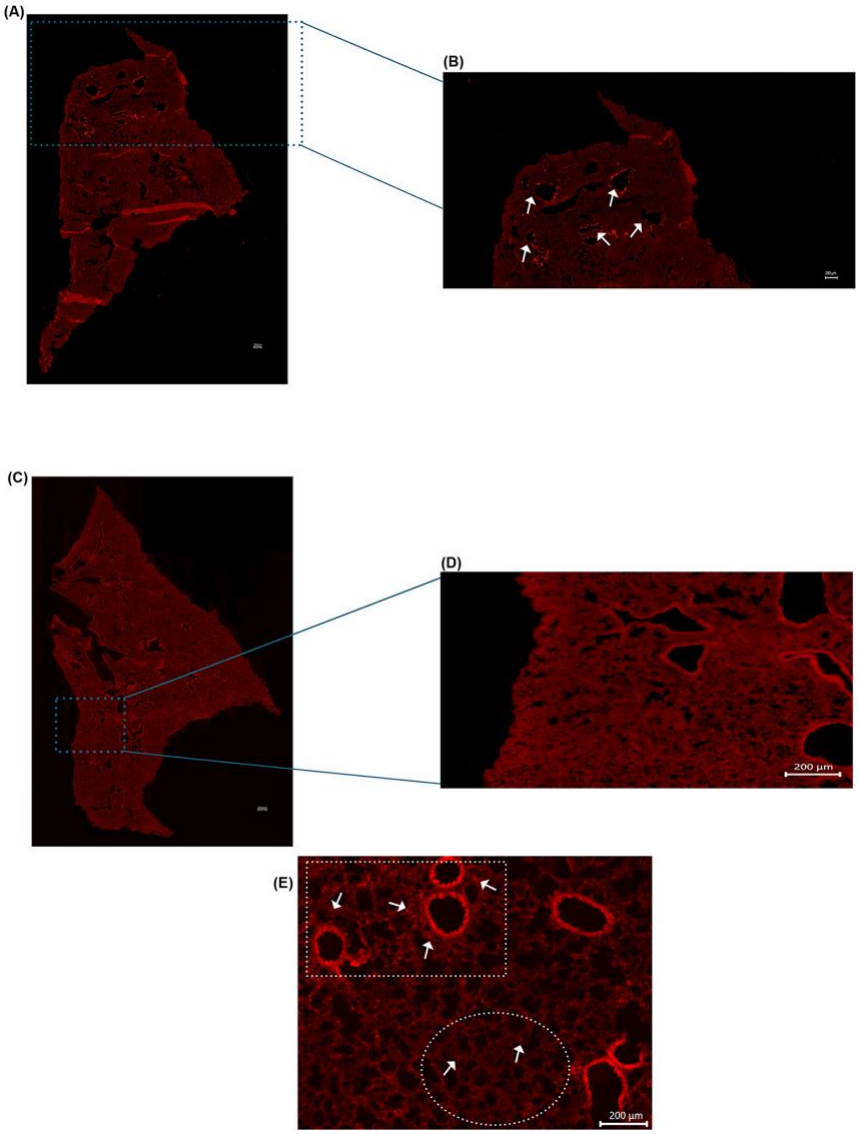

Figure 2.6 – Inconsistent deposition and cellular recruitment in intranasally exposed mice. (A) Tile stitched fluorescence image of full left lobe of intranasally exposed WT mouse illustrating microsphere deposition at apex of the lung only. **(B)** Enlarged image of Figure **(A)** to highlight deposition in apex of lung. Arrows highlight clustering of microspheres around airways. **(C)** Representative tile stitched fluorescence image of full left lobe of control WT mouse exposed to PBS intranasally **(D)** Enlarged image of Figure **(C). (E)** Fluorescence image of PGRP+ mouse intranasally exposed to LPS illustrating preferential clustering around airways. White square highlights neutrophil clustering surrounding airways. White circle highlights minimal neutrophil deposition in parenchyma of lung. Arrows highlight PGRP+ cells recruited into the lung.

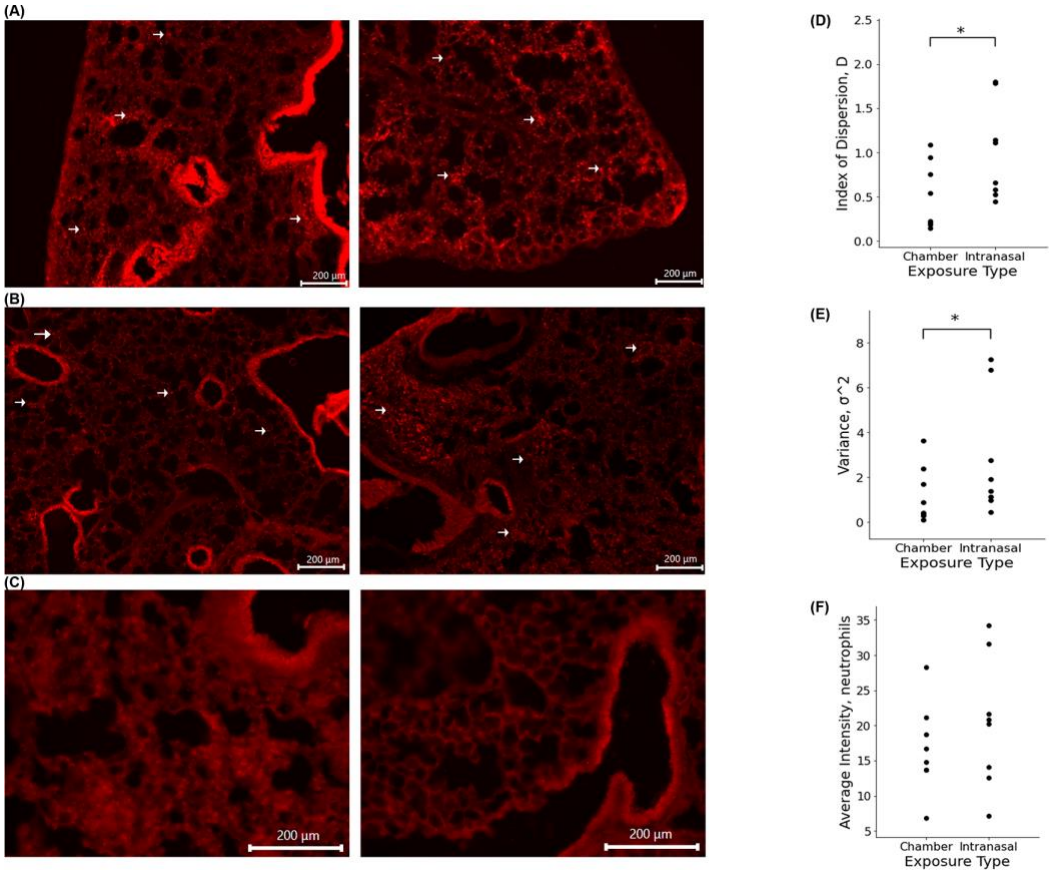

Figure 2.7 – Cellular recruitment in PGRP+ mice. (A) Fluorescence images of cellular recruitment in PGRP+ mouse exposed to LPS via exposure chamber. **(B)** Fluorescence images of cellular recruitment in PGRP+ mouse exposed to LPS intranasally. Arrows highlight PGRP+ cells recruited into the lungs. **(C)** Fluorescence images of control lung. **(D)** Index of Dispersion of chamber and intranasally exposed PGRP+ mice. **p-value= 0.009467 (E)** Raw variance of chamber and intranasally exposed PGRP+ mice. **p-value= 0.042693 (F)** Average neutrophil density comparison of chamber and intranasally exposed mice. **p-value= 0.251384**

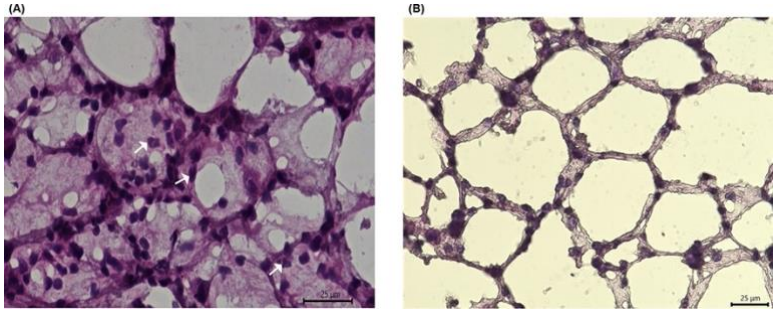

Figure 2.8 - Histological characterization of infiltrating cells. **(A)** 60X hematoxylin and eosin stain of PGRP-S-dsRed model exposed to LPS intranasally. Arrows highlight infiltrating neutrophils. **(B)** 60X hematoxylin and eosin stain of WT control mice exposed to PBS intranasally.

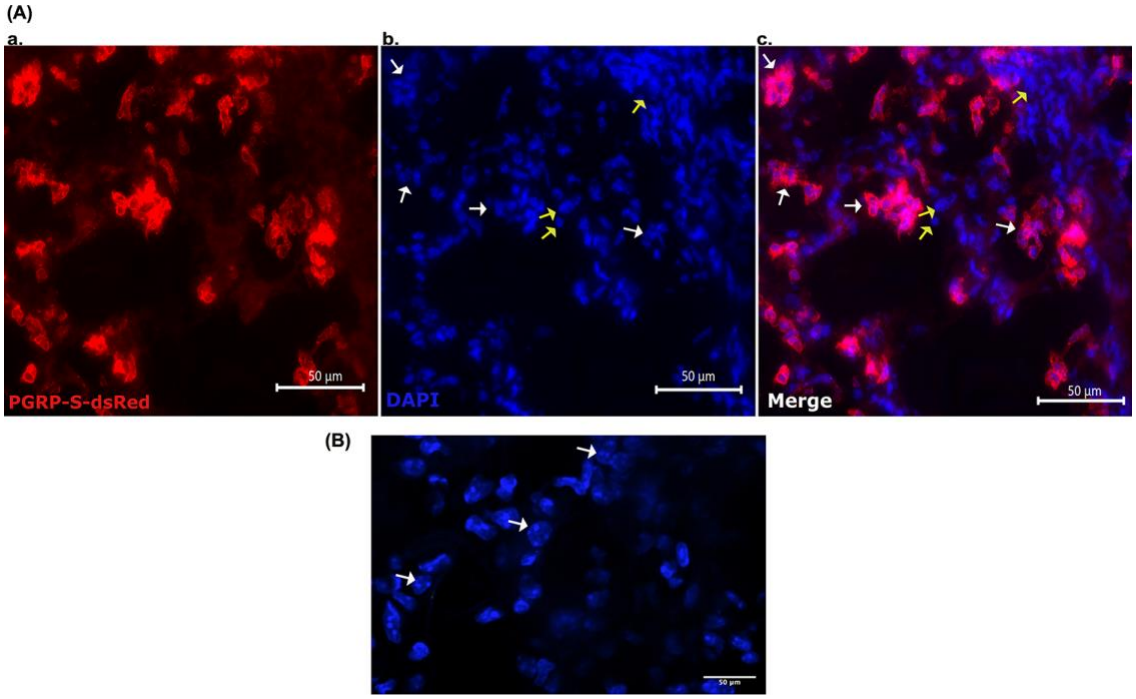

Figure 2.9 - Fluorescence images of I.N. LPS exposed mice (Red=PGRP signal, Blue=DAPI). **A) a.**60X PGRP **b.** 60X DAPI, yellow arrows signify epithelial cell nuclei; white arrows signify neutrophil nuclei **c.** 60X Merge of PGRP and DAPI. **B)** 63X magnified DAPI stain to show multilobular neutrophil nuclei.

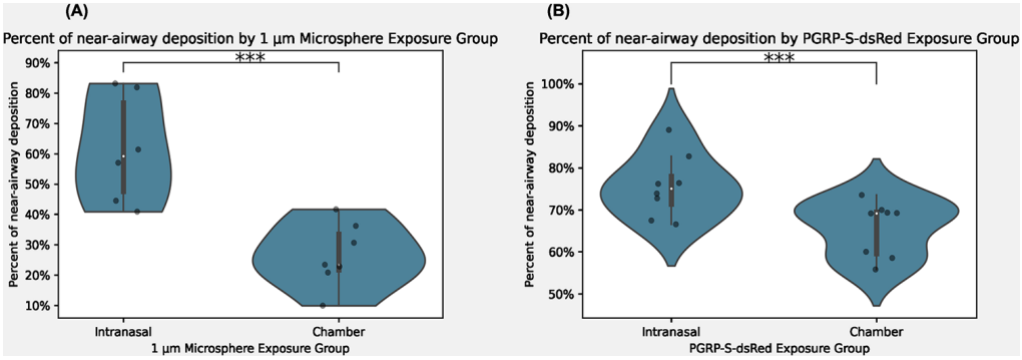

Figure 2.10 – Percent of near-airway deposition. (A) Percent of near-airway deposition of microspheres in intranasal and chamber exposed animals. **p-value= 0.004496 (B)** Percent of near-airway deposition of recruited neutrophils in intranasal and chamber exposed animals. **p-value= 0.011466.**

Exposure Condition	Method of administration	Index of dispersion	Average Variance	% Peri-airway Deposition
Microsphere exposure	Aerosol chamber	0.627	0.266	26.48%
Microsphere exposure	Intranasal administration	41.90	2043.0	52.68%
Lipopolysaccharide exposure	Aerosol chamber	0.981	1.224	65.68%
Lipopolysaccharide exposure	Intranasal administration	0.509	2.833	75.60%

Table 2.1 - Summary of results.

Chapter 3: Salton Sea Aerosol Exposure in Mice Induces a Pulmonary Response Distinct From Allergic Inflammation

Abstract

In communities surrounding the Salton Sea, high rates of asthma are associated with high aerosol dust levels. However, the Salton Sea itself may play an additional role in pulmonary health. Therefore, to investigate a potential role of the Salton Sea on pulmonary health, we exposed mice to aerosolized Salton Sea water for 7 days and assessed tissue responses, including cellular infiltration and gene expression changes. For reference, mice were also exposed to aerosolized fungal allergen (Alternaria sp.) and Pacific Ocean aerosols. Exposure to aerosolized Alternaria sp. induced dramatic allergic inflammation, including neutrophil and eosinophil recruitment to the bronchoalveolar lavage fluid (BALF) and lung tissue. By contrast, Salton Sea “spray” induced only B cell recruitment to the lung tissue without increased inflammatory cell numbers in BALF. However, there were consistent gene expression changes suggestive of an inflammatory response. The response to the Salton Sea spray was notably distinct from the response to Pacific Ocean water, which induced some B cell recruitment but without an inflammatory gene expression profile. Our studies suggest that soluble components in Salton Sea water promote induction of a unique inflammation-associated response, though any relationship to asthma remains to be explored.

Introduction

The Salton Sea is a 345 mi2 inland body of water located in California's Riverside and Imperial counties. The Sea is primarily fed by agricultural runoff as well as inflow from the Alamo, New, and Whitewater rivers. In recent decades, the Sea has been undergoing a rapid retreat. This retreat is causing increased exposure of dry lakebed (playa), resulting in increased dust production which is spreading throughout the region and impacting the surrounding population. Moreover, the drying Sea has become hypersaline, at approximately 74 parts per thousand, more than twice that of Pacific Ocean water[1]. The consequent rapid change in the Sea's ecology has resulted in periodic algal blooms, and fish and migratory bird die-offs[2,3]. Pesticide and herbicide use from agricultural areas located to the southeast and northwest of the Sea[3], as well as heavy metal contamination from elements such as selenium[4], paint an overall picture of ill-health in the Sea itself.

This ecosystem's ill health is also reflected in the surrounding communities. The human population surrounding the Salton Sea includes a high proportion of migrant workers, with high rates of poverty and poor access to health care. Area residents suffer from one of the highest rates of childhood asthma in California at 20%–22.4%, compared to an average of 14.5% for the rest of the State[5]. Predictably, the surrounding area also has one of the highest

rates of hospitalization for asthma[6], making it a serious health crisis in an already underserved community.

Asthma is a disease of airway restriction, defined as an increase in airway hyperreactivity, and usually associated with allergies (referred to as “atopic” asthma), characterized by increased immunoglobulin E (IgE) production, Th2 cytokine secretion and the recruitment of eosinophils to the lungs[7]. Atopic asthma exacerbations can occur in response to exposure to environmental or household allergens[8]. High levels of particulate matter (PM) have also been known to exacerbate asthma[9]. Unfortunately for the communities surrounding the Salton Sea, there are many potential allergens and asthma exacerbating particles. The region has consistently high levels of particulate matter between 10 μm and 2.5 μm in diameter (PM10) and under 2.5 μm in diameter[10, 11,12]. Indoor household allergens, such as Alternaria alternata, and other fungi, are also prevalent[13]. Up to 70% of patients with fungal allergies show a positive skin test response to Alternaria[14]. Additionally, household Alternaria exposure is linked to an increased odds ratio for developing asthma symptoms[15].

However, the region's rampant asthma may have more complex origins than simple dust levels, largely pointing to the Salton Sea itself. Studies have identified a variety of pesticides, including DDT, organophosphates and

pyrethroid, in both the water and the sediment of sites around and within the Sea [16]. Organophosphates have been linked to increased risk of childhood asthma[17]. Additionally, the Sea experiences periodic algal blooms and has been shown to contain low levels of microcystin-LR and YR, cyanotoxins known to cause ill-health[2]. These microcystins have been shown to cause damage to the lungs after chronic exposure[18,19]. Some algal blooms, such as red tides off the coast of Florida, have also been directly linked to the development of asthma and asthma exacerbations[20,21]. Additionally, cyanobacteria, which make up a large part of algal blooms, may serve directly as sensitizing allergens, exacerbating the harmful effects of the algae[22].

Despite suggestive associations between the Salton Sea and asthma, more direct mechanistic information on Salton Sea aerosols and their potential impact on pulmonary health are still needed. To address this issue, we began studies to simulate chronic aerosol exposures in a mouse model of pulmonary inflammation. In the present study, we focused on the direct effect of Salton Sea “spray” aerosols on lung responses.

Materials and methods

Water sample collection

Two batches of Salton Sea water were collected at the edge of Salton City. The first was collected on March 2nd, 2019 (33°19′25.9″N 115°56′18.3″W) and the second was collected on May 13th, 2020 (33°19′53.2″N 115°56′30.0″W). Water samples were collected with a homemade raft; because aerosols are most likely generated at the surface layer of the sea, the design of the raft aims to collect water from the top few centimeters of the water column. Four sampling ports were square distributed, sticking out of the bottom of the raft at a length of 2 in., to ensure sampling surface water only and avoiding floating debris. Two 4.96 m poles were installed and used to move the raft to places with large depth. Water samples were taken by a hand pump on the shore. The whole system was sterilized thoroughly by bleach solution and flushed by MilliQ water before being used on site. More than 2 L of water samples were taken before sample collection to rinse the system. The collected water was stored on ice while transported to the University of California, Riverside campus. Once there, water samples were stored at 4 °C until processed.

Pacific Ocean water was also collected in two batches. The first was collected at Torrey Pines on March 9th, 2019. The second was also collected at Torrey Pines on October 2nd, 2020 (32°55′51.4″N 117°15′37.7″W). Water was

collected directly by containers without using the raft since ocean water is relatively well mixed due to tides. Samples were stored at 4 °C until processed.

Water processing

Before using for aerosolization studies, the water was filtered through an acid-washed, sterilized glass funnel using a sterile 0.2 μm filter (47-mm diameter; Pall Supor 200 Sterile Grid filters, Pall Corporation, Por Washington) into an acid-washed sterilized collecting flask below via vacuum filtration. After filtration, filtrate was either stored at 4 °C or as aliquots archived at −80 °C for long-term storage. The pH of all filtrates was measured; all filtrates were approximately pH 7.0 (±0.8%). The filtered water was stored for various periods from weeks to several months between collection and use in the chamber exposure studies; we were unable to detect any difference in the magnitude of the reported effects on mouse lung responses associated with storage time.

Animals

Animal studies were performed in accordance with UCR institutional IACUC and NIH guidelines and approved protocols. Adult male and female (8–9 weeks old) C57BL/6 J mice were purchased from Jackson Labs, Sacramento. Mice were acclimated for one week in the University of California, Riverside SPF vivarium before being placed into the exposure chamber when they were 9–10

weeks old. Mice were kept 3–4 to a cage and given food and water ad libitum, with bedding being changed at least once weekly. A 12-hour day/night cycle was provided.

Exposure studies were performed in dual animal chambers (an exposure chamber and a control chamber) developed from the chamber described in Peng (2019)[23]. When in the exposure chamber, mice were given a mixture of dry filtered air (0.5–1 lpm) and aerosolized spray (dried by silica gel, 3.5–4.5 lpm) with a total particle concentration of approximately 1500 μg m−3. The three types of PM were generated from solutions of Alternaria alternata and Alternaria tenuis filtrate (Greer Laboratories, Lenoir, NC, USA; 0.4 g/L), Salton Sea water (133-200× dilution), or Pacific Ocean water (40× dilution) with proper concentrations or dilution ratios, respectively. Example of typical exposure PM levels for different PM types are shown in Fig. 3.1a with weekly averaged PM level being 1425 μg m−3 for Alternaria, 1377 μg m−3 for Pacific Ocean spray, and 1523 μg m−3 for Salton Sea spray. Sample aerosolization was accomplished by using a homemade nebulizer with silica-gel dryers (Peng et al., 2019). Mice in the control chamber were given filtered dry air (5.0 lpm) only, with other conditions the same as the exposure chamber, including bedding replacement, food and water supplies, and corresponding day/night cycle. Particulate matter was only monitored within the exposure chamber by a scanning mobility particle sizer (SMPS, including Series 3080 Electrostatic Classifier and Ultrafine Condensation

Particle Counter 3776, TSI) to assist in maintaining stable PM concentration of 1500 μg m−3. Concentration was similar to our previous study in Peng et al. (2018),24 where 1500 μg m−3 of Alternaria was sufficient to generate neutrophil and eosinophil recruitment to the lungs. Relative humidity (40–60%) and ammonia (weekly averaged [NH4] < 25 ppm) were selectively measured in some of the exposures to ensure consistent quality control. For each exposure, we used an equal number of male and female mice. Each exposure had a control air cohort that matched the number and sex of the exposure group. The number of mice for each exposure is as follows: 8 mice for the 3/2/2019 Salton Sea collection, 10 mice for the 5/13/2020 Salton Sea collection, 4 mice for the 3/9/2019 Pacific Ocean collection, 6 mice for the 10/2/2020 Pacific Ocean collection, 10 mice for the Alternaria exposure.

Figure 3.1: Quantification of *Alternaria* (ALT), Pacific Ocean (PO) and Salton Sea (SS) aerosols. PM mass concentration was measured by a scanning mobility particle sizer. Chemical composition was determined by AMS. **(A)** PM mass concentration during 7-day exposure of SS, PO and ALT. Dash line shows the 7-day averaged mass concentration of PM. All units are in μg m^{-3}. **(B)** Averaged mobility diameter distribution of different PM used in exposure experiments. **(C)** Chemical composition of dry particulate matters generated from different materials collected in different season (mm/yr). Other includes metals (sodium, calcium, magnesium), trace metals and other inorganics. (Key: SS0319, Salton Sea/March 2019; SS0520, Salton Sea/May 2020; PO0319, Pacific Ocean/March 2019; PO1020, Pacific Ocean/October 2020; ALT, Alternaria filtrate).

After 7 days, the mice were removed from the chamber, anesthetized via isoflurane and sacrificed by cervical dislocation. The mice were then processed for either RNA extraction and flow cytometry or histological analysis. For the RNA extraction/flow cytometry mice, BALF was collected via 3 injections of 0.8 mL PBS, after which the right lung lobe was extracted and flash frozen in liquid nitrogen and kept at −80 °C until RNA extraction, while the left lobe was digested using 0.5 mg/mL collagenase D (Roche Diagnostics, Mannheim, Germany), 50 U/mL DNAse I (Sigma Aldrich, St. Louis, USA) in RPMI 1640 (Gibco, Grand Island, USA) supplemented with 10% heat-inactivated FBS (Gibco, Grand Island, USA) preheated to 37 °C. The lung was left to digest for 30 min at 37 °C before being diced into small (~1–2 mm) sections and pushed through a cell strainer (Corning, Corning, USA). The cell strainer was rinsed with RPMI 1640 with 10% heat-inactivated FBS before being centrifuged and resuspended for use in Flow Cytometry. For the histological mice, the lung was inflated with 0.7 mL of a 1:1 OCT:PBS mixture before being flash frozen via liquid nitrogen in an OCT block.

Flow cytometry

BALF and post-digested lungs were centrifuged at 1,500 rpm before being resuspended in 100 µL of a 1:50 dilution of Mouse BD FC block (BD Pharmingen, San Jose, USA; Clone 2.4G2) in FACS Buffer. Cells were stained using fluorescent antibodies: anti-CD45 FITC (BioLegend, San Diego, USA; Clone 30-F11), anti-CD19 PE-Cy5 (eBioscience, San Diego, USA; Clone MB19-

1), anti-CD3 Alexa Fluor 700 (BioLegend, San Diego, USA; Clone 17A2), anti-Ly6G BV510 (BioLegend, San Diego, USA; Clone 1A8), anti-CD11b BV421 (BioLegend, San Diego, USA; Clone M1/70), anti-CD11c PE-Cy7 (BioLegend, San Diego, USA; Clone N418) and anti-SiglecF APC (BioLegend, San Diego, USA; Clone S17007L). Samples were run on a MoFlo Astrios (Beckman Coulter, Carlsbad, USA). Gating and analysis were performed using FlowJo (Version 10.71, Ashland, USA). Note that the Figures show different Y-axis ranges in order to best illustrate the magnitude of the differences in cells recovered from lavage versus tissue; however, the absolute values are also presented in the text.

RNA extraction

RNA was extracted using TRIzol© (Ambion, Carlsbad, USA). Briefly, ~100 mg of frozen lung tissue was placed in a mortar, covered with liquid nitrogen, then ground into dust using a pestle before adding to TRIzol©. Chloroform was added, mixed and centrifuged. The aqueous phase was removed and mixed with isopropanol and centrifuged, leaving a pellet which was then washed 3× with 75% ethanol before drying at room temperature. The pellet was resuspended in DEPC-Treated water (Ambion, Austin, USA). Concentration and purity of RNA was checked via NanoDrop 2000 (Thermo Scientific, Carlsbad, USA).

NanoString analysis

Purified RNA was analyzed using an nCounter® Sprint Profiler (NanoString Technologies, Seattle, USA) with the nCounter® Mouse Immunology Panel according to manufacturer protocols. Gene expression was analyzed using the nSolver® 4.0 software (NanoString Technologies, Seattle, USA). Statistical analysis was done using nSolver® Advanced Analysis 2.0 (NanoString Technologies, Seattle, USA); false discovery rates (FDR) were calculated using the Benjamini-Hochberg method.

Differences in lung immune gene expression profiles (from nCounter® Mouse Immunology Panel) for each mouse sampled were analyzed using Principal Component Analyses (PCA) using the “prcomp” function in R version 4.0.3 (R version 4.0.3; R Core Team, 2020). Normalized and log transformed gene expression data matrices were constructed as data points were projected onto the 2-D plane, such that the variance is maximized. As dimensions were reduced, they spread out in two directions to explain most of the differences in the data. X-axes (labeled as PC1) in the ordination space represent the first principal component, which separates data points to represent the most variation in the dataset; y-axes (labeled as PC2) are orthogonal to PC1 and separate data points to represent the next greatest amount of variation within these gene expression datasets, across exposure types. We used the ggplot2 package and

the “stat ellipse” function, with 95% confidence intervals, to visualize these PCA plots in R (R version 3.2.1).

Histology

OCT embedded lungs were sectioned at 20 μm in a Cryostat. Sections were stored at −80 °C until staining. Before staining with H&E, slides were fixed with 4% PFA for 10 min. Histological images were taken using a Keyence BZ-X710 (Keyence Corporation of America, Itasca, USA).

Aerosol mass spectrometry

Chemical composition of aerosolized particles was measured by an HR-ToF-AMS[24]. Particles were generated using the same atomizer system as chamber exposures, as described by Peng et al. (2018)[23]. The outlet of our atomizer system was split into two ports, with one connected to the sampling inlet of the aerosol mass spectrometer (AMS) and the other venting through a HEPA filter. The Salton Sea and Pacific Ocean stock samples were diluted 10× with MilliQ water to generate particles at suitable concentrations. Alternaria solutions were the same concentrations as those used in chamber exposures. ToF-AMS Analysis Toolkit 1.57 and PIKA 1.16 on Igor Pro 6.36 were used in data processing.

Statistical analysis

All statistical analysis was done using GraphPad Prism 6 (GraphPad, San Diego, USA). p-Value was calculated using the Mann-Whitney U test for nonparametric data. We analyzed multivariate homogeneity of group dispersions (variances) using PERMDISP2 procedures in the R package vegan, with the function “betadisper” in R. Euclidean distances between objects and group centroids were handled by reducing the original distances to principal coordinates. We used Tukey's Honest Significant Difference methods as “TukeyHSD.betadisper” to create 95% confidence intervals on differences between mean distance-to-centroids across exposures, as compared with mice in chambers containing control air.

Results

Control of exposure to aerosol particulate levels

To ensure consistent levels of simulated chronic environmental aerosol exposures, our environmental chamber system was set up to continuously monitor suspended aerosols by particulate size as well as steady-state mass concentrations. In this study, we performed exposure studies using aerosolized suspensions generated from aqueous solutions of Alternaria filtrate, Salton Sea water, and Pacific Ocean water. Mass concentrations of PM generated from different sources were stable over 7 days, with averaged mass concentrations

around 1500 μg m−3 (±10%; Fig. 3.1a). Average size distributions of the different types of PM were generated using the same atomizer system, under identical conditions (Fig. 3.1b). Only minor differences in average particle size were observed between samples; peak particle mobility diameter for Pacific Ocean PM was 79.1 nm; Alternaria PM was 88.2 nm, and Salton Sea PM was 94.7 nm. Because the injection method was consistent between each exposure, minor differences in PM size distribution were primarily due to composition differences of each aerosolized solution. Moreover, differences in particle densities were seen with higher “salty” PM densities, as compared to the “organic” PM (Alternaria PM 1.36 g cm−3 < Pacific Ocean PM 1.96 g cm−3 < Salton Sea PM 2.07 g cm−3). Importantly, a majority of PM was either fine (PM with a diameter between 0.1 μm–2.5 μm) or ultrafine (PM with a diameter of less than 0.1 μm), with the vast majority of PM under 1 μm in mobility diameter. This is critical to consistent exposure effects, as ultrafine PM is expected to be able to travel deep into lung tissue down to the alveoli.

PM surface area has been proposed to be an important factor in studies on the health effects of PM on lungs. However, as all three types of PM used in this experiment were generated from aqueous solutions, with no inert components; the particles were – by their nature – highly water soluble. Accordingly, particle size could change within the lung due to the high relative humidity of the lung microenvironment[25]; therefore, for comparability across

different material exposures, we chose to control the total mass concentration of the different types of PM instead of total surface area.

Due to the complexity of multiple factors, including particle size and depth of penetration into lung tissue, as well as the extent of animal activity, age, or relative humidity fluctuation, it is difficult to estimate the actual dose of material deposited in the lung of a mouse over the course of a 7-day exposure. Since we maintained a target mass concentration in the chamber, with similar particle size distributions across each of three aerosol suspensions, we expect that particle suspensions of all three materials were delivered in similar fashion. Moreover, since the particles were all generated using aqueous solutions, it is likely that all particles coming into direct contact with lung tissue (i.e., alveolar or airway epithelium) will similarly fully dissolve and release their components to diffuse into the tissue.

PM chemical composition analysis by aerosol mass spectrometer

Since the aerosol suspensions of particles were all using aqueous solutions with no inert particulate matter, the biological impacts of the exposures are expected to be based on the release of soluble components of particulates into the tissue, rather than on the particulate physical properties. Thus, we determined the soluble composition of the aqueous solutions using AMS. There

was a large difference in the organic fraction between PM from the Salton Sea (5.9–6.6%), Pacific Ocean (12–20%) and the Alternaria (82%). Additionally, Alternaria PM had a notable fraction of NO3 (10%) compared to the others (<0.1%). Detectable levels of NH4 (1.01%) were only measured for the Alternaria PM. There were also key differences between the “salty” PMs (Salton Sea and Pacific Ocean). The Salton Sea PM was lower in organic content than the Pacific Ocean PM. In contrast, the fraction of metal ions and other inorganics were higher in the Salton Sea PM than in the Pacific Ocean PM (Fig. 3.1c).

Alternaria elicited allergic immune cell recruitment to lungs

To assess whether Salton Sea exposure can trigger allergic asthma, it was important to establish reference characteristics of a canonical allergic lung inflammation. Thus, we exposed C57BL/6 J mice to Alternaria alternata and Alternaria tenuis filtrate mixture (hereafter referred to as “Alternaria”) at a chamber mass concentration of approximately 1500 μg m−3 for 7 days. A group of mice were held in the exposure chamber, while a control group was simultaneously held in a parallel chamber that had only filtered air pumped into it. Following the exposure, BALF and lung tissues were assessed for inflammatory cell infiltration. H&E staining of the lung showed marked cellular infiltration around the airways compared to the controls (Fig. 3.2a), indicating an inflammatory response to the Alternaria. Additionally, there was a significant

increase in the number of cells in the BALF (1.7 × 106 ± 2.7 × 105 vs. 2.5 × 105 ± 4.9 × 104 control, $p < 0.0001$; Fig. 3.2b) compared to the controls.

Figure 3.2: Inflammatory cell recruitment due to *Alternaria* aerosols. Mice were exposed to either filtered control air or aerosolized *Alternaria* filtrate for 7 days in dual environmental chambers. Following exposure, bronchoalveolar lavage fluid (BALF) was collected and the left lobe was digested and analyzed via flow cytometry. **(A)** Lungs inflated with a 1:1 OCT:PBS solution and frozen in OCT blocks were sectioned and stained with H&E. (*, Interstitial infiltrate). **(B)** Total cells in the BALF were counted via hemocytometer (Left, Control air, n = 9; Right, *Alternaria*, n = 10). **(C–F)** Cells were represented as a percentage of $CD45^+$ cells in digested lungs or BALF. Representative dot plots for control air and *Alternaria* exposed are shown. Eosinophils are $CD45^+CD11c^-SiglecF^+$ (Left diagram: Left, Control air BALF, n = 9; Right, *Alternaria* BALF, n = 10; Right diagram: Left, Control Air Lung, n = 6, Right, *Alternaria* Lung, n = 6). Neutrophils are $CD45^+CD11b^+Ly6G^+$ (Left diagram: Left, Control air BALF, n = 9; Right, *Alternaria* BALF, n = 10; Right diagram: Left, Control air, n = 6, Right, *Alternaria,* n = 6). B cells are $CD45^+SSC^{low}CD19^+$ (Left diagram: Left, Control air BALF, n = 9; Right, *Alternaria* BALF, n = 10; Right diagram: Left, Control air, n = 6, Right, *Alternaria,* n = 6). T cells are $CD45^+SSC^{low}CD3^+$ (Left diagram: Left, Control air BALF, n = 9; Right diagram: Right, *Alternaria* BALF, n = 10; Left, Control air, n = 6, Right, *Alternaria,* n = 6). ** = $p < 0.01$; **** = $p < 0.0001$.

BALF cells were stained for analysis by flow cytometry to identify infiltrating inflammatory cells. The differential proportions of neutrophils (CD11b+, Ly6G+), eosinophils (CD11c−, Siglec F+), T cells (SSClow, CD3+), and B cells (SSClow, CD19+) were quantified as a proportion of CD45+ cells, with the remaining cells mainly being alveolar macrophages. Similar to our previous studies (Peng et al., 2018), the BALF of Alternaria exposed mice showed an expected increase in neutrophils (72.1 ± 11.1% vs. 0.2 ± 0.1% control, p <

0.0001; Fig. 3.2d) and eosinophils (8.3 ± 1.7% vs. ~0% control, $p < 0.0001$; Fig. 3.2c). T cells made up a higher, though small, percent of the BALF after Alternaria exposure (2.5 ± 0.4% vs 0.2 ± 0.1% control, $p < 0.0001$; Fig. 3.2f). B cells were essentially undetectable in the BALF (0.2 ± 0.1% vs. 0.2 ± 0.1% control; Fig. 3.2e).

Infiltrating inflammatory cells may be limited to the interstitial compartment of the tissue, and so might not be detected among lung lavage cells. Differences in BALF versus tissue infiltrating cells may also reveal differences in the way inflammatory cells are recruited as well as differences in their impact on tissue remodeling, which has a critical impact on airway resistance. Thus, tissue infiltrating cells were also isolated by enzymatic digestion of lung tissues and stained for analysis by flow cytometry. Interestingly, we found that while there were some similarities in the types of cells detected, the proportions of different infiltrating cell types were notably different. For example, the proportion of neutrophils in Alternaria exposed lungs, while higher than in the control lungs (21.8 ± 1.3% vs. 11.1 ± 1.8% control, $p < 0.01$; Fig. 3.2d), was nonetheless smaller than the 70% + proportion of neutrophils in the BALF. In the case of eosinophils, there also were low numbers of cells detected in controls; however, Alternaria-exposed lung actually showed a higher proportion in the digested tissue (12.3 ± 1.0% vs. 3.6 ± 0.3% control $p < 0.01$; Fig. 3.2c) compared to ~8.3% in the BALF. These contrasting ratios of neutrophils and eosinophils in

BALF versus digested tissue are consistent with the possibility that neutrophils may play a more important role in clearing microbes from alveolar and airway spaces, while eosinophils are more important in the interstitial spaces, where they may contribute to tissue remodeling.

Lymphocytes were also more easily detected in lung digests compared to BALF. T cells were higher in digested tissue (13.6 ± 0.9% vs. 13.9 ± 1.4% control) compared to BALF, but the Alternaria exposed lungs showed no significant difference compared to controls (Fig. 3.2f); an expected increase in recruited CD4 T cells21 was likely diluted by the infiltrating granulocytes. The percentage of B cells was also higher in digests (8.8 ± 0.6% vs. 17.4 ± 1.0% control, $p < 0.01$) than in BALF, but the proportion of B cells detected in exposed lungs was decreased relative to controls, also possibly due to the increased proportion of granulocytes (Fig. 3.2e).

Response to Salton Sea and Pacific Ocean water

With the inflammatory response to Alternaria exposure as a reference, we exposed mice to filtered and aerosolized Salton Sea water. Exposures were performed using water samples collected at different times and sites at the Sea, but all exposures were performed at a similar mass concentration. Following the exposures, mice were analyzed in the same manner as the Alternaria exposure.

In contrast to the picture in Alternaria exposed mice, the lungs from mice exposed to aerosolized Salton Sea water did not contain granulocyte recruitment in either the BALF or digested lung tissue. Moreover, H&E stained lung sections (Fig. 3.3a) showed no evidence for cellular recruitment after exposure to aerosolized Salton Sea water. Total BALF cell counts also showed no differences between exposure and control (5.2 × 105 ± 1.6 × 105 vs. 3.8 × 105 ± 7.9 × 104 control; Fig. 3.3b). Flow cytometry analysis of digested lung tissue revealed minimal inflammatory cell recruitment: eosinophils (3.7 ± 0.6% vs. 2.4 ± 0.5% control; Fig. 3.3c), neutrophils (12.2 ± 1.2 vs. 15.3 ± 2.7% control; Fig. 3.3d), and T cells (10.7 ± 0.7% vs. 10.2 ± 0.8% control; Fig. 3.3f) showed no significant differences. Interestingly, B cells in digested lung tissue were increased after exposure to the Salton Sea water (18.5 ± 1.5% vs. 12.3 ± 0.7% control, $p < 0.05$; Fig. 3.3e). All four cell types were essentially not present in the BALF (data not shown).

Figure 3.3: **Inflammatory cell recruitment due to Salton Sea and Pacific Ocean aerosols.** Mice were exposed to filtered control air, filtered and aerosolized Salton Sea water, or filtered and aerosolized Pacific Ocean water for 7 days. BALF was collected and tissue was digested for flow cytometry. **(A)** Lungs were inflated with a 1:1 OCT:PBS mixture and frozen, sectioned and stained with H&E. **(B)** Total cells in the BALF were counted via hemocytometer (Left diagram: Left, Control air, n = 8; Right, Salton Sea, n = 9; Right diagram: Left, Control Air, n = 4; Right, Pacific Ocean, n = 6). **(C–F)** Digested lung was stained and analyzed via flow cytometry. Cells populations are represented as the percentage of $CD45^+$ cells. Representative dot plots for the control air, Salton Sea exposed, and Pacific Ocean exposed mice are shown. Aerosolized Salton Sea and Pacific Ocean exposed mice are compared to their contemporaneous controls. Eosinophils are $CD45^+CD11c^-SiglecF^+$ (Left diagram: Left, Control air, n

= 6; Right, Salton Sea, n = 6; Right Diagram: Left, Control air, n = 6; Right, Pacific Ocean, n = 6). Neutrophils are $CD45^{+}CD11b^{+}Ly6G^{+}$ (Left diagram: Left, Control air, n = 6; Right, Salton Sea, n = 6; Right Diagram: Left, Control air, n = 6; Right, Pacific Ocean, n = 6). B cells are $CD45^{+}SSC^{low}CD19^{+}$ (Left diagram: Left, Control air, n = 6; Right, Salton Sea, n = 6; Right Diagram: Left, Control air, n = 6; Right, Pacific Ocean, n = 6). T cells are $CD45^{+}SSC^{low}CD3^{+}$ (Left diagram: Left, Control air, n = 6; Right, Salton Sea, n = 6; Right Diagram: Left, Control air, n = 6; Right, Pacific Ocean, n = 6). * = $p < 0.05$.

To determine whether this response was due to unique characteristics of the Salton Sea spray particles or a general response to Sea spray, we exposed mice to aerosolized Pacific Ocean water, also collected at multiple dates. Communities living near the Pacific Ocean do not show the high asthma rates found near the Salton Sea, so any differences observed may provide clues to potential links between Salton Sea aerosols and asthma. Inflammatory cell recruitment from Salton Sea and Pacific Ocean exposures turned out to be very similar, as there was no difference in the BALF cell counts (3.8 × 105 ± 7.6 × 104 vs 2.6 × 105 + 3.3 × 104 control; Fig. 3.3b) nor increase in the percentage of tissue digest eosinophils (2.6 ± 0.3% vs. 2.8 ± 0.3% control; Fig. 3.3c), neutrophils (11.9 ± 2.7% vs. 16.8 ± 6.8% control; Fig. 3.3d), or T cells (15.5 ± 1.3% vs. 10.7 ± 1.4% control; Fig. 3.3f). Moreover, there was a similar significant increase in B cell percentage (21.1 ± 1.2% vs. 13.9 ± 1.9% control, $p < 0.05$; Fig. 3.3e). Once again, all four cell types were essentially absent in the BALF (data not shown).

Gene expression changes in the response to aerosols

While assays for cellular infiltrates and histological changes can reveal significant inflammatory responses to exposures, more subtle tissue responses were revealed from analyses of gene expression profiles. In these studies, we focused on a subset of immune-associated genes assayed using a panel of short sequence tag probes (NanoString). This method quantifies expressed genes by direct counting of hybridized tagged gene probes and includes a set of general "housekeeping gene" probes. As a set, this approach allowed broad internal normalization of the assayed gene expression profiles, which in turn enabled direct comparisons of different RNA profiles from different samples and studies. Principal Component Analysis (PCA) of gene expression profiles collapses the complex gene expression data sets and helps provide overall comparisons among individual mice in different treatment groups.

Our reference allergic inflammatory response to Alternaria exposure illustrates a reproducible and characteristic gene expression pattern, as seen by the distance between centroids from the control air group to the Alternaria group ($d = 19.84$) in this PCA ordination; we observed tight clustering within the control air group and Alternaria groups and clear differentiation between the groups in the PCA, despite multiple replicates (Fig. 3.4a). We identified 213 differentially regulated genes (FDR < 0.10) of which 166 were significantly upregulated vs 47 which were significantly downregulated (Fig. 3.4b). These genes are diverse in

function, but the strongest change in regulation falls into immune defense responses and chemokine production, consistent with the observed recruitment of inflammatory cells into the lung. Among the top 20 regulated genes are Ig receptors (Fcgr2b, Pigr, Fcgr3), chemokines (Cxcl3, Ccl9, Ccl8, Ccl3 Ccl22), immune regulatory genes (Tgfbi, Lilrb4, IL33, Ctss, Ptafr, Ctsc) and innate immune genes (Cfb, Muc1).

Figure 3.4: Gene expression changes due to *Alternaria* aerosol exposure. After a 7-day exposure to either filtered control air (n = 10) or *Alternaria* filtrate (n = 10), lung RNAs were analyzed for gene expression using a defined immunology gene panel (NanoString); **(A)** PCA of the gene expression data with red squares representing mouse lung immune gene expression profiles from individual animals exposed to aerosolized *Alternaria* sp., as compared to green circles, which are from mouse samples exposed to control air. **(B)** Volcano plot depicting the differential expression profile of the *Alternaria* exposed mice compared to a baseline of control air. The X-axis depicts the log2 fold change while the Y-axis depicted the -log10 (Benjamini-Hochberg adjusted p-value). The 40 most significant gene by Benjamini-Hochberg adjusted p-value are labeled.

By contrast, analysis of gene expression profiles from exposures to aerosolized Salton Sea water revealed a distinctively different pattern (Fig. 3.5a). The PCA shows an overall distinction between control air and Salton Sea exposed groups; however, the extent of these orthogonal axes did not explain as much of the variance, nor did they illustrate as great of a separation as was detected for the Alternaria exposures. Euclidean distance between centroids of control air and Salton Sea exposed groups (d = 3.08) within the PCA ordination was shorter than was found in the PCA for the Alternaria exposures.

Figure 3.5: Gene expression changes due to Salton Sea aerosol exposure. After a 7-day exposure to either filtered control air (n = 18) or aerosolized Salton Sea water (n = 17), lung RNAs were analyzed for gene expression using a defined immunology gene panel (NanoString). **(A)** PCA of the gene expression data with purple triangles representing mouse lung immune gene expression profiles from individual animals exposed to aerosolized Salton Sea water, as compared to green circles, which are from mouse samples exposed to control air. **(B)** Volcano plot depicting the differential expression profile of the aerosolized Salton Sea exposed mice compared to a baseline of control air. The X-axis depicts the log2 fold change while the Y-axis depicted the -log10 (Benjamini-Hochberg adjusted p-value). The 40 most significant gene by Benjamini-Hochberg (BH) adjusted p-value are labeled.

This exposure triggered significant gene expression changes, with 151 differentially expressed genes (Fig. 3.5b). Of these, 146 genes were significantly upregulated while only 5 were significantly downregulated (FDR < 0.10). The regulated genes were primarily associated with phosphorylation pathways (Jak1, Jak2, Jak3, Stat5b, Tnfrsf14), T cell activation (Ifnar1, Ifngr1), and NF-KB signaling (Ikbkb). Additionally, a preference toward MHC I/Th1 response predominates (Ifnar1, Ifngr1, Tap1), although there were some Th2-related receptors upregulated (Il6ra). It should be noted that the magnitude of gene expression changes, while statistically significant, were relatively small, with the vast majority (134 of the 146 upregulated genes) showing less than 0.5 Log2 fold change. Despite the lower magnitude changes, the regulated genes were consistent across replicate exposures and multiple Salton Sea samples, illustrated by the clustering of the Salton Sea data points relative to control data in the PCA.

As noted above, both Salton Sea and Pacific Ocean exposures induced some recruitment of B cells into lung tissue. Interestingly, this similarity was not seen in the gene expression profiles; in replicate studies with different Pacific Ocean samples, aerosolized Pacific Ocean exposed mice showed no significant changes in gene expression compared to controls (Fig. 3.S2). It is likely that if there were any induced genes related to B cell recruitment, they were not represented in the probe set used. More importantly however, these comparisons suggest that Salton Sea water exposures had a characteristic biological effect, unrelated to any general effect of exposure to sea water.

Our analysis of gene regulation in response to Alternaria versus Salton Sea exposures showed that each induced a reproducible and characteristic set of gene expression changes, with tight clustering within the groups and little intergroup overlap. Additionally, both Salton Sea and Alternaria produced responses distinct from the Pacific Ocean exposed mice (Fig. 3.6a). It is especially notable, however, that the Alternaria and Salton Sea exposures each induced strikingly different sets of genes (Fig. 3.6b; Pacific Ocean excluded due to a lack of differentially expressed genes). Of the 166 upregulated genes in Alternaria exposed mice and the 146 in the Salton Sea exposed mice, only 55 are upregulated in both. Even more notable is that of the 47 downregulated genes in the Alternaria exposed mice and 5 downregulated genes in the Salton

Sea exposed, only 1 was downregulated in both. Additionally, 13 genes which were upregulated in Salton Sea exposed mice were downregulated in Alternaria while 2 genes which were upregulated in Alternaria exposed mice were downregulated in mice exposed to aerosolized Salton Sea. Thus, while it appeared that both types of exposures regulated genes associated with at least some aspect of innate and adaptive immunity, their overall impacts were on rather different components of the immune or inflammatory response.

Figure 3.6: Comparisons between *Alternaria*, Salton Sea and Pacific Ocean exposures. Mice were exposed to either control air, *Alternaria*, or aerosolized Salton Sea for 7-days before lung tissue was collected. Extracted RNA was analyzed using a Mouse Immunology Panel (NanoString). **(A)** PCAs were generated using the "prcomp" function in R (version 4.0.3), to compare Pacific Ocean (blue stars), Salton Sea (purple triangles) and *Alternaria* (red squares) exposures, and visualized PCA as in Methods. Comparisons are made between *Alternaria* exposed mice (n = 10) and their contemporaneous controls (n = 10) or aerosolized Salton Sea exposed mice (n = 17) and their contemporaneous controls (n = 18). 213 genes were differentially regulated in the *Alternaria* comparison (FDR < 0.10), of which 166 were upregulated and 47 were downregulated. 151 genes were differentially regulated in the Salton Sea comparison (FDR < 0.10), of which 146 were upregulated and 5 were downregulated. 55 genes were upregulated in both comparisons, 1 gene was downregulated in both comparisons, 13 were upregulated in the Salton Sea comparison but downregulated in the *Alternaria* comparison while 2 were upregulated in the *Alternaria* comparison but downregulated in the Salton Sea comparison. 78 genes were uniquely upregulated, and 2 genes were uniquely downregulated in the Salton Sea comparison while 109 genes were uniquely upregulated and 33 were uniquely downregulated in the *Alternaria* comparison.

Discussion

The studies reported here were principally aimed at determining whether the aqueous components (which may include microbial components and toxins) in Salton Sea water might have effects on pulmonary tissues in response to chronic delivery into the lung as aerosolized particles. We found that aerosolized Salton Sea water was able to induce a distinct inflammatory gene expression profile despite a lack of cell recruitment to the BALF as well as neutrophil and eosinophil recruitment to the lung tissue. It is important to note that these studies do not test the biological effects of actual dust generated at the Salton Sea exposed playa; these effects are the subject of ongoing studies and will be reported separately. Since the impact of dust exposure among residents in the region is dependent on a variety of factors, including prevailing wind patterns, dust events, and proximity to the Salton Sea, such studies will need to take these other additional factors into account.

To investigate the effect that Salton Sea spray may have on the communities surrounding the Sea, we exposed C57BL/6 mice to approximately 1500 μg m−3 of aerosolized Salton Sea for 7 days. While this is meant to simulate a chronic exposure condition, there are still some limitations associated with our model. Residents surrounding the Salton Sea are exposed to variable levels of aerosols over a period of years, unlike the consistent 7-day exposure in our study. As perfectly matching both the exposure time and aerosol

concentration the residents are exposed to is impractical, we focused on a reasonable timeframe and aerosol concentration that showed demonstrable results. As this timeframe and concentration was sufficient to reliably induce large changes in Alternaria exposed mice and gene expression changes in Salton Sea exposed mice while the Pacific Ocean exposed mice showed no change, we believe our methodology is capable of providing real insights into the health effects of these aerosols. While direct measurement of airway hyperreactivity was beyond the scope of this study, our initial results call for future studies into this topic.

For this study, we used aerosols generated from filtered aqueous solutions. While this excluded the potential effects of larger inert dust particles, it allowed us to specifically focus on the effects of the dissolved components in the water. Separating the effects of the dissolved aqueous components and inert dust particles is critical as inert dust particles can have their own biological effects, including triggering of airway irritant receptors[26]. Additionally, larger dust particles (e.g., 1 μm or larger) may affect the delivery of soluble components carried on their surface, since they would not be as capable of penetrating deep into alveolar spaces. Exclusion of these larger particles was also important for generating a consistent PM (all PM in the study had a mobility diameter well under 1 μm); thus, particle size was unlikely to be a limiting factor for distribution. Effects due directly to minor differences in particle size are most likely negligible,

as exposure to Pacific Ocean water failed to induce gene expression changes, indicating that the specific composition of the aerosol is the primary driving agent for gene expression changes and cell recruitment. Our AMS breakdown was unable to pinpoint a broad category for reactive agents, as there was no consistent ratio between the composition and the effects. Thus, future studies should focus on specific components that may be present in the Salton Sea water. As we found some aspects of the NF-KB pathway upregulated (Ikbkb, RelA), care should be taken to investigate sources of reactive oxygen species (ROS). In particular, pesticides and heavy metal ions [16,12,27], both of which have been detected in the Salton Sea, should be investigated, as they are known to induce ROS[28,29].

The studies reported here are only among the first steps in studies identifying the potential aerosols contributing to lung disease in residents near the Salton Sea. The sea spray aerosols produced at the Salton Sea surface are certainly not the only contributor to inhaled aerosols and the proportions of other components in the inhaled aerosols may vary widely depending on the aggregation of sea spray among other ambient dust particles generated at the playa or more distant sources. Indeed, these studies should not be interpreted to suggest that Salton Sea water aerosols are the only source of potential aerosol toxins in the region. Also, actual exposures well depend on an individual's geographic position relative to the Salton Sea, seasonal winds, and other factors.

The main observation reported here is that soluble components of Salton Sea water are able to induce a unique pattern of gene expression changes in chronically exposed lungs, and that this pattern is strikingly distinct from the characteristic allergic inflammation induced by the common household fungal allergens in Alternaria filtrate. In the context of the observed high incidence of asthma in the Salton Sea region, our findings suggest that the Salton Sea water soluble components by themselves appear to induce significant lung responses, but they are clearly distinct from the characteristic allergic inflammatory responses typified by Alternaria exposures. However, the distinctive effect of Salton Sea exposures does not entirely rule out potential impacts on asthma. A number of receptors were significantly upregulated, including Il6r, CD97, Ifngr1 and Ifnar1. IL-6 is associated with IL-4 production, which is critical for Th2 differentiation[30]. The soluble form of Il6r has also been associated with asthma severity[31]. CD97 is a known costimulatory factor on CD4+ T cells[32]. In contrast to the previous receptors, Ifngr1 and Ifnar1 are associated with Th1 response. However, Th1-polarization has been linked to nonallergic asthma[33]. Additionally, our previous studies showed that Th1 inflammatory responses could not only co-exist with allergic Th2 inflammatory responses, they could show additive effects[34]. Salton Sea exposures also induced a number of genes associated with signaling pathways, such Jak1, Jak2 and Jak3. As these signaling pathways are known to have critical roles in pulmonary eosinophilia, airway hyperreactivity and mucus hypersecretion[35], upregulation of these components could potentially

provide additive or synergistic effects in the presence of other triggers, including environmental or household allergens.

Conclusion

Our results suggest two main points. First, Salton Sea exposure is unable to generate an inflammatory response similar to a potent allergen, as characterized in our study by Alternaria. However, aerosolized Salton Sea was able to trigger an inflammatory response distinct from a potent allergen, unlike aerosolized Pacific Ocean water, which did not trigger an inflammatory response. Thus, while Salton Sea spray may not be sufficient to generate asthma alone, it could play a key role in the progression to asthma or other inflammatory diseases. Future studies should explore the role of this inflammatory response in the context of the full range of aerosols to which the communities surrounding the Salton Sea are exposed.

Fig 3.S1: Gating strategy for flow cytometry. Lungs of mice were collected and digested after 7 days of a given exposure condition. The digested lungs were treated with BD FC Block in order to prevent nonspecific binding. Afterwards, the digested lung was stained with anti-$CD45^+$ FITC, anti-CD19 PE-Cy5, anti-CD3 Alexa Fluor 700, anti-CD11b BV421, anti-Ly6G BV510 or anti-SiglecF APC. The gating strategy used to identify different immune cell subpopulations are shown above. First, debris is gated out using SSC and FSC height. Following that, doublets are gated out using SSC area and SSC height. Then $CD45^+$ cells are selected. These $CD45^+$ cells are then subdivided into B cells (SSC^{low}, $CD19^+$), T cells (SSC^{low}, $CD3^+$), neutrophils ($CD11b^+$, $Ly6G^+$) and eosinophils ($CD11c^-$, Siglec F^+).

Fig. 3.S2. Gene expression changes due to Pacific Ocean aerosols. After a 7-day exposure to either filtered control air (n = 10) or aerosolized Pacific Ocean exposed (n = 10), lung RNAs were analyzed for gene expression using a defined immunology gene panel (NanoString). **(A)** PCA of the gene expression data with blue stars representing mouse lung immune gene expression profiles from individual animals exposed to aerosolized Pacific Ocean, as compared to green circles, which are from mouse samples exposed to control air. PCAs were generated as described in Methods. **(B)** Volcano plot depicting the differential expression profile of the aerosolized Pacific Ocean exposed mice compared to a baseline of control air. The X-axis depicts the log2 fold change while the Y-axis depicted the -log10 (Benjamini-Hochberg adjusted p-value). The 40 most significant gene by Benjamini-Hochberg adjusted p-value are labeled.

References

1. Bureau of Reclamation. “Lower Colorado Region | Bureau of Reclamation.” *Www.usbr.gov*, 29 Nov. 2022, www.usbr.gov/lc/region/programs/saltonsea.html
2. Carmichael, Wayne W, and RenHui Li. “Cyanobacteria Toxins in the Salton Sea.” *Saline Systems*, vol. 2, no. 1, 2006, p. 5, https://doi.org/10.1186/1746-1448-2-5
3. Xu, Elvis Genbo, et al. “Spatial and Temporal Assessment of Environmental Contaminants in Water, Sediments and Fish of the Salton Sea and Its Two Primary Tributaries, California, USA, from 2002 to 2012.” *Science of the Total Environment*, vol. 559, July 2016, pp. 130–140, https://doi.org/10.1016/j.scitotenv.2016.03.144
4. Zhou, Chuanqi, et al. “Effects of Selenite on Microcystis Aeruginosa: Growth, Microcystin Production and Its Relationship to Toxicity under Hypersalinity and Copper Sulfate Stresses.” *Environmental Pollution*, vol. 223, Apr. 2017, pp. 535–544, https://doi.org/10.1016/j.envpol.2017.01.056
5. Farzan, Shohreh F., et al. “Assessment of Respiratory Health Symptoms and Asthma in Children near a Drying Saline Lake.” *International Journal of Environmental Research and Public Health*, vol. 16, no. 20, 11 Oct. 2019, p. 3828, www.ncbi.nlm.nih.gov/pmc/articles/PMC6843482/

6. Environmental Health Hazard Assessment. “CalEnviroScreen 3.0.” *Ca.gov*, 2020, www.oehha.ca.gov/calenviroscreen/report/calenviroscreen-30

7. Bousquet, Jean, et al. “Asthma.” *American Journal of Respiratory and Critical Care Medicine*, vol. 161, no. 5, May 2000, pp. 1720–1745, https://doi.org/10.1164/ajrccm.161.5.9903102

8. Wark, P A B. “Asthma Exacerbations 3: Pathogenesis.” *Thorax*, vol. 61, no. 10, 1 Oct. 2006, pp. 909–915, www.ncbi.nlm.nih.gov/pmc/articles/PMC2104753/

9. Guarnieri, Michael, and John R Balmes. “Outdoor Air Pollution and Asthma.” *The Lancet*, vol. 383, no. 9928, 3 May 2014, pp. 1581–1592, www.ncbi.nlm.nih.gov/pmc/articles/PMC4465283/

10. U.S. Environmental Protection Agency. “Story Map Series.” *Www.arcgis.com*, www.arcgis.com/apps/MapSeries/index.html?appid=8fbf9bde204944eeb422eb3ae9fde76

11. Evan, Amato T. “Downslope Winds and Dust Storms in the Salton Basin.” *Monthly Weather Review*, vol. 147, no. 7, 14 June 2019, pp. 2387–2402, https://doi.org/10.1175/mwr-d-18-0357.1

12. Frie, Alexander L., et al. “Dust Sources in the Salton Sea Basin: A Clear Case of an Anthropogenically Impacted Dust Budget.” *Environmental*

Science & Technology, vol. 53, no. 16, 24 July 2019, pp. 9378–9388, https://doi.org/10.1021/acs.est.9b02137

13. Sinclair, Ryan, et al. “Asthma Risk Associated with Indoor Mold Contamination in Hispanic Communities in Eastern Coachella Valley, California.” *Journal of Environmental and Public Health*, vol. 2018, 15 Oct. 2018, pp. 1–7, https://doi.org/10.1155/2018/9350370

14. Bush, Robert K., and Jay J. Prochnau. “Alternaria-Induced Asthma.” *The Journal of Allergy and Clinical Immunology*, vol. 113, no. 2, 1 Feb. 2004, pp. 227–234, pubmed.ncbi.nlm.nih.gov/14767434/, https://doi.org/10.1016/j.jaci.2003.11.023

15. Salo, P, et al. “Exposure to Alternaria Alternata in US Homes Is Associated with Asthma Symptoms.” *Journal of Allergy and Clinical Immunology*, vol. 118, no. 4, Oct. 2006, pp. 892–898, https://doi.org/10.1016/j.jaci.2006.07.037

16. LeBlanc, Lawrence A., and Kathryn M. Kuivila. “Occurrence, Distribution and Transport of Pesticides into the Salton Sea Basin, California, 2001–2002.” *Hydrobiologia*, vol. 604, no. 1, 18 Mar. 2008, pp. 151–172, https://doi.org/10.1007/s10750-008-9316-1

17. Shaffo, Frances C., et al. “Mechanisms of Organophosphorus Pesticide Toxicity in the Context of Airway Hyperreactivity and Asthma.” *American Journal of Physiology - Lung Cellular and Molecular Physiology*, vol. 315,

no. 4, 1 Oct. 2018, pp. L485–L501, www.ncbi.nlm.nih.gov/pmc/articles/PMC6230874/

18. Li, Xinxiu, et al. “Chronic Exposure to Microcystin-LR Affected Mitochondrial DNA Maintenance and Caused Pathological Changes of Lung Tissue in Mice.” *Environmental Pollution*, vol. 210, 1 Mar. 2016, pp. 48–56, https://doi.org/10.1016/j.envpol.2015.12.001

19. Wang, Cong, et al. “The Toxic Effects of Microcystin-LR on Mouse Lungs and Alveolar Type II Epithelial Cells.” *Toxicon*, vol. 115, 1 June 2016, pp. 81–88, www.sciencedirect.com/science/article/pii/S0041010116300472?via%3Dihub, https://doi.org/10.1016/j.toxicon.2016.03.007

20. Fleming, Lora E., et al. “Aerosolized Red-Tide Toxins (Brevetoxins) and Asthma.” *CHEST*, vol. 131, no. 1, 1 Jan. 2007, pp. 187–194, journal.chestnet.org/article/S0012-3692(15)49898-8/fulltext, https://doi.org/10.1378/chest.06-1830

21. Zaias, Julia, et al. “Repeated Exposure to Aerosolized Brevetoxin-3 Induces Prolonged Airway Hyperresponsiveness and Lung Inflammation in Sheep.” *Inhalation Toxicology*, vol. 23, no. 4, Mar. 2011, pp. 205–211, https://doi.org/10.3109/08958378.2011.558936

22. Bernstein, Jonathan A., et al. “Cyanobacteria: An Unrecognized Ubiquitous Sensitizing Allergen?” *Allergy and Asthma Proceedings*, vol.

32, no. 2, 1 Mar. 2011, pp. 106–110, https://doi.org/10.2500/aap.2011.32.3434

23. Peng, Xinze, et al. “Establishment and Characterization of a Multi-Purpose Large Animal Exposure Chamber for Investigating Health Effects.” *Review of Scientific Instruments*, vol. 90, no. 3, 1 Mar. 2019, https://doi.org/10.1063/1.5042097

24. DeCarlo, Peter F., et al. “Field-Deployable, High-Resolution, Time-of-Flight Aerosol Mass Spectrometer.” *Analytical Chemistry*, vol. 78, no. 24, Dec. 2006, pp. 8281–8289, https://doi.org/10.1021/ac061249n

25. Löndahl, Jakob, et al. “Size-Resolved Respiratory-Tract Deposition of Fine and Ultrafine Hydrophobic and Hygroscopic Aerosol Particles during Rest and Exercise.” *Inhalation Toxicology*, vol. 19, no. 2, Jan. 2007, pp. 109–116, https://doi.org/10.1080/08958370601051677

26. Sellick, Hilary, and John Widdicombe. “Stimulation of Lung Irritant Receptors by Cigarette Smoke, Carbon Dust, and Histamine Aerosol.” *Journal of Applied Physiology*, vol. 31, no. 1, 1 July 1971, pp. 15–19, https://doi.org/10.1152/jappl.1971.31.1.15

27. D’Evelyn, S.M., et al. “Differential Inflammatory Potential of Particulate Matter (PM) Size Fractions from Imperial Valley, CA.” *Atmospheric Environment*, vol. 244, Jan. 2021, p. 117992, www.ncbi.nlm.nih.gov/pmc/articles/PMC7654835/

28. Abdollahi, Mohammad, et al. “Pesticides and Oxidative Stress: A Review.” *Medical Science Monitor: International Medical Journal of Experimental and Clinical Research*, vol. 10, no. 6, 1 June 2004, pp. RA141-147, pubmed.ncbi.nlm.nih.gov/15173684/

29. Leikauf, George D., et al. “Mechanisms of Ultrafine Particle-Induced Respiratory Health Effects.” *Experimental & Molecular Medicine*, 17 Mar. 2020, https://doi.org/10.1038/s12276-020-0394-0

30. Rincon, Mercedes, and Charles G. Irvin. “Role of IL-6 in Asthma and Other Inflammatory Pulmonary Diseases.” *International Journal of Biological Sciences*, vol. 8, no. 9, 2012, pp. 1281–1290, www.ncbi.nlm.nih.gov/pmc/articles/PMC3491451/?report=classic

31. Capasso, Melania, et al. “Costimulation via CD55 on Human CD4+ T Cells Mediated by CD97.” *The Journal of Immunology*, vol. 177, no. 2, 15 July 2006, pp. 1070–1077, https://doi.org/10.4049/jimmunol.177.2.1070

32. Capasso, Melania, et al. “Costimulation via CD55 on Human CD4+ T Cells Mediated by CD97.” *The Journal of Immunology*, vol. 177, no. 2, 15 July 2006, pp. 1070–1077, https://doi.org/10.4049/jimmunol.177.2.1070

33. Zoratti, Edward, et al. “Differentiating Asthma Phenotypes in Young Adults through Polyclonal Cytokine Profiles.” *Annals of Allergy, Asthma, & Immunology*, vol. 113, no. 1, 1 July 2014, pp. 25–30, https://doi.org/10.1016/j.anai.2014.04.013

34. Li, L., et al. “Th2-Induced Eotaxin Expression and Eosinophilia Coexist with Th1 Responses at the Effector Stage of Lung Inflammation.” *Journal of Immunology (Baltimore, Md.: 1950)*, vol. 161, no. 6, 15 Sept. 1998, pp. 3128–3135, www.ncbi.nlm.nih.gov/pubmed/9743380

35. Hoshino, A. “STAT6-Mediated Signaling in Th2-Dependent Allergic Asthma: Critical Role for the Development of Eosinophilia, Airway Hyper-Responsiveness and Mucus Hypersecretion, Distinct from Its Role in Th2 Differentiation.” *International Immunology*, vol. 16, no. 10, 31 Aug. 2004, pp. 1497–1505, https://doi.org/10.1093/intimm/dxh151

Acknowledgments

Research reported in this publication was supported by the National Institute On Minority Health And Health Disparities of the National Institutes of Health under Award Number U54MD013368. The content is solely the responsibility of the authors and does not necessarily represent the official views of the National Institutes of Health. The authors thank Mary Hamer, Director of the School of Medicine Research Instrumentation Core facility for assistance with flow cytometry data collection, Dr. Meera Nair for assistance in establishing flow cytometry parameters for lung cell populations and for helpful comments on the manuscript, and Mary Mercado for producing the graphical abstract.

Figures

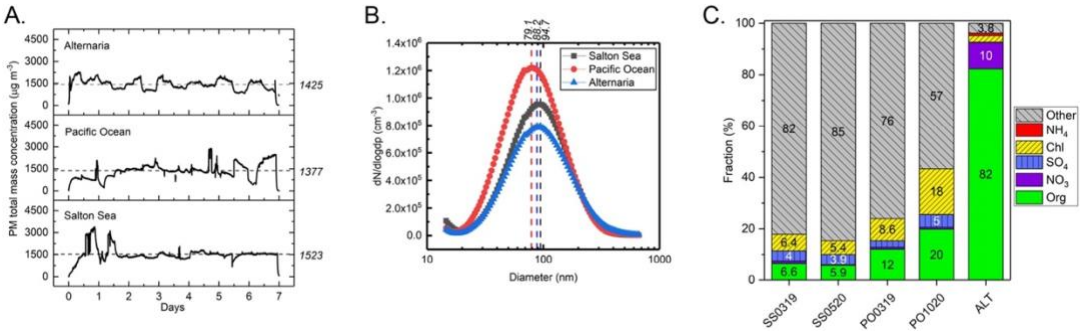

Figure 3.1 - Quantification of *Alternaria* (ALT), Pacific Ocean (PO) and Salton Sea (SS) aerosols. PM mass concentration was measured by a scanning mobility particle sizer. Chemical composition was determined by AMS. **(A)** PM mass concentration during 7-day exposure of SS, PO and ALT. Dash line shows the 7-day averaged mass concentration of PM. All units are in μg m^{-3}. **(B)** Averaged mobility diameter distribution of different PM used in exposure experiments. **(C)** Chemical composition of dry particulate matters generated from different materials collected in different season (mm/yr). Other includes metals (sodium, calcium, magnesium), trace metals and other inorganics. (Key: SS0319, Salton Sea/March 2019; SS0520, Salton Sea/May 2020; PO0319, Pacific Ocean/March 2019; PO1020, Pacific Ocean/October 2020; ALT, Alternaria filtrate).

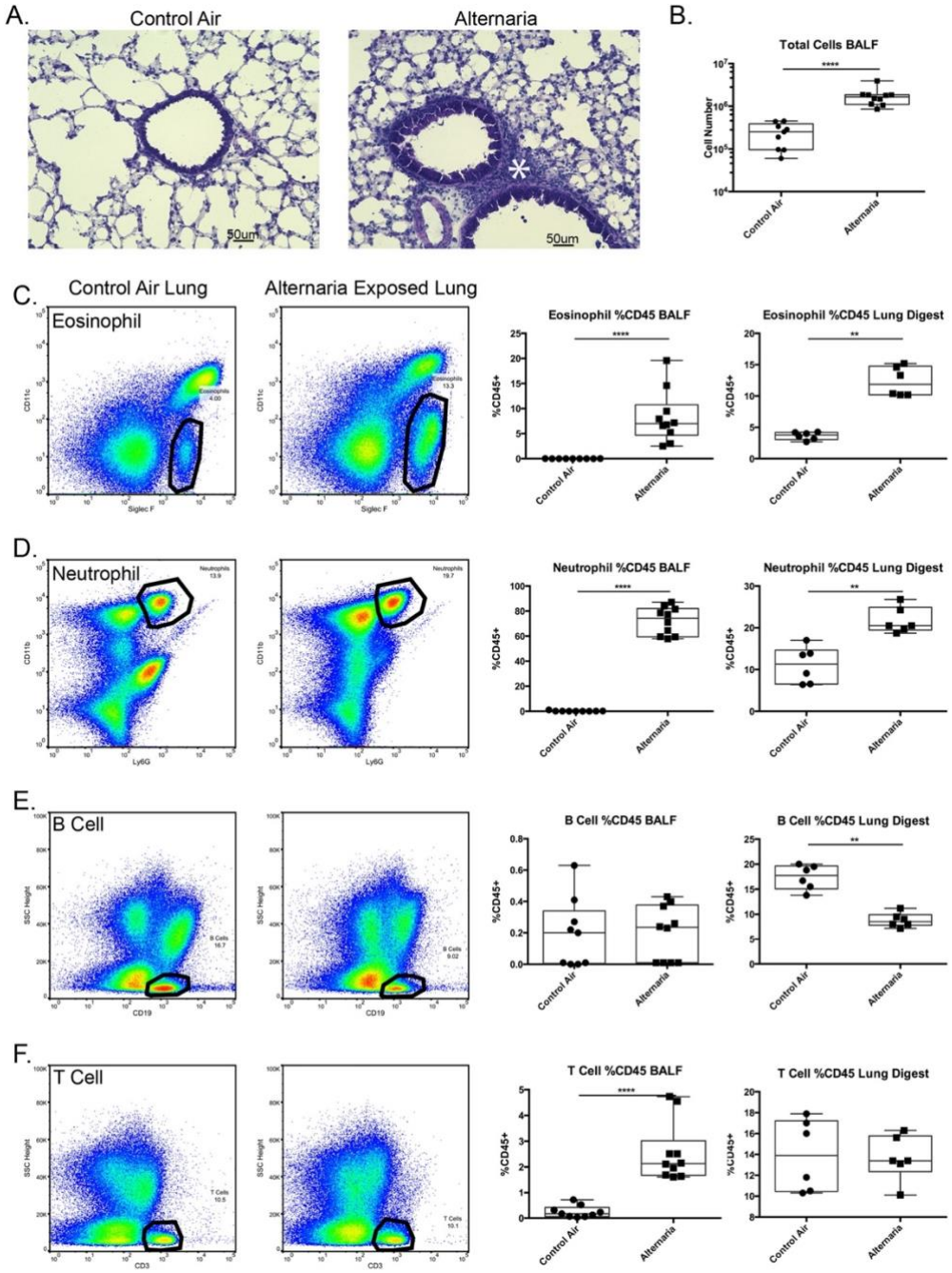
A.
Control Air
Alternaria
50um
50um
B.
Total Cells BALF
Cell Number
Control Air
Alternaria
C.
Control Air Lung
Alternaria Exposed Lung
Eosinophil
Siglec F
CD11c
Eosinophil %CD45 BALF
Eosinophil %CD45 Lung Digest
%CD45+
D.
Neutrophil
Ly6G
CD11b
Neutrophil %CD45 BALF
Neutrophil %CD45 Lung Digest
E.
B Cell
CD19
SSC Height
B Cell %CD45 BALF
B Cell %CD45 Lung Digest
F.
T Cell
CD3
T Cell %CD45 BALF
T Cell %CD45 Lung Digest

Figure 3.2 - Inflammatory cell recruitment due to *Alternaria* aerosols. Mice were exposed to either filtered control air or aerosolized *Alternaria* filtrate for 7 days in dual environmental chambers. Following exposure, bronchoalveolar lavage fluid (BALF) was collected and the left lobe was digested and analyzed via flow cytometry. **(A)** Lungs inflated with a 1:1 OCT:PBS solution and frozen in OCT blocks were sectioned and stained with H&E. (*, Interstitial infiltrate). **(B)** Total cells in the BALF were counted via hemocytometer (Left, Control air, n = 9; Right, *Alternaria*, n = 10). **(C–F)** Cells were represented as a percentage of $CD45^+$ cells in digested lungs or BALF. Representative dot plots for control air and *Alternaria* exposed are shown. Eosinophils are $CD45^+CD11c^-SiglecF^+$ (Left diagram: Left, Control air BALF, n = 9; Right, *Alternaria* BALF, n = 10; Right diagram: Left, Control Air Lung, n = 6, Right, *Alternaria* Lung, n = 6). Neutrophils are $CD45^+CD11b^+Ly6G^+$ (Left diagram: Left, Control air BALF, n = 9; Right, *Alternaria* BALF, n = 10; Right diagram: Left, Control air, n = 6, Right, *Alternaria,* n = 6). B cells are $CD45^+SSC^{low}CD19^+$ (Left diagram: Left, Control air BALF, n = 9; Right, *Alternaria* BALF, n = 10; Right diagram: Left, Control air, n = 6, Right, *Alternaria,* n = 6). T cells are $CD45^+SSC^{low}CD3^+$ (Left diagram: Left, Control air BALF, n = 9; Right diagram: Right, *Alternaria* BALF, n = 10; Left, Control air, n = 6, Right, *Alternaria,* n = 6). ** = $p < 0.01$; **** = $p < 0.0001$.

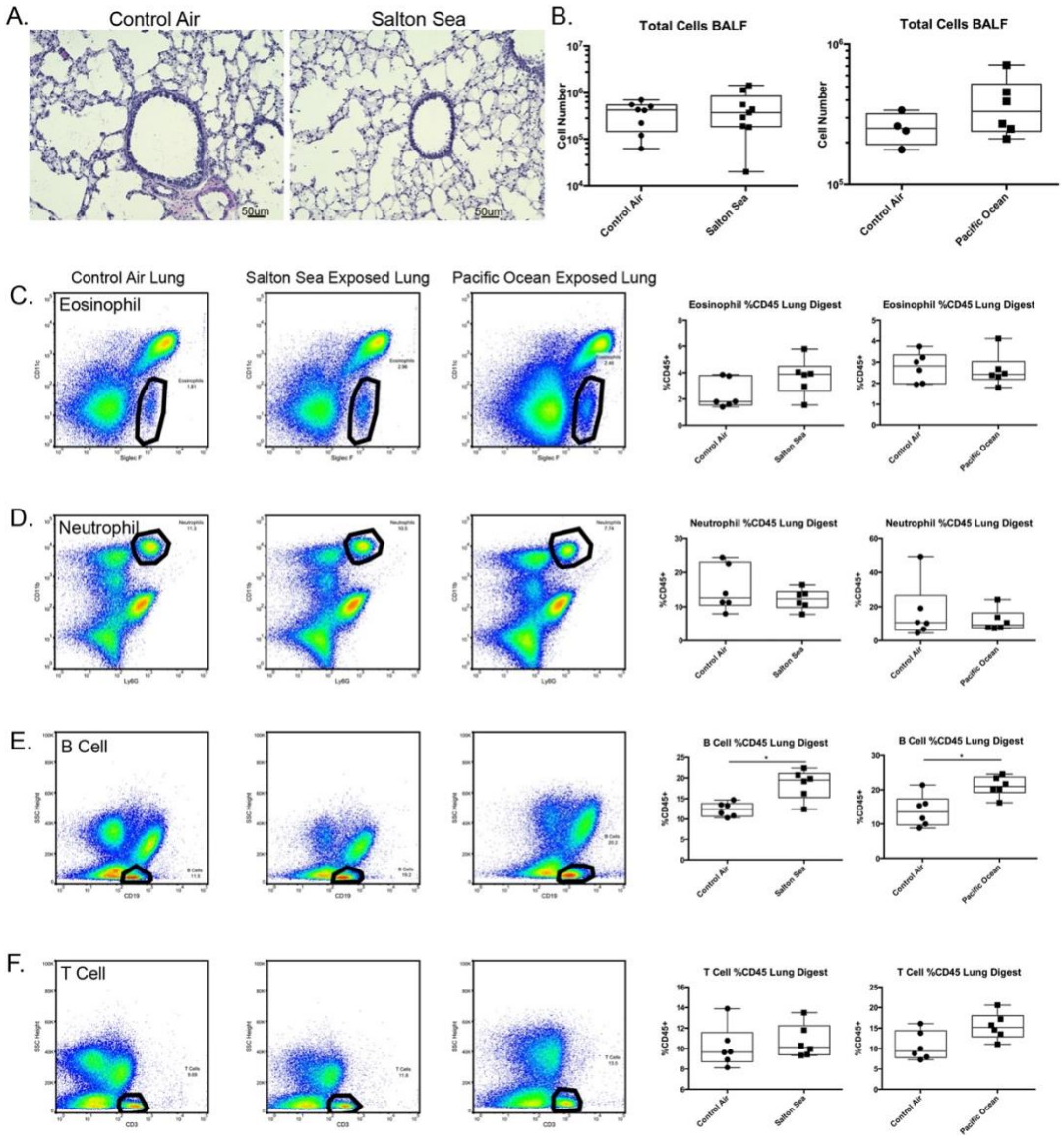

Figure 3.3 - Inflammatory cell recruitment due to Salton Sea and Pacific Ocean aerosols. Mice were exposed to filtered control air, filtered and aerosolized Salton Sea water, or filtered and aerosolized Pacific Ocean water for 7 days. BALF was collected and tissue was digested for flow cytometry. **(A)** Lungs were inflated with a 1:1 OCT:PBS mixture and frozen, sectioned and stained with H&E. **(B)** Total cells in the BALF were counted via hemocytometer (Left diagram: Left, Control air, n = 8; Right, Salton Sea, n = 9; Right diagram: Left, Control Air, n = 4; Right, Pacific Ocean, n = 6). **(C–F)** Digested lung was stained and analyzed via flow cytometry. Cells populations are represented as the percentage of $CD45^+$ cells. Representative dot plots for the control air, Salton

Sea exposed, and Pacific Ocean exposed mice are shown. Aerosolized Salton Sea and Pacific Ocean exposed mice are compared to their contemporaneous controls. Eosinophils are $CD45^{+}CD11c^{-}SiglecF^{+}$ (Left diagram: Left, Control air, n = 6; Right, Salton Sea, n = 6; Right Diagram: Left, Control air, n = 6; Right, Pacific Ocean, n = 6). Neutrophils are $CD45^{+}CD11b^{+}Ly6G^{+}$ (Left diagram: Left, Control air, n = 6; Right, Salton Sea, n = 6; Right Diagram: Left, Control air, n = 6; Right, Pacific Ocean, n = 6). B cells are $CD45^{+}SSC^{low}CD19^{+}$ (Left diagram: Left, Control air, n = 6; Right, Salton Sea, n = 6; Right Diagram: Left, Control air, n = 6; Right, Pacific Ocean, n = 6). T cells are $CD45^{+}SSC^{low}CD3^{+}$ (Left diagram: Left, Control air, n = 6; Right, Salton Sea, n = 6; Right Diagram: Left, Control air, n = 6; Right, Pacific Ocean, n = 6). * = $p < 0.05$.

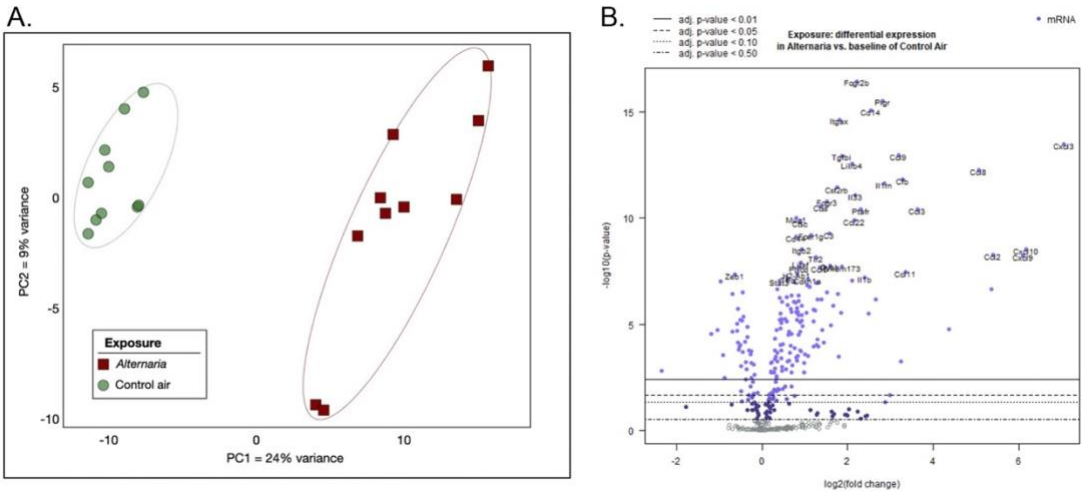

Figure 3.4 - Gene expression changes due to *Alternaria* aerosol exposure. After a 7-day exposure to either filtered control air (n = 10) or *Alternaria* filtrate (n = 10), lung RNAs were analyzed for gene expression using a defined immunology gene panel (NanoString); **(A)** PCA of the gene expression data with red squares representing mouse lung immune gene expression profiles from individual animals exposed to aerosolized *Alternaria* sp., as compared to green circles, which are from mouse samples exposed to control air. **(B)** Volcano plot depicting the differential expression profile of the *Alternaria* exposed mice compared to a baseline of control air. The X-axis depicts the log2 fold change while the Y-axis depicted the -log10 (Benjamini-Hochberg adjusted p-value). The 40 most significant gene by Benjamini-Hochberg adjusted p-value are labeled.

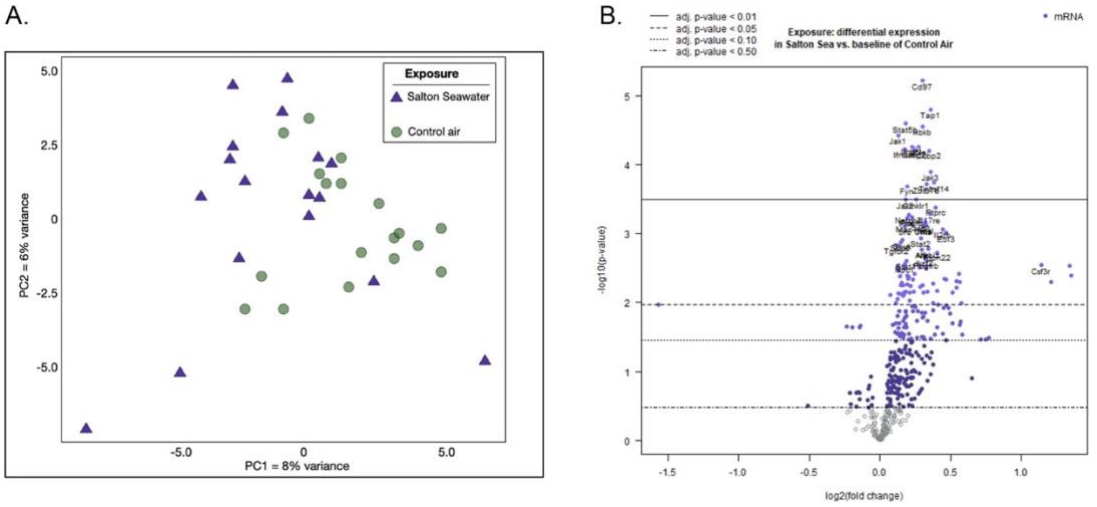

Figure 3.5 - Gene expression changes due to Salton Sea aerosol exposure. After a 7-day exposure to either filtered control air (n = 18) or aerosolized Salton Sea water (n = 17), lung RNAs were analyzed for gene expression using a defined immunology gene panel (NanoString). **(A)** PCA of the gene expression data with purple triangles representing mouse lung immune gene expression profiles from individual animals exposed to aerosolized Salton Sea water, as compared to green circles, which are from mouse samples exposed to control air. **(B)** Volcano plot depicting the differential expression profile of the aerosolized Salton Sea exposed mice compared to a baseline of control air. The X-axis depicts the log2 fold change while the Y-axis depicted the -log10 (Benjamini-Hochberg adjusted p-value). The 40 most significant gene by Benjamini-Hochberg (BH) adjusted p-value are labeled.

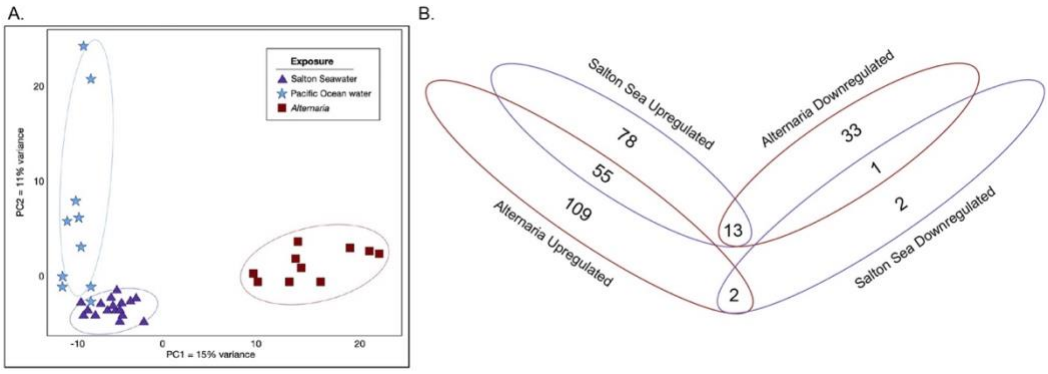

Figure 3.6 - Comparisons between *Alternaria*, Salton Sea and Pacific Ocean exposures. Mice were exposed to either control air, *Alternaria*, or aerosolized Salton Sea for 7-days before lung tissue was collected. Extracted RNA was analyzed using a Mouse Immunology Panel (NanoString). **(A)** PCAs were generated using the "prcomp" function in R (version 4.0.3), to compare Pacific Ocean (blue stars), Salton Sea (purple triangles) and *Alternaria* (red squares) exposures, and visualized PCA as in Methods. Comparisons are made between *Alternaria* exposed mice (n = 10) and their contemporaneous controls (n = 10) or aerosolized Salton Sea exposed mice (n = 17) and their contemporaneous controls (n = 18). 213 genes were differentially regulated in the *Alternaria* comparison (FDR < 0.10), of which 166 were upregulated and 47 were downregulated. 151 genes were differentially regulated in the Salton Sea comparison (FDR < 0.10), of which 146 were upregulated and 5 were downregulated. 55 genes were upregulated in both comparisons, 1 gene was downregulated in both comparisons, 13 were upregulated in the Salton Sea comparison but downregulated in the *Alternaria* comparison while 2 were upregulated in the *Alternaria* comparison but downregulated in the Salton Sea comparison. 78 genes were uniquely upregulated, and 2 genes were uniquely downregulated in the Salton Sea comparison while 109 genes were uniquely upregulated and 33 were uniquely downregulated in the *Alternaria* comparison.

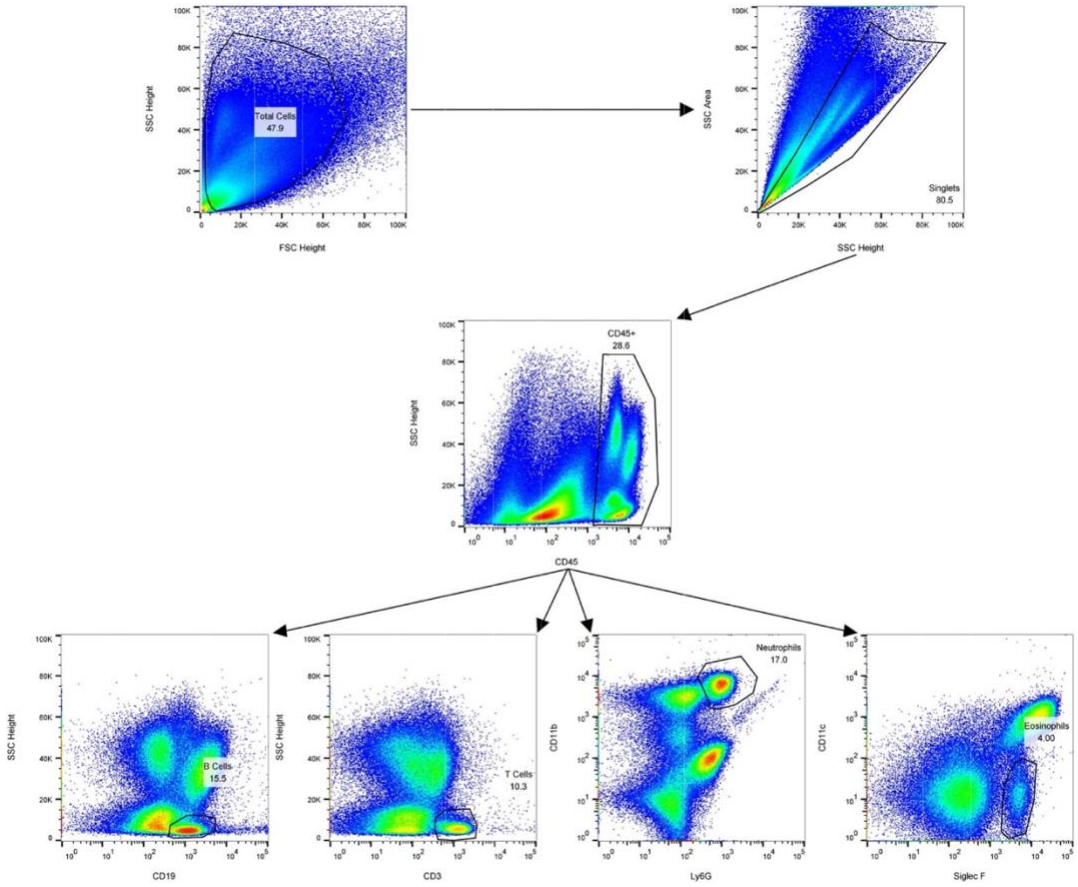

Figure 3.S1 - Gating strategy for flow cytometry. Lungs of mice were collected and digested after 7 days of a given exposure condition. The digested lungs were treated with BD FC Block in order to prevent nonspecific binding. Afterwards, the digested lung was stained with anti-$CD45^+$ FITC, anti-CD19 PE-Cy5, anti-CD3 Alexa Fluor 700, anti-CD11b BV421, anti-Ly6G BV510 or anti-SiglecF APC. The gating strategy used to identify different immune cell subpopulations are shown above. First, debris is gated out using SSC and FSC height. Following that, doublets are gated out using SSC area and SSC height. Then $CD45^+$ cells are selected. These $CD45^+$ cells are then subdivided into B cells (SSC^{low}, $CD19^+$), T cells (SSC^{low}, $CD3^+$), neutrophils ($CD11b^+$, $Ly6G^+$) and eosinophils ($CD11c^-$, Siglec F^+).

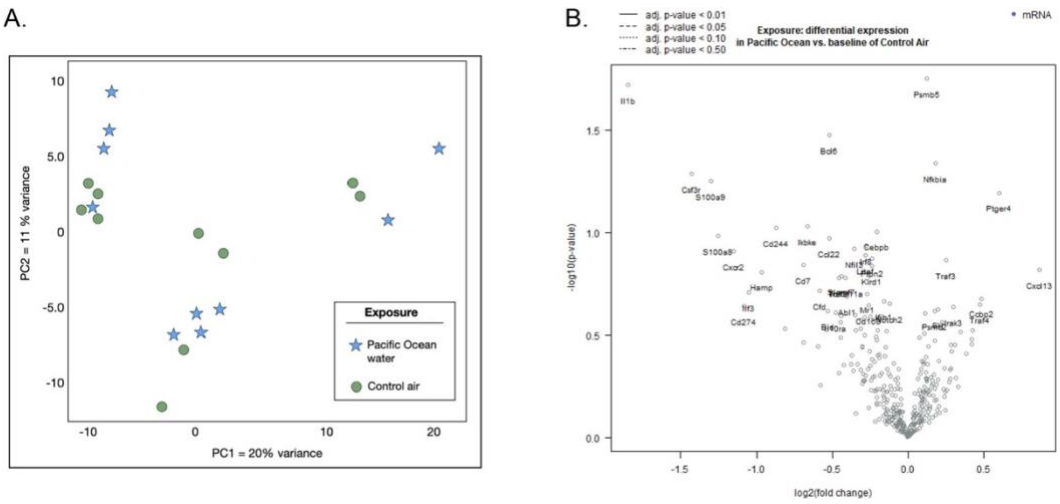

Figure 3.S2 - Gene expression changes due to Pacific Ocean aerosols. After a 7-day exposure to either filtered control air (n = 10) or aerosolized Pacific Ocean exposed (n = 10), lung RNAs were analyzed for gene expression using a defined immunology gene panel (NanoString). **(A)** PCA of the gene expression data with blue stars representing mouse lung immune gene expression profiles from individual animals exposed to aerosolized Pacific Ocean, as compared to green circles, which are from mouse samples exposed to control air. PCAs were generated as described in Methods. **(B)** Volcano plot depicting the differential expression profile of the aerosolized Pacific Ocean exposed mice compared to a baseline of control air. The X-axis depicts the log2 fold change while the Y-axis depicted the -log10 (Benjamini-Hochberg adjusted p-value). The 40 most significant gene by Benjamini-Hochberg adjusted p-value are labeled.

Chapter 4: Aerosolized Aqueous Dust Extracts Collected Near a Drying Lake Trigger Acute Neutrophilic Pulmonary Inflammation Reminiscent of Microbial Innate Immune Ligands

Abstract

In communities surrounding the Salton Sea, high rates of asthma are associated with high aerosol dust levels. However, the Salton Sea itself may play an additional role in pulmonary health. Therefore, to investigate a potential role of the Salton Sea on pulmonary health, we exposed mice to aerosolized Salton Sea water for 7 days and assessed tissue responses, including cellular infiltration and gene expression changes. For reference, mice were also exposed to aerosolized fungal allergen (Alternaria sp.) and Pacific Ocean aerosols. Exposure to aerosolized Alternaria sp. induced dramatic allergic inflammation, including neutrophil and eosinophil recruitment to the bronchoalveolar lavage fluid (BALF) and lung tissue. By contrast, Salton Sea “spray” induced only B cell recruitment to the lung tissue without increased inflammatory cell numbers in BALF. However, there were consistent gene expression changes suggestive of an inflammatory response. The response to the Salton Sea spray was notably distinct from the response to Pacific Ocean water, which induced some B cell recruitment but without an inflammatory gene expression profile. Our studies suggest that soluble components in Salton Sea water promote induction of a unique inflammation-associated response, though any relationship to asthma remains to be explored.

Introduction

The Salton Sea, a 345 mi2 body of water located in California's Coachella Valley and Imperial Valley, is a site of frequent high levels of dust. Already designated a nonattainment area for particulate matter smaller than 10 μm in aerosol diameter (PM10) and particulate matter under 2.5 μm in aerosol diameter (PM2.5)[1], dust in the region may soon worsen. Due to increasing temperatures and ongoing drought conditions, along with a 2003 ordinance shifting water away from the Sea, it has been estimated that 105,000 acres of additional playa will be exposed between 2003 and 2045[2], with the shoreline having retreated substantially between 1985 and 2020 (Fig. 4.1). Exposed playa has been linked to higher levels of dust in general[3,4,5,6], and, in particular, the dust in the Salton Sea Basin is estimated to increase by 11 % between 2018 and 2030[7] with changes in composition due to playa emissions[8].

Figure 4.1: Collection Sites and Changes in Exposed Playa Over Time. Map showing the 3 dust collection sites (Wister, Dos Palmas, Sonny Bono) from around the Salton Sea, along with the desert dust control collection site (Boyd Deep Canyon), playa collection site (Corvina Beach), and water collection site from Biddle et al., 2021 (Salton City). Map also shows the change in playa exposure between 1985 and 2020 due to evaporation of the Salton Sea.

Along with high levels of dust, the communities surrounding the Salton Sea have high levels of childhood asthma. Currently, the asthma rate among children is estimated at 20 %–22.4 %, which is among the highest in the state of California, and noticeably higher than the state average of 14.5 %[9]. Additionally,

the communities surrounding the Salton Sea are among the top percentile for emergency room visits due to asthma[10], though whether this is due to more severe asthma, lack of access to healthcare, high asthma rates, or a combination thereof is currently unknown.

Worryingly little is known about how the dust in the Salton Sea Basin may contribute to asthma and pulmonary disease. Asthma is generally defined as a disease of airway restriction, with an increase in airway hyperreactivity due to an allergen, along with immunoglobulin E (IgE) production, Th2 cytokine secretion and eosinophil recruitment[11]. Typically, asthma development is associated with childhood exposure to aeroallergens, which leads to the development of allergies[12, 13,14]. However, the exact mechanism for asthma development remain elusive, with risk factors including microbial exposure[15,16,17], genetic predisposition[18], and childhood viral and bacterial infections[19,20]. Other pulmonary diseases such as acute lung injury (ALI) instead preferentially recruit neutrophils[21]. Large dust storms, such as those in East Asia, have been linked to increased prevalence of respiratory diseases such as asthma[22,23,24], while organic dust from enclosed swine facilities has been shown to cause neutrophilic inflammation and oxidative stress[25]. Thus, dust can cause a variety of pulmonary disease; however, it is unclear how Salton Sea dust may be contributing, especially in a location which serves as a reservoir for agricultural runoff. Contaminants such as pesticides, herbicides, heavy metals, along with microbial

toxins, have been found in the Salton Sea[26,27,28]. We previously showed that aerosolized Salton Sea water is capable of inducing gene expression changes indicating a mild inflammatory genotype without overt inflammatory cell recruitment[29]. However, in that paper we had not examined the potential contributions of dust in pulmonary disease.

While there have been previous studies examining the toxic effects of dust from the Salton Sea Basin, these studies relied on a single collected site and either an in vitro model[30], or intranasal administration of whole dust without a control dust site[31]. As our study used an environmental exposure chamber to examine the potentially harmful effects of dust from multiple sites, including a desert dust control site, using an in vivo model while mimicking natural inhalation, we believe it offers a more robust and accurate look at dust as a source of pulmonary inflammation around the Salton Sea.

To understand the type of pulmonary inflammation caused by Salton Sea dust extracts, we used the aforementioned environmental exposure chamber, flow cytometry, and whole lung tissue gene expression. The inflammatory cell recruitment to the airways and lung tissue, along with changes in gene expression, were analyzed at either a 48-h or 7-day timepoint. Dust exposed mouse samples were compared to well established acute, innate inflammatory agents lipoteichoic acid (LTA), lipopolysaccharide (LPS), and the chronic,

adaptive inflammatory allergen Alternaria to determine where the dust extracts fall along these axes.

Materials and methods

Sample collection

At each of four sites, we collected dust using passive collectors; our collectors consisted of a modified round bundt pan (Nordic Ware, Minneapolis, MN, USA) coated with Teflon (25.4 cm in diameter), which was lined with Kevlar mesh (Industrial Netting, Maple Grove, MN, USA), as described in Aciego et al.[32] and Maltz et al.[33]. Glass marbles were suspended from the bottom and rested atop the mesh within the pan. Pans were fitted with overarching cross-braced strapping, which was covered in bird repellent (Bird-X, Elmhurst, IL, USA) to deter bird visitation or roosting. All pans, marbles, and mesh were acid washed in 2 M HCl, with rinses of 18.2 M Ω water between each reagent cleaning step, prior to deployment or contact with any dust. We deployed each of our collectors atop wooden posts, 2 m above ground level, within open canopy locations at each field site; this minimized the contribution of local dust inputs from nearby vegetation and local saltation.

On August 14th, 2020, we deployed these passive dust collectors at the “Boyd Deep” site, located in the Boyd Deep Canyon Reserve of the University of California (20 miles from the northwest border of the Salton Sea shoreline; see

Supplemental Table 4.1). On August 30th, 2020, dust collectors were deployed at the “Sonny Bono” site, Sonny Bono Salton Sea National Wildlife Refuge, the “Wister” site, in the Wister Unit of the Imperial Wildlife Area, and the “Dos Palmas” site, in the Dos Palmas Preserve of the Bureau of Land Management. There was a second deployment at the “Wister” site starting on September 18th, 2021. These three sites are located at distances of 0.6, 2.0, and 4.0 miles from the nearest border of the Salton Sea lakebed, respectively (Supplemental Table 4.1; Fig. 4.1). After 81 days (for 2021 Wister dust), 55 days (for Boyd Deep Canyon dust), or 41 days (for Sonny Bono, 2020 Wister, Dos Palmas dust) these dust collectors were taken down, sealed in sterile Whirl-pak collection bags (Nasco, Madison, WI, USA), and transported to the University of California Riverside for further processing. The sampling duration varied due to environmental conditions preventing access to remote areas, and other factors. The Boyd Deep Canyon Site was chosen as a control site as the mountain range protected the site from winds blowing over the Salton Sea. The Sonny Bono, Wister, and Dos Palmas sites were chosen based to give an idea of the dust over several geographic sites near the exposed Salton Sea playa and based on availability of government permits and government lands on which to add the passive dust collectors.

To sample playa, we used sterilized putty knives and flat spatulas to scrape the top layer (3.0–5.0 mm) of playa from the muddy exposed surface at 1.0 m−2.0 m distances from the Salton Sea shoreline at Corvina Beach. From a

0.25 m2 plot, we slid large flat sterilized spatulas into playa material to sever the top layer of playa from the underlying sediment. We used the sterile putty knife to scrape this playa material into sterile Whirl-pak collection bags. Playa samples were frozen prior to subsequent transport and processing at the University of California Riverside.

Sample processing

To recover and archive dust samples from collectors across each of these date ranges, we used 18.2 M Ω water to extract the dust. We rinsed the marbles, mesh, and inner pan from each collector, using sterilized gloves to dislodge dust from these surfaces into the water suspension; we then removed the mesh and marbles and transferred the remaining water and dust suspension to acid-washed 1 L bottles (Nalgene Nunc International Corporation, Rochester, NY, USA; high density polyethylene; HDPE), for further processing and subsequent analyses.

All materials used for filtration and storage of samples were sterilized by acid washing, as described above. Frozen wet playa samples were weighed to 100 g and suspended into 1 L of 18.2 M Ω water within a beaker. Playa suspensions were mixed at the lowest speed on a stir plate at ambient temperatures and then filtered through autoclaved cheese cloth. We then filtered

our playa suspensions into glass funnels through autoclaved 5.0 μm filters (Millipore-Sigma, Burlington, MA, USA).

To ensure that the biological effects of the dust are dependent only on the components and not on physical effects of inert particles, we filtered all playa and dust suspensions into glass funnels through sterile 0.2 μm filters (47-mm diameter; Pall Supor 200 Sterile Grid filters, Pall Corporation, Port Washington, New York, USA) into collecting flasks. The remaining flow-through of playa (i.e., playa filtrate) was analyzed and subsequently used for mouse chamber exposures. Dust filtrates were frozen at a 45° angle in Fast Freeze Flasks, prior to lyophilization on a Labconco FreeZone 2.5 L − 50 °C benchtop freeze dryer (i.e., lyophilizer, Labconco Corp., Kansas City, MO, USA). Lyophilized dust filtrate was subsequently normalized by dust mass (mg) in an aqueous suspension for use in mouse chamber exposures.

Animals

All animal studies were done following the UCR institutional IACUC and NIH guidelines. Both male and female 8–9-week-old C57BL/6J mice were purchased from Jackson Labs, Sacramento and acclimated for one week in the University of California, Riverside SPF vivarium. After acclimation, mice were placed in an environmental exposure chamber for experimentation. Mice were kept 3–4 to a cage and allowed food and water ad libitum. A 12-hour day/night

cycle was provided. Exposure lasted for either 48-hours or 7 days. The 48-hour timepoint was chosen to reflect an acute innate response, while the 7-day timepoint was chosen as we found that Alternaria was capable of generating an allergic-type response by 7 days[29].

Chamber operation

Exposure studies were performed in dual 540 L animal chambers (an exposure chamber and a control chamber) developed as described in Peng et al. (2019) and as used in Biddle et al. (2021) [34,29]. The relative humidity, temperature, and atmospheric pressure were measured in both chambers, with ammonia selectively measured in some exposures to ensure consistent exposure conditions were maintained. Mice in the exposure chamber were continuously fed a mixture of dry filtered air (0.5–1 lpm) and aerosolized spray (dried by two in-line silica gel columns, 3.5–4.5 lpm). The PM was generated from solutions of Alternaria alternata and Alternaria tenuis filtrate (Greer Laboratories, Lenoir, NC, USA; 0.4 g/L), lipoteichoic acid (LTA) from Staphylococcus aureus (Sigma Aldrich, St. Louis, USA), Lipopolysaccharide (LPS) from Escherichia coli O55:B5 (Sigma Aldrich, St. Louis, USA), and playa or dust collected from various sites in the region near the Salton Sea (0.025–0.100 g/L). The aerosol sources for the exposure were each tested in advance in order to determine chemical composition (high-resolution time-of-flight aerosol mass spectrometer (HR-ToF-AMS), Aerodyne) and aerosol density (aerosol particle

mass analyzer (APM), Kanomax) to prepare the solutions to yield the targeted particle mass concentration. Sample aerosolization was accomplished by using a homemade nebulizer with silica-gel dryers[34]. Mice in the control chamber were given filtered dry air (5.0 lpm) only, with other conditions matching the exposure chamber, including bedding replacement, food and water supplies, and corresponding day/night cycle. Particulate matter was only monitored within the exposure chamber by a scanning mobility particle sizer (SMPS, including Series 3080 Electrostatic Classifier and Ultrafine Condensation Particle Counter 3776, TSI) to assist in maintaining stable PM concentration. The target PM concentrations were as follows: 750 μg/m3 for the Alternaria mixture, 150 μg/m3 for LTA, 1 μg/m3 for LPS, and 1500 μg/m3 for environmental samples. Alternaria, LTA, and LPS doses were set at levels that promoted inflammatory cell recruitment without an accompanying cytokine storm (data not shown). The environmental sample concentration was similar to our previous studies in Biddle et al. (2021)[29], where 1500 μg m−3 of water from Salton City was capable of inducing differential gene expression in the lungs by 7-days of exposure. For each exposure (n = 6–12), we used an equal number of male and female mice. Each exposure had a control air cohort that matched the number and sex of the exposure group. Mice were kept in the chamber for either 48-h or 7-days depending on the study.

Animal processing

After either 48 h or 7-days, the mice were removed from the environmental exposure chamber. They were then anesthetized using isoflurane and euthanized by cervical dislocation. Bronchoalveolar lavage fluid (BALF) was collected by flushing the lungs 3 times with 0.8 mL of PBS. Afterwards, the lungs were dissected out for digestion or RNA extraction. The right lung lobes were flash frozen in liquid nitrogen and kept at –80 °C until RNA extraction. The left lobe minced into small (∼1–2 mm) sections and digested using 0.5 mg/mL collagenase D (Roche Diagnostics, Mannheim, Germany) and 50 U/mL DNase I (Sigma Aldrich, St. Louis, USA) in RPMI 1640 (Gibco, Grand Island, USA) fortified with 10 % heat-inactivated FB (Gibco, Grand Island, USA) preheated to 37 °C. After incubating 30 min at 150 rpm in 37 °C, the lung was agitated using an 18-gauge needle and incubate for another 15 min under the same conditions. Following digestion, the lung was pushed through a 100 μm cell strainer (Corning, Corning, USA). The cell strainer was then washed with RPMI 1640 with 10 % heat-inactivated FBS before centrifugation and resuspension for use in flow cytometry.

Some mice were set aside for histology. After being anesthetized and euthanized, the lungs were inflated using 0.7 mL of a 1:1 OCT: PBS mixture. The whole lungs were excised, placed into OCT, and flash frozen in liquid nitrogen before being stored at −80 °C until further processing.

Histology

OCT embedded lungs were sectioned at 15 µm in a Cryostat. Sections were stored at −80 °C until staining. Before staining with H&E, slides were fixed with 4 % PFA for 10 min. Histological images were taken using a Keyence BZ-X710 (Keyence Corporation of America, Itasca, USA).

Flow cytometry

BALF and post-digested lungs were centrifuged at 1500 rpm before resuspension in 100 µL of a 1:100 dilution of Zombie Yellow™ dye (Biolegend, San Diego, USA). After staining, cells were washed in FACS Buffer, centrifuged, and resuspended in 100 µL of a 1:50 dilution of Mouse BD FC block (BD Pharmigen, San Joe, USA). Cells were then stained using the following fluorescent antibodies: anti-CD45 FITC (BioLegend, San Diego, USA; Clone 30-F11), anti-CD19 Percp-Cy5.5 (eBioscience, San Diego, USA; Clone eBio1D3), anti-CD3 Alexa Fluor 700 (BioLegend, San Diego, USA; Clone 17A2) or anti-CD3 APC-Cy7 (BioLegend, San Diego, USA; Clone 17A2), anti-Ly6G BV510 (BioLegend, San Diego, USA; Clone 1A8), anti-CD11b BV421 (BioLegend, San Diego, USA; Clone M1/70), anti-CD11c PE-Cy7 (BioLegend, San Diego, USA; Clone N418) and anti-SiglecF APC (BioLegend, San Diego, USA; Clone S17007L).

Cells stained with Zombie Yellow™ dye were excluded from further analysis. Cell populations were determined using the following surface markers: neutrophils were CD45+CD11b+Ly6G+SiglecF−CD11c−, eosinophils were CD45+CD11b+SiglecF+CD11c−, T cells were CD45+CD3+SiglecF−CD11c−, and B cells were CD45+CD19+SiglecF+CD11c−

Samples were run on a NovoCyte Quanteon (Agilent Technologies, Santa Clara, USA). Gating and analysis were performed using FlowJo (Version 10.81, Ashland, USA).

RNA extraction

RNA was purified from the frozen right lung lobes using a TRIzol© (Ambion, Carlsbad, USA) based method. ~100 mg of frozen lung tissue (half of the right lobe) was placed in a mortar, frozen with liquid nitrogen, and ground into dust using a pestle. After, the ground lung tissue was placed in TRIzol©. Chloroform was added, and the solution was mixed and centrifuged. The surface aqueous phase was mixed with isopropyl alcohol and centrifuged. The RNA pellet was then washed 3 times with 75 % ethanol before drying at room temperature. This pellet was then resuspended in DEPC-Treated water (Ambion, Austin, USA). Concentration and purity of the RNA was checked via NanoDrop 2000 (Thermo Scientific, Carlsbad, USA).

NanoString analysis

50 ng of purified RNA was analyzed using an nCounter® Sprint Profiler (NanoString Technologies, Seattle, USA) with the nCounter® Mouse Immunology Panel according to manufacturer protocols. The nSolver® 4.0 software (NanoString Technologies, Seattle, USA) was used to normalize gene counts based on housekeeping genes and positive controls. Differential expression was calculated using the nSolver® Advanced Analysis 2.0 software (NanoString Technologies, Seattle, USA), and p-values were adjusted using the Benjamini-Hochberg method.

Normalized log2 gene counts and differential expression data were imported into R version 4.1.2 using readr and readxl and visualized using the ggplot2 package and the Khroma package. Principal Component Analyses were calculated using the normalized log2 gene count and the “prcomp” function. This data was visualized using the ggforitify package. Dendrograms were generated using the average log2 gene count for each type of exposure and the built-in hclust function using the Ward.D2 method. They were visualized as an unrooted dendrogram using the ape package.

Statistical analysis

Statistical analysis for inflammatory cell infiltration was done using GraphPad Prism 9 (GraphPad, San Diego, USA). P-value was calculated using

the Mann-Whitney U test for nonparametric data. Results shown include all mice, along with the average ± the standard error (SE). P-value for gene expression was calculated using nSolver® 4.0 and was false discovery rate (FDR) adjusted using the Benjamini-Hochberg method. A p-value of <0.05 and an FDR adjusted p-value of <0.1 were considered significant.

Results

Pulmonary inflammation due to Salton Sea dust extract compared to a desert dust extract control

To assess the biological effects of inhalation of these dusts in the Salton Sea region, we made aqueous extracts from collected dust, filtering out inert and larger particulate material. We injected suspensions of fine aerosols (~100 nm diameter) into an environmental chamber for chronic exposures of mice. In previous studies on exposure to aerosols generated from Salton Sea water ("sea spray"), the exposed lungs showed induction of sets of genes associated with low level immune activation; however, no active tissue inflammation (i.e., recruitment of inflammatory cells such as neutrophils, eosinophils, lymphocytes) was detected above background[29]. In striking contrast, in mice exposed for 7 days to aerosolized extracts from Salton Sea dust collected at the Imperial Wister Unit, there was infiltration by granulocytes around the major airways (Figure 4.2b). Additionally, there was dramatic recruitment of neutrophils in bronchoalveolar lavage fluid (BALF) (13.9 % ± 8.8 % vs 0.08 ± 0.04 %; Figure

4.2c). T cells were also preferentially recruited to the airways (2.4 ± 0.7 % vs 0.5 ± 0.2 %; Figure 4.2e), though B cells (Figure 4.2f) and eosinophils (Figure 4.2d) were not detected above background levels. Moreover, gene expression patterns were consistent with activation of acute immune inflammation (Figure 4.2h). The most highly expressed genes included several neutrophil chemokines (Cxcl3, Cf2rb), among other inflammatory chemokine (Ccl6, Ccl9). Additionally, several innate immune receptors

Figure 4.2: Pulmonary inflammation triggered by Salton Sea (Wister) Dust extract and by Desert (Boyd Deep Canyon) Dust extract. (A) 20× magnification H&E stain of lung tissue from mice exposed to Boyd Deep Canyon Dust extract. Insets are 60× magnification. **(B)** 20× magnification H&E stain of lung tissue from mice exposed to Wister Dust extract. Insets are 60× magnification. **(C)** Neutrophilic infiltration into the bronchoalveolar lavage fluid measured as a percentage of total immune cells (CD45+) as determined by flow cytometry. Neutrophil were defined as $CD45^{+}CD11b^{+}Ly6G^{+}SiglecF^{-}CD11c^{-}$. **(D)** Eosinophilic infiltration into the bronchoalveolar lavage fluid measured as a percentage of total immune cells (CD45+) as determined by flow cytometry. Eosinophils were defined as $CD45^{+}CD11b^{+}SiglecF^{+}CD11c^{-}$. **(E)** T cell infiltration into the bronchoalveolar lavage fluid measured as a percentage of total immune cells (CD45+) as determined by flow cytometry. T cells were defined as $CD45^{+}CD3^{+}SiglecF^{-}CD11c^{-}$. **(F)** B cell infiltration into the bronchoalveolar lavage fluid measured as a percentage of total immune cells (CD45+) as determined by flow cytometry. B cells were defined as $CD45^{+}CD19^{+}SiglecF^{+}CD11c^{-}$. All Boyd Deep Canyon Dust extract (*n = 4*) and Wister Dust extract (*n = 6*) exposed mice were compared to contemporaneous sex- and age-matched mice exposed to filtered house air. **(G)** Differential expression plot for Boyd Deep Canyon Dust extract exposed mice (*n = 6*) compared to contemporaneous sex- and age-matched mice exposed to filtered house air (*n = 6*). **(F)** Differential expression plot for Wister Dust extract exposed mice (*n = 9*) compared to contemporaneous sex- and age-matched mice exposed to filtered house air (*n = 9)*. Gene expression was measured by a Nanostring Sprint Profiler using the mouse immunology panel; analysis was done using the accompanying nSolver software and visualized using *ggplot2*. Labeled genes have a log2 fold change >1 or less than negative 1 and an Benjamini-Hochberg adjusted False Discovery Rate of

<0.01. * $p < 0.05$. ** $p < 0.01$. *p*-value determined using the Mann-Whitney *U* test for nonparametric data.

For comparison, exposure to extracts of dust collected at Boyd Deep Canyon, a site in the desert distant from the prevailing winds of the Salton Sea, showed no significant inflammation in either the lung tissue (Figure 4.2a), BALF (Figure 4.2c,d,e,f), nor a gene expression pattern indicative of active inflammation (Figure 4.2g). While there were some inflammatory chemokines upregulated (Cxcl3, Ccl9), they were approximately 25–50 % lower than in mice exposed to extract from around the Salton Sea. Additionally, control extracts failed to elicit upregulation in innate immune receptors or cytokines.

Comparison of 48-hour and 7-day timepoints for Salton Sea dust extract and reference microbial toxins LTA, LPS, and allergen Alternaria

Interestingly, although communities near the sea appear to suffer from a high incidence of asthma, the inflammatory response seen here did not show eosinophil recruitment nor Th2 gene regulation, which are hallmarks of allergic inflammation. This is not a limitation of the relatively short term (7d) aerosol exposure, as similar exposure to aerosols of the fungal allergen Alternaria produces robust allergic inflammation within 4 to 7 days [29,35]. Second, exposures of only 48 h induced the strongest neutrophil recruitment (63.9 ± 3.5 % vs 0.1 ± 0.03 % in the airways; Figure 4.3a; 41.2 ± 10.4 % vs 8.6 ± 0.6 % in the digested lung tissue; Figure 4.3c) with strong but slightly lower persistent inflammation

present after 7 days of exposure (Figure 4.3a) and no recruitment of eosinophils at either timepoint (Figure 4.3b,d). Allergic stimuli such as Alternaria tend to have a stronger response at 7 days, as 48 h does not appear to be enough to generate an adaptive response. Both neutrophilic and eosinophilic recruitment was greater at 7 days in Alternaria exposed mice (Figure 4.3a,b). Thus, material from dust at the Salton Sea induced strong pulmonary inflammation, but not the allergic profile more commonly associated with clinical asthma.

Figure 4.3: Changes from 48-h to 7-day timepoints for Salton Sea (Wister) Dust extract, *Alternaria*, LTA, and LPS exposed mice. (A) Neutrophil infiltration at 48-h and 7-days in the bronchoalveolar lavage fluid (BALF) as a percent of total immune cells (CD45+) for Wister Dust extract, *Alternaria*, LTA, and LPS exposed mice. **(B)** Eosinophil infiltration at 48-h and 7-days in the bronchoalveolar lavage fluid (BALF) as a percent of total immune cells (CD45+) for Wister Dust extract, *Alternaria*, LTA, and LPS exposed mice. **(C)** Neutrophil infiltration at 48-h and 7-days in the lung tissue as a percent of total immune cells (CD45+) for Wister Dust extract, *Alternaria*, LTA, and LPS exposed mice. **(D)** Eosinophil infiltration at 48-h and 7-days in the lung tissue as a percent of total immune cells (CD45+) for Wister Dust extract, *Alternaria*, LTA, and LPS exposed mice. Neutrophils were defined as $CD45^{+}CD11b^{+}Ly6G^{+}SiglecF^{-}CD11c^{-}$, while eosinophils were defined as $CD45^{+}CD11b^{+}SiglecF^{+}CD11c^{-}$. All timepoint and exposure combinations were compared to contemporaneous sex- and age-matched mice exposed to filtered house air. $n = 4–6$ **(E)** PCA plot showing the changes from the 48-h timepoints to 7-day timepoints for Wister Dust extract, *Alternaria*, LTA, and LPS exposed mice. PCA was generated using the *prcomp* function in R and visualized using *ggplot2*. Each point represents the average location of the specific timepoint and exposure combination on PC1 and PC2. Arrows highlight trend line from 48-h to 7-day for each exposure. $n = 6–9$. * $p < 0.05$, ** $p < 0.01$. p-value calculated using the Mann-Whitney U test for nonparametric data.

The kinetics and types of inflammatory cells recruited matched conventional patterns of responses to innate immune triggers such as LPS and

LTA, ligands for the innate receptors Toll-like receptor 4 (TLR4) and Toll-like receptor 2 (TLR2) respectively. These microbial components triggered strong, acute neutrophilic inflammation at 48-h; however, over the course of chronic 7-day exposure the inflammatory response was significantly attenuated. The attenuation over the course of 7 days for Salton Sea dust extracts and innate immune triggers vs the increasing response after exposure to allergen is also shown at the gene expression level. The average log2 fold change decreased in all three exposures, from 0.476 to 0.219 for Wister extract, 0.266 to 0.177 for LPS, and 0.243 to 0.191 for LTA but increased from 0.226 to 0.683 for Alternaria. By the 7-day timepoint, the Salton Sea dust extracts, LPS, and LTA had attenuated to the point that their gene expression patterns clustered closer to the mice given only filtered air while the allergic inflammation gene expression patterns in mice exposed to Alternaria were clearly distinct at 7-days (Figure 4.3e). This tendency towards resolution is not seen in an allergic model, as the Alternaria response matured over the course of 7 days.

Gene expression comparison of multiple Salton Sea collection sites

To confirm that neutrophil recruitment and innate immune activation were representative of the entire Salton Sea basin rather than specifically the Imperial Wister Unit, we exposed mice to dust extract collect from two additional sites around the Salton Sea, the Dos Palmas Preserve and Sonny Bono. As the response was higher at 48-h for dust extract from the Imperial Wister Unit, we

used this timepoint for analysis. We found that dust extract from these locations triggered neutrophil infiltration to the BALF and gene expression profiles (Figure 4.S1) consistent with dust collected from the Imperial Wister Unit. This gene expression profile clustered with the other innate immune triggers and the Alternaria mixture before maturation into a Th2 response (Figure 4.4a). By contrast, mice exposed to extracts of playa (dry exposed lakebed), one of the major potential sources of dust, failed to recruit significant neutrophil responses and showed few gene expression changes (Figure 4.S2), with only Marco and Il1a being significantly upregulated.

Figure 4.4: Gene expression comparisons for 48 h and 7-day timepoints. **(A)** PCA plot comparing Salton Sea Dust extract (Wister, Sonny Bono, Dos Palmas), Salton Sea Playa extract (Corvina Beach), LTA, LPS and *Alternaria* exposed mice at 48-h (*n = 6)*. **(B)** PCA plot comparing Salton Sea Dust extract (Wister), Desert Dust extract (Boyd Deep Canyon), LTA, LPS and *Alternaria* exposed mice at 7-days (*n = 6–9)*. PCA was generated using the *prcomp* function in R and visualized using *ggplot2*. **(C)** Dendrogram showing the relationship between Salton Sea Dust extract (Wister, Sonny Bono, Dos Palmas), Salton Sea Playa extract (Corvina Beach), LTA, LPS and *Alternaria* exposed mice at 48-h (*n = 6*). **(D)** Dendrogram showing the relationship between Salton Sea Dust extract (Wister), Desert Dust extract (Boyd Deep Canyon), LTA, LPS and *Alternaria* exposed mice at 7-days (*n = 6–9).* Dendrograms were generated using the log2 value for each gene averaged by the exposure. This average was then used with the hclust function (method = Ward.D2) and visualized using the *ape* package.

To better characterize the relationship between the chronic exposures, we performed a similar analysis using our 7-day exposures. We found that there was significant overlap between the control air and the Boyd Deep Canyon Dust extract exposed mice. LTA exposed mice, whom had the most significant

attenuation of inflammation by 7-days, also overlapped heavily with the control air. The LPS and Wister Dust extract exposed mice were distinct from the controls, but not to the extent of the Alternaria exposed mice. Thus, while LPS and Wister Dust do not have a maturation of the immune response by 7-days, they appear to have not fully resolved, indicating a potential for low-level inflammation over a longer time course (Figure 4.4b). It should be noted that LPS and Wister responses were distinct from each other, with minimal overlap. Thus, they are unlikely to be triggering inflammation through the same mechanism.

The relationship between the different exposures is summarized in the dendrograms in Figure 4.4c and d. For the 48-h exposures, the response to playa is at one end, with the majority of exposures on the other branch. The Wister dust has the longest branch, as it has the strongest response and is unique among the other exposures. The others are closely related, with minor separation. For the 7-day exposures, Alternaria is entirely separated from the other exposures. The control dust extract is on the opposite side from the innate immune-like responses, which all have little distinction from each other.

Discussion

The response to Salton Sea dust showed similarities to innate immune ligands LTA and LPS in the overall kinetics and patterns of gene induction. These responses started with high levels of neutrophil, but not eosinophil,

recruitment to the airways before decreasing to nonexistent (LTA) or minimal (LPS) levels by 7 days of continuous exposure, along with an attenuation of inflammatory gene expression. This is wholly distinct from an adaptive immune Th2 response to the allergen Alternaria which started with a low level of neutrophil recruitment before maturing into a stronger response highlighted by high levels of neutrophils, eosinophils, and an increase in genes related to Th2 responses. As the Salton Sea dust followed the kinetics of the innate immune ligands, it appears unlikely to be triggering an adaptive response.

Yet the effects of Salton Sea dust did not strictly match reference innate ligands. Salton Sea dust triggered neutrophil recruitment that was persistent for at least 7 days, which was not the case in mice exposed to LTA. Additionally, we found upregulation of TLR2 in our Salton Sea Dust exposed mice, but not in LTA or LPS exposed mice, indicating potential for exacerbation after dust exposure, even in the case of selective tolerance to the dust. All Salton Sea dusts induced persistent upregulation of Il1a through 7 days of exposure; no other 7-day exposure in our study induced significant upregulation of Il1a. Il1a has been associated with neutrophil recruitment by cigarette smoke, as well as promoting inflammatory cytokine release and inhibiting fibrotic extracellular matrix (ECM) release and healing by lung fibroblasts[36,37,38]. The persistent upregulation of Il1a could be a key culprit in the pattern of inflammation caused by chronic Salton Sea dust exposure and contribute to long term lung pathology without conforming

to either microbial toxin-driven innate nor adaptive immune patterns of immunity. This is important as other innate immune triggers such as LPS tend to attenuate and provide immune tolerance[39], which may not be the case in Salton Sea dust exposure (Fig. 4.4).

It is important to clarify that the patterns of inflammation compared in this study are similar to familiar innate immune triggers composed of microbial components (cell wall, endotoxin, etc.) that are not by themselves directly toxic, and are mediated instead through innate immune receptors such as TLR2 and TLR4. These should be viewed as rather distinct from the effects of actual microbial toxins (e.g., cyanotoxins, microbicidins, etc.), produced by a variety of microbes including both bacteria and algae. The effects of these types of toxins on lung inflammation are not within the scope of this study, and while Salton Sea water is known to have detectable levels of some cyanotoxins, it is not known if the cyanotoxins can aerosolize and cause pulmonary inflammation nor it is known whether Salton Sea dust contains harmful concentrations of these toxins[40]. However, studies have cited the potential impact of microbial toxins in triggering or exacerbating asthma symptoms when present in red tides[41],[42].

In addition to the ways that Salton Sea dust may directly cause pulmonary disease, the dust may interact with allergens to modify asthma development. Exposure to LPS during allergic sensitization to ovalbumin or house dust mite

can worsen Th2 asthma or shift it towards a corticosteroid resistant Th17-type asthma[43,44,45,46,47]. As Salton Sea dust triggers inflammation similar to LPS, it may work in similar ways. This would have significant implications for the communities surrounding the Salton Sea, as different forms of asthma require different treatments.

The similarity of the Salton Sea dust responses to innate immunity that can be triggered by “Pathogen-Associated Molecular Patterns” – that is, bacterial components such as endotoxin, cell wall, and other materials – raises the question of whether specific microbial species in the Salton Sea or accompanying playa dust are particularly pro-inflammatory in lungs. While a comprehensive microbiome analysis of the aeolian microbiota has yet to be published, several studies have analyzed the composition of the Salton Sea and the sediment. Proteobacteria, particularly Gammaproteobacteria and Alphaproteobacteria, make up the majority of the bacteria in the Salton Sea and in the sediment, followed by Bacteroidetes[48,49,50]. These types of bacteria are known major contributors to LPS in the gut[51], and can be carried on dust particles over large distances[52], indicating a potential source of microbial inflammatory substances, particularly LPS. Understanding the interplay between the water, playa and aeolian microbiota is likely critical to understanding the pulmonary inflammation due to Salton Sea Dust[53].

As our preparation method filters out whole bacteria, our results would be due to the products produced by the bacteria rather than an immune response towards the bacteria itself. The diverse bacteria and other microorganisms in the dust and playa samples we processed for these exposures produce a wide and diverse range of primary and secondary compounds. While our induced pulmonary inflammation results from dust extracts were similar to LPS, there were clear differences. Thus, while LPS may be a contributing compound to dust-driven pulmonary inflammation, it is unlikely to be the only factor.

Conclusion

In summary, our results provide insight into the pulmonary health effects of a drying terminal lake. The dust collected from around the Salton Sea was uniquely toxic when compared to desert dust collected from a location protected from the prevailing winds around the sea. While there is likely a unique ecology and contaminants to the Salton Sea Basin, we believe the more general features of the drying lake, associated aerosol dusts, and consequent health impact, has broad relevance to other regions plagued by chronic drought and drying lakes. These regions are unique as they have rapidly increasing levels of dust, which has the unique property of triggering high levels of pulmonary inflammation that is likely to worsen the pulmonary health of already vulnerable nearby communities. By understanding the inflammation triggered by the dust, the mechanisms behind the inflammation, and how it interacts with allergens and

allergic development, we may be better equipped to handle the negative health impacts of the dust and developed tailored strategies to address them.

Figure 4.S1: Dos Palmas and Sonny Bono Cell infiltration and Gene expression. (A) Neutrophilic infiltration into the bronchoalveolar lavage fluid in mice exposed to Dos Palmas Dust extract for 48-h measured as a percentage of total immune cells (CD45+) as determined by flow cytometry. **(B)** Neutrophilic infiltration into the bronchoalveolar lavage fluid in mice exposed to Sonny Bono Dust extract for 48-h measured as a percentage of total immune cells (CD45+) as determined by flow cytometry. Neutrophil were defined as $CD45^{+}CD11b^{+}Ly6G^{+}SiglecF^{-}CD11c^{-}$. All Dos Palmas Dust extract (*n = 4*) and Sonny Bono Dust extract (*n = 6*) exposed mice were compared to contemporaneous sex- and age-matched mice exposed to filtered house air. **(C)** Differential expression plot for Dos Palmas Dust extract exposed mice (*n = 6*) compared to contemporaneous sex- and age-matched mice exposed to filtered house air (*n = 6)*. **(D)** Differential expression plot for Sonny Bono Dust extract exposed mice (*n = 6*) compared to contemporaneous sex- and age-matched mice exposed to filtered house air (*n = 6*). Gene expression was measured by a Nanostring Sprint Profiler using the mouse immunology panel; analysis was done using the accompanying nSolver software and visualized using *ggplot2*. Labeled genes have a log2 fold change >1 or less than negative 1 and an Benjamini-Hochberg adjusted False Discovery Rate of <0.01. * $p < 0.05$. ** $p < 0.01$. *p*-value determined using the Mann-Whitney *U* test for nonparametric data. Average ± standard error shown.

Figure 4.S2: Response to Corvina Beach Playa. (A) Neutrophilic infiltration into the bronchoalveolar lavage fluid in mice exposed to Corvina Beach Playa extract for 48-h Neutrophil were defined as $CD45^{+}CD11b^{+}Ly6G^{+}SiglecF^{-}CD11c^{-}$. Corvina Beach Playa extract (*n = 4*) exposed mice were compared to contemporaneous sex- and age-matched mice exposed to filtered house air. **(B)** Differential expression plot for Corvina Beach Playa extract exposed mice (*n = 6*) compared to contemporaneous sex- and age-matched mice exposed to filtered house air (*n = 6*). Gene expression was measured by a Nanostring Sprint Profiler using the mouse immunology panel; analysis was done using the accompanying nSolver software and visualized using *ggplot2*. Labeled genes have a log2 fold change >1 or less than negative 1 and an Benjamini-Hochberg adjusted False Discovery Rate of <0.01. * $p < 0.05$. ** $p < 0.01$. p-value determined using the Mann-Whitney U test for nonparametric data. Average ± standard error shown.

References

1. US EPA, OAR. “Nonattainment Areas for Criteria Pollutants (Green Book).” *Www.epa.gov*, 14 Apr. 2016, www.epa.gov/green-book

2. Evan, Amato T. “Downslope Winds and Dust Storms in the Salton Basin.” *Monthly Weather Review*, vol. 147, no. 7, 14 June 2019, pp. 2387–2402, https://doi.org/10.1175/mwr-d-18-0357.1

3. Bullard, Joanna, et al. “Sub-Basin Scale Dust Source Geomorphology Detected Using MODIS.” *Geophysical Research Letters*, vol. 35, no. 15, 12 Aug. 2008, https://doi.org/10.1029/2008gl033928

4. Hossein Mardi, Ali, et al. “The Lake Urmia Environmental Disaster in Iran: A Look at Aerosol Pollution.” *The Science of the Total Environment*, vol. 633, 15 Aug. 2018, pp. 42–49, pubmed.ncbi.nlm.nih.gov/29573690/, https://doi.org/10.1016/j.scitotenv.2018.03.148

5. Reheis, Marith C. “Dust Deposition Downwind of Owens (Dry) Lake, 1991-1994: Preliminary Findings.” *Journal of Geophysical Research: Atmospheres*, vol. 102, no. D22, 1 Nov. 1997, pp. 25999–26008, https://doi.org/10.1029/97jd01967

6. Reynolds, Richard L., et al. “Dust Emission from Wet and Dry Playas in the Mojave Desert, USA.” *Earth Surface Processes and Landforms*, vol. 32, no. 12, 2007, pp. 1811–1827, https://doi.org/10.1002/esp.1515

7. Parajuli, Sagar P., and Charles S. Zender. “Projected Changes in Dust Emissions and Regional Air Quality due to the Shrinking Salton Sea.” *Aeolian Research*, vol. 33, Aug. 2018, pp. 82–92, https://doi.org/10.1016/j.aeolia.2018.05.004

8. Frie, Alexander L., et al. “The Effect of a Receding Saline Lake (the Salton Sea) on Airborne Particulate Matter Composition.” *Environmental Science & Technology*, vol. 51, no. 15, 21 July 2017, pp. 8283–8292, https://doi.org/10.1021/acs.est.7b01773

9. Farzan, Shohreh F., et al. “Assessment of Respiratory Health Symptoms and Asthma in Children near a Drying Saline Lake.” *International Journal of Environmental Research and Public Health*, vol. 16, no. 20, 11 Oct. 2019, p. 3828, www.ncbi.nlm.nih.gov/pmc/articles/PMC6843482/

10. California Office of Environmental Health Hazard Assessment. “CalEnviroScreen 4.0.” *CA.gov*, 2021, oehha.ca.gov/calenviroscreen/report/calenviroscreen-40.

11. Bousquet, Jean, et al. “Asthma.” *American Journal of Respiratory and Critical Care Medicine*, vol. 161, no. 5, May 2000, pp. 1720–1745, https://doi.org/10.1164/ajrccm.161.5.9903102

12. Anderson, Halie M., and Daniel J. Jackson. “Microbes, Allergic Sensitization, and the Natural History of Asthma.” *Current Opinion in*

Allergy & Clinical Immunology, vol. 17, no. 2, Apr. 2017, pp. 116–122, dx.doi.org/10.1097%2FACI.0000000000000338, https://doi.org/10.1097/aci.0000000000000338

13. Simpson, Angela, et al. “Beyond Atopy.” *American Journal of Respiratory and Critical Care Medicine*, vol. 181, no. 11, June 2010, pp. 1200–1206, https://doi.org/10.1164/rccm.200907-1101oc

14. Stoltz, D. J., et al. “Specific Patterns of Allergic Sensitization in Early Childhood and Asthma & Rhinitis Risk.” *Clinical & Experimental Allergy*, vol. 43, no. 2, 18 Jan. 2013, pp. 233–241, https://doi.org/10.1111/cea.12050

15. Ege, Markus J., et al. “Exposure to Environmental Microorganisms and Childhood Asthma.” *New England Journal of Medicine*, vol. 364, no. 8, 24 Feb. 2011, pp. 701–709, https://doi.org/10.1056/nejmoa1007302

16. Lynch, Susan V., et al. “Effects of Early-Life Exposure to Allergens and Bacteria on Recurrent Wheeze and Atopy in Urban Children.” *Journal of Allergy and Clinical Immunology*, vol. 134, no. 3, Sept. 2014, pp. 593-601.e12, https://doi.org/10.1016/j.jaci.2014.04.018

17. Stein, Michelle M., et al. “Innate Immunity and Asthma Risk in Amish and Hutterite Farm Children.” *New England Journal of Medicine*, vol. 375, no. 5, 4 Aug. 2016, pp. 411–421, https://doi.org/10.1056/nejmoa1508749

18. Chang, Jen-Chieh, et al. “Perinatal Gene-Gene and Gene-Environment Interactions on IgE Production and Asthma Development.” *Clinical and Developmental Immunology*, vol. 2012, 2012, pp. 1–9, https://doi.org/10.1155/2012/270869

19. Jackson, Daniel J., et al. “Wheezing Rhinovirus Illnesses in Early Life Predict Asthma Development in High-Risk Children.” *American Journal of Respiratory and Critical Care Medicine*, vol. 178, no. 7, Oct. 2008, pp. 667–672, https://doi.org/10.1164/rccm.200802-309oc

20. James, Kristina M., et al. “Risk of Childhood Asthma Following Infant Bronchiolitis during the Respiratory Syncytial Virus Season.” *Journal of Allergy and Clinical Immunology*, vol. 132, no. 1, July 2013, pp. 227–229, https://doi.org/10.1016/j.jaci.2013.01.009

21. Blázquez-Prieto, Jorge, et al. “The Emerging Role of Neutrophils in Repair after Acute Lung Injury.” *American Journal of Respiratory Cell and Molecular Biology*, vol. 59, no. 3, Sept. 2018, pp. 289–294, https://doi.org/10.1165/rcmb.2018-0101ps

22. Chen, Yong-Shing, et al. “Effects of Asian Dust Storm Events on Daily Mortality in Taipei, Taiwan.” *Environmental Research*, vol. 95, no. 2, June 2004, pp. 151–155, https://doi.org/10.1016/j.envres.2003.08.008

23. Kwon, Ho-Jang, et al. “Effects of the Asian Dust Events on Daily Mortality in Seoul, Korea.” *Environmental Research*, vol. 90, no. 1, Sept. 2002, pp. 1–5, https://doi.org/10.1006/enrs.2002.4377

24. Watanabe, Masanari, et al. “Correlation between Asian Dust Storms Worsening Asthma in Western Japan.” *Allergology International*, vol. 60, no. 3, 1 Jan. 2011, pp. 267–275, https://doi.org/10.2332/allergolint.10-oa-0239

25. Poole, Jill A., and Debra J. Romberger. “Immunological and Inflammatory Responses to Organic Dust in Agriculture.” *Current Opinion in Allergy and Clinical Immunology*, vol. 12, no. 2, Apr. 2012, pp. 126–132, https://doi.org/10.1097/aci.0b013e3283511d0e

26. Carmichael, W.W., Li, R. “Cyanobacteria toxins in the Salton Sea.” *Aquat. Biosyst.* **2**, 5 (2006). https://doi.org/10.1186/1746-1448-2-5

27. Xu, Elvis Genbo, et al. “Spatial and Temporal Assessment of Environmental Contaminants in Water, Sediments and Fish of the Salton Sea and Its Two Primary Tributaries, California, USA, from 2002 to 2012.” *Science of the Total Environment*, vol. 559, July 2016, pp. 130–140, https://doi.org/10.1016/j.scitotenv.2016.03.144

28. Zhou, Chuanqi, et al. “Effects of Selenite on Microcystis Aeruginosa: Growth, Microcystin Production and Its Relationship to Toxicity under

Hypersalinity and Copper Sulfate Stresses." *Environmental Pollution*, vol. 223, Apr. 2017, pp. 535–544, https://doi.org/10.1016/j.envpol.2017.01.056

29. Biddle, Trevor A., et al. "Salton Sea Aerosol Exposure in Mice Induces a Pulmonary Response Distinct from Allergic Inflammation." *Science of the Total Environment*, vol. 792, Oct. 2021, p. 148450, https://doi.org/10.1016/j.scitotenv.2021.148450

30. D'Evelyn, S.M., et al. "Differential Inflammatory Potential of Particulate Matter (PM) Size Fractions from Imperial Valley, CA." *Atmospheric Environment*, vol. 244, Jan. 2021, p. 117992, https://doi.org/10.1016/j.atmosenv.2020.117992

31. Burr, Abigail C, et al. "Lung Inflammatory Response to Environmental Dust Exposure in Mice Suggests a Link to Regional Respiratory Disease Risk." *Dovepress*, vol. Volume 14, 1 Aug. 2021, pp. 4035–4052, https://doi.org/10.2147/jir.s320096

32. Aciego, S. M., et al. "Dust Outpaces Bedrock in Nutrient Supply to Montane Forest Ecosystems." *Nature Communications*, vol. 8, no. 1, 28 Mar. 2017, https://doi.org/10.1038/ncomms14800

33. Maltz, Mia R., et al. "Landscape Topography and Regional Drought Alters Dust Microbiomes in the Sierra Nevada of California." *Frontiers in*

Microbiology, vol. 13, 28 June 2022, https://doi.org/10.3389/fmicb.2022.856454

34. Peng, Xinze, et al. “Establishment and Characterization of a Multi-Purpose Large Animal Exposure Chamber for Investigating Health Effects.” *Review of Scientific Instruments*, vol. 90, no. 3, 1 Mar. 2019, https://doi.org/10.1063/1.5042097

35. Peng, Xinze, et al. “Continuous Inhalation Exposure to Fungal Allergen Particulates Induces Lung Inflammation While Reducing Innate Immune Molecule Expression in the Brainstem.” *ASN Neuro*, vol. 10, 1 Jan. 2018, p. 175909141878230-175909141878230, https://doi.org/10.1177/1759091418782304

36. Botelho, Fernando M, et al. “IL-1α/IL-1R1 Expression in Chronic Obstructive Pulmonary Disease and Mechanistic Relevance to Smoke-Induced Neutrophilia in Mice.” *PLOS ONE*, vol. 6, no. 12, 6 Dec. 2011, pp. e28457–e28457, https://doi.org/10.1371/journal.pone.0028457

37. Osei, Emmanuel T., et al. “Interleukin-1α Drives the Dysfunctional Cross-Talk of the Airway Epithelium and Lung Fibroblasts in COPD.” *European Respiratory Journal*, vol. 48, no. 2, 13 July 2016, pp. 359–369, https://doi.org/10.1183/13993003.01911-2015

38. Suwara, M I, et al. “IL-1α Released from Damaged Epithelial Cells Is Sufficient and Essential to Trigger Inflammatory Responses in Human Lung Fibroblasts.” *Mucosal Immunology*, vol. 7, no. 3, 30 Oct. 2013, pp. 684–693, https://doi.org/10.1038/mi.2013.87

39. Natarajan, Sudha, et al. “CHRONIC PULMONARY LPS TOLERANCE INDUCES SELECTIVE IMMUNOSUPPRESSION WHILE MAINTAINING the NEUTROPHILIC RESPONSE.” *Shock*, vol. 33, no. 2, 1 Feb. 2010, p. 162, https://doi.org/10.1097/SHK.0b013e3181aa9690

40. Carmichael, Wayne W, and RenHui Li. “Cyanobacteria Toxins in the Salton Sea.” *Saline Systems*, vol. 2, no. 1, 2006, p. 5, https://doi.org/10.1186/1746-1448-2-5

41. Fleming, Lora E., et al. “Aerosolized Red-Tide Toxins (Brevetoxins) and Asthma.” *CHEST*, vol. 131, no. 1, 1 Jan. 2007, pp. 187–194, https://doi.org/10.1378/chest.06-183

42. Zaias, Julia, et al. “Repeated Exposure to Aerosolized Brevetoxin-3 Induces Prolonged Airway Hyperresponsiveness and Lung Inflammation in Sheep.” *Inhalation Toxicology*, vol. 23, no. 4, Mar. 2011, pp. 205–211, https://doi.org/10.3109/08958378.2011.558936

43. Barboza, Renato, et al. “Endotoxin Exposure during Sensitization to Blomia Tropicalis Allergens Shifts TH2 Immunity towards a TH17-

Mediated Airway Neutrophilic Inflammation: Role of TLR4 and TLR2." *PLoS ONE*, vol. 8, no. 6, 21 June 2013, p. e67115, https://doi.org/10.1371/journal.pone.0067115

44. Li, L., et al. "Th2-Induced Eotaxin Expression and Eosinophilia Coexist with Th1 Responses at the Effector Stage of Lung Inflammation." *Journal of Immunology (Baltimore, Md.: 1950)*, vol. 161, no. 6, 15 Sept. 1998, pp. 3128–3135, www.ncbi.nlm.nih.gov/pubmed/9743380

45. Kaori Sadakane, et al. "Effects of Co-Exposure of Lipopolysaccharide and β-Glucan (Zymosan A) in Exacerbating Murine Allergic Asthma Associated with Asian Sand Dust." *JAT. Journal of Applied Toxicology/Journal of Applied Toxicology*, vol. 39, no. 4, 12 Dec. 2018, pp. 672–684, https://doi.org/10.1002/jat.3759

46. Thakur, Vandana R., et al. "An Experimental Model of Asthma in Rats Using Ovalbumin and Lipopolysaccharide Allergens." *Heliyon*, vol. 5, no. 11, 1 Nov. 2019, p. e02864, https://doi.org/10.1016/j.heliyon.2019.e02864

47. Yu, Qian-Lin, and Zhangbo Chen. "Establishment of Different Experimental Asthma Models in Mice." *Experimental and Therapeutic Medicine*, 8 Jan. 2018, https://doi.org/10.3892/etm.2018.5721

48. Dillon, Jesse G., et al. “Seasonal Changes in Bacterial Diversity in the Salton Sea.” *Hydrobiologia*, vol. 632, no. 1, 28 June 2009, pp. 49–64, https://doi.org/10.1007/s10750-009-9827-4

49. Hawley, E. R., et al. “Metagenomic Sequencing of Two Salton Sea Microbiomes.” *Genome Announcements*, vol. 2, no. 1, 23 Jan. 2014, https://doi.org/10.1128/genomea.01208-13

50. Swan, Brandon K, et al. “Archaeal and Bacterial Communities Respond Differently to Environmental Gradients in Anoxic Sediments of a California Hypersaline Lake, the Salton Sea.” *Applied and Environmental Microbiology*, vol. 76, no. 3, 1 Feb. 2010, pp. 757–768, https://doi.org/10.1128/aem.02409-09

51. d’Hennezel, Eva, et al. “Total Lipopolysaccharide from the Human Gut Microbiome Silences Toll-like Receptor Signaling.” *MSystems*, vol. 2, no. 6, 14 Nov. 2017, https://doi.org/10.1128/msystems.00046-17

52. Tang, Kai, et al. “Characterization of Atmospheric Bioaerosols along the Transport Pathway of Asian Dust during the Dust-Bioaerosol 2016 Campaign.” *Atmospheric Chemistry and Physics*, vol. 18, no. 10, 24 May 2018, pp. 7131–7148, https://doi.org/10.5194/acp-18-7131-2018

53. Freund, Hannah, et al. “Microbiome Interactions and Their Ecological Implications at the Salton Sea.” *California Agriculture*, vol. 76, no. 1, Apr. 2022, pp. 16–26, https://doi.org/10.3733/ca.2022a0002

Acknowledgments

TAB led experiments and was the primary author of the manuscript. KY, TMT, DDC and MLS helped with mouse dissections and processing. RD, QL, and DG ran and monitored environmental exposure chamber. HF, MPS, MRM collected and processed dust. JY assisted in creation of Fig. 4.1 JKB designed environmental dust collectors. EA and DRCIII helped with experimental design and processing. DDL assisted with experimental design and editing the manuscript. This research used the site and facilities of the University of California, Natural Reserve System, Philip L. Boyd Deep Canyon Desert Research Center, doi:10.21973/N3V66D.

Figures

Figure 4.1 - Collection Sites and Changes in Exposed Playa Over Time. Map showing the 3 dust collection sites (Wister, Dos Palmas, Sonny Bono) from around the Salton Sea, along with the desert dust control collection site (Boyd Deep Canyon), playa collection site (Corvina Beach), and water collection site from Biddle et al., 2021 (Salton City). Map also shows the change in playa exposure between 1985 and 2020 due to evaporation of the Salton Sea.

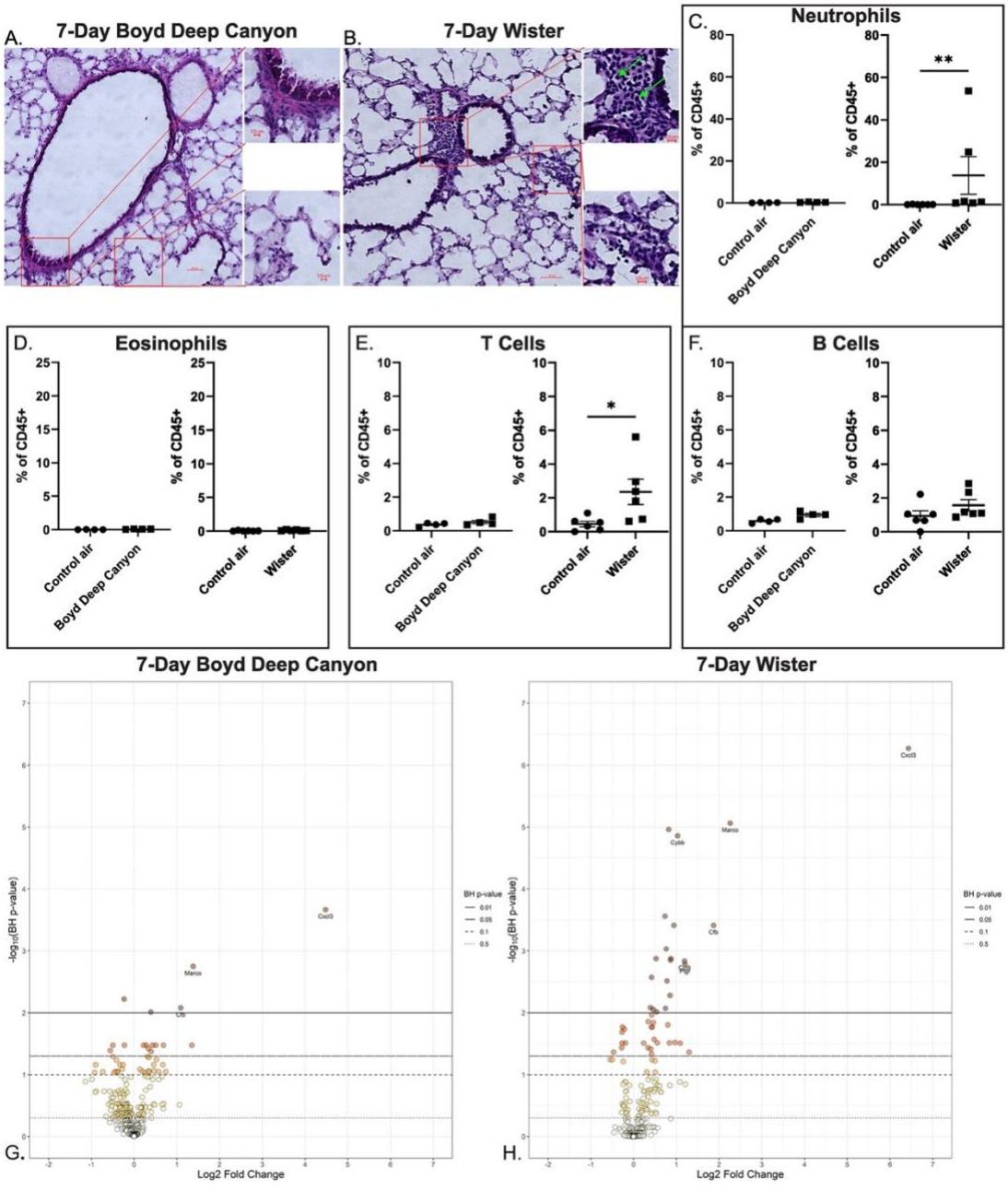

Figure 4.2 - Pulmonary inflammation triggered by Salton Sea (Wister) Dust extract and by Desert (Boyd Deep Canyon) Dust extract. (A) 20× magnification H&E stain of lung tissue from mice exposed to Boyd Deep Canyon Dust extract. Insets are 60× magnification. **(B)** 20× magnification H&E stain of lung tissue from mice exposed to Wister Dust extract. Insets are 60× magnification. **(C)** Neutrophilic infiltration into the bronchoalveolar lavage fluid

measured as a percentage of total immune cells (CD45+) as determined by flow cytometry. Neutrophil were defined as $CD45^{+}CD11b^{+}Ly6G^{+}SiglecF^{-}CD11c^{-}$. **(D)** Eosinophilic infiltration into the bronchoalveolar lavage fluid measured as a percentage of total immune cells (CD45+) as determined by flow cytometry. Eosinophils were defined as $CD45^{+}CD11b^{+}SiglecF^{+}CD11c^{-}$. **(E)** T cell infiltration into the bronchoalveolar lavage fluid measured as a percentage of total immune cells (CD45+) as determined by flow cytometry. T cells were defined as $CD45^{+}CD3^{+}SiglecF^{-}CD11c^{-}$. **(F)** B cell infiltration into the bronchoalveolar lavage fluid measured as a percentage of total immune cells (CD45+) as determined by flow cytometry. B cells were defined as $CD45^{+}CD19^{+}SiglecF^{+}CD11c^{-}$. All Boyd Deep Canyon Dust extract (*n* = *4*) and Wister Dust extract (*n* = *6*) exposed mice were compared to contemporaneous sex- and age-matched mice exposed to filtered house air. **(G)** Differential expression plot for Boyd Deep Canyon Dust extract exposed mice (*n* = *6*) compared to contemporaneous sex- and age-matched mice exposed to filtered house air (*n* = *6*). **(F)** Differential expression plot for Wister Dust extract exposed mice (*n* = *9*) compared to contemporaneous sex- and age-matched mice exposed to filtered house air (*n* = *9)*. Gene expression was measured by a Nanostring Sprint Profiler using the mouse immunology panel; analysis was done using the accompanying nSolver software and visualized using *ggplot2*. Labeled genes have a log2 fold change >1 or less than negative 1 and an Benjamini-Hochberg adjusted False Discovery Rate of <0.01. * $p < 0.05$. ** $p < 0.01$. *p*-value determined using the Mann-Whitney *U* test for nonparametric data.

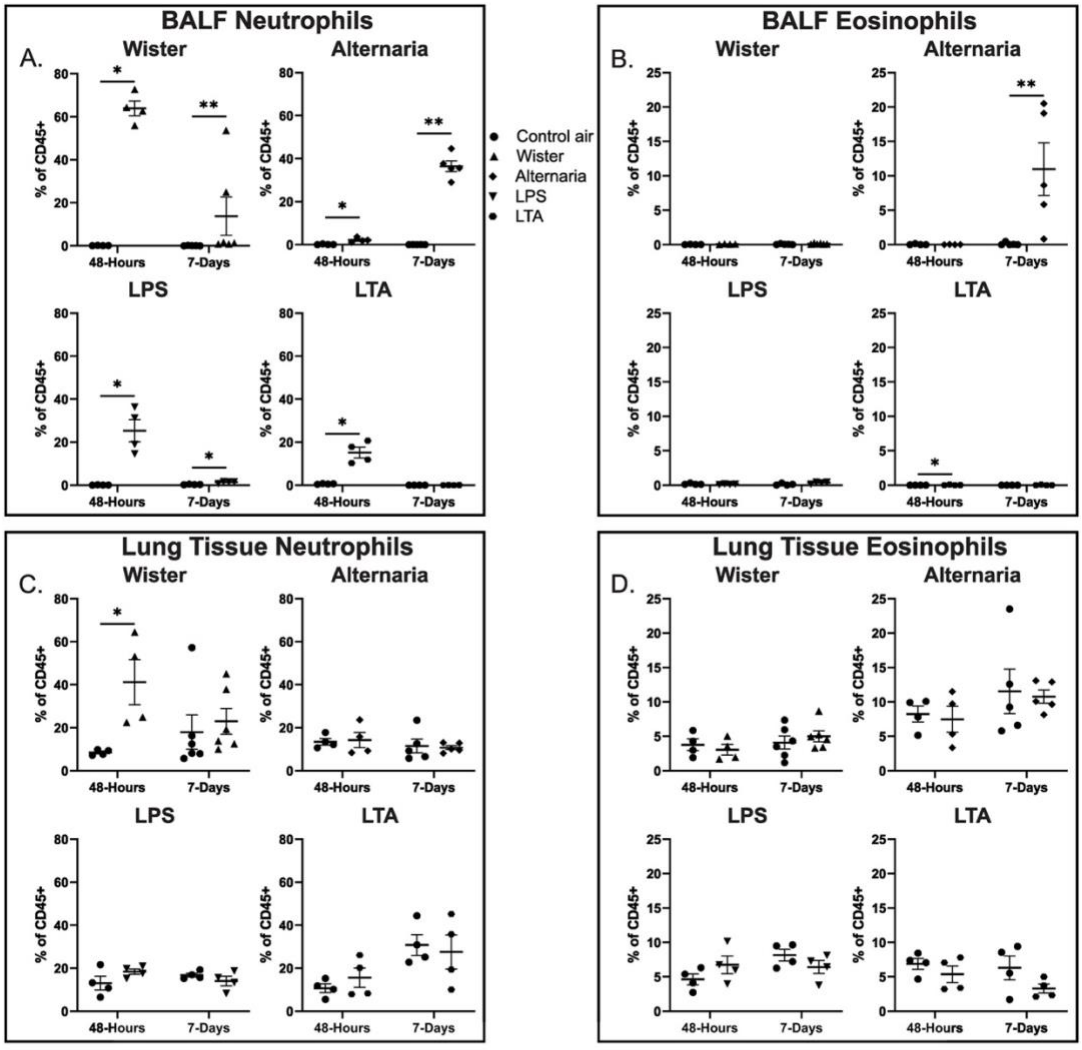
BALF Neutrophils
A.
Wister
Alternaria
LPS
LTA
% of CD45+
48-Hours
7-Days
Control air
Wister
Alternaria
LPS
LTA
BALF Eosinophils
B.
Lung Tissue Neutrophils
C.
Lung Tissue Eosinophils
D.

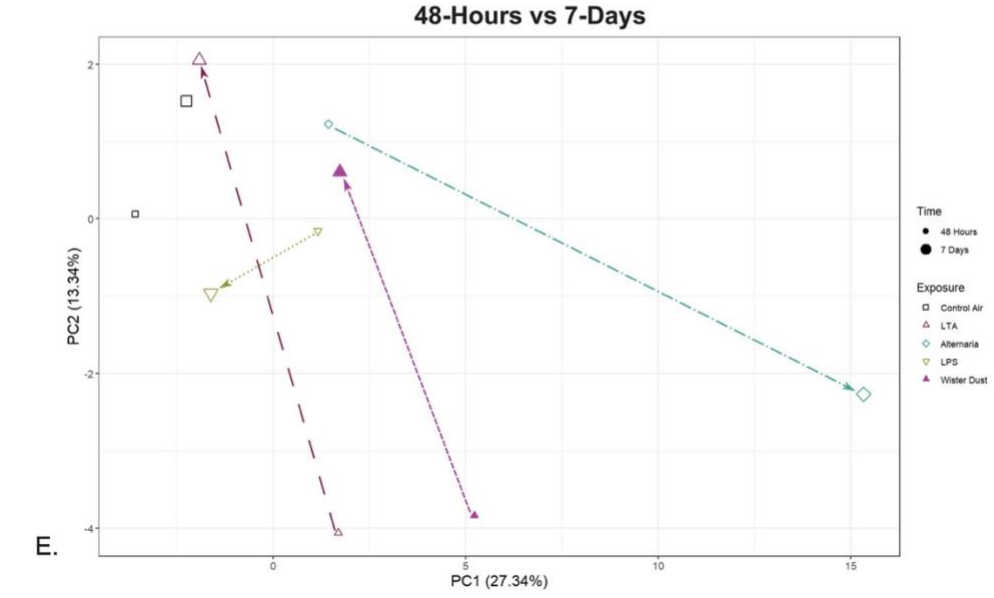
48-Hours vs 7-Days
E.
PC1 (27.34%)
PC2 (13.34%)
Time
48 Hours
7 Days
Exposure
Control Air
LTA
Alternaria
LPS
Wister Dust

Figure 4.3 - Changes from 48-h to 7-day timepoints for Salton Sea (Wister) Dust extract, *Alternaria*, LTA, and LPS exposed mice. (A) Neutrophil infiltration at 48-h and 7-days in the bronchoalveolar lavage fluid (BALF) as a percent of total immune cells (CD45+) for Wister Dust extract, *Alternaria*, LTA, and LPS exposed mice. **(B)** Eosinophil infiltration at 48-h and 7-days in the bronchoalveolar lavage fluid (BALF) as a percent of total immune cells (CD45+) for Wister Dust extract, *Alternaria*, LTA, and LPS exposed mice. **(C)** Neutrophil infiltration at 48-h and 7-days in the lung tissue as a percent of total immune cells (CD45+) for Wister Dust extract, *Alternaria*, LTA, and LPS exposed mice. **(D)** Eosinophil infiltration at 48-h and 7-days in the lung tissue as a percent of total immune cells (CD45+) for Wister Dust extract, *Alternaria*, LTA, and LPS exposed mice. Neutrophils were defined as $CD45^{+}CD11b^{+}Ly6G^{+}SiglecF^{-}CD11c^{-}$, while eosinophils were defined as $CD45^{+}CD11b^{+}SiglecF^{+}CD11c^{-}$. All timepoint and exposure combinations were compared to contemporaneous sex- and age-matched mice exposed to filtered house air. $n = 4–6$ **(E)** PCA plot showing the changes from the 48-h timepoints to 7-day timepoints for Wister Dust extract, *Alternaria*, LTA, and LPS exposed mice. PCA was generated using the *prcomp* function in R and visualized using *ggplot2*. Each point represents the average location of the specific timepoint and exposure combination on PC1 and PC2. Arrows highlight trend line from 48-h to 7-day for each exposure. $n = 6–9$. * $p < 0.05$, ** $p < 0.01$. p-value calculated using the Mann-Whitney U test for nonparametric data.

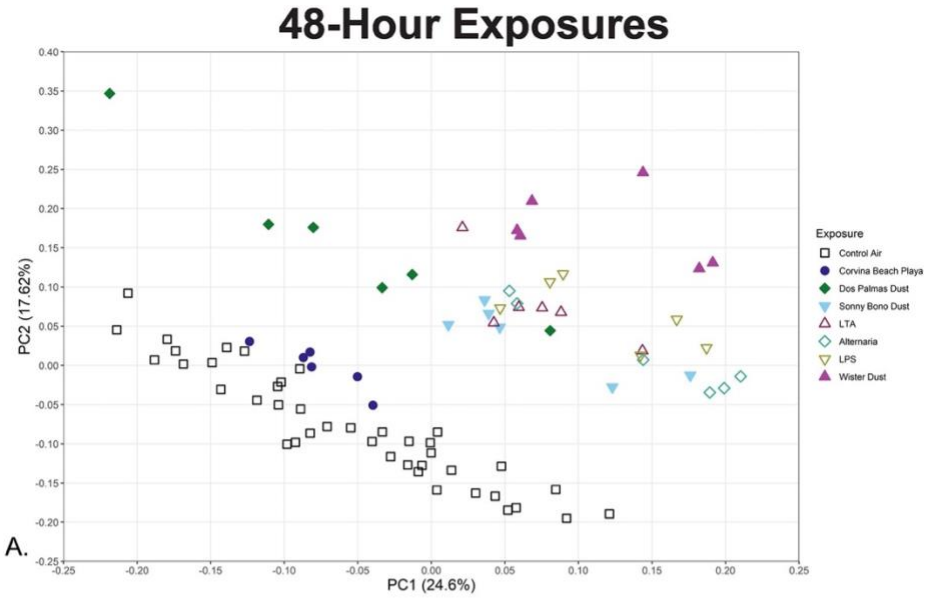
48-Hour Exposures
A.
PC2 (17.62%)
PC1 (24.6%)
Exposure
Control Air
Corvina Beach Playa
Dos Palmas Dust
Sonny Bono Dust
LTA
Alternaria
LPS
Wister Dust

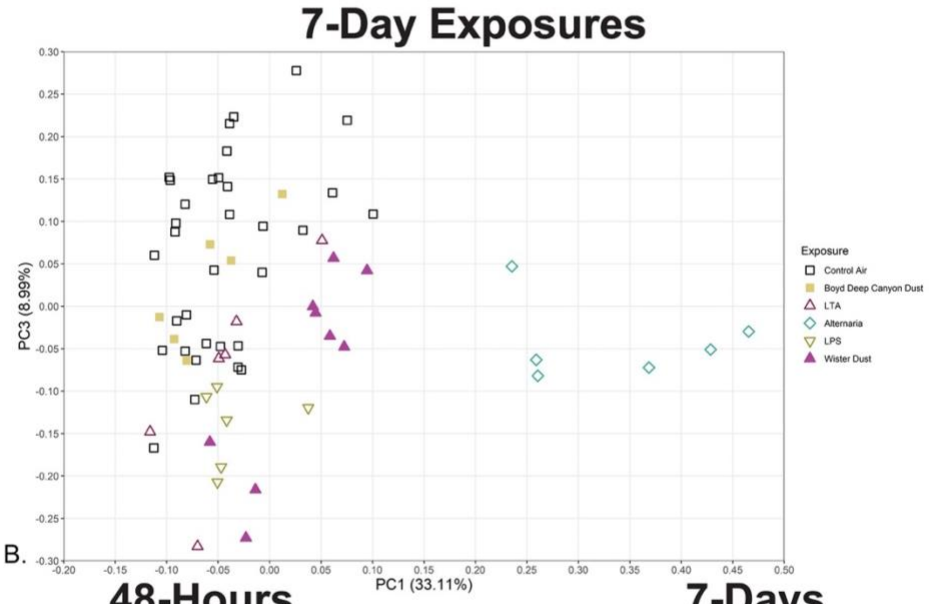
7-Day Exposures
B.
PC3 (8.99%)
PC1 (33.11%)
Exposure
Control Air
Boyd Deep Canyon Dust
LTA
Alternaria
LPS
Wister Dust

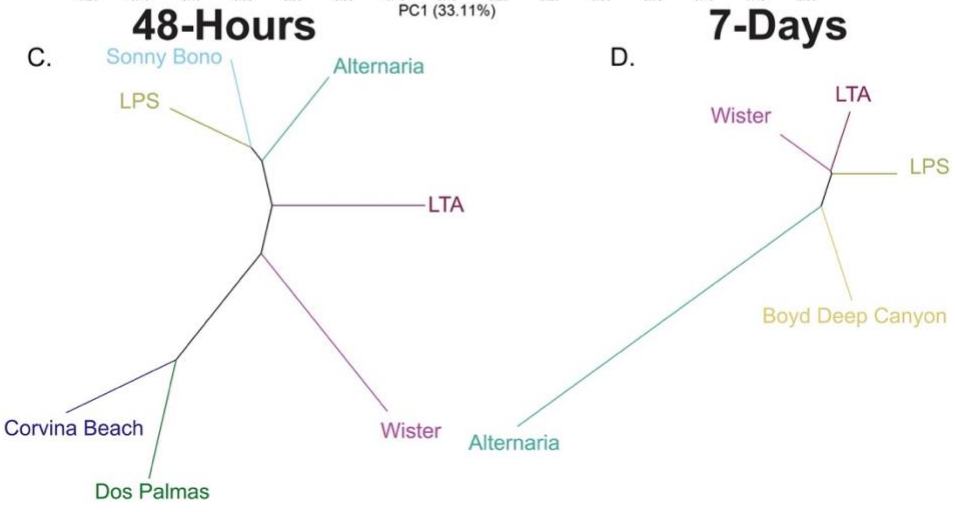
48-Hours
C.
Sonny Bono
Alternaria
LPS
LTA
Corvina Beach
Wister
Dos Palmas
7-Days
D.
LTA
Wister
LPS
Boyd Deep Canyon
Alternaria

Figure 4.4 - Gene expression comparisons for 48 h and 7-day timepoints. **(A)** PCA plot comparing Salton Sea Dust extract (Wister, Sonny Bono, Dos Palmas), Salton Sea Playa extract (Corvina Beach), LTA, LPS and *Alternaria* exposed mice at 48-h (*n = 6)*. **(B)** PCA plot comparing Salton Sea Dust extract (Wister), Desert Dust extract (Boyd Deep Canyon), LTA, LPS and *Alternaria* exposed mice at 7-days (*n = 6–9)*. PCA was generated using the *prcomp* function in R and visualized using *ggplot2*. **(C)** Dendrogram showing the relationship between Salton Sea Dust extract (Wister, Sonny Bono, Dos Palmas), Salton Sea Playa extract (Corvina Beach), LTA, LPS and *Alternaria* exposed mice at 48-h (*n = 6*). **(D)** Dendrogram showing the relationship between Salton Sea Dust extract (Wister), Desert Dust extract (Boyd Deep Canyon), LTA, LPS and *Alternaria* exposed mice at 7-days (*n = 6–9).* Dendrograms were generated using the log2 value for each gene averaged by the exposure. This average was then used with the hclust function (method = Ward.D2) and visualized using the *ape* package.

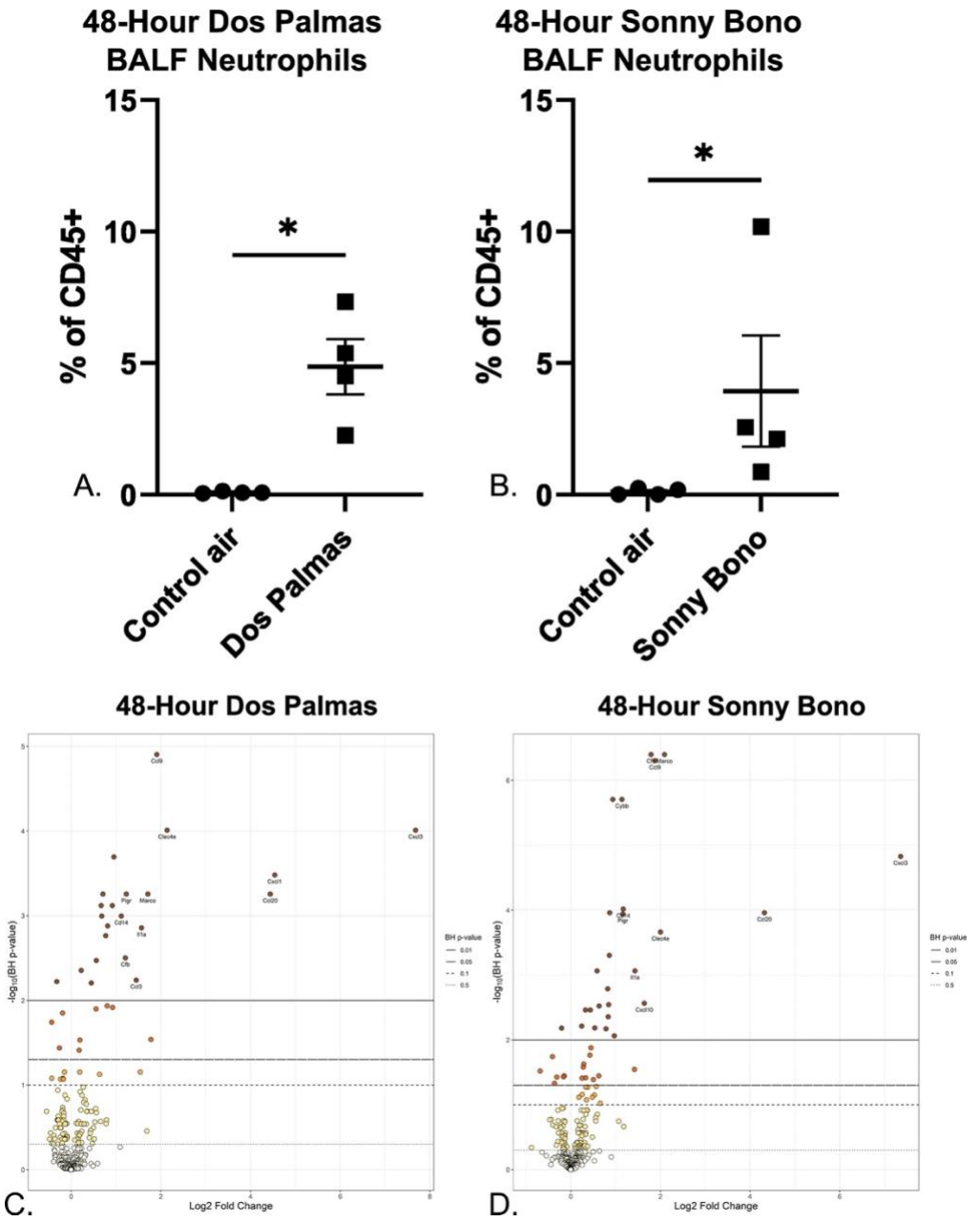

Figure 4.S1 - Dos Palmas and Sonny Bono Cell infiltration and Gene expression. (A) Neutrophilic infiltration into the bronchoalveolar lavage fluid in mice exposed to Dos Palmas Dust extract for 48-h measured as a percentage of total immune cells (CD45+) as determined by flow cytometry. **(B)** Neutrophilic infiltration into the bronchoalveolar lavage fluid in mice exposed to Sonny Bono

Dust extract for 48-h measured as a percentage of total immune cells (CD45+) as determined by flow cytometry. Neutrophil were defined as $CD45^{+}CD11b^{+}Ly6G^{+}SiglecF^{-}CD11c^{-}$. All Dos Palmas Dust extract (*n = 4*) and Sonny Bono Dust extract (*n = 6*) exposed mice were compared to contemporaneous sex- and age-matched mice exposed to filtered house air. **(C)** Differential expression plot for Dos Palmas Dust extract exposed mice (*n = 6*) compared to contemporaneous sex- and age-matched mice exposed to filtered house air (*n = 6)*. **(D)** Differential expression plot for Sonny Bono Dust extract exposed mice (*n = 6*) compared to contemporaneous sex- and age-matched mice exposed to filtered house air (*n = 6*). Gene expression was measured by a Nanostring Sprint Profiler using the mouse immunology panel; analysis was done using the accompanying nSolver software and visualized using *ggplot2*. Labeled genes have a log2 fold change >1 or less than negative 1 and an Benjamini-Hochberg adjusted False Discovery Rate of <0.01. * $p < 0.05$. ** $p < 0.01$. *p*-value determined using the Mann-Whitney *U* test for nonparametric data. Average ± standard error shown.

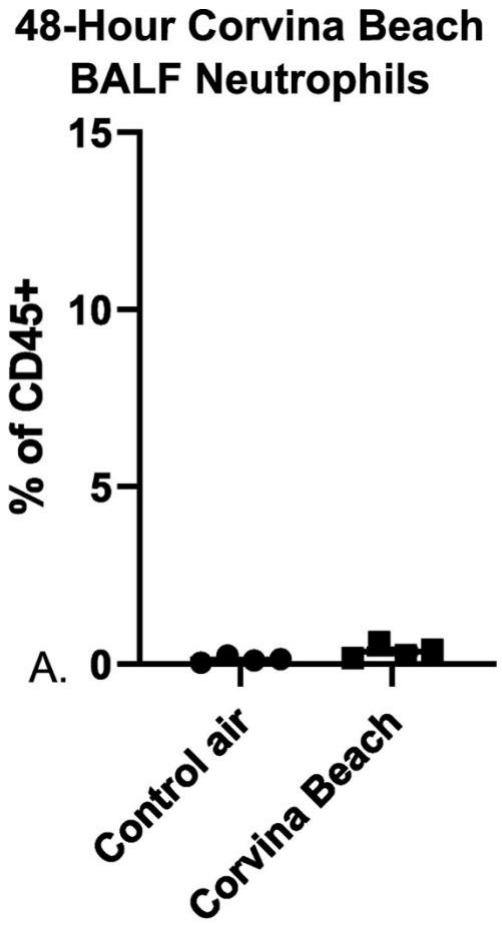
48-Hour Corvina Beach
BALF Neutrophils
% of CD45+
15
10
5
0
A.
Control air
Corvina Beach

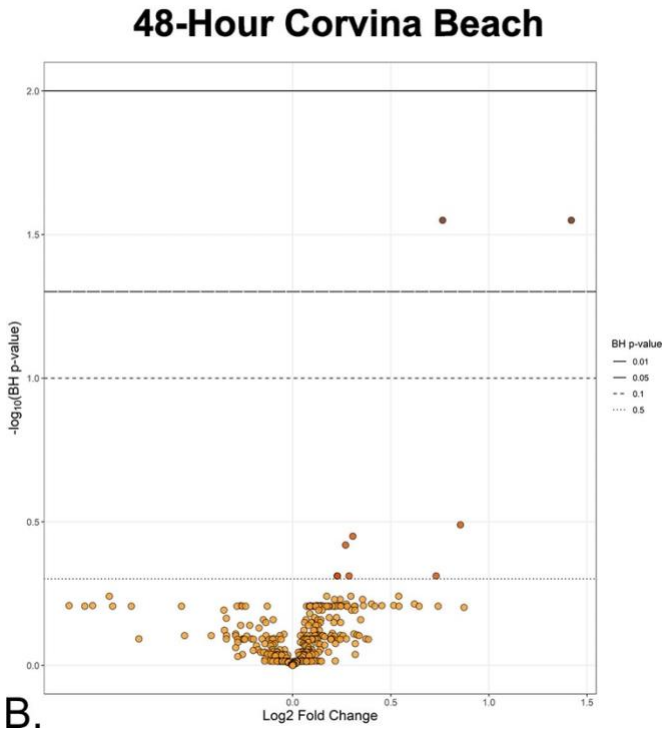
48-Hour Corvina Beach
-log10(BH p-value)
Log2 Fold Change
BH p-value
0.01
0.05
0.1
0.5
B.

Figure 4.S2 - Response to Corvina Beach Playa. (A) Neutrophilic infiltration into the bronchoalveolar lavage fluid in mice exposed to Corvina Beach Playa extract for 48-h Neutrophil were defined as $CD45^{+}CD11b^{+}Ly6G^{+}SiglecF^{-}CD11c^{-}$. Corvina Beach Playa extract (*n* = *4*) exposed mice were compared to contemporaneous sex- and age-matched mice exposed to filtered house air. **(B)** Differential expression plot for Corvina Beach Playa extract exposed mice (*n* = *6*) compared to contemporaneous sex- and age-matched mice exposed to filtered house air (*n* = *6*). Gene expression was measured by a Nanostring Sprint Profiler using the mouse immunology panel; analysis was done using the accompanying nSolver software and visualized using *ggplot2*. Labeled genes have a log2 fold change >1 or less than negative 1 and an Benjamini-Hochberg adjusted False Discovery Rate of <0.01. * $p < 0.05$. ** $p < 0.01$. p-value determined using the Mann-Whitney U test for nonparametric data. Average ± standard error shown.

Site	Latitude (ºN)	Longitude (ºW)	Sampling dates	Deployment (days)	Sample type
Corvina Beach	33°28'36.5	115°53'31.3	08/21/21	n/a	playa
Boyd Deep	33°39'04.0	116°22'22.9	08/14/20-10/08/20	55	dust
Sonny Bono	33°11'16.0	115°35'57.3	08/30/20-10/10/20	44	dust
Wister	33°17'01.7	115°36'00.3	08/30/20-10/10/20, 09/18/21-12/08/21	44, 81	dust
Dos Palmas	33°29'22.1	115°50'06.3	08/30/20-10/10/20	44	dust

Supplemental Table 4.1. Site and sampling characteristics. Coordinates and deployment dates for each of five sites Salton Sea Basin of California.

Chapter 5: Evidence for Aerosolized Bacterial Endotoxin as an Environmental Health Hazard

Abstract

The high incidence of asthma in communities near California's Salton Sea has been attributed to dust produced at the exposed lakebed. In previous studies, aerosol exposures of mice to local dust resulted in lung inflammation dominated by neutrophils without significant recruitment of eosinophils. These results suggested that asthma symptoms in the Salton Sea region may be from a non-allergic inflammatory pathology. Our aim was to compare the mouse exposure studies to environmental and clinical information in the Salton Sea region, to assess whether mouse responses to dust were predictive of asthma-like symptoms and indicate potential causes of symptoms among residents in the region. To determine whether the mouse exposure studies were predictive of the clinical setting in the Salton Sea region, we used mouse exposures to assess inflammatory responses to Salton Sea dust. To relate dust exposure data to clinical outcomes, a community survey of clinical symptoms with geospatial tags was conducted across the Salton Sea region. Exploratory spatial regressions were constructed to investigate the relationship between households' clinical outcomes and demographic and environmental variables in the study area. Mouse exposure studies revealed inflammatory responses, with different dust samples showing a geographic gradient from northwest to southeast in the magnitude of responses. Interestingly, a community symptom survey showed a

very similar pronounced geographic gradient with the incidence of families with asthma symptoms reaching upwards of 35% in northern Imperial Valley, results that were confirmed by geospatial models. The pattern of response in exposed mice indicated an innate immune response to bacterial endotoxin, confirmed in transgenic mice lacking endotoxin receptors. Moreover, dust samples from the southern end of the Salton Sea inducing high inflammatory responses also showed concentrations of endotoxin far higher than those in samples from the northern end of the region. Our studies show that Salton Sea dust induces lung inflammation in mice with the magnitude of responses showing a northwest to southeast geographic gradient. Interestingly, this matches the geographic gradient in the incidence of asthma symptoms in residents of the region, along with the predominant wind direction in the study area. The mouse inflammatory response was shown to be due to bacterial endotoxin in the dust samples, and high concentrations of endotoxin in the dust were also found in samples collected nearest the highest incidence of clinical symptoms. The results are consistent with a model in which agriculture nutrient runoff drives bacterial growth and production of endotoxin that is entrained in the dust. Inhalation of the endotoxin in dust may account for the high incidence of asthma symptoms, suggesting that asthma in the region may be a non-allergic innate response to endotoxin rather than an environmental allergen.

Introduction

The Salton Sea is California's largest inland lake; its desert location means that its continued existence cannot rely on rainfall or mountain snowpack runoff, so it can only be maintained by excess Colorado River irrigation water from nearby agricultural activity[1,2]. The lake continues to retreat due to evaporation and declining freshwater inputs, with increasing areas of exposed lakebed (playa) emitting high levels of dust[3]. Residents in the region suffer from high levels of asthma that is generally attributed to this playa dust[3,4], though the specific contribution or mechanism of induction of asthma symptoms has not been determined. In nearby communities such as Palm Springs, residents are also exposed to aerosol particulate matter (PM) during acute dust events as well as chronic exposure to ambient PMs, but the incidence of asthma is far lower, similar to baseline levels across the state[5]. Thus, triggers of asthma symptoms among Salton Sea residents are likely to be from specific components generated at or near the lake itself.

A Salton Sea-specific aerosol component has not yet been identified, but a number of environmental factors have been raised as possibilities. These include a variety of heavy metal contaminants in the groundwater, including arsenic and selenium[6]. The active agriculture industry in the region also contributes a variety of pesticides, including residual long-lasting pesticides such as DDT[6]. Unfortunately, these potential environmental components are not

known for their induction of pulmonary symptoms, so despite their presence in and around the Salton Sea, their contribution to the high incidence of asthma in the region is uncertain.

Asthma symptoms are usually seen in the context of allergic inflammation, so specific local allergenic agents could include pollen from plants growing near Salton Sea, or fungi or mold in household environments[7]. Unfortunately, these allergens are also common to environments outside of the Salton Sea region, so their unique contribution to the induction of disease in this region has not been demonstrated. In addition, bacterial or algal toxins, including cyanotoxins, domoic acid, or other microbial components, are also known to exacerbate asthma symptoms[8], though they are not allergens per se, and have not yet been detected in significant amounts in the environment. Thus, while there are a number of potential factors that may contribute to the incidence of asthma in the region, they have not yet been shown to be unique to the Salton Sea environment, or present in sufficient amounts to induce symptoms.

In this report, we extend previous studies on the biological effects of dust material collected from locations around the Salton Sea region. We found that mice exposed to dust material from the Salton Sea region demonstrated strong neutrophilic lung inflammation, supporting the notion that this dust may be a major factor in pulmonary disease in the region. In this report we provide additional focus on identifying the component(s) likely to produce asthma-like

symptoms. Complementary studies with a community-wide symptom survey with geospatial tagging also provided information on the distribution of disease symptoms. Together, the data are consistent with a model in which microbial production of endotoxin in the Salton Sea or exposed playa causes chronic exposure to this inflammatory toxin among residents, leading to a non-allergic lung inflammation with asthma-like symptoms. Thus, this study provides an argument for monitoring levels of aerosolized endotoxin as an environmental pollutant correlating with pulmonary disease.

Materials and methods

In vivo environmental exposures

8-9-week-old male and female C57BL/6J mice were purchased from Jackson Laboratory. Mice were housed under a 12-hour light cycle within their home cages with ad libitum food and water. After 1-week of acclimation, mice were housed 2-3 mice per cage, placed in an environmental aerosol exposure chamber, and exposed to dust from the Salton Sea region for 48 hours. Upon completion of exposure, mice were sacrificed immediately and analyzed for cellular recruitment, gene regulation, and histological alterations.

Salton Sea dust collection and extraction

Passive dust collectors were placed at different areas surrounding the sea to collect dust. These collectors consist of a round bundt pan coated with Teflon

lined with Kevlar mesh containing glass marbles as described in Biddle at al. (2023)[9].To recover material from the collectors, marbles were rinsed with water and the resulting dust suspension was filtered through sterile 0.2 um filters, lyophilized, and resuspended for aerosolization in our environmental exposure chambers.

Exposure Chambers

Exposure studies were performed in dual animal chambers as described in Peng et al (2019)[10]. Relative humidity, temperature, and atmospheric pressure were measured in the chambers. Particulate matter size and concentration were also monitored using a scanning mobility particle sizer (SMPS) to maintain consistent PM concentrations for the duration of the exposure. Utilizing these chambers, animals were exposed to either filtered air, serving as a control exposure, or to aerosolized dust collected from the Salton Sea region for 48 hours.

Flow Cytometry

Bronchoalveolar lavage fluid (BALF) and left lung lobes were collected for flow cytometry analysis. BALF and digested lung tissue were stained for the following surface markers: anti-CD45 FITC, anti-CD19 Percpcy5.5, anti-CD3 AF700, anti-CD4 BV711, anti-CD8 PE-CF594, anti-SiglecF APC, anti-Ly6G BV510, anti-CD11c PE-Cy7, anti-CD11b BV421, and anti-IgE PE. Cells were

fixed in 1% PFA and samples were run the following day using the Agilent NovoCyte Quanteon Flow Cytometer. Upon excluding dead cells identified by positive staining with Zombie Yellow dye, cellular populations were identified using the following surface markers: $CD45^+CD11c^+$ $SiglecF^+$ for alveolar macrophages, $CD45^+CD11b^+Ly6G^+$ for neutrophils, $CD45^+CD11b^+SiglecF^+$ for eosinophils, $CD45^+CD3^+$ for T cells, and $CD45^+CD19^+$ for B cells. All gating and analysis were performed using FlowJo analysis software. This data was then transferred into PRISM for production of graphs and statistical analysis. Statistical analysis for cellular infiltration was conducted using GraphPad Prism 9, and p-values were calculated using the Mann-Whitney U test.

Gene expression profiling (Nanostring)

RNA was extracted from flash frozen right lung lobes of exposed and control animals for NanoString analysis. RNA was extracted using a TRIzol based extraction method. Approximately 100 mg of tissue was ground using liquid nitrogen in a mortar and pestle to pulverize the tissue into a fine dust. Following this, tissues were placed in TRIzol and centrifuged for dissociation of RNA. The supernatant was then collected and mixed with Chloroform to allow for further separation before centrifugation. The aqueous phase of the centrifuged product was mixed with isopropyl alcohol and centrifuged before a series of washes with 75% ethanol. RNA was resuspended in DEPC-Treated water and concentration and purity were measured using a Nanodrop 2000

spectrophotometer. For Nanostring analysis, 50 ng of RNA was analyzed using the NanoString nCounter Mouse Immunology Panel to assess gene regulatory changes. Differential expression was calculated and normalized based on housekeeping genes. Statistical analysis for Nanostring data was calculated using nSolver with a p-value of <0.05 used to determine significance. Positive controls and p-values were adjusted using the Benjamini-Hochberg method.

Limulus Amebocyte Lysate Assay

Dust and water samples collected from around the Salton Sea were tested for endotoxin concentrations using the ToxinSensor Chromogenic LAL Endotoxin Assay Kit (GenScript, ABIN491527). Samples were processed via manufacturer instructions and run neat, as well as at 1:10, 1:50, 1:5000, and 1:10000 dilution concentrations. Absorbance values were measured at a wavelength of 545 nm using a SpectraMax ID5. Concentrations were then back calculated from the standard curve and dilution factors were corrected for to give final endotoxin concentrations for each sample. Values for dust samples were then standardized based on the length of time that the dust collectors were out for collection of material.

Sandwich ELISA assay

LPS was measured in samples through a competitive ELISA (absorbance 450 nm; ELISA Kit - LS-F15272, LSBio, Seattle, WA), following manufacturer's

specifications, using a SpectraMax iD5 microplate reader (Molecular Devices, San Jose, CA). Samples from Salton Sea collection sites were run neat and in three 1:5 serial dilutions. An additional positive control of lipopolysaccharides from *E. coli* O55:B5 (LPS; L2880) at a concentration of 0.1ng/mL with three 5-fold serial dilutions was also measured. Endotoxin units were calculated based on a serial fold dilution of an endotoxin standard provided by the manufacturer.

Histology

For histological analysis, lungs were inflated with 0.3 ml of 10% neutral buffered formalin (NBF). Lungs were then excised and placed in 10% NBF overnight. Lungs were washed in 1x PBS and transferred to 70% ethanol. Tissues were shipped to University of Irvine and were paraffin embedded and sectioned at 15 um using a microtome. Sections were deparaffinized and stained with hematoxylin and eosin (H&E) to analyze cellular recruitment and histological alterations.

Community clinical symptom survey

The clinical symptom survey study was approved by the University of California, Riverside Institutional Review Board, protocol HS22-154. HARC and HDR@UCR drafted a survey with 42 questions, which was modeled on a standardized questionnaire from the Global Asthma Network, originating from the International Study of Asthma and Allergies in Childhood (ISAAC) program[11].

Results are from an address-based survey of households in eastern Riverside County and northern Imperial County. HARC (via Ace Printing) mailed a “survey package,” which included an invitation letter (in English and Spanish), a paper survey in English, a paper survey in Spanish, a pre-paid return envelope, and a $2 bill as a pre-incentive that the recipient could keep regardless of whether they took the survey. Further, the invitation letter explained that the first 1,000 households to complete and submit the survey would receive a $20 Visa card as compensation. Ace Printing purchased a list of 6,941 households likely to have children and mailed the survey package to these households. In addition, a flyer with a URL link and QR code (to take the survey online) was mailed to an additional 18,000 households (regardless of whether they were likely to have children or not). These flyers likewise offered a $20 Visa card. The mailed instructions asked the adult in the household most familiar with the child to take the survey (the survey thus was often completed by the child’s parent or grandparent). If a household had more than one child, the survey questions concerned the oldest child under the age of 18 in the home. The survey was launched on August 18, 2023, and the survey was closed on October 31, 2023. A total of 840 completed surveys were received. All paper survey results were entered into the online survey platform, Sogolytics. The final results were downloaded, cleaned, and analyzed using SPSS (Statistical Package for the Social Sciences). *Demographics*: The average age for surveyed children was 12 years old. Among surveyed children, 55.8% were boys, and 44.2% were girls.

About 93.8% were Hispanic/Latino. The median household size was 5.0 people. Nearly half (49.4%) of households had a total annual income of less than $35,000, and a majority (50.9%) of households were at or below the federal poverty level.

Geospatial analysis correlating symptom survey results and environmental data

In addition to the surveyed households, environmental and water contaminant data were collected for the study area. Specifically, groundwater contaminant data were sourced from the California Water Boards Groundwater Ambient Monitoring and Assessment Program (GAMA)[12], municipal water contaminant data from the Safe Drinking Water Information System (SDWIS)[13], air quality data from the Environmental Protection Agency[14], and wind direction from the Global Wind Atlas[15]. From the municipal water and groundwater data, ten chemicals were used, based on the possible mechanisms of interest: arsenic, iron, aluminum, nitrates, nitrites, phosphates, selenium, uranium, chromium, and manganese.

In our study area, there were six different municipal water suppliers present. Each of these municipalities publishes contaminant data for each of our chemicals of interest at each site monitored. The surveyed households located within the borders of a municipal water supplier (95% of households surveyed)

were assigned contaminant data based on the average of the farthest downstream sampling sites for each municipality. The GAMA data, meanwhile, are a composite dataset of sampled locations from at least nine different organizations. The sampling locations were used to construct interpolated surfaces for each contaminant of interest for our study area, and those surfaces were used to assign contaminant values for the five percent of households located outside the boundary of any municipal water supplier. The same interpolation process was used to generate a continuous surface of the atmospheric pollutant PM10, with the resulting values assigned to each household. The predominant wind direction across the Salton Sea is along its long axis, from the northwest to the southeast. Each surveyed household was given a vectorized value that denotes its position relative to the predominant wind direction, as in Figure 5.4. The relative angle between a vector drawn between each household and the midpoint of the Salton Sea and the predominant wind direction was calculated.

Dummy variables were constructed for asthma and rash incidence for the households, and these were used as dependent variables for the models, while the groundwater/municipal water contaminant, surface water contaminant, air quality, wind direction, and demographic data were used as independent variables. Several models were constructed depending on the mechanism of interest, and all models were spatially lagged regressions – several of the input

variables exhibit significant spatial autocorrelation, as did the residuals of a spatially agnostic ordinary least squares model. The resulting models function as exploratory tools, shedding light on the explanatory power of each of the independent variables on asthma and rash incidence rates.

Surface phosphate and nitrate concentrations along the tributaries, tributary mouths (Alamo and New River), and in the Salton Sea in Figure 5.3 were collected from publicly available community organized Salton Sea Environmental Timeseries[16], Imperial Irrigation District[17], California Environmental Data Exchange Network[18], Bureau of Reclamation[19], as well as USGS Westmoreland[20,21,22].

Results

Lung inflammatory responses in exposed mice suggest a geographic gradient across the region

To identify environmental components that may trigger or drive chronic inflammatory lung disease or asthma, we studied the effects of aerosols generated from materials collected near the Salton Sea using an in vivo environmental exposure system[23]. We found that sea spray from the lake's water could induce some lung gene expression changes consistent with promotion of immune responses, however, overt inflammatory disease was not induced[23]. When filtrates of dust samples were used, many of the samples induced

significant acute neutrophilic inflammation. The patterns of cell recruitment and gene expression contrasted with the allergic inflammatory response to an aerosolized fungal allergen, suggesting that the driving component in the dust was not allergenic[9].

In the present study, we found that exposures to dust samples collected at different sites in the area induced similar patterns of neutrophilic inflammation, although the magnitude of the response varied among samples across the region (Figure 5.1). This variation showed an apparent geographic gradient, with lower inflammatory responses to samples collected at the northern end compared to higher responses to samples collected at the southern end of the region, most evident for 7-day exposures (Figure 5.1A). This geographic gradient suggests that environmental factors contributing to the inflammatory potential of the dust are not uniformly distributed across the region and may help provide clues to the source of the inflammatory component. Acute neutrophil responses were evident in 48-hour exposures as well (Figure 5.1B).

Figure 5.1 - Mouse response to Salton Sea dust from various collection sites. Numbers show the mouse inflammatory responses (percentage of neutrophils among CD45+ cells in lavage) to 7-1day exposures **(A)** and 48-hour exposures **(B)** in control air and dust exposed mice.

Asthma-related clinical symptoms show a similar geographic gradient across the region

Studies on the inflammation induced in mice were designed on the expectation that they are predictive of health impacts on residents in the region, who are subject to long term chronic exposures to these same dusts. Thus, the epidemiology of clinical pulmonary symptoms and their geographic distribution would be expected to be similar to the range seen in mouse responses. Accordingly, we performed a clinical symptom survey to assess the incidence and distribution of specific symptoms across the Salton Sea region. From previous discussions with local residents, major concerns included asthma, skin rashes, and nosebleeds, so a questionnaire was developed to query related symptoms along with demographic information.

The survey gathered approximately 830 responses from families across the region from Eastern Coachella Valley to Imperial Valley, each response including geospatial information. In this region, the population is predominantly Latino/Hispanic, with relatively low household income and related socioeconomic indicators. The distribution of demographic indicators was uniform across the region showing no clear geographic gradients.

Previous estimates of asthma incidence have been less detailed, with relatively small numbers grouped into relatively large geographic regions such as

zip codes (e.g., HARC, CHIS), which make it more difficult to associate symptoms with proximity to potential sources of disease triggers. Therefore, to correlate symptom incidence with more detailed geographic information, we aggregated responses into local population cohorts. The incidence of asthma diagnosis, as well as related clinical symptoms such as wheezing, showed an apparent geographical gradient from north to south within the region (Figure 5.2). The percentage of families reporting asthma-related symptoms was 13-19% at the northern end of the Salton Sea region, rising to approximately 35% in communities at the southern end. This gradient was specific to asthma-related symptoms; in contrast, the geographic distribution of skin rash and nosebleeds showed distinct patterns, with a concentration of skin rash notably increased at the northern end of the region.

Figure 5.2. Map of survey responses, distribution of skin rash, asthma, and wheezing. Survey responses were grouped in local cohorts for purposes of calculating symptom incidence. Note that the incidence reflects the percentage of responding families with the specific symptom, rather than the total incidence in the population. **(A)** green dots indicate survey respondents; these were mainly found within population centers. **(B)** Incidence of skin rash, showing highest incidence in communities at the North Shore and Imperial, with a possible northern gradient near the Salton Sea (blue arrow). **(C) (D)** Incidence of asthma diagnosis and wheezing, showing an apparent northwest to southeast gradient (purple arrows).

Asthma-related symptoms compared to environmental factors

As with the mouse exposure studies, the incidence of asthma symptoms showed a geographic distribution with increasing incidence in an apparent

northwest to southeast gradient. This gradient suggests a distribution of environmental factors contributing to disease incidence; these may include a variety of factors, including contributions from the region's geochemistry, such as groundwater contaminants, as well as air quality and other environmental pollutants.

In general, the groundwater and municipal water contaminant data was not a good explainer of asthma incidence rates. This is reasonable considering that asthma would most likely be induced in this population by inhaled aerosols. In addition, water sources are less likely to be a factor since the majority of households receive municipal water. This results in a lower degree of freedom than might otherwise be expected given the sample size, since nearly 800 of the households share one of only six values for each of the contaminants (one for each of the municipal water suppliers present in the study area).

Figure 5.3 - Surface water nutrient levels. Concentrations of nitrate and phosphate in surface water are shown across the region. Highest concentrations were found at the extreme northern and southern ends of the Salton Sea, where agriculture activity and runoff are high.

Surface water nutrient levels (nitrates, phosphates) also do not appear to be direct contributors to asthma incidence (Figure 5.3); because the amounts of nitrogen and phosphorous in both the north and south of the Salton Sea are

similar, those data are also not good explainers of asthma incidence differences between northern and southern households. However, it is worth noting that the levels of nitrogen and phosphorous measured in tributaries to the Salton Sea are very high, with nitrogen levels measured around 8 mg/L and phosphate levels around 1.3 mg/L[16-22,24]. Although there is some seasonal variation in these measurements, they have been consistently high for the last decade or more. For comparison, healthy rivers typically exhibit nitrate levels between 0.9 and 3.5 mg/L and phosphorous levels between 0.02 and 0.04 mg/L[25]. The levels measured in rivers feeding the Salton Sea are well in excess of the thresholds at which phytoplankton, bacteria, and algae growth is encouraged in freshwater lakes[26,27].

Figure 5.4 - Asthma and wind direction. Only a small subset of the surveyed households is displayed for clarity. For each household shown, a vector was drawn between it and the midpoint of the Salton Sea, and the angle between that vector and the predominant wind direction was assigned. In this example, the two households to the southeast of the Salton Sea end up with a low relative angle (<10°), the household to the west has a higher angle, (100°), and the household to the northwest has an even higher angle (170°).

Meanwhile, the levels of PM10 and the relative location of each household to the predominant wind direction were strong predictors of asthma in the population. Both of these variables exhibit moderate collinearity – enough that the exclusion of one variable from the regressions does not significantly impact the R^2 value of the model. The concentration of PM10 is higher to the south of the Salton Sea than to the north, but not by very much – this may be a function of

the relative sparsity and non-uniform distribution of air quality testing stations in our study area. This results in a positive but small coefficient in the regressions. Similarly, wind direction is a consistently strong predictor of asthma (Figure 5.4). Households that are downwind of the Salton Sea and in the direct path of the predominant wind direction in the area report higher asthma incidence rates. Interestingly, survey participants' household incomes and race/ethnicity data were not significant predictors of asthma. Although this finding may seem contrary to national trends, in which asthma is often correlated with lower socioeconomic measures, it is likely because the survey's population is fairly homogeneous – most of the participants were Latino/Hispanic and report a relatively low household income. Table 5.1 shows the regression results for these factors – note that due to their collinearity, the displayed results are those of two different regressions (one for each independent variable), and not for a single multiple regression.

Table 5.1 - Regression results for PM10, wind direction, and asthma incidence.

Inflammatory responses to dust are due to endotoxin from environmental bacteria

Notably, the lung inflammatory response to Salton Sea dust showed characteristics of an innate immune response[9], including an early peak with

declining cell recruitment after one week of exposure and similarity to responses to aerosolized innate ligands[9]. We next examined the possibility that LPS derived from Gram-negative bacteria is the likely inflammatory ligand in the dust; Figure 5.5 shows a reference response to a commercial preparation of LPS. In which mice were exposed to aerosolized LPS at a concentration of 15u/m^3 as characterized in (Yisrael et al. 2023)[28], however, to represent chronic aerosol exposure, here, mice were exposed for a period of 7-days. As previously reported[9], these responses also included dramatic neutrophil recruitment as well as some detectable eosinophil recruitment, but these were part of a general inflammatory response which were determined from cellular recruitment and gene expression patterns to be distinct from conventional allergic inflammatory responses to a fungal allergen.

Figure 5.5 - Cellular recruitment into the airways after 7 days of continuous exposure to 15ug/m^3 aerosolized commercial LPS. **(A)** cell numbers in Bronchoalveolar lavage fluid (BALF), **(B)** cell recruitment shown as percentage of CD45+ BALF cells, **(C)** flow cytometry dot plots showing gating of neutrophils.

To test whether the response to Salton Sea dust is indeed a response to LPS, we measured the response of mice lacking receptors for LPS (TLR4 knockout mice), and the receptor for cell wall peptidoglycan and related components of Gram-positive bacteria (TLR2 knockout). We also included mice lacking the innate adaptor protein MyD88 to test the overall requirement for innate immune signaling, as distinct from adaptive immunity to dust components

(e.g., allergic inflammation). Mice with genetic knockouts for the innate receptors TLR4, TLR2, and MyD88 were exposed to a Salton Sea dust sample known to induce a strong inflammatory response. Wildtype and TLR2 knockout mice showed similar strong lung inflammatory responses, while TLR4 and MyD88 knockouts had nearly absent inflammatory cellular recruitment (Figures 5.6 and 5.7).

While the magnitude of inflammatory cell recruitment was reduced in TLR2 knockout mice, the pattern of gene expression shown in the Principal Component Analysis (Figure 5.7) showed that both TLR4 and MyD88 knockout mice showed dramatically different responses, while the TLR2 knockout response co-localized with the response of wild type mice. Thus, the inflammatory response to Salton Sea dust appears to be primarily due to the response to LPS.

Figure 5.6 - Histology of neutrophilic recruitment from exposure to Salton Sea dust (AG site dust). (A) Lung sections showing infiltration of neutrophils and histological alterations in lung tissue of wildtype mice after exposure to Salton Sea dust. **(B)** Lung sections showing lack of neutrophil infiltration in lung tissue of TLR4-/- mice after exposure to Salton Sea dust.

Figure 5.7 - Response of innate immune receptor knockout mice to Salton Sea dust. (A) Bronchoalveolar lavage fluid cell numbers recovered from wild type (WT), and MyD88, TLR2 and TLR4 knockout mice exposed to Salton Sea dust (AG sample site); **(B)** cell percentages of CD45+ BALF cells; **(C)** flow cytometry dot plots showing neutrophils; **(D)** Principal Component Analysis (PCA) of gene expression profiling of lung tissue showing colocalization of WT

and TLR2 knockout profiles, distinct from the profiles of TLR4 and MyD88 knockout mice.

In our studies on dust collected from sites around the Salton Sea region, mice showed differences in the magnitude of inflammatory responses induced by aerosol exposures (Figure 5.1), so if LPS were the main component driving these responses, then LPS concentrations might show similar variation across the geographic range. We found that LPS concentrations measured in the dust and water samples across the region varied significantly with the highest concentrations in samples collected near the Salton Sea, both at the extreme northern and southern ends of the lake (Figure 5.8), with the highest concentrations by far found in both dust and water samples at the southeastern end, near Wister.

Figure 5.8 - LPS concentrations in dust and water samples from the Salton Sea region. (A) map showing collection sites; **(B)** LPS concentrations measured in water samples collected from the shoreline of Salton Sea, using limulus and ELISA assays; **(C)** LPS concentrations measured in dust samples, using limulus and ELISA assays. Limulus assays produced a higher signal than ELISA assays, with the ELISA often showing undetectable signals.

Importantly, the detection of LPS in the dust may be related to its biological origin. Aerosolized endotoxin has been described as a critical health issue in other locations, notably at places such as along the San Diego coast, where raw sewage dumped into the water at the US-Mexico border resulting in high levels of coliform bacterial LPS in the water as well as in aerosols[29]. Similar concerns have been raised about untreated sewage entering Salton Sea. In our testing for LPS, we used two different assays, one using a biological assay based on the limulus amebocyte extract, where an enzyme cascade is activated by LPS, causing a quantitative colorimetric output. The second was a competitive

ELISA assay, which is a structural rather than biological assay, in which antibodies against LPS are used to detect the molecules.

The biological amebocyte assay relies on evolutionarily conserved reactivity to LPS that is present as far back as invertebrate organisms, and so it was able to detect LPS in all of our samples, with an effective range of at least three logs. By contrast, the sandwich ELISA is based on antibodies specific for clinical LPS molecules, such as those produced by common human pathogens such as *E. coli*. The manufacturer confirmed that this type of assay is not suitable for detecting LPS from environmental bacteria since environmental LPS has different structures in the outer core carbohydrate. Indeed, this assay was unable to detect signal in most of the samples that showed very high activity using the limulus assay (Figure 5.8). These results suggest that the main inflammatory LPS found in our dust samples was likely produced by environmental bacteria. Interestingly, some LPS activity was detectable by the ELISA assay in samples from the southern and western collection sites; it is possible that these samples may also have LPS from clinical pathogens, contributed by runoff from livestock farming as well as possible untreated sewage[30, 31].

Discussion

Environmental factors present complex patterns of health hazards across the Salton Sea region

This study aimed to identify potential environmental factors contributing to the high incidence of clinical asthma symptoms in the Salton Sea communities. An important step was obtaining more detailed epidemiologic data on clinical symptoms and distribution in the region. These data were then correlated with several data sets, including our experimental studies on inflammation induced by dust samples, as well as publicly available data on several environmental factors geospatially mapped across the region. Publicly available data on environmental factors included groundwater contamination by heavy metals, as well as wind direction and ambient PM10 levels across the region. The data sets examined so far point to ambient air quality as a major factor, including PM10 levels, wind direction, and the dust that we subsequently found to contain significant concentrations of bacterial endotoxin, presumably from environmental microbes at the Salton Sea.

While our original studies were aimed at identifying a possible allergen to account for the high incidence of asthma in the community, our data suggest that the clinical symptoms are instead due to innate immune inflammation in response to chronic inhalation of aerosolized bacterial endotoxin from environmental microbes. This conclusion suggests that the health impacts of dust

at terminal lakes such as the Salton Sea are due to a novel clinical syndrome related to chronic inhalation of environmental endotoxin, which has important implications for diagnosis and treatment of pulmonary disease in these settings. Aerosolized endotoxin likely induces a rather different array of pathogenic mechanisms, and new studies focusing on this clinical syndrome are clearly needed.

While asthma symptoms mapped with a northwest to southeast gradient, the skin rash incidence showed a contrasting pattern, which appeared to be highest mainly in the Eastern Coachella Valley region. When compared to available data on environmental factors, there was a potential correlation with groundwater arsenic levels (not shown). Indeed, one of the symptoms of arsenic exposure is skin rash. In this region, exposure to contaminated groundwater may be greater for those residents using ground water sources (e.g., well water) rather than municipal water sources, but more detailed studies will be required to assess any relationship of symptoms to environmental exposures.

Another data set that may inform our analysis of environmental hazard is the concentration of surface water nutrients across the region. Agricultural activity, especially at the extreme northern and southern ends of the Salton Sea, contributes to high levels of phosphates and nitrates in the rivers that feed the Salton Sea. These nutrients can drive microbial growth in the water, and we

found that concentrations of bacterial endotoxin in both surface water and dust are high at the northern and southern ends of Salton Sea, where runoff boosts water nutrient levels. Notably, the highest levels of LPS were detected at the southeastern end of the lake near Wister, both in the dust and water samples, consistent with the notion that the high concentration of LPS in the water may directly contribute to LPS in the dust. While the surface water nutrient levels are not directly geographically colocalized with the highest incidence of asthma symptoms, they may be connected by promoting microbial growth and LPS production, which subsequently becomes aerosolized and transported by the prevailing winds to the population centers to the southeast, which showed the highest incidence of asthma symptoms.

Significant levels of LPS were also detected at the northern end of Salton Sea, where runoff also contributes to high levels of surface water nutrients. Its impact on local asthma symptom incidence may still be significant, but the prevailing wind direction may drive toxic dusts to the south, helping to reduce its impact in the northern region, but potentially augmenting the effects at the southern end.

Although several details remain to be worked out, the information gathered so far is consistent with a scenario (Figure 5.9) in which (1) agriculture activity runoff feeds nutrients into the surface water at the Salton Sea which drive

microbial growth, including among halophilic gram negative bacteria; (2) the LPS in the cell wall of the halophilic bacteria are released and entrained in dust at the playa; (3) inhalation of the LPS induces lung neutrophilic inflammation, with symptoms of non-allergic asthma. This scenario provides a logic model that suggests a set of mechanisms by which environmental factors lead to significant human health hazards; more detailed studies are clearly needed to identify key mechanisms as well as possible points where intervention may be helpful to public health outcomes.

Figure 5.9 - Scenario of LPS production and impacts. See text for details.

Combining data sets and methods to identify environmental health hazards

The present report is an attempt to draw attention to potential mechanistic links between environmental factors and health outcomes by combining different types of data sets, including in vivo environmental exposures, clinical surveys, and combined geospatial mapping of both types of data. This combination of disparate yet complementary data enable an analysis that points to a specific environmental toxin as a factor in a significant public health issue. Moreover, by directly connecting a bacterial toxin from the Salton Sea to pulmonary health impacts we have also posed a potential mechanism by which a degraded

ecosystem poses an environmental health hazard in the absence of direct anthropogenic pollutants.

Many environmental factors might only have an indirect relationship to specific health impacts, though they may contribute to a web of interacting factors leading to development of toxic aerosols. Our hypothetical scenario connecting nutrient runoff levels to asthma requires establishing several proposed links as well as confirming a number of mechanistic assumptions. For example, the measurements of surface water nutrients are geographically separate from the asthma-affected communities. Therefore, among the connections that need to be confirmed are (1) the production of LPS by nutrient-promoted halophilic bacterial growth in the water, (2) entrainment of LPS into aerosol dusts, and (3) airborne delivery of the toxic dusts to the nearby population centers in Imperial Valley.

For each of these steps however, there is additional information that provides some support to this scenario. In step 1, environmental bacteria, especially halophilic species, may perform modification of the LPS to allow them to manage the osmotic stress of high salt conditions. These modifications may also affect their stability in the environment as well as their biological potency[32]. Thus, nutrient-driven growth under high salt conditions may favor production of high levels of LPS that may be more easily entrained in the dust. For step 2, sea

spray or evaporation of Salton Sea water at the exposed playa concentrate organic material including LPS, separating it from salt crystals at the surface. Structural studies suggest that LPS can form larger complexes in the presence of Calcium or Magnesium ions, which might be more stable and thus more easily entrained as larger molecular complexes[33,34]. Finally, regarding step 3, the entrained dust from playa or sea spray will be carried by prevailing winds, which despite seasonal and diurnal variation, are predominantly from the northwest to the southeast. This would carry dusts generated at the Salton Sea directly into the population centers described above which may explain their high incidence of asthma symptoms.

This scenario also suggests topics needing additional research. The highly saline ecosystem of the Salton Sea apparently sustains a variety of halophilic bacteria capable of producing inflammatory LPS that can be detected by a biological assay, but not an assay specific for clinical LPS. This suggests that environmental Gram-negative bacteria are capable of producing LPS that presents a significant environmental health hazard, yet little is known about which microbes produce this LPS, or its toxicity relative to LPS from known clinical sources. More studies are needed to provide sensitive practical assays for aerosolized endotoxin from environmental sources, as well as broader monitoring for its presence in other settings.

Our studies also point to an unexpected potential role for environmental aerosolized LPS as a factor in non-allergic asthma symptoms, especially in settings where other anthropogenic causes (e.g., industrial particulates, diesel exhaust) are less likely. Conventional notions of innate immune triggers such as LPS are assumed to drive only acute but transient (a few days) inflammatory responses[34]; moreover, innate immune agonists have been shown in lab settings to induce tolerance or non-responsiveness[36]. On the other hand, under different conditions, including different timing and dose, LPS responsiveness to repeat exposure can actually be enhanced in what is called “trained immunity” and can include differentiation of myeloid cells toward a stable condition of increased reactivity[37]. Accordingly, our evidence from chronic or continuous exposures to LPS both in laboratory environmental chamber exposures, as well as in environmental settings, may drive chronic lung inflammatory disease, with symptoms that may be conflated with allergic asthma.

Conclusion

In sum, the studies and preliminary analyses are consistent with the scenario described here and offer a number of additional topics needing investigation to confirm key elements. Overall, there is sufficient support for the notion that Salton Sea aerosols carry significant concentrations of bacterial LPS, which are able to induce lung inflammation in mouse exposure studies. The mouse inflammatory responses and LPS concentrations also appear to correlate

with the geographic distribution of asthma symptoms in Salton Sea communities, offering the possibility that aerosolized LPS is a significant environmental aerosol toxin, contributing to overall environmental hazard within the region.

References

1. *Regions*. CDFW. (n.d.). https://wildlife.ca.gov/Regions/6/Salton-Sea-Program/Background

2. O'Dowd, P. (2023, February 22). *Future of the Salton Sea is tied to fate of imperiled Colorado River*. WBUR. https://www.wbur.org/hereandnow/2023/02/22/salton-sea-colorado-river-water

3. Nate Seltenrich. (2023). A Terminal Case? Shrinking Inland Seas Expose Salty Particulates and More. *Environmental Health Perspectives*, *131*(6). https://doi.org/10.1289/ehp12835

4. Ann Marie Cheney, Ortiz, G., Trinidad, A., Rodriguez, S., Moran, A., Gonzalez, A., Chavez, J., & Pozar, M. (2023). Latinx and Indigenous Mexican Caregivers' Perspectives of the Salton Sea Environment on Children's Asthma, Respiratory Health, and Co-Presenting Health Conditions. *International Journal of Environmental Research and Public Health*, *20*(11), 6023–6023. https://doi.org/10.3390/ijerph20116023

5. California Breathing County Asthma Data Tool. (2022, May 26). Www.cdph.ca.gov. https://www.cdph.ca.gov/Programs/CCDPHP/DEODC/EHIB/CPE/Pages/CaliforniaBreathingCountyAsthmaProfiles.aspx

6. Brouwer, R., Langford, I. H., Bateman, I. J., & Turner, R. K. (2002). Characteristics and contaminants of the Salton Sea sediments.

Environmental and Resource Economics, 24, 263–288. https://doi.org/10.1023/A:1016509113214

7. Sinclair, R., Russell, C., Kray, G., & Vesper, S. (2018). Asthma Risk Associated with Indoor Mold Contamination in Hispanic Communities in Eastern Coachella Valley, California. *Journal of Environmental and Public Health*, *2018*, 1–7. https://doi.org/10.1155/2018/9350370

8. Earl, C. S., An, S., & Ryan, R. P. (2015). The changing face of asthma and its relation with microbes. *Trends in Microbiology*, *23*(7), 408–418. https://doi.org/10.1016/j.tim.2015.03.005

9. Biddle, T. A., Yisrael, K., Drover, R., Li, Q., Maltz, M. R., Topacio, T. M., Yu, J., Del Castillo, D., Gonzales, D., Freund, H. L., Swenson, M. P., Shapiro, M. L., Botthoff, J. K., Aronson, E., Cocker, D. R., & Lo, D. D. (2023). Aerosolized aqueous dust extracts collected near a drying lake trigger acute neutrophilic pulmonary inflammation reminiscent of microbial innate immune ligands. *Science of the Total Environment*, *858*, 159882. https://doi.org/10.1016/j.scitotenv.2022.159882

10. Peng, Xinze, et al. “Establishment and Characterization of a Multi-Purpose Large Animal Exposure Chamber for Investigating Health Effects.” *Review of Scientific Instruments*, vol. 90, no. 3, 1 Mar. 2019, https://doi.org/10.1063/1.5042097

11. Ellwood, P., et al. “Global Asthma Network Phase I Manual.” *Globalasthmanetwork.org*, Aug. 2015, www.globalasthmanetwork.org/

12. *The Groundwater Ambient Monitoring and Assessment (GAMA) Program | California State Water Resources Control Board*. (n.d.). Www.waterboards.ca.gov. https://www.waterboards.ca.gov/gama/

13. “Public Drinking Water Watch.” *Sdwis.waterboards.ca.gov*, https://www.sdwis.waterboards.ca.gov/PDWW/

14. US EPA,OAR. (2014, July 8). *Outdoor Air Quality Data | US EPA*. US EPA. https://www.epa.gov/outdoor-air-quality-data

15. Global Wind Atlas. (2022). *Global Wind Atlas*. Globalwindatlas.info. https://globalwindatlas.info/en

16. “Salton Sea Environmental Timeseries.” *Salton Sea Environmental Timeseries*, https://saltonseascience.org/

17. Imperial Irrigation District. “Water Quality | Imperial Irrigation District.” *Www.iid.com*, www.iid.com/water/water-supply/water-quality

18. “CEDEN AdvancedQueryTool.” *Ceden.waterboards.ca.gov*, https://ceden.waterboards.ca.gov/

19. “Lower Colorado Region | Bureau of Reclamation.” *Www.usbr.gov*, www.usbr.gov/lc/region/programs/saltonsea.html

20. “New R NR Westmorland CA.” *Waterdata.usgs.gov*, https://waterdata.usgs.gov/monitoring-location/10255550/#parameterCode=00065&period=P7D

21. “Salton Sea NR Westmorland CA.” *Waterdata.usgs.gov*, http://waterdata.usgs.gov/monitoring-location/10254005/#parameterCode=62614&period=P7D%20and%20Niland%20(Site%20ID%2010254730)

22. “Alamo R NR Niland CA.” *Waterdata.usgs.gov*, https://waterdata.usgs.gov/monitoring-location/10254730/#parameterCode=00065&period=P7D&showMedian=false

23. Biddle, T. A., Li, Q., Maltz, M. R., Tandel, P. N., Chakraborty, R., Yisrael, K., Drover, R., Cocker, D. R., & Lo, D. D. (2021). Salton Sea aerosol exposure in mice induces a pulmonary response distinct from allergic inflammation. *Science of the Total Environment*, *792*, 148450. https://doi.org/10.1016/j.scitotenv.2021.148450

24. Hung, C., Diamond, C., Sinclair, R., Lee, M.-C., Stenstrom, M., Arzeno-Soltero, I.B., Freilich, M.A., Montgomery, Q., Marquez, C., Lyons, T. (2024) Nutrient loading is the root cause of short- and long-term ecological degradation and human threats in the Salton Sea region. Personal communication.

25. Poikane, S., Kelly, M. G., Várbíró, G., Borics, G., Erős, T., Hellsten, S., Kolada, A., Lukács, B. A., Lyche Solheim, A., Pahissa López, J., Willby, N. J., Wolfram, G., & Phillips, G. (2022). Estimating nutrient thresholds for eutrophication management: Novel insights from understudied lake types. *Science of the Total Environment*, *827*, 154242. https://doi.org/10.1016/j.scitotenv.2022.154242

26. Miettinen, I T, et al. “Phosphorus and Bacterial Growth in Drinking Water.” *Applied and Environmental Microbiology*, vol. 63, no. 8, 1997, pp. 3242–3245, https://doi.org/10.1128/aem.63.8.3242-3245.1997

27. Zeng, Qinghui, et al. “Critical Nutrient Thresholds Needed to Control Eutrophication and Synergistic Interactions between Phosphorus and Different Nitrogen Sources.” *Environmental Science and Pollution Research*, vol. 23, no. 20, 4 Aug. 2016, pp. 21008–21019, https://doi.org/10.1007/s11356-016-7321-x

28. Yisrael, Keziyah, et al. “Route of Administration Significantly Affects Particle Deposition and Cellular Recruitment.” *PloS One*, vol. 18, no. 11, 27 Nov. 2023, pp. e0289373–e0289373, https://doi.org/10.1371/journal.pone.0289373

29. Singh, Maanvi. “Heavy Metals and E Coli: Raw Sewage in Tijuana River Endangers California Communities.” *The Guardian*, 15 Feb. 2024, www.theguardian.com/environment/2024/feb/15/us-mexico-california-tijuana-river-illness-public-health

30. James, Ian. “This River Is Too Toxic to Touch, and People Live Right next to It.” *Desertsun.com*, Palm Springs Desert Sun, 10 Dec. 2018, www.desertsun.com/in-depth/news/environment/border-pollution/poisoned-cities/2018/12/05/toxic-new-river-long-neglect-mexico-border-calexico-mexicali/1381599002/

31. California Water Boards. “New River Introduction |Colorado River Regional Water Quality Control Board.” *Www.waterboards.ca.gov*, 24 Sept. 2020, www.waterboards.ca.gov/rwqcb7/water_issues/programs/new_river/nr_intro.html

32. Caroff, Martine, and Alexey Novikov. “LPS Structure, Function, and Heterogeneity.” *Endotoxin Detection and Control in Pharma, Limulus, and Mammalian Systems*, 2019, pp. 53–93, https://doi.org/10.1007/978-3-030-17148-3_3

33. P. Selvarengan, et al. “Complexation of Carboxyl Groups in Bacterial Lipopolysaccharides: Interactions of H+, Mg2+, Ca2+, Cd2+, and UO22+ with Kdo and Galacturonate Molecules via Quantum Mechanical Calculations and NMR Spectroscopy.” *Chemical Geology*, vol. 273, no. 1-2, 1 Apr. 2010, pp. 55–75, https://doi.org/10.1016/j.chemgeo.2010.02.012

34. Lee, Christopher, et al. “Cation-Driven Lipopolysaccharide Morphological Changes Impact Heterogeneous Reactions of Nitric Acid with Sea Spray

Aerosol Particles." *The Journal of Physical Chemistry Letters*, vol. 12, no. 20, 22 May 2021, pp. 5023–5029, https://doi.org/10.1021/acs.jpclett.1c00810

35. Kumar, Vinay, Abul Abbas, Nelson Fausto, and Jon C. Aster, eds. Pathologic Basis of Disease, Eighth edition (Saunders Elsevier, Philadelphia) 2010. pp. 43-69.

36. Gillen, Joseph, et al. "LPS Tolerance Inhibits Cellular Respiration and Induces Global Changes in the Macrophage Secretome." *Biomolecules*, vol. 11, no. 2, 1 Feb. 2021, p. 164, www.mdpi.com/2218-273X/11/2/164

37. Trim Lajqi, et al. "LPS Induces Opposing Memory-like Inflammatory Responses in Mouse Bone Marrow Neutrophils." *International Journal of Molecular Sciences*, vol. 22, no. 18, 10 Sept. 2021, pp. 9803–9803, https://doi.org/10.3390/ijms22189803

Acknowledgments

Research reported in this publication was supported by the National Institute On Minority Health And Health Disparities of the National Institutes of Health under Award Number U54MD013368, and the U.S. Department of the Interior, Bureau of Reclamation, award number R24AP00194. The content is solely the responsibility of the authors and does not necessarily represent the official views of the National Institutes of Health or the U.S. Department of the Interior.

Figures

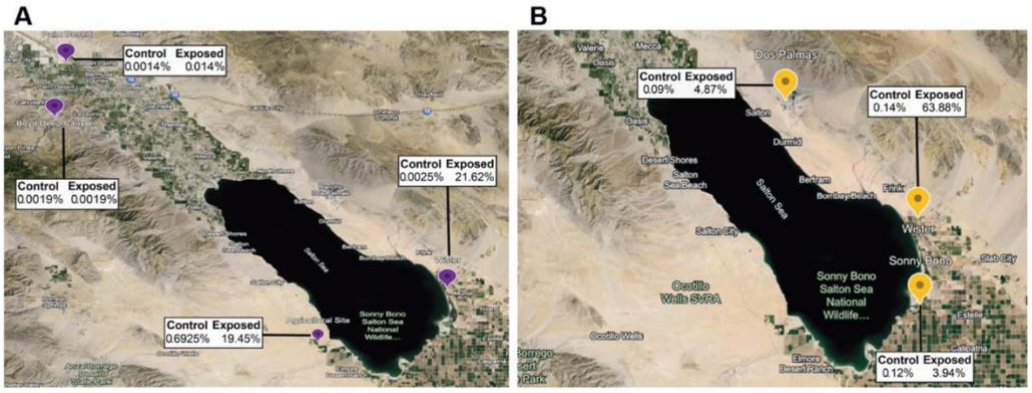

Figure 5.1 - Mouse response to Salton Sea dust from various collection sites. Numbers show the mouse inflammatory responses (percentage of neutrophils among CD45+ cells in lavage) to 7 day-exposures (**A**) and 48-hour exposures (**B**) in control air and dust exposed mice.

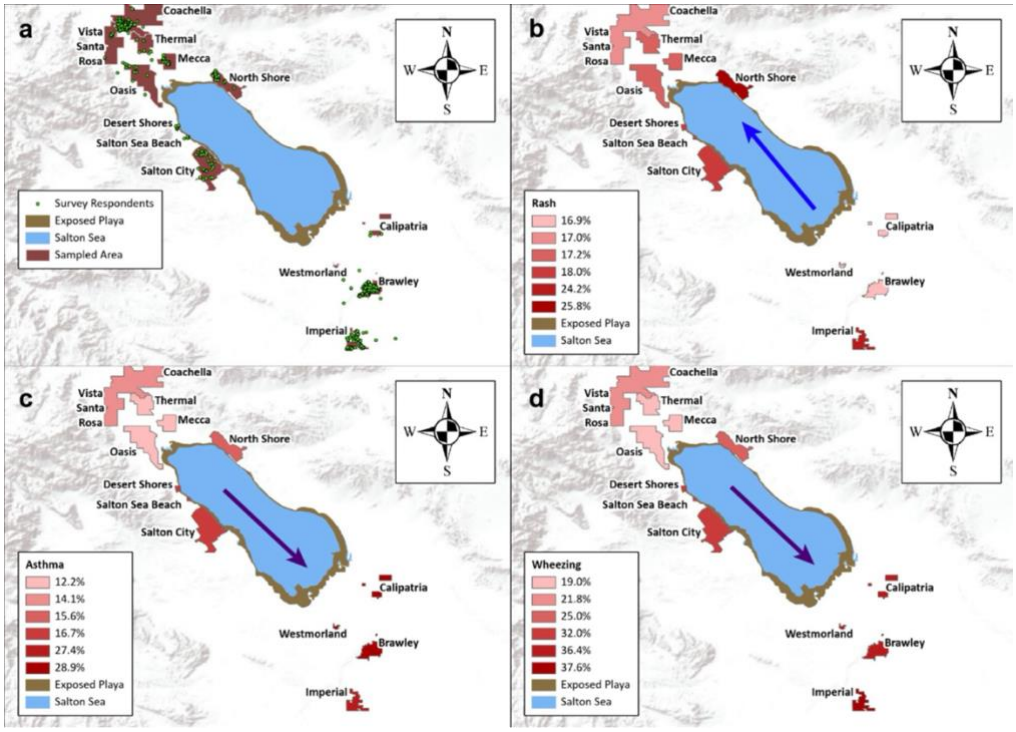

Figure 5.2 - Map of survey responses, distribution of skin rash, asthma, and wheezing. Survey responses were grouped in local cohorts for purposes of calculating symptom incidence. Note that the incidence reflects the percentage of responding families with the specific symptom, rather than the total incidence in the population. **a,** green dots indicate survey respondents; these were mainly found within population centers. **b,** Incidence of skin rash, showing highest incidence in communities at the North Shore and Imperial, with a possible northern gradient near the Salton Sea (blue arrow). **c, d,** Incidence of asthma diagnosis and wheezing, showing an apparent northwest to southeast gradient (purple arrows).

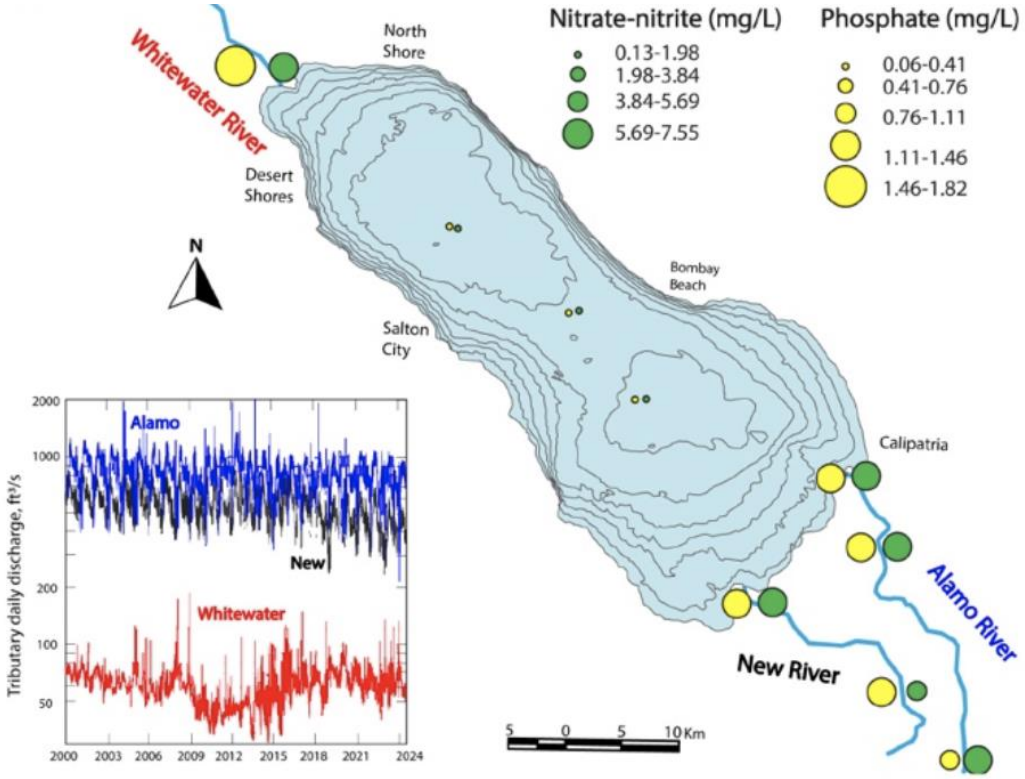

Figure 5.3 - Surface water nutrient level. Map shows nitrate and phosphate concentrations (mg/L) in surface waters of the Salton Sea and its tributaries (Whitewater, Alamo, and New Rivers). Bathymetric contours (1.5 m) are based on 1999 Bureau of Reclamation data. Nutrient data for the lake and Alamo/New Rivers were collected on March 19, 2019 (source: CEDEN, IID, Bureau of Reclamation). Whitewater River mouth data are from December 3, 2022 (source: Salton Sea Environmental Time Series, https://saltonseascience.org/). Tributary daily discharge (ft3/m) are shown for Alamo, New and Whitewater rivers (source: USGS NWIS) from year 2000 to 2024.

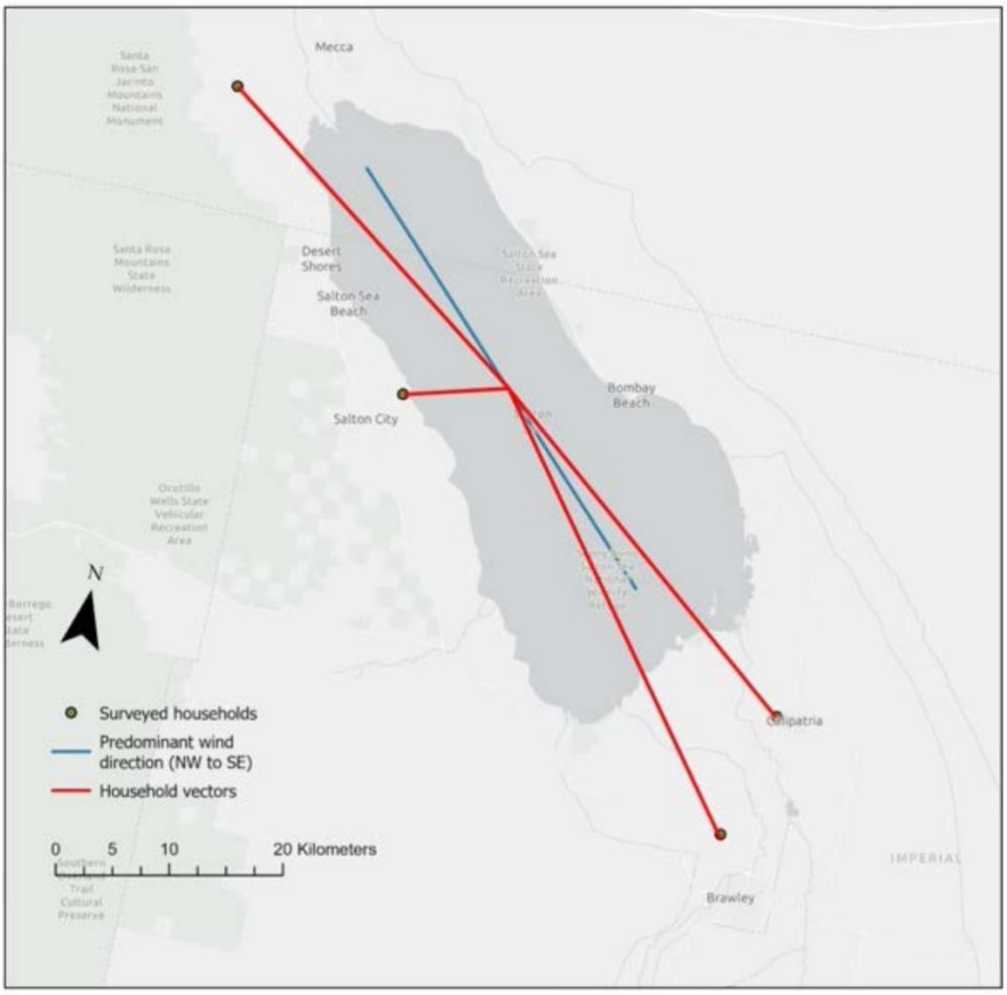

Figure 5.4 - Asthma and wind direction. Only a small subset of the surveyed households is displayed for clarity. For each household shown, a vector was drawn between it and the midpoint of the Salton Sea, and the angle between that vector and the predominant wind direction was assigned. In this example, the two households to the southeast of the Salton Sea end up with a low relative angle (<10°), the household to the west has a higher angle, (100°), and the household to the northwest has an even higher angle (170°).

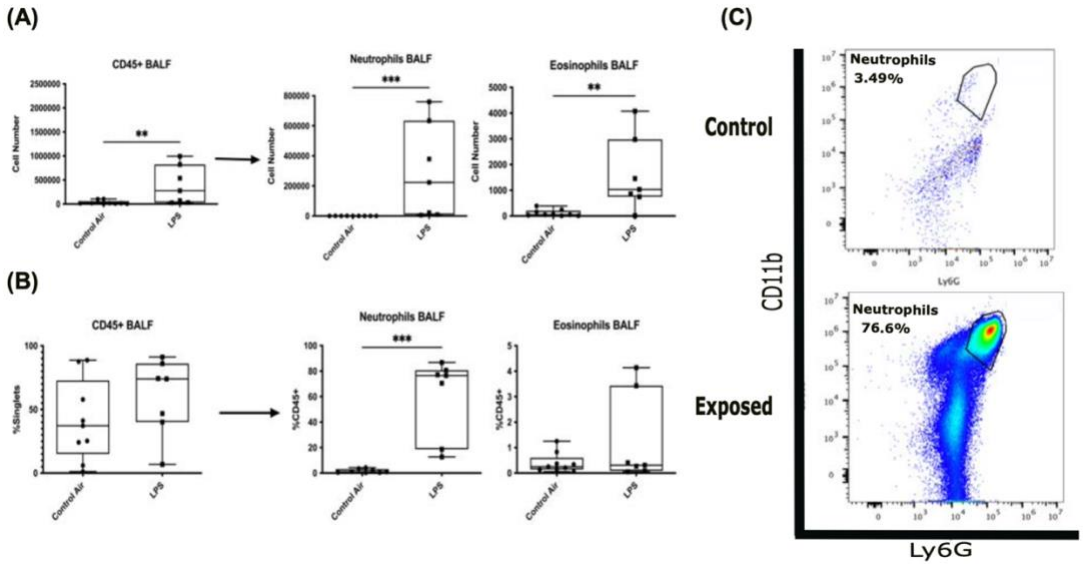

Figure 5.5 - Cellular recruitment into the airways after 7 days of continuous exposure to 15ug/m3 aerosolized commercial LPS. **(A)** cell numbers in Bronchoalveolar lavage fluid (BALF), **(B)** cell recruitment shown as percentage of CD45+ BALF cells, **(C)** flow cytometry dot plots showing gating of neutrophils. (P-values. For cell counts, Neutrophils WT vs LPS: 0.0002. Eosinophils WT vs LPS 0.0079. For cell percentages, Neutrophils WT vs LPS:0.0003. Eosinophils WT vs LPS: ns.)

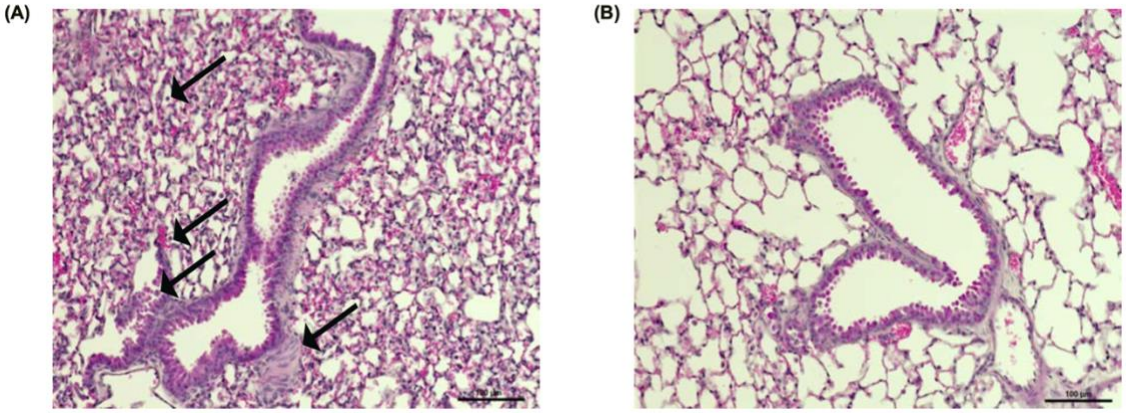

Figure 5.6 - Histology of neutrophilic recruitment from exposure to Salton Sea dust (AG site dust). (A) Lung sections showing infiltration of neutrophils and histological alterations in lung tissue of wildtype mice after exposure to Salton Sea dust. **(B)** Lung sections showing lack of neutrophil infiltration in lung tissue of TLR4-/- mice after exposure to Salton Sea dust.

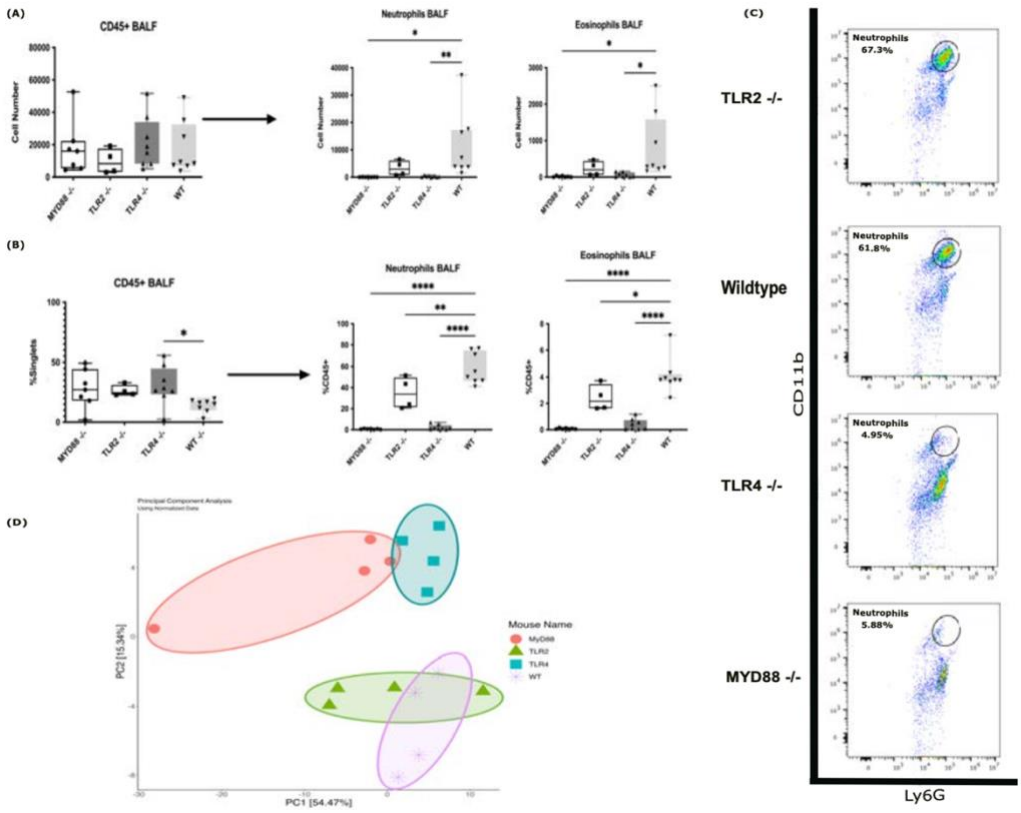

Figure 5.7 - Response of innate immune receptor knockout mice to Salton Sea dust. (A) Bronchoalveolar lavage fluid cell numbers recovered from wild type (WT), and MyD88, TLR2 and TLR4 knockout mice exposed to Salton Sea dust (AG sample site); **(B)** cell percentages of CD45+ BALF cells; **(C)** flow cytometry dot plots showing neutrophils; **(D)** Principal Component Analysis (PCA) of gene expression profiling of lung tissue showing colocalization of WT and TLR2 knockout profiles, distinct from the profiles of TLR4 and MyD88 knockout mice. (P-values. For cell counts, Neutrophils WT vs TLR2ko: 0.1588; vs TLR4ko: 0.0091; vs MyD88ko: 0.0102. Eosinophils WT vs TLR2ko: ns; vs TLR4ko: 0.0164; vs MyD88ko: 0.0136. For cell percentages, Neutrophils WT vs TLR2ko: 0.0024; vs TLR4ko: <0.0001; vs MyD88ko: <0.0001. Eosinophils WT vs TLR2ko: 0.0110; vs TLR4ko: <0.0001; vs MyD88ko: <0.0001.).

(A)

(B)

LPS concentrations in water samples

Site	LAL LPS Concentration (EU/mL)	ELISA LPS Concentration (EU/mL)	Coordinates	Number on Map
North Shore	0.81	0.010	33°30'38"N 115°55'52"W	1
Salton City	9.07	0.025	33°15'43"N 115°44'27"W	7
Wister	338.57	0.025	33°18'49"N 115°37'52"W	3b

(C)

LPS concentrations in dust samples

Site	LAL LPS Concentration (EU/mL/month)	ELISA LPS Concentration (EU/mL/month)	Coordinates	Number on Map
Boyd Deep Canyon (BDC)	0.044	n.d.	33°39'14"N 116°22'27"W	9
Dos Palmas (DP)	0.808	n.d.	33°29'17"N 115°50'05"W	2
Community Center (CC)	0.309	0.121	33°32'40"N 116°06'47"W	8
Lot	0.085	0.062	33°17'52"N 115°55'31"W	6
Agricultural Site (AG)	0.728	0.002	33°10'06"N 115°51'20"W	5
Red Hill Bay (RHB)	0.141	0.023	33°11'58"N 115°36'44"W	4
Wister (WI)	2912.33	n.d.	33°19'29"N 115°34'58"W	3a

Figure 5.8 - LPS concentrations in dust and water samples from the Salton Sea region. (A) map showing collection sites; (B) LPS concentrations measured in water samples collected from the shoreline of Salton Sea, using limulus and ELISA assays; (C) LPS concentrations measured in dust samples, using limulus and ELISA assays. Limulus assays produced a higher signal than ELISA assays, with the ELISA often showing undetectable signals.

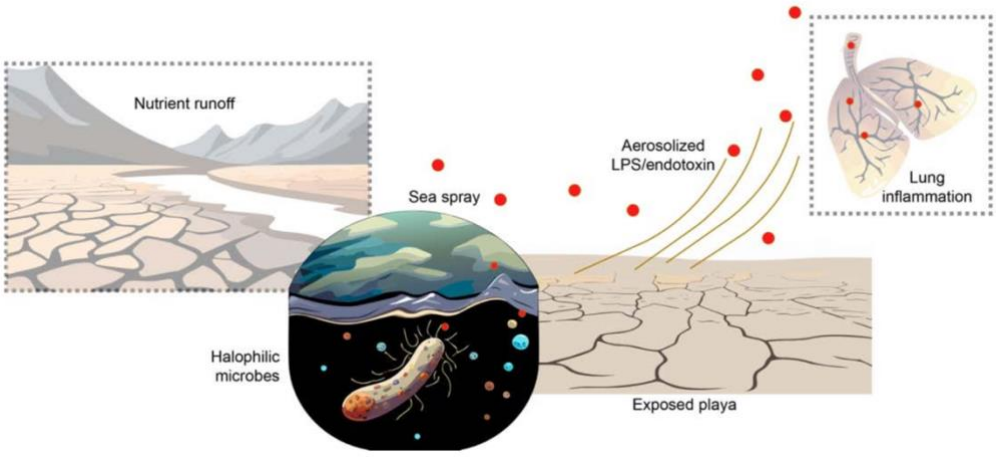

Figure 5.9 - Scenario of LPS production and impacts.

Variable	Coefficient	p-value
Relative angle	-1.163	<0.001
PM10	0.081	<0.001

Table 5.1 - Regression results for PM10, wind direction, and asthma incidence.

Chapter 6: Effects of TGF-βRI Signaling Prevention on Protection From Airway Remodeling in Murine Model of Allergic Inflammation

Abstract

Our research aims to investigate the underlying mechanisms of airway remodeling by studying a key contributor in asthma disease progression, transforming growth factor beta 1 (TGF-β), in a clinically representative model of allergic disease. Airway remodeling (AWR) is a complex molecular process which leads to irreversible structural changes to the lung tissue of patients suffering from chronic respiratory illnesses such as asthma. These physical alterations include subepithelial fibrosis, neovascularization, glandular enlargement, goblet cell hyperplasia, and increased smooth muscle and collagen deposition. Research shows these changes to lung physiology are linked to both an increase in asthma severity as well as nonresponsiveness to current treatment methods (e.g., corticosteroids)[1,2]. AWR is often directly correlated with chronic allergic asthma due to various Th2 cytokines serving as main driving factors behind this mechanism such as IL-13 and IL-4 are central mediators in the molecular process of AWR[3]. Although the driving mechanisms for the involvement of these cytokines are not yet well known, it is hypothesized that IL-13 stimulates collagen production by activating airway fibroblasts and macrophages potentially in a Matrix Metalloproteinase (MMP) and TGF-B dependent manner9. It is known, however, that activation of these cell types via IL-13 leads to increased deposition of collagen in the extracellular matrix of

affected lungs[4]. To investigate the effect of inhibition of TGF- β signaling on inflammation and airway remodeling, animals were treated with Vactosertib, an anti-TGF-βRI drug, and exposed to *Alternaria alternata* and inflammatory responses and airway structural changes were analyzed.

Introduction

Airway remodeling and asthma

Asthma is a chronic respiratory disease characterized by the presentation of clinical symptoms such as wheezing, coughing, excessive mucus production, and chest tightness/pain. Asthma is a complex disease possessing multiple subsets. The most prevalent forms being allergic and nonallergic asthma. Allergic asthma is characterized by severe eosinophilia, differentiation of T cells into Th2 cells, as well as production of allergy associated antibodies such as IgE. Allergic inflammation is the most common form of asthma and is typically well managed through the use of corticosteroids, antibodies, and beta agonists[5]. While nonallergic asthma, although much less common, is a more severe form of the disease, described by infiltration of neutrophils into the tissues and airways of the lung and skewing of T cells towards Th1 or Th17 phenotypes[6]. Nonallergic pulmonary inflammation presents with more severe symptoms not addressed by current treatment methods.

Although possessing different inflammatory phenotypes, both forms of the disease can be complicated by the development of airway remodeling (AWR). AWR refers to the physiological changes within the lung in conditions of sustained pulmonary inflammation. These changes included basement membrane thickening of the airway epithelium, goblet cell hyperplasia, smooth muscle proliferation, collagen deposition, as well as other changes within the extracellular matrix[7]. AWR can significantly affect the severity of disease manifestation in asthmatics with increased degrees of AWR correlating directly with increased severity of symptom manifestation. Those suffering from severe airway remodeling are prone to increased frequency of disease exacerbation, corticosteroid insensitivity, as well as an overall worse prognosis.

TGF-β and asthma

TGF-β is implicated in both the progression of asthma and the development of airway remodeling. In literature, TGF-β demonstrates the ability to induce production of Th2 cytokines (e.g., IL-4 and IL-13) from CD4+ T cells, directly aiding in the development of pulmonary fibrosis. TGF-β is a pleotropic cytokine which controls cellular proliferation, differentiation, apoptosis, as well as many other molecular functions[8]. In relation to airway remodeling, this protein is known to be involved in goblet cell proliferation, subepithelial fibrosis, and direct fibroblast proliferation− major hallmarks of airway remodeling[9]. Although eosinophils have been believed to be the primary producers of TGF-β during

allergic inflammation, recent literature demonstrates that various immune and structural cells (e.g., macrophages, fibroblasts, lymphocytes, epithelial, endothelial, and smooth muscle cells) can also produce and secrete TGF-β during asthma induction[10]. Although AWR is a very complex process compiled of many simultaneous processes, many are centered around TGF- β and its potent ability to promote pulmonary fibrosis. For this reason, the use of therapeutics which target this protein may be a viable approach to disease management and prevention of progression of airway remodeling.

TGF-β signaling

The multifunctional protein, TGF-β, is secreted by a variety of cells into the extracellular matrix (ECM) as precursor proteins. This reservoir of inactive TGF-β in the ECM is associated with its latency-associated peptide (LAP) to allow for tightly regulated processes due to the pleiotropic properties of TGF-β[11]. This latent form of the protein can be activated by a variety of triggers such as low pH, integrins, matrix metalloproteinases (MMP2/MMP9), reactive oxygen species, and thrombospondin-1[11]. The cleavage of TGF-β from LAP initiates binding and signaling through TGF-βRI and TGF-βRII. Binding of TGF-β to TGF-βRII causes receptor dimerization with TGF-βRI and phosphorylates TGF-βRI to allow for the recruitment and phosphorylation of transcription factors SMAD 2/3[11,12]. Phosphorylated SMAD 2/3 complex translocates to the nucleus for regulation of genes involved in cellular proliferation, survival, ECM production, fibrosis, and

many other biological processes[13]. By targeting the activity of this pleotropic protein, we hope to mitigate fibrosis and inflammation to aid in disease manifestation and lung function.

Vactosertib

Vactosertib is a potent inhibitor of transforming growth factor beta (TGF-β) receptor type 1, a serine/threonine kinase[14]. It has been recognized for its antineoplastic activity for various cancers such as esophageal, colorectal, osteosarcoma, and others. However, its potential for use in cases of asthma has not yet been addressed. The mechanism of action of Vactosertib is via binding to TGF-β receptor I and preventing downstream signaling[15]. Due to the potential of Vactosertib in ongoing cancer trials, we hypothesized that it could potentially serve therapeutic purposes in cases of asthma with extensive airway remodeling[15]. To investigate its efficacy in this instance, we created murine models of allergic inflammation by exposing mice to *Alternaria alternata* either by aerosol exposure chamber or intranasal administration and investigated the efficacy of Vactosertib at inhibiting proinflammatory and profibrotic processes.

Alternaria alternata

Alternaria alternata is a common household fungus known to induce allergic asthma[16]. This fungus is commonly used to generate murine models of clinical allergic disease. *Alternaria* is known to stimulate the immune system by

activation of PAR2, a G protein-coupled receptor (GPCR)[17]. *Alternaria* alkaline serine protease (AASP) has potent protease activity and activates PAR2 by cleavage of the extracellular amino terminus[17]. This activation induces downstream signaling via Gαq and β-arrestin-dependent pathways[18]. Signaling through these adaptor proteins ultimately result in production of allergy associated chemokine such as CCL5, known to induce eosinophil recruitment, a characteristic feature of allergic inflammation[19]. Exposure to *Alternaria* in murine models leads to distinctive allergic responses in mice characterized by increased IgE production, airway hyperreactivity (AHR), as well as increased expression of Th2 cytokines such as IL-4 and IL-13. Although there are hypothesized to be various allergens of *Alternaria*, AASP/PAR2 immune activation is the most well characterized.

To mimic physiological exposure, we exposed mice to *Alternaria alternata* fungal filtrate in an environmental aerosol exposure chamber described in Peng et. al.[20]. Additionally, we exposed mice to this allergen by intranasal administration. In the aerosol exposure group, mice were administered drug via implantation of an Alzet osmotic pump and exposed to allergen. The Alzet pump is an osmotically regulated infusion pump that allows for consistent delivery of a drug over extended periods of time[21]. In this group of mice, no potential anti-inflammatory or anti-fibrotic activity was observed. However, in animals administered Vactosertib intraperitoneally (I.P.) and exposed to allergen, we

observed an anti-inflammatory phenotype described by significant inhibition of eosinophil recruitment into airways of allergen challenged mice.

Materials and methods

Animals

8-week-old C57BL/6J (B6) male and female mice were obtained from Jackson Laboratories, Sacramento. Animals are allowed to acclimate for one week in the University of California, Riverside SPF vivarium. All mice are housed 3-4 to a cage and are giving food and water ad libitum. Animals were placed on a 12-hour day/night light cycle.

Surgery

For the experimental group being exposed to *Alternaria* via aerosol, all mice underwent surgical implantation of Alzet pumps to administer either PBS or Vactosertib (2.5 mg/kg/day). Mice were anesthetized using isoflurane and administered buprenorphine (0.1 mg/kg) before beginning surgery. Surgical area was shaved and cleaned with 70% ETOH and povidone iodine before one incision was made on the dorsal side of the animal closer to the nape to create a pocket between the skin and muscle layers. Alzet pumps were then inserted into the pocket and the incision was closed using surgical clamps. Antibiotic ointment was applied and carprofen (5 mg/kg) was administered once a day for three days

following surgery. Mice were individually housed and allowed to rest for 1 week before exposure studies were conducted.

Mice were divided into 5 study groups outlined below: positive controls who received PBS via Alzet pump and exposed to Alternaria, the experimental group which received Vactosertib via Alzet pump and exposed to Alternaria, negative controls which received PBS via the pump and exposed to filtered air, drug controls which received Vactosertib but exposed to filtered air, and vehicle controls in which animals received DMSO and exposed to filtered air.

Exposures and treatment

Aerosol Exposure

8-week-old female and male mice were purchased from Jackson Laboratory. The aerosol exposure group underwent surgical implantation of an Alzet pump to allow for consistent delivery of Vactosertib or PBS for the duration of the exposure. Mice were anesthetized with isoflurane before proceeding with surgery. Animals were administered 0.1 mg/kg buprenorphine and placed in a prone position to expose its back. The surgical area was then shaved to remove fur before swabbing the area three times in sequence with 70% ethanol, surgical scrub, and gently wiped with an alcohol swab. A small incision was made on the back side and a hemostat was then inserted into the incision to create a pocket. Preloaded Alzet pumps were surgically implanted under the skin. Wound clips

were used to close the incision and animals were administered 1-week following surgical implantation of the Alzet pump**,** mice were exposed to 750 ug/m^3 *Alternaria alternata* in an aerosol exposure chambers for 2-weeks.

Intranasal Exposure

B6 mice were divided into 5 groups as specified below: Positive controls in which animals received (50ug in 20 ul) *Alternaria* by intranasal administration (I.N.) and given Vactosertib (0.658mg in 100 ul) Intraperitoneally (IP), the experimental group which received Alternaria I.N. and Vactosertib I.P., negative controls which were administered PBS I.P. and PBS I.N., drug controls which received PBS I.N. and Vactosertib I.P., as well as vehicle controls which were administered DMSO I.N. and PBS I.P. Animals were treated for 4 consecutive days and allowed to rest for 3 days before sacrifice. Upon sacrifice, flow cytometry and NanoString analysis were performed to assess pulmonary inflammation by cellular recruitment and gene regulation.

Flow Cytometry

Following exposure, bronchoalveolar lavage fluid (BALF) and left lung lobes are analyzed via flow cytometry. Mice are anesthetized with isoflurane before cervical dislocation. Chest cavities are opened to expose lungs and an incision is made in the trachea. Tubing connected to a 23G needle is inserted into the trachea to allow for administration of 0.8 mL of PBS into the airways.

Airways are washed a total of 3x to collect BALF and processed for flow cytometry analysis. After collection of BALF, left lung lobes are collected and digested using 0.5 mg/mL collagenase, and 50 u/mL DNase and digested into a single cell mixture using the Miltenyi Biotec GentleMACS tissue dissociator. This cell mixture is then treated with ACK lysis buffer (Gibco), to lyse red blood cells. Cells then undergo a series of PBS washes before being fixed and stained. Cells isolated from the airways as well as the lung tissue are stained using the following antibody-fluorophore panel: anti-CD45 FITC (BioLegend, San Diego, USA; Clone 30-F11), anti-CD19 PerCP-Cy5.5 (Invitrogen, San Diego, USA; Clone
eBio1D3 (1D3)), anti-SiglecF APC (BioLegend, San Diego, USA; Clone S17007L), anti-CD11c PE-Cy7 (BioLegend, San Diego, USA; Clone N418), anti-CD3 Alexa Fluor 700 (BioLegend, San Diego, USA; Clone 17A2), anti-Ly6G BV510 (BioLegend, San Diego, USA; Clone 1A8), and anti-CD11b BV421 (BioLegend, San Diego, USA; Clone M1/70). Samples were run using the Novocyte Quanteon flow cytometer and all gating and analysis was done using FlowJo software.

RNA extraction and Nanostring

RNA was extracted from right lobes of each exposure group using a TRIzol (Ambion) based protocol. An estimate of 100 mg of frozen right lung lobes was placed in a mortar and pestle. Liquid nitrogen was then added, and the

tissues were ground into a fine dust. This sample is then treated with TRIzol to initiate RNA extraction from protein and DNA before treatment with chloroform to further extract RNA from other material. Upon addition of chloroform, samples are mixed and centrifuged. Aqueous phase containing RNA is collected and undergoes a series of alcohol washes and centrifuge steps for product cleanup. Resulting pellets were resuspended in DEPC-treated water (Invitrogen) and concentration and purity were analyzed via a NanoDrop 2000 (Thermo Scientific).

Extracted RNA was analyzed using an nCounter Sprint Profiler (NanoString Technologies, USA) with the nCounter Mouse Immunology Panel. All statistical analysis was performed using nSolver Advanced Analysis software and false discovery rates were calculated using the Benjamini-Hochberg method.

SHG

Second Harmonic generation (SHG) microscopy technique was utilized as a method to measure fibrosis. This technique allows for the autofluorescence of collagen fibers due to their noncentrosymmetric structure[22]. Left lung lobes were excised and fixed overnight in 4% PFA. Following fixation, tissues were washed in 1x PBS and left overnight in 30% sucrose to minimize drying artifacts. The following day, lungs are then frozen in OCT compound (Fisher HealthCare) over a block of dry ice using a 15mmx15mm tissue cassette. Tissues are stored in -20

degrees before sectioning at 15mm using a cryostat. These tissues are then mounted on a slide, mounting media (Prolong Gold No DAPI) is applied, and slides are mounted using a cover slip. Samples are then imaged using the Nikon Multiphoton Microscope.

Flexivent

Lung function measurements were taken utilizing flexivent instrumentation (SCIREQ). Mice were administered 80 mg/120 mg ketamine/xylazine in 1x PBS intraperitoneally (IP). After 10 minutes, a toe pinch reflex test was conducted to ensure anesthetization before proceeding. Anesthetized mice were placed on a 50 degrees Celsius heating pad to maintain temperature throughout surgery. 70% ethanol was used to clean the surgical area prior to making a small incision to remove skin and muscle layers atop of the trachea. The trachea was then exposed, and a small incision was made between two cartilage rings of the trachea. A cannula was then inserted and tied off to secure, and mice were connected to the Flexivent instrument. Lung hyperreactivity, resistance, elasticity, and Pressure-volume data was collected and analyzed using PRISM.

Histology

For histological analysis, lungs were inflated with 0.3mL of 10% neutral buffered formalin (NBF), excised, and placed in 10mL of 10% NBF for 24 hours. Tissues were then washed in 1x PBS before placing in 70% ethanol. NBF fixed

tissue was then shipped to University of Irvine for paraffin embedding and sectioning at 15 um using a microtome. Sections were deparaffinized and stained with hematoxylin and eosin (H&E) to analyze cellular recruitment and histological alterations.

Results

Alternaria induces allergic inflammation in exposed mice

Flow cytometry

Both aerosol and intranasally exposed groups demonstrated significant inflammation of both the airways and the parenchyma in experimental, positive control, as well as vehicle and drug control groups.

Aerosol group

In the aerosol exposed group, there was no significant difference of cellular recruitment profiles among the positive control group and the experimental, treated groups (Fig. 6.1). Treatment with Vactosertib was not sufficient to inhibit inflammation in neither the lungs nor the airways of *Alternaria* exposed mice. Histology, Flexivent, and SHG were not performed on this group as this experiment is still in preliminary stages and requires optimization of drug delivery methods before testing its effects. For this reason, the following sections will highlight results from all intranasal experiments.

Figure 6.1 - Cellular recruitment in BALF and lungs of aerosolized *Alternaria alternata* exposed animals. (A) Cell numbers in BALF **(B)** Cell numbers in lung **(C)** Cell percentages in BALF **(D)** Cell percentages in lung.

I.N. group

Among all groups exposed to Alternaria intranasally, with exception of saline exposed mice, there were no differences between recruitment of T cells, B cells, or neutrophils in bronchoalveolar lavage fluid (Fig. 6.2A and C). However, the population of recruited eosinophils in the airways significantly decreased when treated with Vactosertib (Fig. 6.2A and 2C). In the lungs of treated mice, there was no significant difference between the recruitment of eosinophils in the treated vs positive control groups (Fig. 6.2B and 2D). These results suggest direct inhibitory activity of Vactosertib on eosinophil recruitment into the airways specifically.

Figure 6.2 - Cellular recruitment in BALF and lungs of intranasal *Alternaria alternata* exposed animals. (A) Cell numbers in BALF **(B)** Cell numbers in lung **(C)** Cell percentages in BALF **(D)** Cell percentages in lung.

SHG

Although Vactosertib treated mice did not demonstrate statistically significant differences in collagen deposition when compared to controls, there was a slight trend towards decreasing collagen deposition observed in treated animals (Fig. 6.3). Additional studies including a larger sample size will be conducted to further elucidate the effect of TGF-β signaling inhibition.

Figure 6.3 - Second Harmonic Analysis of lungs of intranasal *Alternaria alternata* exposed animals. (A) SHG of left lobe of control mouse **(B)** SHG of left lobe of *Alternaria* exposed mouse **(C)** SHG of left lobe of *Alternaria* exposed and Vactosertib treated mouse.

Histology

Histological changes within the tissue of exposed and control animals were not significant. However, minute differences were observed. Alternaria exposed animals demonstrated increased cellular infiltration as well as increased smooth muscle deposition surrounding larger airways (Fig. 6.4).

Figure 6.4 - H&E images of lungs of intranasal *Alternaria alternata* exposed animals. (A) H&E of control mouse **(B)** H&E of *Alternaria* exposed mouse. Black arrows highlighting cellular recruitment in airways. Yellow arrow highlighting increased smooth muscle deposition surrounding airway. **(C)** H&E of *Alternaria* exposed and Vactosertib treated mouse.

Nanostring

No significant gene regulatory differences were observed. However, when compared to the nontreated group, there was slight downregulation in collagen biosynthesis and fibroblast migration related genes such as Ccl11 and Pdgfrb. These proteins demonstrated a negative log2fold change of -0.871 and -0.964, respectively (Table 6.1). Additionally, both NF-kB activation and myofibroblast regulation were decreased in the treated group. Although not significant, this trend in decreasing collagen biosynthesis, NF-kB signaling, and myofibroblast regulation lightly supports decreased fibrosis and inflammation in Vactosertib

treated animals (Fig. 6.5). Additional studies will need to be done in order to increase sample size and overall significance.

Table 6.1 - Table of log fold change of Ccl11 and Pdgfrb in Vactosertib treated mice.

Figure 6.5 - NF-kB signaling and myofibroblast regulation in intranasal *Alternaria* alternata exposed mice. (A) NF-kB signaling in *Alternaria* (Exposed) mice vs *Alternaria* exposed and Vactosertib treated mice (Treated). **(B)** Myofibroblast regulation in *Alternaria* (Exposed) mice vs *Alternaria* exposed and Vactosertib treated mice (Treatment).

Flexivent

Flexivent analysis revealed significant mechanical changes within the lung tissue. Although no differences were observed in airway resistance, significant differences were identified in both tissue resistance as well as tissue elastance (Fig. 6.6A-C). Untreated animals exposed to *Alternaria* demonstrated an increased tissue resistance when compared to Vactosertib treated animals, signifying decreased collagen deposition in the parenchyma of mice treated with the drug (Fig. 6.6B). Additionally, tissue elasticity was significantly decreased in treated mice, demonstrating decreased deposition of elastic fibers in the tissue as well as the extracellular matrix (Fig. 6.6C). Vactosertib treated animals also exhibited an increase in inspiratory capacity when compared to *Alternaria* exposed mice (Fig. 6.6D).

Pressure-volume curves (PV loops) were generated to elucidate mechanical behavior of the respiratory system. PV curves are advantageous in representing the dynamic interaction of changes between pressure and volume during inspiration and exhalation. Pressure-volume changes in Alternaria exposed animals demonstrated a PV loop indicative of an emphysema-like phenotype (Fig. 6.6E). However, when animals were treated with Vactosertib, this phenotype diminished, and lung mechanics were similar to those of the controls. This data suggests the ability of Vactosertib to mitigate the structural and mechanical changes to lung parenchyma induced by *Alternaria* exposure.

Figure 6.6 - Flexivent analysis of intranasal *Alternaria alternata* and PBS exposed mice. (A) Airway resistance measurements in Alternaria mice vs Alternaria exposed and Vactosertib treated mice vs. Vactosertib and I.N. PBS treated animals. **(B)** Tissue resistance measurements in Alternaria mice vs Alternaria exposed and Vactosertib treated mice vs. Vactosertib and I.N. PBS treated animals. **(C)** Tissue elastance measurements in Alternaria mice vs Alternaria exposed and Vactosertib treated mice vs. Vactosertib and I.N. PBS treated animals. **(D)** Pressure-volume curves for Alternaria mice vs Alternaria exposed and Vactosertib treated mice vs. Vactosertib and I.N. PBS treated animals. **(E)** Inspiratory capacity values for Alternaria mice vs Alternaria exposed and Vactosertib treated mice vs. Vactosertib and I.N. PBS treated animals.

Discussion

TGF-β has been documented to be a key player in driving allergic inflammation and more specifically, airway remodeling[23]. Here, using an animal model of allergic pulmonary inflammation, we demonstrate that Vactosertib may be a promising therapeutic approach to treating AWR. In summary, animals

treated with Vactosertib, we noted significant decreases in eosinophils recruited into the airways, decreased tissue resistance and elastance, a PV loop and inspiratory capacity demonstrating a rescued phenotype. While it is documented that in the context of allergic inflammation, eosinophils are a major contributor to TGF-β production, direct effects of TGF-β signaling on eosinophil recruitment are less clear. While a few studies point to a strong correlation between TGF-β expression and eosinophil burden, others relate TGF-β to proapoptotic programming in eosinophils[24,25]. The controversy surrounding this topic deserves more attention to elucidate the specific role of TGF-β in these processes; however, this may prove difficult as TGF-β is pleotropic protein with a variety of functions varying with altering biological cues. Due to this, it is likely that this protein can recruit and induce apoptosis in eosinophils, perhaps varying with the environment, stimulus, and other biological features. In this model, the data suggests that TGF-β signaling acts as a chemoattractant for eosinophils, as demonstrated by increased recruitment of eosinophils in animals which were exposed to *Alternaria*.

While the effects of TGF-β on eosinophils in allergic asthma requires more in-depth studies, our findings suggest potential use for Vactosertib in managing pulmonary inflammation. Although Nanostring analysis did not reveal any differences in gene regulation, this outcome could be attributed to this to the 3-day rest period before sample collection. During this time, it is likely that the

inflammatory responses are likely to return to baseline values, potentially masking any observable changes. Minute changes observed in histological sections could also be explained by a partial resolution of inflammatory responses. However, noticeable differences in deposition of airway smooth muscle were observed and suggest the potential role of Vactosertib in alleviation of smooth muscle deposition and hypertrophy due to persistent allergen exposure. The absence of significant changes in airway resistance observed via flexivent may also be explained by the mitigation of αSMA deposition. During asthmatic episodes, hypertrophy and hyperplasia of smooth muscle contribute to bronchoconstriction and airway hyperreactivity of the airways, phenomena not observed in mice treated with Vactosertib[26].

Lung function changes such as tissue elasticity, resistance, as well as inspiratory capacity appeared to be rescued by treatment with Vactosertib. This data suggests the ability of Vactosertib in inhibiting deposition of collagen and elastin fibers which directly increase tissue resistance and elasticity, respectively[27,28]. Deposition of collagen and elastin fibers due to fibrotic processes causes rigidity within the lung tissue, increasing tissue resistance and elasticity, while decreasing inspiratory capacity. However, in treated mice, values of tissue resistance and elastance were significantly decreased compared to untreated, *Alternaria* exposed animals, demonstrating a rescuing of fibrotic processes due to Vactosertib treatment. Additionally, pressure-volume curves

indicated an increase in lung compliance in treated animals, indicating decreased fibrotic processes and fiber deposition due to treatment.

Conclusion

Our studies provide valuable insights into the complex interplay between TGF-β signaling, allergic inflammation, and airway remodeling in asthma. By utilizing Vactosertib, and inhibitor of TGF-β receptor type I, we aimed to investigate its potential therapeutic efficacy in mitigating the pathophysiological processes associated with airway remodeling in a murine model of allergic asthma.

Our findings demonstrate that treatment with Vactosertib significantly reduced eosinophil recruitment into the airways of mice intranasally exposed to *Alternaria*, highlighting its potential as an anti-inflammatory agent in allergic asthma. Additionally, while not reaching statistical significance, there was a notable trend towards decreased collagen deposition and improved lung function in treated mice, as demonstrated by SHG microscopy and Flexivent analysis, respectively. This data suggest inhibition of TGF-β signaling with Vactosertib may attenuate some aspects of AWR, offering promise for managing severe structural changes in the lungs caused by chronic pulmonary inflammation.

Additionally, our studies demonstrate the multifaceted role of TGF-β in orchestrating fibrotic responses and inflammatory processes in asthma. Despite

the complexity of AWR, targeting TGF-β signaling pathways could represent a therapeutic strategy to alleviate disease progression and improve clinical outcomes in patients suffering from asthma. Further studies with enhanced molecular analyses are warranted to further elucidate the therapeutic potential of Vactosertib in asthma and AWR management. Ultimately, this study highlights the need for developing effective treatment modalities aimed at mitigating the detrimental effects of airway remodeling in many chronic respiratory diseases even extending beyond asthma.

References

1. Bergeron, Céline, et al. “Airway Remodelling in Asthma: From Benchside to Clinical Practice.” *Canadian Respiratory Journal*, vol. 17, no. 4, 2010, pp. e85–e93, https://doi.org/10.1155/2010/318029
2. Jang, An-Soo. “Steroid Response in Refractory Asthmatics.” *The Korean Journal of Internal Medicine*, vol. 27, no. 2, 1 Jan. 2012, pp. 143–143, https://doi.org/10.3904/kjim.2012.27.2.143
3. Firszt, R., et al. “Interleukin-13 Induces Collagen Type-1 Expression through Matrix Metalloproteinase-2 and Transforming Growth Factor- 1 in Airway Fibroblasts in Asthma.” *European Respiratory Journal*, vol. 43, no. 2, 16 May 2013, pp. 464–473, https://doi.org/10.1183/09031936.00068712
4. Barron, Luke, and Thomas A. Wynn. “Fibrosis Is Regulated by Th2 and Th17 Responses and by Dynamic Interactions between Fibroblasts and Macrophages.” *American Journal of Physiology - Gastrointestinal and Liver Physiology*, vol. 300, no. 5, 1 May 2011, pp. G723–G728, www.ncbi.nlm.nih.gov/pmc/articles/PMC3302189/, https://doi.org/10.1152/ajpgi.00414.2010
5. Schatz, Michael, and Lanny Rosenwasser. “The Allergic Asthma Phenotype.” *The Journal of Allergy and Clinical Immunology: In Practice*, vol. 2, no. 6, Nov. 2014, pp. 645–648, https://doi.org/10.1016/j.jaip.2014.09.004

6. Romanet-Manent, S., et al. “Allergicvsnonallergic Asthma: What Makes the Difference?” *Allergy*, vol. 57, no. 7, July 2002, pp. 607–613, https://doi.org/10.1034/j.1398-9995.2002.23504.x

7. Hough, Kenneth P., et al. “Airway Remodeling in Asthma.” *Frontiers in Medicine*, vol. 7, no. 7, 21 May 2020, p. 191, https://doi.org/10.3389/fmed.2020.00191

8. Sino Biological. “What Is TGF-Beta.” *Www.sinobiological.com*, www.sinobiological.com/resource/cytokines/what-is-tgf-beta

9. Makinde, Toluwalope, et al. “The Regulatory Role of TGF- *β* in Airway Remodeling in Asthma.” *Immunology & Cell Biology*, vol. 85, no. 5, 27 Feb. 2007, pp. 348–356, https://doi.org/10.1038/sj.icb.7100044

10. Denney, Laura, et al. “Pulmonary Epithelial Cell-Derived Cytokine TGF-β1 Is a Critical Cofactor for Enhanced Innate Lymphoid Cell Function.” *Immunity*, vol. 43, no. 5, Nov. 2015, pp. 945–958, https://doi.org/10.1016/j.immuni.2015.10.012

11. Chen, Pei-Yu, et al. “TGFβ Signaling Pathways in Human Health and Disease.” *Frontiers in Molecular Biosciences*, vol. 10, 1 June 2023, https://doi.org/10.3389/fmolb.2023.1113061

12. Rojas, Andres, et al. “TGF-β Receptor Levels Regulate the Specificity of Signaling Pathway Activation and Biological Effects of TGF-β.” *Biochimica*

et Biophysica Acta (BBA) - Molecular Cell Research, vol. 1793, no. 7, July 2009, pp. 1165–1173, https://doi.org/10.1016/j.bbamcr.2009.02.001

13. Cabezas, Felipe, et al. “Participation of the SMAD2/3 Signalling Pathway in the down Regulation of Megalin/LRP2 by Transforming Growth Factor Beta (TGF-ß1).” *PLOS ONE*, vol. 14, no. 5, 23 May 2019, p. e0213127, https://doi.org/10.1371/journal.pone.0213127
14. “NCI Thesaurus.” *Ncithesaurus.nci.nih.gov*, www.ncithesaurus.nci.nih.gov/ncitbrowser/ConceptReport.jsp?dictionary=NCI_Thesaurus&ns=ncit&code=C116357
15. Lee, Ji Eun, et al. “Vactosertib, TGF-β Receptor I Inhibitor, Augments the Sensitization of the Anti-Cancer Activity of Gemcitabine in Pancreatic Cancer.” *Biomedicine & Pharmacotherapy*, vol. 162, 1 June 2023, p. 114716, https://doi.org/10.1016/j.biopha.2023.114716
16. Salo, Päivi M., et al. “Dustborne Alternaria Alternata Antigens in U.S. Homes: Results from the National Survey of Lead and Allergens in Housing.” *The Journal of Allergy and Clinical Immunology*, vol. 116, no. 3, 1 Sept. 2005, pp. 623–629, https://doi.org/10.1016/j.jaci.2005.05.030
17. Rivas, Candy M., et al. “Alternaria Alternata-Induced Airway Epithelial Signaling and Inflammatory Responses via Protease-Activated Receptor-2 Expression.” *Biochemical and Biophysical Research Communications*, vol.

591, 5 Feb. 2022, pp. 13–19, pubmed.ncbi.nlm.nih.gov/34990903/, https://doi.org/10.1016/j.bbrc.2021.12.090

18. Yee, Michael B, et al. “Protease-Activated Receptor-2 Signaling through β-Arrestin-2 Mediates *Alternaria* Alkaline Serine Protease-Induced Airway Inflammation.” *American Journal of Physiology-Lung Cellular and Molecular Physiology*, vol. 315, no. 6, 1 Dec. 2018, pp. L1042–L1057, https://doi.org/10.1152/ajplung.00196.2018

19. “RANTES - an Overview | ScienceDirect Topics.”, www.sciencedirect.com/topics/pharmacology-toxicology-and-pharmaceutical-science/rantes

20. Peng, Xinze, et al. “Establishment and Characterization of a Multi-Purpose Large Animal Exposure Chamber for Investigating Health Effects.” *Review of Scientific Instruments*, vol. 90, no. 3, 1 Mar. 2019, https://doi.org/10.1063/1.5042097

21. Theeu, F, and ves d. “Principles of the Design’ and Operation of Generic Osmotic Pumps for the Delivery of Semisolid or Liquid Drug Formulations.” *ANNALS of BIOMEDICAL ENGiNEERING*, vol. 4, no. 4, 1976, www.alzet.com/wp-content/uploads/2019/05/R0002.pdf

22. Williams, Rebecca, et al. “Interpreting Second-Harmonic Generation Images of Collagen I Fibrils.” *Biophysical Journal*, vol. 88, no. 2, 1 Feb. 2005, pp. 1377–1386, https://doi.org/10.1529/biophysj.104.047308

23. “Role of Transforming Growth Factor-β in Airway Remodeling in Asthma.” *American Journal of Respiratory Cell and Molecular Biology*, vol. 44, no. 2, 1 Feb. 2011, pp. 127–133, https://doi.org/10.1165/rcmb.2010-0027TR

24. Janulaityte, Ieva, et al. “In Vivo Allergen-Activated Eosinophils Promote Collagen I and Fibronectin Gene Expression in Airway Smooth Muscle Cells via TGF-β1 Signaling Pathway in Asthma.” *International Journal of Molecular Sciences*, vol. 21, no. 5, 6 Mar. 2020, p. 1837, https://doi.org/10.3390/ijms21051837

25. Alam, Rafeul, et al. *Transforming Growth Factor B Abrogates the Effects of Hematopoietins on Eosinophils and Induces Their Apoptosis* . Mar. 1994, www.rupress.org/jem/article-pdf/179/3/1041/1675568/1041.pdf
Prakash, Y. S. “Airway Smooth Muscle in Airway Reactivity and Remodeling: What Have We Learned?” *American Journal of Physiology-Lung Cellular and Molecular Physiology*, vol. 305, no. 12, 15 Dec. 2013, pp. L912–L933, https://doi.org/10.1152/ajplung.00259.2013

26. Liu, Lumei, et al. “Role of Collagen in Airway Mechanics.” *Bioengineering*, vol. 8, no. 1, 16 Jan. 2021, p. 13, https://doi.org/10.3390/bioengineering8010013

27. Starcher, B C. “Elastin and the Lung.” *Thorax*, vol. 41, no. 8, 1 Aug. 1986, pp. 577–585, https://doi.org/10.1136/thx.41.8.577

Figures

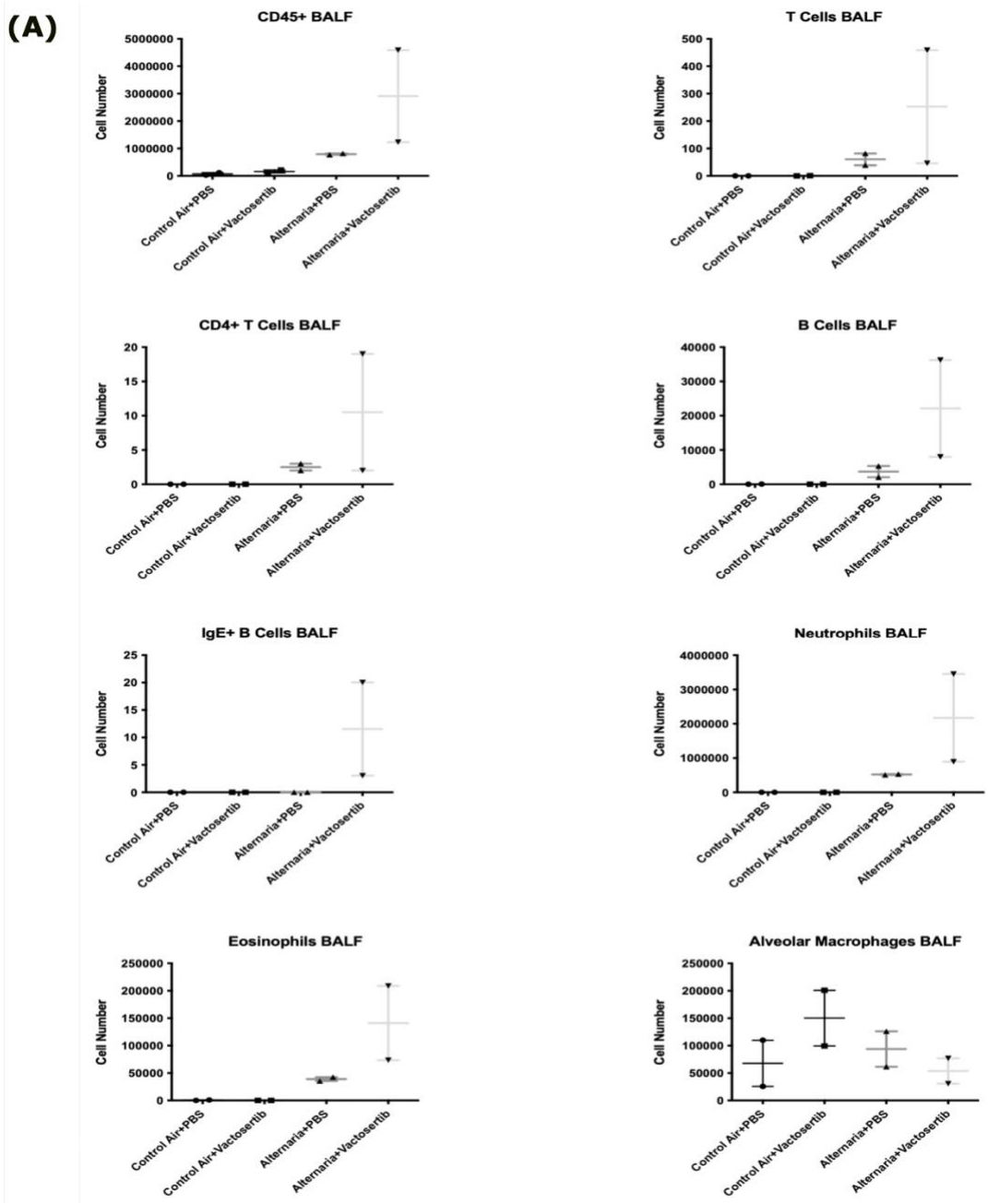
(A)
CD45+ BALF
Cell Number
5000000
4000000
3000000
2000000
1000000
0
Control Air+PBS
Control Air+Vactosertib
Alternaria+PBS
Alternaria+Vactosertib
T Cells BALF
Cell Number
500
400
300
200
100
0
Control Air+PBS
Control Air+Vactosertib
Alternaria+PBS
Alternaria+Vactosertib
CD4+ T Cells BALF
Cell Number
20
15
10
5
0
Control Air+PBS
Control Air+Vactosertib
Alternaria+PBS
Alternaria+Vactosertib
B Cells BALF
Cell Number
40000
30000
20000
10000
0
Control Air+PBS
Control Air+Vactosertib
Alternaria+PBS
Alternaria+Vactosertib
IgE+ B Cells BALF
Cell Number
25
20
15
10
5
0
Control Air+PBS
Control Air+Vactosertib
Alternaria+PBS
Alternaria+Vactosertib
Neutrophils BALF
Cell Number
4000000
3000000
2000000
1000000
0
Control Air+PBS
Control Air+Vactosertib
Alternaria+PBS
Alternaria+Vactosertib
Eosinophils BALF
Cell Number
250000
200000
150000
100000
50000
0
Control Air+PBS
Control Air+Vactosertib
Alternaria+PBS
Alternaria+Vactosertib
Alveolar Macrophages BALF
Cell Number
250000
200000
150000
100000
50000
0
Control Air+PBS
Control Air+Vactosertib
Alternaria+PBS
Alternaria+Vactosertib

(B)

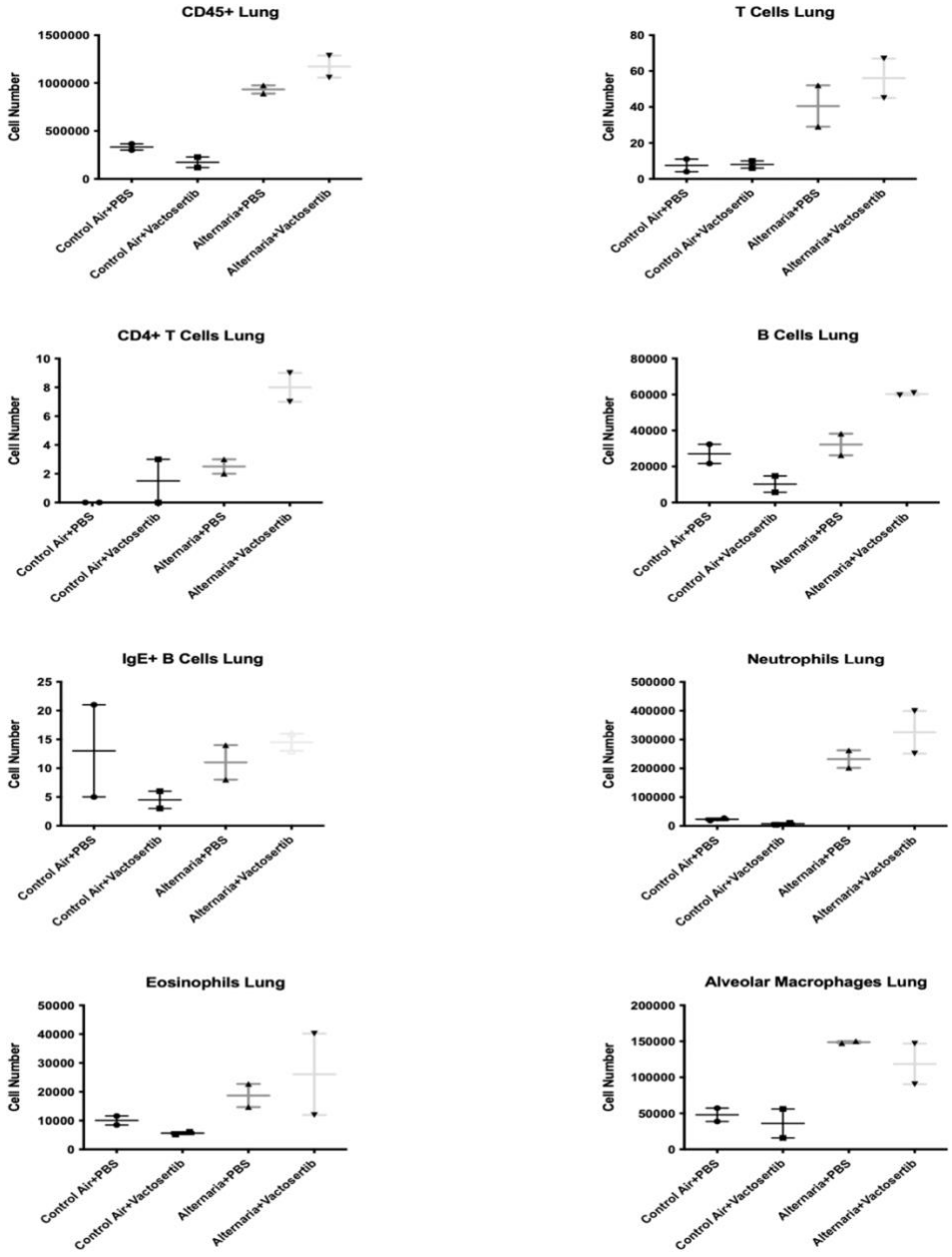
CD45+ Lung
Cell Number
1500000
1000000
500000
0
Control Air+PBS
Control Air+Vactosertib
Alternaria+PBS
Alternaria+Vactosertib
T Cells Lung
Cell Number
80
60
40
20
0
Control Air+PBS
Control Air+Vactosertib
Alternaria+PBS
Alternaria+Vactosertib
CD4+ T Cells Lung
Cell Number
10
8
6
4
2
0
Control Air+PBS
Control Air+Vactosertib
Alternaria+PBS
Alternaria+Vactosertib
B Cells Lung
Cell Number
80000
60000
40000
20000
0
Control Air+PBS
Control Air+Vactosertib
Alternaria+PBS
Alternaria+Vactosertib
IgE+ B Cells Lung
Cell Number
25
20
15
10
5
0
Control Air+PBS
Control Air+Vactosertib
Alternaria+PBS
Alternaria+Vactosertib
Neutrophils Lung
Cell Number
500000
400000
300000
200000
100000
0
Control Air+PBS
Control Air+Vactosertib
Alternaria+PBS
Alternaria+Vactosertib
Eosinophils Lung
Cell Number
50000
40000
30000
20000
10000
0
Control Air+PBS
Control Air+Vactosertib
Alternaria+PBS
Alternaria+Vactosertib
Alveolar Macrophages Lung
Cell Number
200000
150000
100000
50000
0
Control Air+PBS
Control Air+Vactosertib
Alternaria+PBS
Alternaria+Vactosertib

(C)

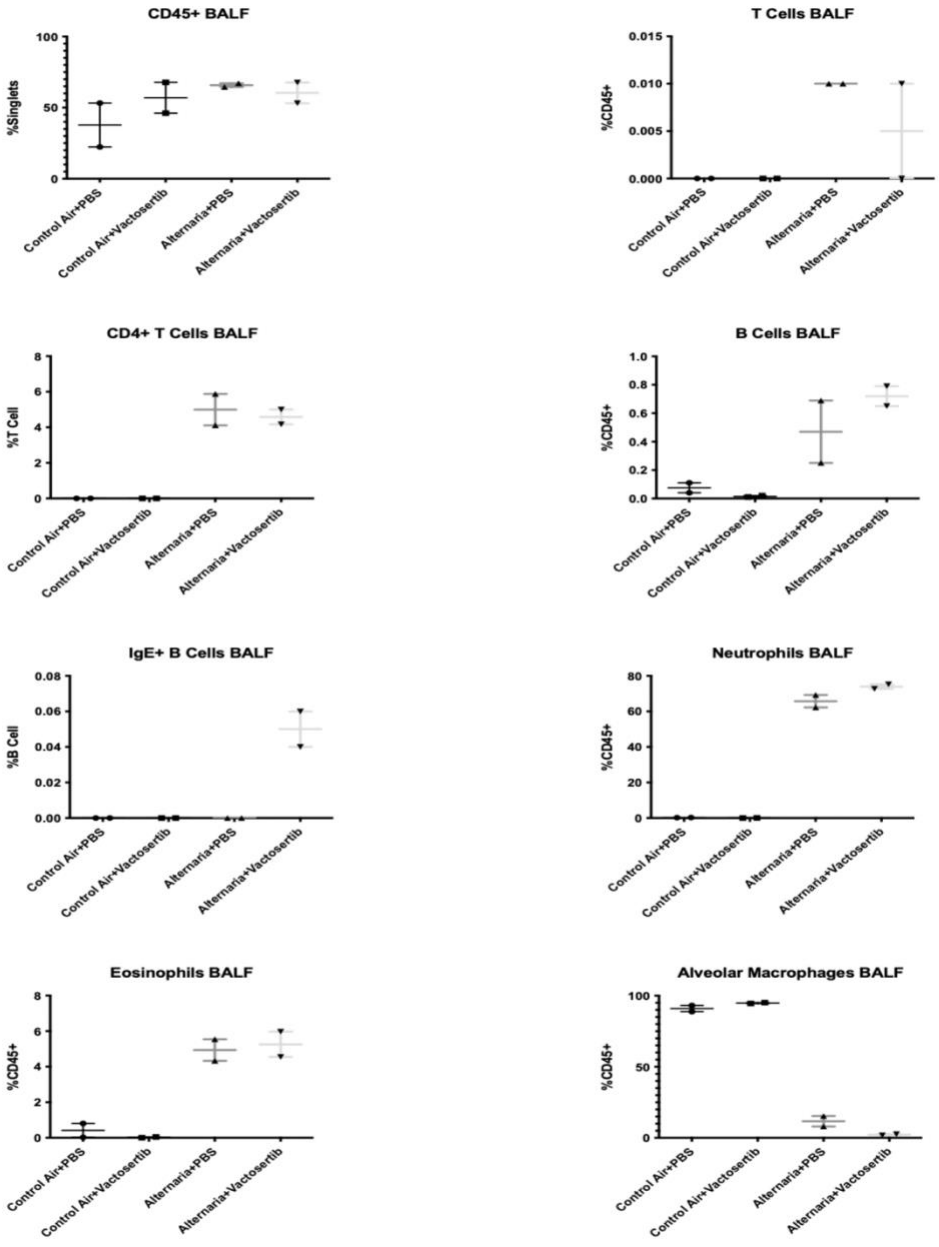
CD45+ BALF
%Singlets
100
50
0
Control Air+PBS
Control Air+Vactosertib
Alternaria+PBS
Alternaria+Vactosertib
T Cells BALF
%CD45+
0.015
0.010
0.005
0.000
CD4+ T Cells BALF
%T Cell
8
6
4
2
0
B Cells BALF
%CD45+
1.0
0.8
0.6
0.4
0.2
0.0
IgE+ B Cells BALF
%B Cell
0.08
0.06
0.04
0.02
0.00
Neutrophils BALF
%CD45+
80
60
40
20
0
Eosinophils BALF
%CD45+
Alveolar Macrophages BALF
%CD45+

(D)

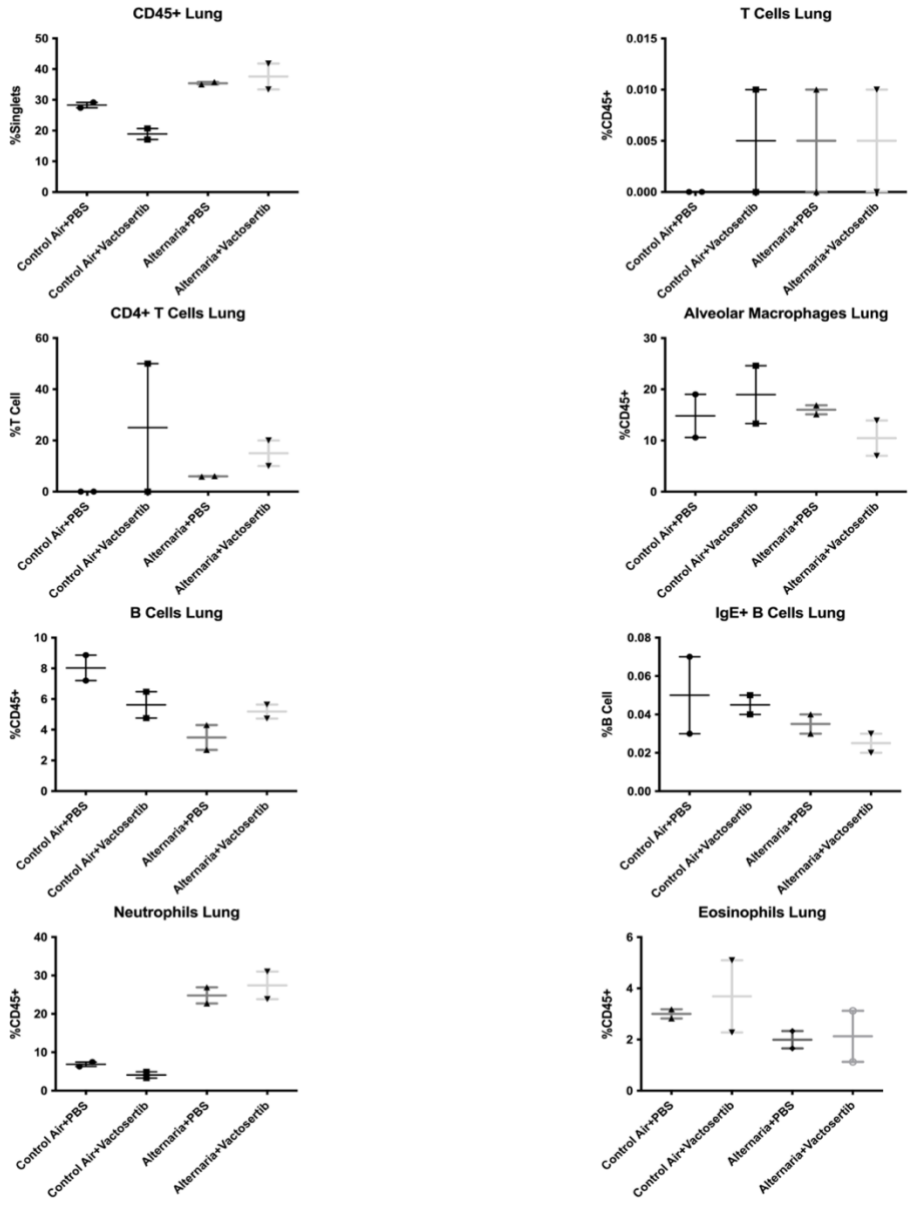
CD45+ Lung
%Singlets
T Cells Lung
%CD45+
CD4+ T Cells Lung
%T Cell
Alveolar Macrophages Lung
%CD45+
B Cells Lung
%CD45+
IgE+ B Cells Lung
%B Cell
Neutrophils Lung
%CD45+
Eosinophils Lung
%CD45+
Control Air+PBS
Control Air+Vactosertib
Alternaria+PBS
Alternaria+Vactosertib

Figure 6.1 - Cellular recruitment in BALF and lungs of aerosolized *Alternaria alternata* exposed animals. (A) Cell numbers in BALF **(B)** Cell numbers in lung **(C)** Cell percentages in BALF **(D)** Cell percentages in lung.

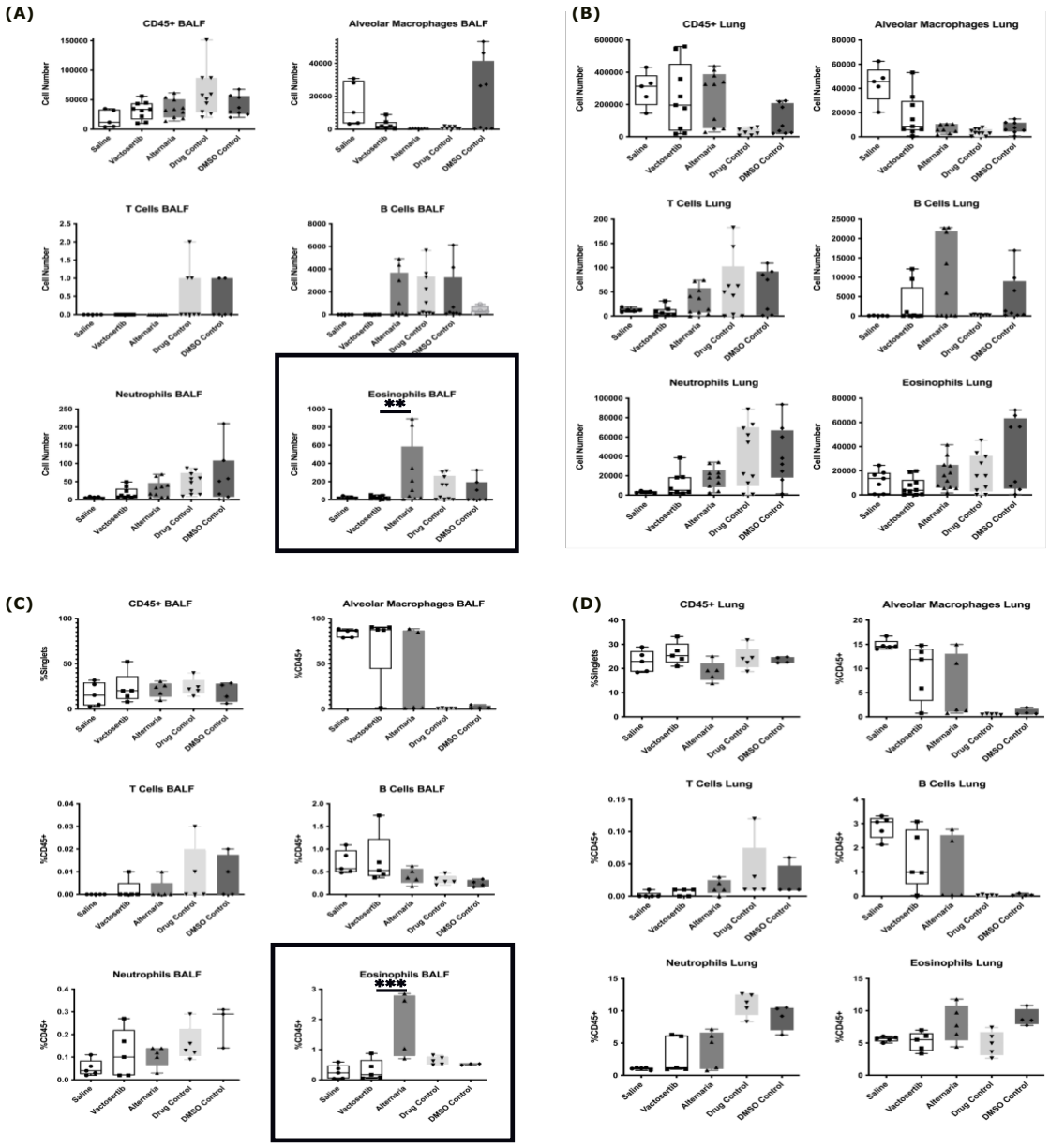

Figure 6.2 - Cellular recruitment in BALF and lungs of intranasal *Alternaria alternata* exposed animals. (A) Cell numbers in BALF **(B)** Cell numbers in lung **(C)** Cell percentages in BALF **(D)** Cell percentages in lung.

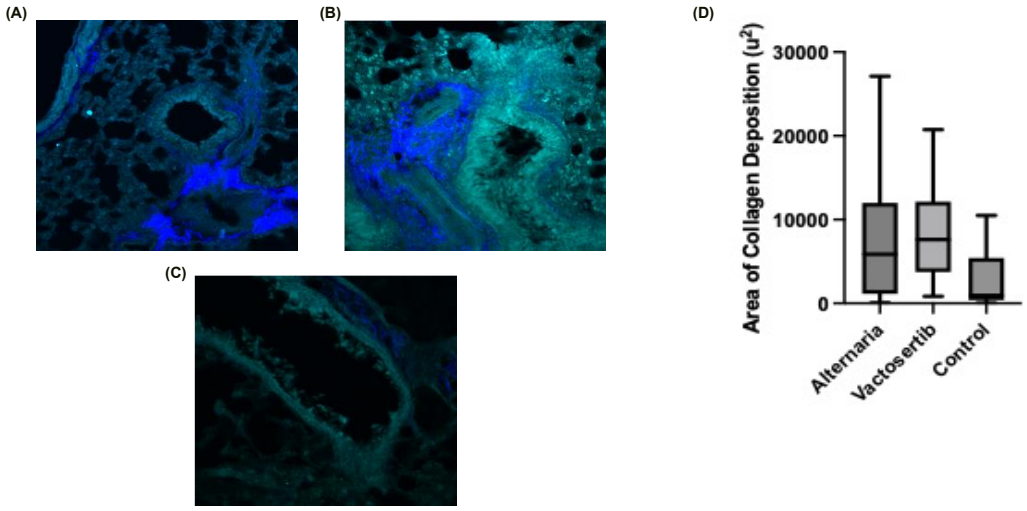

Figure 6.3 - Second Harmonic Analysis of lungs of intranasal *Alternaria alternata* exposed animals. (A) SHG of left lobe of control mouse **(B)** SHG of left lobe of *Alternaria* exposed mouse **(C)** SHG of left lobe of *Alternaria* exposed and Vactosertib treated mouse. **(D)** Quantification of area of collagen deposition in lung.

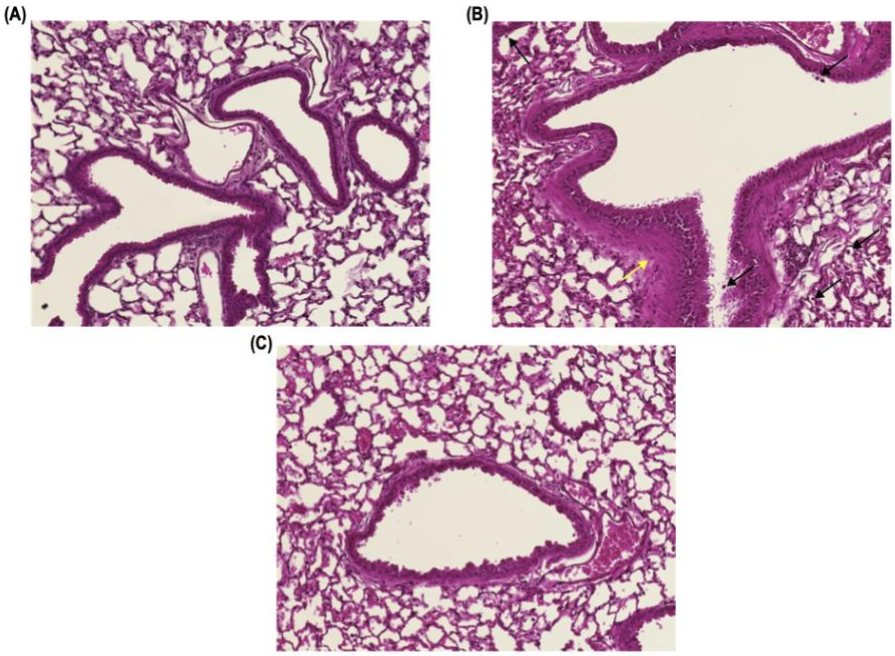

Figure 6.4 - H&E images of lungs of intranasal *Alternaria alternata* exposed animals. (A) H&E of control mouse **(B)** H&E of *Alternaria* exposed mouse. Black arrows highlighting cellular recruitment in airways. Yellow arrow highlighting increased smooth muscle deposition surrounding airway. **(C)** H&E of *Alternaria* exposed and Vactosertib treated mouse.

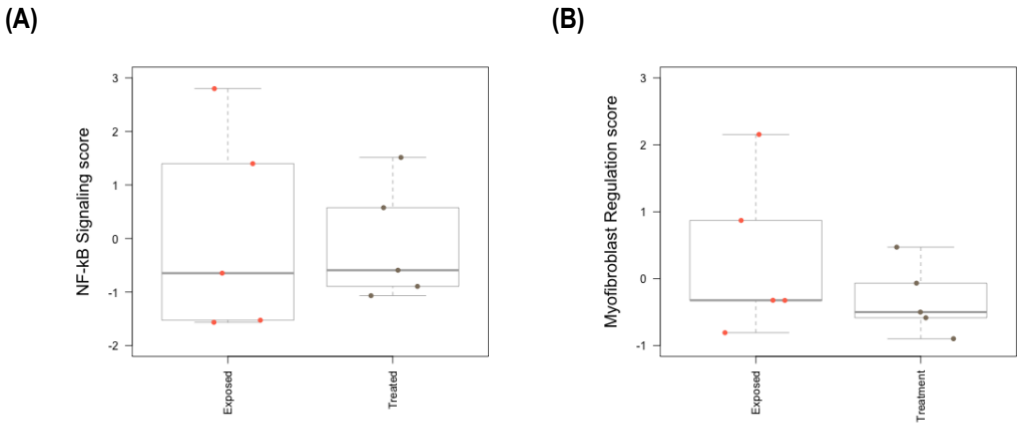

Figure 6.5 - NF-kB signaling and myofibroblast regulation in intranasal *Alternaria* alternata exposed mice. (A) NF-kB signaling in *Alternaria* (Exposed) mice vs *Alternaria* exposed and Vactosertib treated mice (Treated). **(B)** Myofibroblast regulation in *Alternaria* (Exposed) mice vs *Alternaria* exposed and Vactosertib treated mice (Treatment).

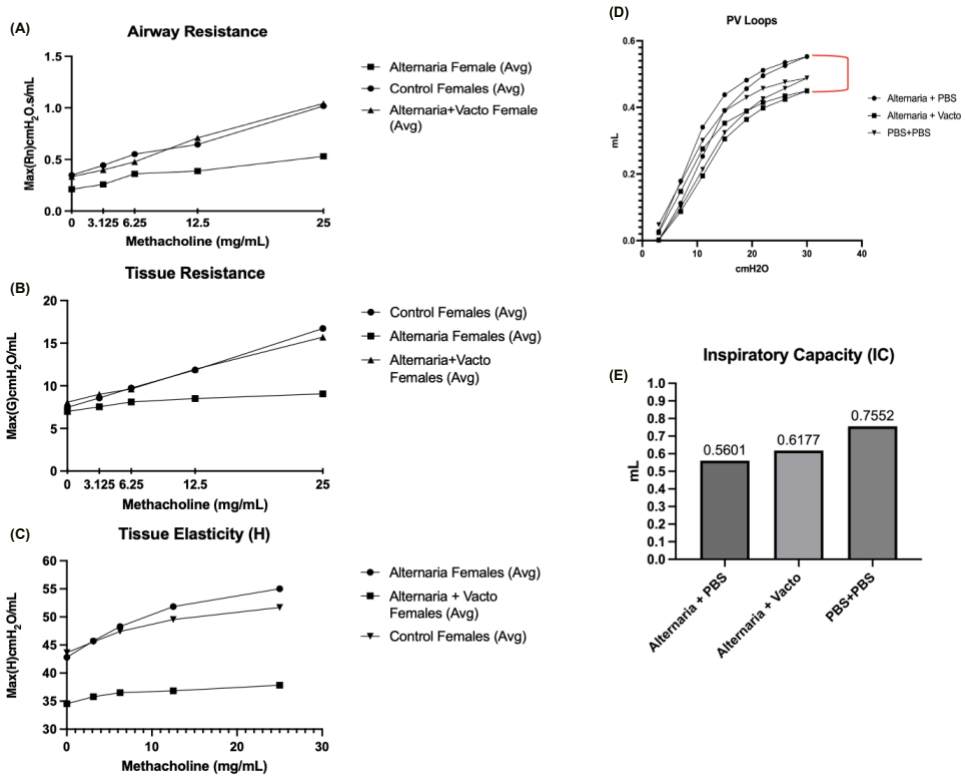

Figure 6.6 - Flexivent analysis of intranasal *Alternaria alternata* and PBS exposed mice. (A) Airway resistance measurements in Alternaria mice vs Alternaria exposed and Vactosertib treated mice vs. Vactosertib and I.N. PBS treated animals. **(B)** Tissue resistance measurements in Alternaria mice vs Alternaria exposed and Vactosertib treated mice vs. Vactosertib and I.N. PBS treated animals. **(C)** Tissue elastance measurements in Alternaria mice vs Alternaria exposed and Vactosertib treated mice vs. Vactosertib and I.N. PBS treated animals. **(D)** Pressure-volume curves for Alternaria mice vs Alternaria exposed and Vactosertib treated mice vs. Vactosertib and I.N. PBS treated animals. **(E)** Inspiratory capacity values for Alternaria mice vs Alternaria exposed and Vactosertib treated mice vs. Vactosertib and I.N. PBS treated animals.

	Log2 fold change	std error (log2)	P-value	BH.p.value
Ccl11-mRNA	-0.88	1.78	0.638	1
Pdgfrb-mRNA	-0.964	3.61	0.798	1

Table 6.1 - Table of log fold change of Ccl11 and Pdgfrb in Vactosertib treated mice.

Chapter 7: Antimicrobial Activity of Stable Antimicrobial Peptides Extracted From the Citrus-greening Huanglongbing Resistant Australian Finger Lime Plant

Abstract

Citrus Huanglongbing (HLB) is the most destructive disease affecting citrus trees globally[1]. HLB exists as a significant economic concern as it ravages through citrus plants, significantly reducing both the lifespan of the tree as well as the quality of the fruit. Citrus plants infected with HLB produce small poorly colored fruit with juices low in soluble solids, high in acids, and bitter. The financial strain this puts on the citrus industry is enormous and can lead to catastrophic outcomes[2]. Current efforts to treat HLB involve toxic measures which pose significant risk to human health. Our lab investigated the susceptibility of antimicrobial peptides isolated from HLB resistant trees in three clinically relevant pathogenic strains of bacteria: *Salmonella typhimurium*, *Pseudomonas aeruginosa*, and *Klebsiella pneumoniae*. The stable antimicrobial peptide (SAMP) demonstrated bacteriostatic potential in *Salmonella typhimurium* and *P. aeruginosa* while *K. pneumoniae* demonstrated resistance to peptide activity. Another isolated peptide, 104, demonstrated varying levels of effectiveness, progressively increasing with increasing concentrations of the peptide. These antimicrobial peptides may be potentially useful in treatment of disease caused by these strains of bacteria.

Introduction

Citrus Huanglongbing (HLB), also known as citrus greening disease, is the most destructive disease affecting citrus trees globally. HLB is a bacterial disease caused by the bacteria phloem-limited bacterium Candidatus liberobacter asiaticus[3]. The bacterium is easily spread by a sap-sucking insect known as the Asian citrus psyllid (ACP)[3]. ACP has been documented to have spread HLB as far west as Louisiana, Texas, and California, severely affecting the global citrus industry. Upon infection, most trees only survive for a few years due to the detrimental effects of the disease as well as the lack of available treatments[4]. This disease poses a significant economic threat, costing billions of dollars in annual production losses. Despite current research efforts, there are still no effective treatments to treat infected crops or to prevent new infection. While currently, a lot of the utilized methods to treat HLB is by coating the citrus trees with insecticide chemicals and antibiotics[1]. Both of which pose significant risks to human, animal, as well as overall environmental health. Due to this, it is necessary to investigate and develop alternative treatment methods to rid HLB and prevent further damage to economic revenue brought in by the citrus industry[1]. There are a few strains of citrus trees which remain unsusceptible to disease, one of which is the *Microcitrus australiasica, also known as the* Australian finger lime[1]*.* In collaboration with Dr. Hailing Jin's lab, potential antimicrobial peptides have been identified and isolated from this resistant

species in order to investigate their effectiveness not only as a treatment for HLB but also as a broad antimicrobial treatment for pathogenic bacterial strains. Given this hypothesis, our lab began testing the effectiveness of clinically relevant bacterial strains such as *Salmonella typhimurium*, *Klebsiella pneumoniae*, and *Pseudomonas aeruginosa* to stable antimicrobial peptides (SAMPs) as well as the isolated peptide 104.

Salmonella typhimurium is a gram-negative enteric pathogen which is often the causative agent of common food-borne illnesses[5]. This pathogen is typically contracted by consumption of undercooked or raw meat, poultry, and eggs but can also be transmitted by contaminated water, the environment, and other infected humans or animals[6,7]. Infection with this pathogen poses as a major public health threat and can lead to diarrhea, blood in stool, dehydration, and prolonged vomiting. Pseudomonas aeruginosa, also a gram-negative bacterium, often leads to much more severe infections and is a frequent nosocomial contaminant[8]. Presenting a significant risk for serious infections such as endocarditis, meningitis, septicemia, respiratory failure, pneumonia, and many other illnesses[9,10,11]. The gram-negative bacterium, Klebsiella pneumoniae, has also been associated with pneumonia in immunocompromised individuals and is considered the most common cause of nosocomial pneumonia in the United States[12]. Klebsiella is known to have very high degrees of virulence and antibiotic resistance, complicating treatment in infected patients[12]. Each of these gram-

negative bacteria pose significant risk in clinical settings. Additionally, these bacteria are pathogenic bacteria capable of producing biofilms[13,14]. Although most healthy individuals can clear these pathogens after some time, immunocompromised individuals may experience additional life-threatening complications and require hospitalization and undergo extensive treatment[5]. Due to the risk posed by these bacteria as well as their clinical implication, we sought to investigate the potential antimicrobial activity of SAMP and 104 in these pathogenic bacterial strains. Our studies show that there is potential for the use of these peptides in a clinical setting as we noted compelling results of antimicrobial activity against the above-mentioned bacterial species.

Materials and methods

Culturing bacteria

Salmonella typhimurium was grown from an in-house glycerol stock while Klebsiella pneumoniae and Pseudomonas aeruginosa were purchased from ATCC. Glycerol stocks of each bacterium were streaked onto a Luria Broth (LB) agar petri dish and incubated at 37 degrees Celsius overnight. One colony of each bacterium was isolated from the LB agar petri dishes and were grown overnight in LB liquid media overnight shaking at 125 rpm. Following incubation, 1 mL of each bacterial culture was aliquoted into a 1.5mL eppendorf tube and centrifuged for 4 minutes at 4,000 g. Supernatant was then removed and each bacterium was

resuspended in 1mL of 150 uM NaCl. OD600 of the resuspended culture was measured and each culture was diluted to an OD600 of 0.2.

Testing peptides

Cultures at an OD600 of 0.2 were incubated for 5 hours with either Ceftazidime (antibiotic), 0.1% Triton-x, 10uM SAMP, 50uM 104, left untreated, or boiled for 30 minutes. After 5 hours, each culture was incubated with Biotium viability dye (30027) for 30 minutes and analyzed via confocal microscopy.

Imaging

All images were taken on the Zeiss Laser Scanning Confocal at 63X using FITC and mCherry visualization channels.

Results

In this study, we investigated the effectiveness of two antimicrobial peptides, SAMP and 104, against three clinical bacterial strains: *Salmonella typhimurium*, *Pseudomonas aeruginosa*, and *Klebsiella pneumoniae*. For *Salmonella typhimurium*, SAMP exhibited 65% effectiveness in the first repeat (Fig. 7.1D), though the second repeat indicated difficulty in quantifying the effectiveness (Fig. 7.2) but suggested some impact on biofilms (Fig. 7.2D)**.** Additional experiments are required under the same conditions for additional confirmation. In contrast, peptide 104 showed approximately 90% effectiveness

at a 10 μm concentration in the first repeat, but no effect in the second (Fig. 7.1E and 7.2E). The third repeat ranged from 70% to 90% effectiveness across 10, 50, and 90 μM concentrations (Fig. 7.3). Due to inconsistencies, further testing, particularly at the most effective concentration, 50 μM, is necessary to validate these findings (Fig. 7.3C).

Figure 7.1 - First experiment- 63X images of *Salmonella typhimurium*. (A) Untreated *S.typhimurium.* **(B)** Boiled treated *S.typhimurium.* **(C)** Ceftazidime treated *S.typhimurium.* **(D)** 10 μM SAMP treated *S.typhimurium.* **(E)** 10 μM 104 treated *S.typhimurium.*

Figure 7.2 - Second experimental repeat- 63X images of *Salmonella typhimurium*. (A) Untreated *S.typhimurium.* **(B)** Boiled *S.typhimurium.* **(C)** Ceftazidime treated *S.typhimurium.* **(D)** 10 μM SAMP treated *S.typhimurium.* **(E)** 10 μM 104 treated *S.typhimurium.*

Figure 7.3 - Third experimental repeat- 63X images of *Salmonella typhimurium*. (A) Untreated *S.typhimurium.* **(B)** 10 μM 104 treated *S.typhimurium.* **(C)** 50 μM 104 treated *S.typhimurium.* **(D)** 90 μM 104 treated *S.typhimurium.*

Regarding *Pseudomonas aeruginosa*, SAMP demonstrated about 80% effectiveness in the first repeat (Fig. 7.4D), with the second repeat again showing difficulty in quantifying the impact but indicating some effect on biofilms (Fig. 7.5D). A repeat under the same conditions is required to verify these results. Peptide 104 showed around 90% effectiveness in the first repeat (Fig. 7.4E), but no effect in the second experiment, and a demonstrated variable effectiveness of

30% to 85% across different concentrations in the third repeat (Fig. 7.6)**.** This data necessitates additional testing at 50 µM for more consistent results.

Figure 7.4 - First experiment- 63X images of *Pseudomonas aeruginosa*. (A) Untreated *P.aeruginosa.* **(B)** Boiled *P.aeruginosa.* **(C)** Ceftazidime treated *P.aeruginosa.* **(D)** 10 µM SAMP treated *P.aeruginosa.* **(E)** 10 µM 104 treated *P.aeruginosa.*

Figure 7.5 - Second experimental repeat- 63X images of *Pseudomonas aeruginosa*. (A) Untreated *P.aeruginosa.* **(B)** Triton-x *P.aeruginosa.* **(C)** Ceftazidime treated *P.aeruginosa.* **(D)** 10 µM SAMP treated *P.aeruginosa.* **(E)** 10 µM 104 treated *P.aeruginosa.*

Figure 7.6 - Third experimental repeat- 63X images of *Pseudomonas aeruginosa*. (A) Untreated *P.aeruginosa.* **(B)** 10 µM 104 treated *P.aeruginosa.* **(C)** 50uM 104 treated *P.aeruginosa.* **(D)** 90 µM 104 treated *P.aeruginosa*

For *Klebsiella pneumoniae*, SAMP showed no effectiveness in the first experiment, suggesting the need for testing at a higher concentration of 100 µM (Fig. 7.7). Peptide 104 exhibited around 70% effectiveness in the second repeat and 70% to 80% effectiveness at 90 and 50 µM (Fig. 7.8C and D). In summary, while SAMP shows promise against *Salmonella typhimurium* and *Pseudomonas aeruginosa*, it is ineffective against *Klebsiella pneumoniae*. Peptide 104 demonstrates high effectiveness against *Salmonella typhimurium* and *Pseudomonas aeruginosa*, with moderate effectiveness against *Klebsiella pneumoniae*. Further testing, concentration adjustments, and statistical analyses are necessary to resolve inconsistencies and confirm these results, however, the

work presented here suggests the potential use of these naturally sourced antimicrobial peptides in clinical settings.

Figure 7.7 - First experiment- 63X images of *Klebsiella pneumoniae*. (A) Untreated *K.pneumoniae.* **(B)** Triton-x treated *K.pneumoniae.* **(C)** Ceftazidime treated *K.pneumoniae.* **(D)** Boiled *K.pneumoniae* **(E)** 10 µM SAMP treated *K.pneumoniae.* **(F)** 10 µM 104 treated *K.pneumoniae.*

Figure 7.8 - Second experimental repeat- 63X images of *Klebsiella pneumoniae*. (A) Untreated *K.pneumoniae.* **(B)** 10 µM 104 treated *K.pneumoniae.* **(C)** 50 µM 104 treated *K.pneumoniae.* **(D)** 90 µM 104 treated *K.pneumoniae*

Discussion

This study aimed to explore the antimicrobial potential of stable antimicrobial peptides (SAMPs) extracted from the Australian Finger Lime plant, a species resistant to Citrus Huanglongbing (HLB). Our research focused on the efficacy of the peptides SAMP and 104 against three clinically significant bacterial strains: Salmonella typhimurium, Pseudomonas aeruginosa, and Klebsiella pneumoniae.

In this section, we reiterate the purpose of the study: to evaluate the antimicrobial capabilities of peptides derived from the Australian Finger Lime plant, specifically targeting their effectiveness against three important bacterial pathogens. This sets the stage for discussing the outcomes and significance of our findings.

The results demonstrated that SAMP exhibited considerable bacteriostatic activity against Salmonella typhimurium and Pseudomonas aeruginosa, albeit

with some variability across experiments. Peptide 104 showed high efficacy against Salmonella typhimurium and Pseudomonas aeruginosa, with effectiveness ranging between 70% and 90% at higher concentrations. However, Klebsiella pneumoniae displayed resistance to SAMP, while peptide 104 achieved moderate effectiveness.

Ultimately, SAMP showed significant bacteriostatic effects on two of the tested bacteria, but its efficacy was inconsistent, suggesting the need for further investigation. Peptide 104 was more consistently effective, especially at higher concentrations, but Klebsiella pneumoniae remained resistant to SAMP. This highlights the varied responses of different bacterial strains to these peptides.

A noteworthy finding from our study is the potential of these peptides to disrupt biofilms. Biofilms are complex communities of bacteria that adhere to surfaces and are encased in a protective matrix, making them highly resistant to conventional antibiotics. This resistance often leads to chronic infections, particularly in clinical settings where biofilms can form on medical devices such as catheters, prosthetic joints, and implants.

Conclusion

Our results indicate that both SAMP and peptide 104 may have the ability to interfere with biofilm formation and stability. This is particularly significant for clinical applications, as biofilm-associated infections are notoriously difficult to

treat and contribute to the persistence of chronic, life-threatening infections and increased healthcare costs. The ability to disrupt biofilms could enhance the effectiveness of existing treatments and reduce the incidence of biofilm-associated complications.

Inconsistent results across some replicates highlight the need for further testing to verify these findings and optimize concentrations. Despite these challenges, the data suggest that these peptides have significant potential as antimicrobial agents. The natural origin of these peptides offers a promising alternative to current treatments, which often involve harmful chemicals.

We acknowledge the inconsistencies observed in the experimental data, emphasizing the necessity for additional testing to confirm the results and optimize peptide concentrations for maximum efficacy. This section underscores the potential of these naturally sourced peptides as safer alternatives to traditional antimicrobial treatments, which often pose health and environmental risks.

Future research will focus on standardizing testing conditions, exploring higher peptide concentrations, and conducting comprehensive statistical analyses to establish the clinical viability of SAMP and peptide 104. This could

pave the way for the development of novel, safer antimicrobial treatments derived from HLB-resistant citrus plants.

References

1. Huang, Chien-Yu, et al. “A Stable Antimicrobial Peptide with Dual Functions of Treating and Preventing Citrus Huanglongbing.” *Proceedings of the National Academy of Sciences*, vol. 118, no. 6, 9 Feb. 2021, www.pnas.org/content/118/6/e2019628118.short
2. Alvarez, Sergio, et al. “Citrus Greening Disease (Huanglongbing) in Florida: Economic Impact, Management and the Potential for Biological Control.” *Agricultural Research*, vol. 5, no. 2, 12 Mar. 2016, pp. 109–118, https://doi.org/10.1007/s40003-016-0204-z
3. Wang, Nian. “Candidatus Liberibacter Asiaticus (Citrus Greening).” *CABI Compendium*, vol. CABI Compendium, 7 Jan. 2022, https://doi.org/10.1079/cabicompendium
4. U.S. Department of Agriculture. “Citrus Greening | Animal and Plant Health Inspection Service.” *Www.aphis.usda.gov*, 16 May 2024, www.aphis.usda.gov/plant-pests-diseases/citrus-diseases/citrus-greening#:~:text=Citrus%20greening%2C%20also%20called%20Huanglongbing
5. Fabrega, Anna, and Jordi Vila. “Salmonella Enterica Serovar Typhimurium Skills to Succeed in the Host: Virulence and Regulation.” *Clinical*

Microbiology Reviews, vol. 26, no. 2, 1 Apr. 2013, pp. 308–341, www.ncbi.nlm.nih.gov/pmc/articles/PMC3623383/, https://doi.org/10.1128/cmr.00066-12

6. Sjölund-Karlsson, Maria, et al. “Occurrence of β-Lactamase Genes among Non-TyphiSalmonella EntericaIsolated from Humans, Food Animals, and Retail Meats in the United States and Canada.” *Microbial Drug Resistance*, vol. 19, no. 3, June 2013, pp. 191–197, https://doi.org/10.1089/mdr.2012.0178
7. Punchihewage-Don, Anuradha Jeewantha, et al. “The Outbreaks and Prevalence of Antimicrobial Resistant Salmonella in Poultry in the United States: An Overview.” *Heliyon*, vol. 8, no. 11, 1 Nov. 2022, p. e11571, www.sciencedirect.com/science/article/pii/S2405844022028596, https://doi.org/10.1016/j.heliyon.2022.e11571
8. Qin, Shugang, et al. “Pseudomonas Aeruginosa: Pathogenesis, Virulence Factors, Antibiotic Resistance, Interaction with Host, Technology Advances and Emerging Therapeutics.” *Signal Transduction and Targeted Therapy*, vol. 7, no. 1, 25 June 2022, https://doi.org/10.1038/s41392-022-01056-1
9. Bodey, G. P., et al. “Infections Caused by Pseudomonas Aeruginosa.” *Clinical Infectious Diseases*, vol. 5, no. 2, 1 Mar. 1983, pp. 279–313, https://doi.org/10.1093/clinids/5.2.279

10. Ashurst, John V., and Adam Dawson. “Klebsiella Pneumonia.” *PubMed*, StatPearls Publishing, 2021, www.ncbi.nlm.nih.gov/books/NBK519004/#:~:text=Klebsiella%20pneumoniae%20is%20a%20gram

11. Wilson, Mina G., and Shivlal Pandey. *Pseudomonas Aeruginosa*. *Www.ncbi.nlm.nih.gov*, StatPearls Publishing, 8 Aug. 2023, www.ncbi.nlm.nih.gov/books/NBK557831/

12. Davies, G., et al. “The Effect of Pseudomonas Aeruginosa on Pulmonary Function in Patients with Bronchiectasis.” *European Respiratory Journal*, vol. 28, no. 5, 12 July 2006, pp. 974–979, https://doi.org/10.1183/09031936.06.00074605

13. Childers, Brandon M, et al. “MrkD $_{1P}$ from Klebsiella Pneumoniae Strain IA565 Allows for Coexistence with Pseudomonas Aeruginosa and Protection from Protease-Mediated Biofilm Detachment.” *Infection and Immunity*, vol. 81, no. 11, 1 Nov. 2013, pp. 4112–4120, https://doi.org/10.1128/iai.00521-13

14. Harrell, Jaikin E., et al. “Salmonella Biofilm Formation, Chronic Infection, and Immunity within the Intestine and Hepatobiliary Tract.” *Frontiers in Cellular and Infection Microbiology*, vol. 10, 2 Feb. 2021, https://doi.org/10.3389/fcimb.2020.624622

Figures

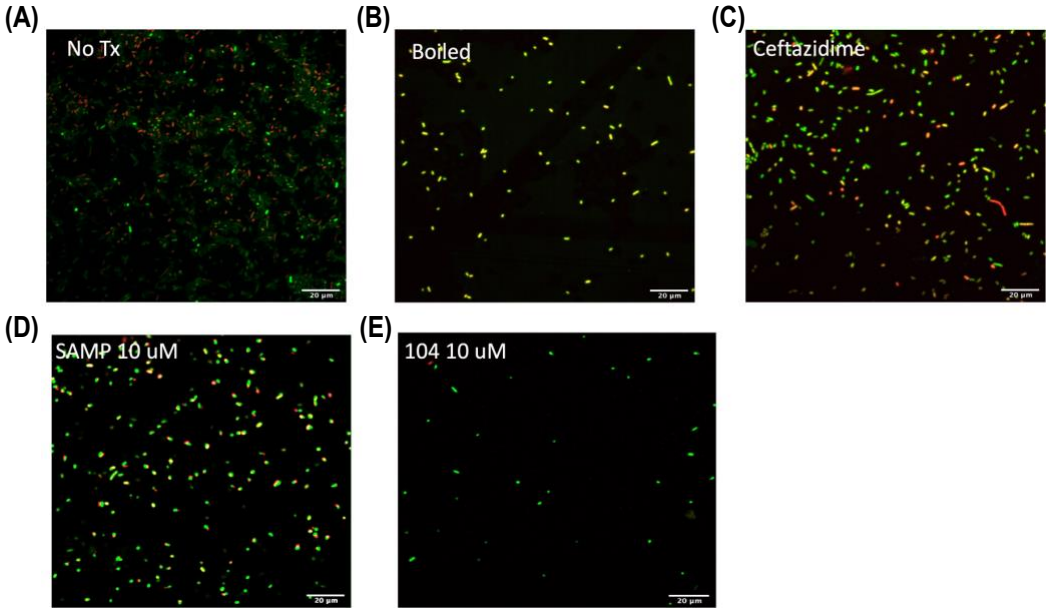

Figure 7.1 - First experiment- 63X images of *Salmonella typhimurium*. (A) Untreated *S.typhimurium.* **(B)** Boiled treated *S.typhimurium.* **(C)** Ceftazidime treated *S.typhimurium.* **(D)** 10 µM SAMP treated *S.typhimurium.* **(E)** 10 µM 104 treated *S.typhimurium.*

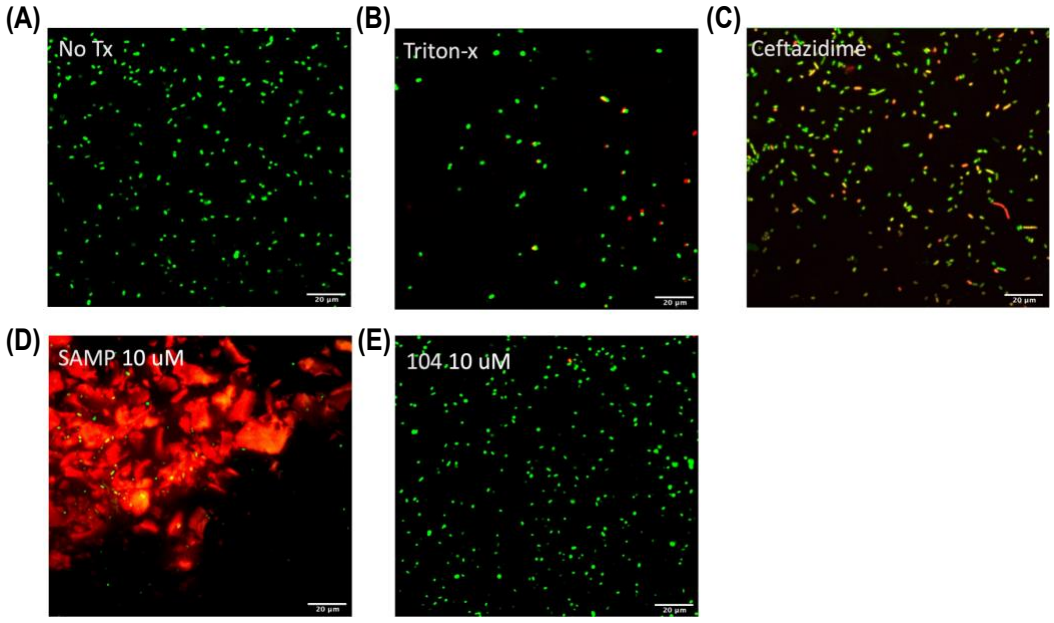

Figure 7.2 - Second experimental repeat- 63X images of *Salmonella typhimurium*. (A) Untreated *S.typhimurium.* **(B)** Triton-x *S.typhimurium.* **(C)** Ceftazidime treated *S.typhimurium.* **(D)** 10 µM SAMP treated *S.typhimurium.* **(E)** 10 µM 104 treated *S.typhimurium*

.

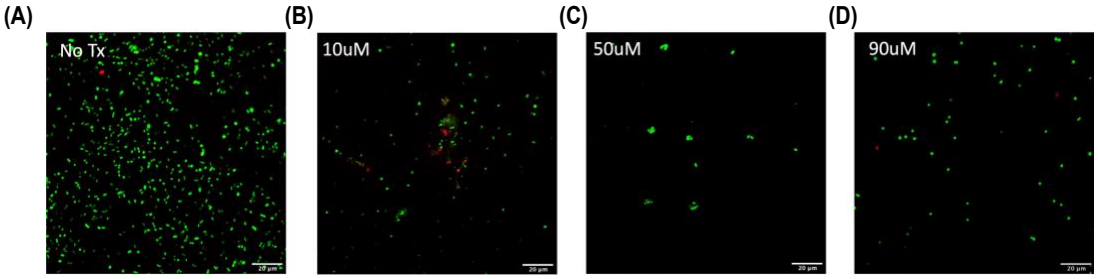

Figure 7.3 - Third experimental repeat- 63X images of *Salmonella typhimurium*. (A) Untreated *S.typhimurium.* **(B)** 10 µM 104 treated *S.typhimurium.* **(C)** 50 µM 104 treated *S.typhimurium.* **(D)** 90 µM 104 treated *S.typhimurium.*

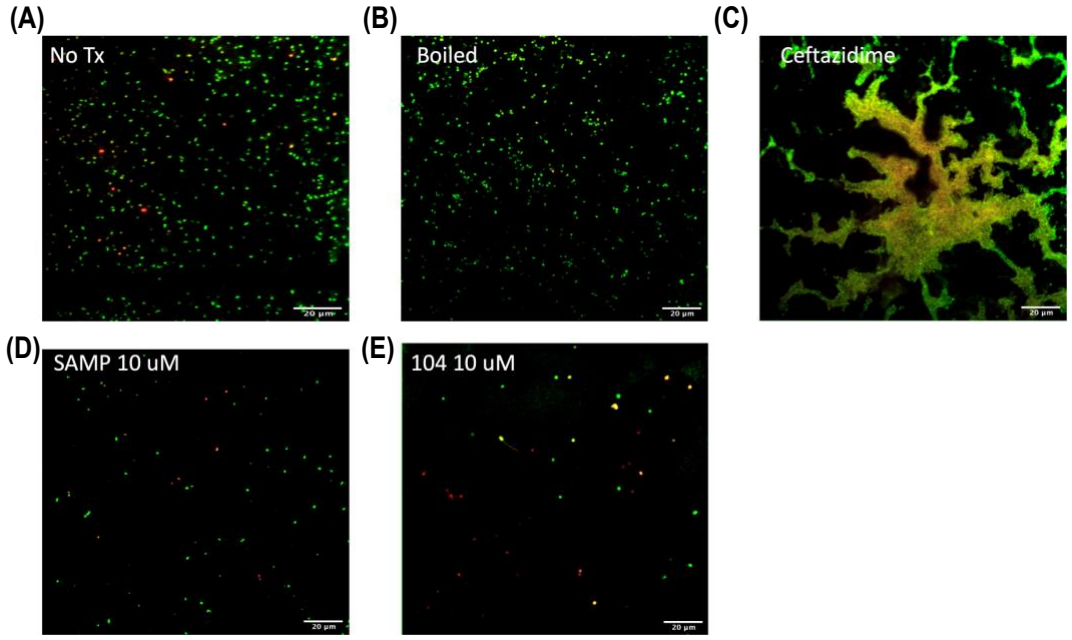

Figure 7.4 - First experiment- 63X images of *Pseudomonas aeruginosa*. (A) Untreated *P.aeruginosa.* **(B)** Boiled *P.aeruginosa.* **(C)** Ceftazidime treated *P.aeruginosa.* **(D)** 10 μM SAMP treated *P.aeruginosa.* **(E)** 10 μM 104 treated *P.aeruginosa.*

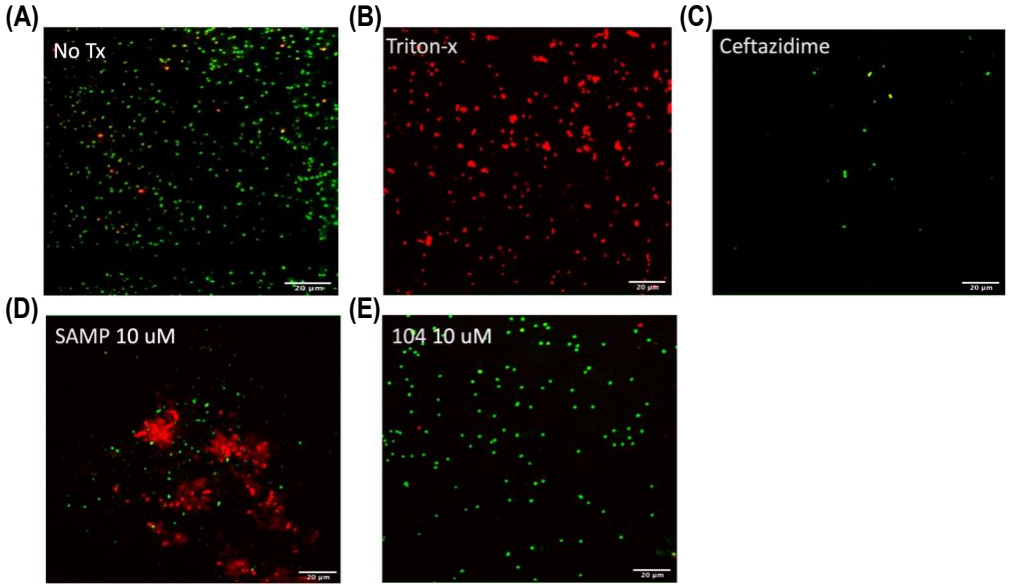

Figure 7.5 - Second experimental repeat- 63X images of *Pseudomonas aeruginosa*. (A) Untreated *P.aeruginosa.* **(B)** Triton-x *P.aeruginosa.* **(C)** Ceftazidime treated *P.aeruginosa.* **(D)** 10 μM SAMP treated *P.aeruginosa.* **(E)** 10 μM 104 treated *P.aeruginosa.*

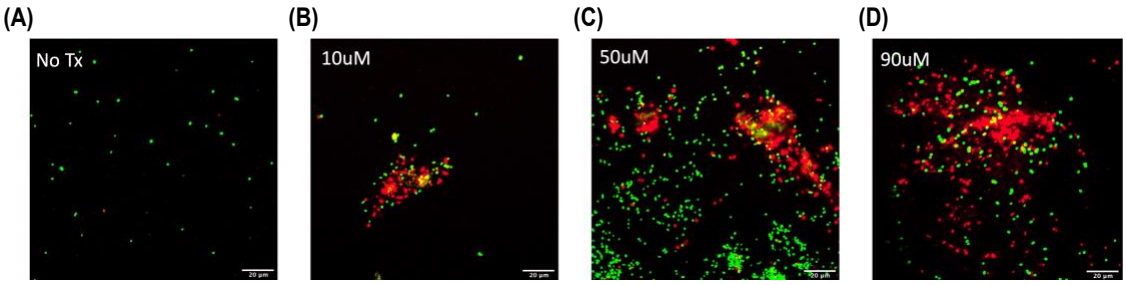

Figure 7.6 - Third experimental repeat- 63X images of *Pseudomonas aeruginosa*. (A) Untreated *P.aeruginosa.* **(B)** 10 µM 104 treated *P.aeruginosa.* **(C)** 50 µM 104 treated *P.aeruginosa.* **(D)** 90 µM 104 treated *P.aeruginosa*

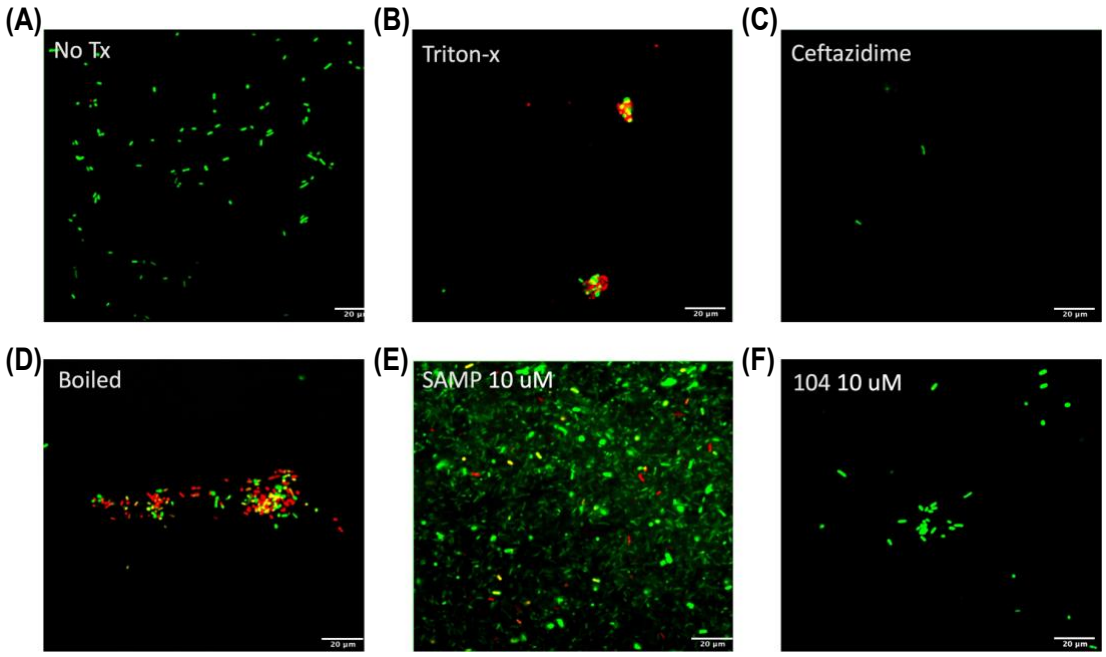

Figure 7.7 - First experiment- 63X images of *Klebsiella pneumoniae*. (A) Untreated *K.pneumoniae.* **(B)** Triton-x treated *K.pneumoniae.* **(C)** Ceftazidime treated *K.pneumoniae.* **(D)** Boiled *K.pneumoniae* **(E)** 10 µM SAMP treated *K.pneumoniae.* **(F)** 10 µM 104 treated *K.pneumoniae.*

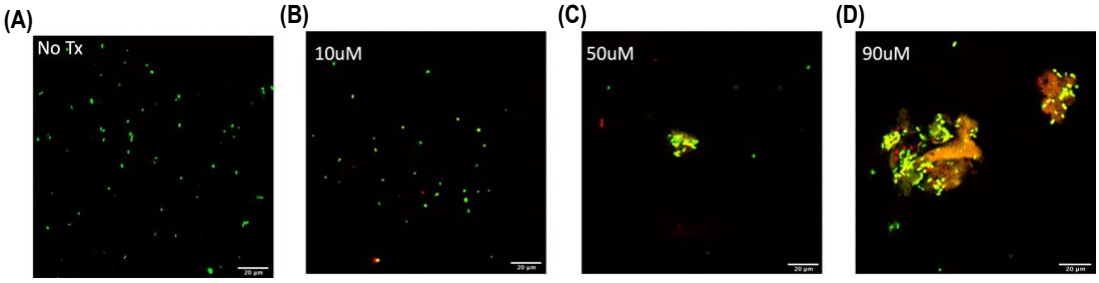

Figure 7.8 - Second experimental repeat- 63X images of *Klebsiella pneumoniae*. (A) Untreated *K.pneumoniae.* **(B)** 10 µM 104 treated *K.pneumoniae.* **(C)** 50 µM 104 treated *K.pneumoniae.* **(D)** 90 µM 104 treated *K.pneumoniae*

Chapter 8: Conclusion

This dissertation explored various biological mechanisms and environmental factors impacting pulmonary health, with a specific focus on inflammatory responses, airway remodeling, and antimicrobial activities. The chapters collectively aimed to uncover insights into both disease pathology and potential therapeutic interventions, addressing the complex interplay between environmental exposures and immune responses in respiratory health. The detailed examination of these interconnected areas provides a comprehensive understanding of the challenges and potential solutions in the field of pulmonary health.

Our studies on the role of TGF-β signaling in allergic asthma demonstrated that inhibition of this pathway through Vactosertib significantly reduced eosinophil recruitment and alleviated fibrotic responses in lung tissues. This finding suggests the therapeutic potential of targeting TGF-β in managing airway remodeling and chronic pulmonary inflammation. Eosinophils are key effector cells in allergic inflammation, contributing to tissue damage and remodeling. By reducing the recruitment of eosinophils, a key cell type involved in allergic responses, and mitigating fibrosis, Vactosertib may help prevent the progression of asthma and improve lung function. The mechanism of action involves the inhibition of TGF-β receptors, which play a critical role in signaling pathways that lead to inflammation and fibrosis. This therapeutic approach could

be particularly beneficial for patients with severe or treatment-resistant asthma, offering a new avenue for intervention beyond standard anti-inflammatory therapies. The study further highlights the importance of molecular-targeted therapies in chronic inflammatory diseases, providing a foundation for the development of new treatment strategies that address the underlying causes of inflammation and tissue remodeling.

Investigations into the pulmonary health effects of aerosolized particles from different sources, including Salton Sea dust and *Alternaria*, revealed distinct inflammatory and gene expression profiles. The use of a novel aerosol exposure chamber provided insights into the real-world implications of chronic particulate matter exposure, highlighting the necessity for accurate and clinically relevant exposure models. Chronic exposure to particulate matter has been linked to various respiratory diseases, including asthma and chronic obstructive pulmonary disease (COPD). The findings from these investigations indicated that different sources of particulate matter could trigger unique inflammatory responses and gene expression changes, which might influence disease severity and progression. For example, Salton Sea dust was found to induce a specific set of inflammatory markers distinct from those induced by *Alternaria* exposure. Moreover, the development and utilization of the aerosol exposure chamber allowed for controlled, reproducible studies that better simulate human exposure scenarios, enhancing the translatability of the results. This model addresses the

limitations of traditional exposure methods, which often fail to replicate the continuous and varied nature of human exposure to environmental pollutants. By providing a more accurate representation of how pollutants affect respiratory health over time, this research contributes to our understanding of the mechanisms through which particulate matter exacerbates respiratory diseases.

The Salton Sea studies are particularly important as it addresses severe health concerns in an impoverished and underserved community. This region has been plagued by high rates of respiratory diseases for decades. The community around the Salton Sea, predominantly composed of low-income and minority populations, has long suffered from limited access to healthcare, exacerbating the impact of environmental health issues. The research highlighted the elevated incidence of respiratory ailments in the region, with studies showing that residents in the Salton Sea area have higher rates of asthma compared to national averages. This project provided crucial insights into the specific environmental factors contributing to these health problems, identifying the dust emissions from the rapidly desiccating Salton Sea as a significant causative agent. The discovery of the bacterial endotoxin, lipopolysaccharide, in the dust provided a clear link between environmental degradation and public health, explaining the high asthma rates and other respiratory issues in the area.

Additionally, the study on antimicrobial peptides (SAMP and 104) isolated from the HLB-resistant Australian Finger Lime showed promising bacteriostatic effects against pathogens such as *Salmonella typhimurium* and *Pseudomonas aeruginosa*. This discovery highlights the potential use of these peptides in developing alternative treatments for bacterial infections, especially in the context of rising antibiotic resistance. Antibiotic resistance is a growing global health threat, driven by the overuse and misuse of antibiotics. These peptides demonstrated a strong ability to inhibit bacterial growth, suggesting they could be harnessed as novel antimicrobial agents. The mechanism of action of these peptides involves disrupting bacterial cell membranes, leading to cell lysis and death. Given the global challenge of antibiotic resistance, the identification of effective, naturally derived antimicrobials is of significant importance. This research opens the door to further exploration of plant-derived compounds as a source of new therapeutics, which could complement or replace traditional antibiotics, reducing the burden of resistant infections. Furthermore, these peptides could be developed into topical applications, inhalable formulations, or systemic therapies, expanding their potential uses in clinical settings.

The dissertation integrates findings from environmental health, immunology, and microbiology to provide a comprehensive understanding of pulmonary health challenges and potential solutions. The demonstrated efficacy of Vactosertib in reducing airway remodeling underscores the importance of

targeted molecular therapies in chronic inflammatory diseases. By specifically inhibiting pathways that contribute to tissue remodeling and fibrosis, targeted therapies like Vactosertib could offer more precise and effective treatment options for patients with chronic respiratory conditions. Meanwhile, the aerosol exposure studies emphasize the critical need for realistic exposure models to understand environmental health impacts accurately. Traditional exposure models often fail to replicate the continuous and varied nature of human exposure to environmental pollutants. The aerosol chamber model addresses this gap, providing a more accurate representation of how pollutants affect respiratory health over time. This research could inform regulatory policies and public health interventions aimed at reducing exposure to harmful pollutants. Finally, the exploration of antimicrobial peptides opens new avenues for combating bacterial infections, offering a sustainable alternative to traditional antibiotics. These peptides could be developed into new classes of antimicrobial agents, providing options for treating infections that are no longer responsive to existing antibiotics. The findings highlight the importance of continued research into alternative treatments, particularly in the face of evolving bacterial resistance.

Future research should focus on enhanced molecular analysis to further dissect the pathways influenced by TGF-β signaling and its broader implications in asthma as well as other pulmonary diseases. Advanced molecular techniques,

such as single-cell RNA sequencing, could provide deeper insights into the specific cellular and molecular changes driven by TGF-β signaling in the context of chronic inflammation and fibrosis. Understanding the precise molecular mechanisms will enable the development of more effective and targeted therapies, potentially improving outcomes for patients with severe asthma and other inflammatory lung diseases. Prolonged exposure studies using the aerosol chamber could better mimic chronic human exposure to environmental pollutants, providing more accurate data on long-term health impacts and informing public health policies. By extending the duration and complexity of exposure studies, researchers can better understand the cumulative effects of pollutants and identify critical thresholds for adverse health outcomes. This research could lead to the identification of biomarkers for early detection and monitoring of pollutant-related respiratory diseases, as well as the development of preventive strategies and interventions. Additionally, continued exploration and optimization of plant-derived antimicrobial peptides could lead to the development of novel therapeutic agents, crucial in the fight against multidrug-resistant bacterial infections. Efforts to enhance the stability, potency, and delivery methods of these peptides will be essential for their successful translation into clinical use. This research could pave the way for the development of a new generation of antimicrobial treatments, addressing one of the most pressing challenges in modern medicine.

In conclusion, this dissertation contributes to a holistic understanding of pulmonary health, emphasizing the interplay between environmental factors, immune responses, and potential therapeutic interventions. The findings pave the way for future research and innovation in improving respiratory health and managing chronic pulmonary diseases. By addressing the complex interactions between environmental exposures and biological responses, this work provides a foundation for developing more effective treatments and preventive strategies for respiratory diseases, ultimately improving health outcomes and quality of life for affected individuals. The comprehensive approach taken in this dissertation underscores the importance of interdisciplinary research in tackling complex health issues and highlights the potential for scientific advancements to make a significant impact on public health. The Salton Sea project, in particular, exemplifies how targeted research can uncover the root causes of long-standing health issues in underserved communities, providing a pathway to effective therapeutic interventions and improved health outcomes for vulnerable populations.